



UNIVERSIDAD DE SEVILLA
CONSEJO SUPERIOR DE INVESTIGACIONES CIÉNTIFICAS

Departamento de Química Inorgánica
Instituto de Investigaciones Químicas

Synthesis, Characterization and Cooperative Reactivity of Polarized Bimetallic Systems

Macarena González Alférez

Tesis Doctoral

Sevilla, 2022

Synthesis, Characterization and Cooperative Reactivity of Polarized Bimetallic Systems

Macarena González Alférez

Trabajo presentado para aspirar
al Título de Doctora en Química
Sevilla, 2022

Macarena González Alférez

Directores:

Jesús Campos Manzano
(Científico titular, CSIC)

Celia Maria Maya Diaz
(Profesora titular, US)

TABLE OF CONTENTS

Abbreviations	1
Publications	5
Acknowledgements	6
General considerations	7
Consideraciones generales	10
Chapter I	
I.1. Metal-metal bonds in transition metal complexes	14
I.2. Frustrated Lewis Pairs	17
<i>I.2.1. Transition Metal Frustrated Lewis Pairs (TMFLPs) with a single transition metal element</i>	23
I.2.1.1 Early and mid-transition metals and rare-earth elements	23
I.2.1.2. Late Transition Metals	28
<i>I.2.2. Frustrated Lewis Pairs and Related Systems based on Two Transition Metals</i>	39
I.2.2.1. Transition Metal Only Frustrated Lewis Pairs (TMOFLPs)	40
I.2.2.2. Polarized heterobimetallic compounds	44
I.3. Metal- Ligand Cooperation	54
<i>I.3.1. Metal-ligand cooperation involving boron-based moieties</i>	57
<i>I.3.2. Metal-ligand cooperation involving cyclopentadienyl ligands</i>	62
I.4 References	67
Chapter II	
II.1. Introductory comments	85
II.2. Results and Discussion	88
<i>II.2.1. Synthesis of Rh(I) MOLPs with s-Block Acids</i>	89
<i>II.2.2. Synthesis of Rh(I) MOLPs with p-Block Acids</i>	94
<i>II.2.3. Synthesis of Rh(I) MOLPs with d-Block Acids</i>	100

<i>II.2.4. Computational analysis of Rh→M bonding in Rh(I) MOLPs</i>	105
II. 3. Experimental Section	111
<i>II. 3.1. General considerations</i>	111
II. 3.1.1. NMR Spectroscopy	111
II. 3.1.2. Crystallographic details	112
<i>II. 3.2. Synthesis and characterization of rhodium compounds</i>	114
II.4 References	124
Chapter III	
III.1. Introductory comments	133
III.2. Reactions between rhodium complex Rh(C ₅ Me ₅)(PMe ₃) ₂ (1a) and the gold complexes (PR ₂ Ar)Au(NTf ₂) (2)	134
III.3. DFT Mechanistic studies for the reaction between 1a and 2 ^{Tripp} towards the formation of 4 ^{Tripp}	142
III.4. Isotopic labelling studies on the Rh/CH ₃ hydride migration in complex 4a ^{Cyp}	149
III.5. Reactivity of Rh/Au bimetallic compounds 3a and 4a towards polar E—H bonds (E = O, N)	152
III.6. Modification of phosphine properties of Cp*Rh complexes 1	158
III.7. Substituting the Cp* ligand in compounds 1 by the Indenyl ligand in Rh complexes 6	164
III.8. Experimental procedures	175
<i>III.8.1. General considerations</i>	175
<i>III.8.2. Crystallographic details</i>	176
<i>III. 8. 3. Computational details</i>	178
<i>III.8.4. Synthesis and characterization of new compounds</i>	180
<i>III.8.5. X-H (X = H, C, O, N) bond activation studies using Rh and Au</i>	205
<i>III.8.6. Variable temperatura van 't Hoff study of the equilibrium of 1c and 2^{Cyp} with 3c^{Cyp}</i>	212

III.9 References	213
Chapter IV	
IV.1. Introductory comments	219
IV.2. Reaction of complex 1a with B(C ₆ F ₅) ₃ and HB(C ₆ F ₅) ₂	221
IV.3. Reaction of complex 6d with B(C ₆ F ₅) ₃ and HB(C ₆ F ₅) ₂	228
IV.4. Catalytic studies	234
IV.5. Mechanistic investigations	239
IV.7. Exchange Spectroscopy (EXSY) experiments for complex 13	248
IV.8. Experimental procedures	254
<i>IV.8.1. General considerations</i>	254
<i>IV.8.2. Crystallographic details</i>	254
<i>IV.8.3. Synthesis and characterization of new compounds</i>	256
IV.9 References	266
Generals Conclusions	271
Conclusiones Generales	274

Abbreviations

Å: Angstrom

Anal. Calc.: Analysis Calculated

Ar: Aryl

Ar': m-terphenyl group

Ar^{Dipp2}: 2,6-bis(2,6-diisopropylphenyl)phenyl, -C₆H₃-2,6-Dipp₂

Ar^{Tripp2}: 2,4,6-tri(2,4,6-triisopropylphenyl)phenyl, -C₆H₃-2,4,6-Tripp₂

Ar^{Xyl2}: 2,6-bis(2,6-dimethylphenyl)phenyl, -C₆H₃-2,6-Xyl₂

atm: Atmosphere

BCP: Bond Critical Point

BP: Bond Path

°C: Degree Celsius

CCDC: Cambridge Crystallographic Data Centre

cm: Centimetre

Cp: Cyclopentadienyl, C₅H₅

Cp*: Pentamethylcyclopentadienyl, C₅Me₅

Cyp: Cyclopentyl, C₅H₉

e⁻: Electron

EDA: Energy Decomposition Analysis

ee: Enantiomeric excess

EF: Electric Field

EIE: Equilibrium Isotope Effect

equiv.: Equivalents

Et: Ethyl, -CH₂CH₃

ET: Electron transfer

Et₂O: Diethyl ether, CH₃CH₂OCH₂CH₃

Exp.: Experimental

FLP: Frustrated Lewis Pair

FRP: Frustrated Radical Pair

g: Gram

h: Hour

HOMO: Highest Occupied Molecular Orbital

IMes: 1,3-Dimesitylimidazol-2-ylidene

iPr: Isopropyl, $-\text{CH}(\text{CH}_3)_2$

IR: Infrared

K: Kelvin

K_{eq} : Equilibrium constant

KIE: Kinetic Isotopic Effect

LUMO: Lowest Unoccupied Molecular Orbitals

m: meta

M: Metal

Me: Methyl, $-\text{CH}_3$

mg: Miligram

min: Minutes

mL: Millilitre

MMA: Methyl methacrylate

mmol: Millimol

MOLP: Metal-Only Lewis Pair

MS-ESI: Mass Spectrometry-ElectroSpray Ionization

NBO: Natural Bond Orbital

NTf₂: Bis(trifluoromethane)sulfonimide, $-\text{N}(\text{S}(\text{O})_2\text{CF}_3$

o: ortho

ORTEP: Oak Ridge Thermal Ellipsoid Program (Crystallographic representation)

p: para

Ph: Phenyl, $-\text{C}_6\text{H}_5$

QTAIM: Quantum Theory of Atoms In Molecules

R, R': Alkyl group

RE: Rare-Earth element

ref: Reference

rt: Room temperature

tBu: tert-butyl, CMe₃

THF: Tetrahydrofuran, C₄H₈O

TM: Transition Metal

TMFLP: Transition Metal Frustrated Lewis Pair

TMOFLP: Transition Metal-Only Frustrated Lewis Pair

Tol: Toluene

TON: Turn Over Number

TS: Transition State

vol: Volume

ZPE: Zero-Point Energy

NMR abbreviations

br: Broad

d: Doublet

DOSY: Diffusion Ordered Spectroscopy

EXSY: Exchange Spectroscopy

HMBC: ¹H-¹³C correlation spectroscopy (Heteronuclear Multiple Bond Correlation).

HSQC: ¹H-¹³C correlation spectroscopy (Heteronuclear Single Quantum Coherence).

Hz: Hertz

m: Multiplet

ⁿJ_{AB}: Coupling constant (Hz) between A and B nuclei separated

by n bonds.

NMR: Nuclear Magnetic Resonance

ppm: Parts per million

q: Quartet

s: Singlet

sept: Septet

t: Triplet

vt: Virtual triplet

δ : Chemical shift in ppm

Publications

Chapter II:

S. Bajo[‡], M. G. Alférez[‡], M. M. Alcaide, J. López-Serrano, J. Campos, *Chem. Eur. J.*, **2020**, 26, 16833–16845.

[‡]These authors contributed equally

Chapter III:

Section III.2, III.4, III.5 :

M. G. Alférez, J. J. Moreno, N. Hidalgo, J. Campos. *Angew. Chem. Int. Ed.*, **2020**, 59, 20863-20867.

Other sections:

Manuscript in preparation.

Chapter IV:

Manuscript in preparation.

Others

M. Navarro, M. G. Alférez, M. de Sousa, J. Miranda-Pizarro, J. Campos, *ACS Catal.*, **2022**, 12, 4227-4241.

M. G. Alférez[‡], N. Hidalgo[‡], J. Campos, **2020**. Editors C. Sloatweg and A. Jupp. Springer.

[‡]These authors contributed equally

J. Miranda-Pizarro, M. G. Alférez, M. D. Fernández-Martínez, E. Álvarez, C. Maya, J. Campos, *Molecules*, **2020**, 25, 593.

Acknowledgements

Dr. Joaquín López-Serrano (Instituto de Investigaciones Químicas, CSIC-Universidad de Sevilla) for the computational studies presented in Chapter II.

Dr. Juan José Moreno (Instituto de Investigaciones Químicas, CSIC-Universidad de Sevilla) for the computational studies presented in Chapter III and IV.

General considerations

The results presented in this Thesis are framed into one of the lines of research developed by the Organometallic and Homogeneous Catalysis Chemistry Group of the “Instituto de Investigaciones Químicas” (Centro Mixto CSIC–Universidad de Sevilla), which has among its main goals the study of bimetallic systems for the activation of small molecules and catalysis.

Although the topic of metal-metal bonds has accompanied the development of organometallic chemistry since its early beginnings, the design of bimetallic structures has only enjoyed an intermittent progress along the decades. However, triggered by the current great interest on developing cooperative molecular approaches for bond activation and catalysis, the field of bimetallic complexes is enjoying a bright renaissance. They certainly offer additional tunable features compared to monometallic compounds, including the capacity to modulate metal-metal bond polarity and order and the ability to effect bond activation by multi-site mechanisms.

In this context, our group has largely focused on highly polarized heterobimetallic structures in which one of the metals presents strong Lewis basicity and the other one strong Lewis acidity. This clearly connects to the area of frustrated Lewis pairs (FLPs) and also relates to many metalloenzymes that rely on the similar bimetallic synergisms.

The content of this Thesis was organized into four chapters. The first one contains a general introduction chapter, where a general overview of bimetallic chemistry is provided and where much focus is given to bimetallic designs that behave as FLPs, one of the main original goals of this Thesis. Besides, other types of cooperative chemistry aligned with the concept of metal-ligand cooperation (MLC) are briefly discussed. The second chapter focuses on the Lewis basic behaviour of a Rh(I) compound of formula $[(\eta^5-$

$C_5Me_5Rh(PMe_3)_2$], which has been treated with a broad family of main group and transition metal electrophiles to design bimetallic structures known as metal-only Lewis pairs (MOLPs). The third chapter exploits the basicity of this Rh(I) compound in an attempt to build a transition metal-only frustrated Lewis pair (TMOFLP) based on a Rh(I)/Au(I) pair. These studies evinced the non-innocent character of the cyclopentadienyl ligand, a topic that is thoroughly investigated within this Thesis. In fact, chapter 4 deals with the investigation of this non-innocence to incorporate pendant boron functions on this ligand and on the related indenyl fragment. The goal here was the design of bifunctional aromatic ligands to bind the rhodium center and access cooperative Rh(I)/borane catalysts. Our results on the benchmark hydrogenation of olefins is described in this last chapter.

Whereas chapter 1 describes provides a general overview of the field, chapters 2-4 are organized in the same manner, with some initial introductory remarks, followed by a results and discussion section, conclusion and finally the corresponding experimental part. References are independent in the four chapters, being included at the end of each page and also the whole collection of references is added at the end of the chapter for convenience to the reader. The number of new complexes is independent in the general introduction of chapter 1 with respect to the other three chapters, where the numbering is correlative.

To apply for the *International PhD Mention* this Thesis was written in English, and only the present general considerations, as well as the final conclusions, are included in Spanish as well. Also, in accordance to current regulations to apply for the aforesaid distinction, I, the candidate, spent a period of three months working under the supervision of Prof. Ulrich Hintermair at the University of Bath, UK. I did research on the synthesis and

reactivity of iridium complexes constructed around pincer PNP-type ligands.

Consideraciones Generales

Los resultados presentados en esta Tesis se enmarcan en una de las líneas de investigación desarrolladas por el Grupo de Química Organometálica y de Catálisis Homogénea del Instituto de Investigaciones Químicas (Centro Mixto CSIC-Universidad de Sevilla), que tiene entre sus principales objetivos el estudio de sistemas bimetálicos para la activación de pequeñas moléculas y su uso en aplicaciones catalíticas.

Si bien los enlaces metal-metal han acompañado el desarrollo de la química organometálica desde sus inicios, el diseño de estructuras bimetálicas ha supuesto un progreso intermitente a lo largo de las décadas. Sin embargo, debido al gran interés actual por el desarrollo de sistemas cooperativos para la activación de enlaces y su empleo en catálisis homogénea, el campo de los complejos bimetálicos está disfrutando de un brillante renacimiento. La realidad es que ofrecen características modulables adicionales en comparación con los compuestos monometálicos, incluida la capacidad de modular la polaridad y el orden de los enlaces metal-metal y la capacidad de efectuar la activación de enlaces mediante mecanismos multi-sitios.

En este contexto, nuestro grupo se ha centrado principalmente en estructuras heterobimetálicas altamente polarizadas en las que uno de los metales presenta una fuerte basicidad de Lewis y el otro una fuerte acidez de Lewis. Esto se conecta claramente con el área de los pares de Lewis frustrados (FLP) y también se relaciona con muchas metaloenzimas que se basan en sinergismos bimetálicos similares.

El contenido de esta Tesis se ha organizado en cuatro capítulos. El primero contiene un capítulo de introducción general, donde se proporciona una visión general de la química bimetálica y se presta especial atención a los diseños bimetálicos que se comportan como FLP, uno de los principales

objetivos originales de esta Tesis. Además, se discuten brevemente otros tipos de química cooperativa alineados con el concepto de cooperación metal-ligando (MLC). El segundo capítulo se centra en el comportamiento básico de Lewis de un compuesto Rh(I) de fórmula $[(\eta^5\text{-C}_5\text{Me}_5)\text{Rh}(\text{PMe}_3)_2]$, que ha sido tratado con una amplia familia de electrófilos de metales de transición y de grupo principal para diseñar estructuras bimetalicas conocidas como pares de Lewis de solo metal (MOLP). El tercer capítulo explota la basicidad de este compuesto Rh(I) en un intento de construir un par de Lewis frustrado de solo metales de transición (TMOFLP) basado en un par Rh(I)/Au(I). Estos estudios pusieron de manifiesto el carácter no inocente del ligando ciclopentadienilo, un tema que se investiga a fondo en esta Tesis. De hecho, el capítulo 4 se ocupa de la investigación de esta no inocencia para incorporar funciones colgantes de boro en este ligando y en el fragmento de indenilo relacionado. El objetivo aquí era el diseño de ligandos aromáticos bifuncionales para unirse al centro de rodio y acceder así a catalizadores cooperativos de Rh(I)/borano. Nuestros resultados sobre la hidrogenación de olefinas, empleada como referencia, se describen en este último capítulo.

El capítulo 1 describe una visión general del campo mientras que los capítulos 2-4 están organizados con una misma estructura consistente en algunos comentarios introductorios iniciales, seguidos de una sección de resultados y discusión, otra de conclusiones y finalmente, la parte experimental correspondiente. Las referencias son independientes en los cuatro capítulos y se incluyen al final de cada página, pero además se añade toda la colección de referencias al final del capítulo para la comodidad del lector. La numeración de los complejos es independiente en la introducción general del capítulo 1 con respecto a los otros tres capítulos, donde la numeración es correlativa.

Para optar a la *Mención Internacional de Doctorado* esta Tesis se ha redactado en inglés, y sólo se incluyen en español las presentes consideraciones generales, así como las conclusiones finales. También, de acuerdo con la normativa vigente para solicitar la mencionada distinción, yo, la candidata, pasé un período de tres meses trabajando bajo la supervisión del Prof. Ulrich Hintermair en la Universidad de Bath, Reino Unido. Investigué sobre la síntesis y la reactividad de complejos de iridio estabilizados mediante ligandos de tipo pinza PNP.

CHAPTER I

I.1. Metal-metal bonds in transition metal complexes

In 1913, Alfred Werner received the Nobel prize in chemistry¹ in recognition of his work explaining the structures, the formation, and the nature of bonding in coordination compounds. He proposed they were a single, transition metal atom surrounded by a set of ligands and he postulated that metals exhibit two types of valences: (i) primary valency or oxidative state and (ii) secondary valency or coordination number. After Werner's theory, there was a huge development and refinement of that concept, following progress in numerous areas²: metal carbonyls and other compounds where the metal was formally not an ion; research on the electronic structures of complexes, thermodynamic and kinetics properties and structural studies, increasing the range of geometries; the understanding of the role of metal ions in biological systems; the recognition that ligands were not passive but that their behaviour is often greatly modified when they were attached to a metal atom, in some cases allowing the metal to act catalytically. Such complexes could contain two or more metal atoms but no direct metal-metal bonds could be established.

The development of the chemistry of metal-metal bonds is intimately connected with that of the single-crystal X-ray Diffraction. Thus, although

¹ A. Werner, On the constitution and configuration of higher-order compounds. Nobel Lecture, December 11, 1913. The Nobel Prize <https://www.nobelprize.org/prizes/chemistry/1913/werner/lecture>.

²a) S. Kirschner, *Coordination Chemistry*, Springer New York, NY, 1969, <https://doi.org/10.1007/978-1-4899-6555-4>

b) *Comprehensive Coordination Chemistry II* (Elsevier, 2004).

c) <https://www.wiley.com/en-us/Introduction+to+Coordination+Chemistry-p-978111868140>

in 1935, Brosset³ reported the first examples with M—M⁴ bonds in the Mo and W binuclear anions: [Mo₆Cl₈]⁴⁺ and [W₂Cl₉]³⁻, it was not until 1957 when the unambiguous recognition of M—M bonding was made. More precisely, this involved the determination of the Mn₂(CO)₁₀ structure⁵ by X-ray diffraction, which was a landmark discovery in transition metal chemistry and set the grounds for exciting developments in the field of polynuclear molecular compounds⁶. Only a few years later, in 1964 the existence of multiple bonding between metals was demonstrated by Cotton and co-workers in [Re₂Cl₈]⁷, shattering at the same time the common belief of a maximum bond order of three, as seen in the *p*-block. The area of metal-to-metal bonded compounds has discontinuously evolved since then, in a path teemed with milestones that include, to cite some paradigmatic examples, the first quintuply bonded dimetallic structure [Cr₂{C₆H₃-2,6-Dip₂}₂]⁸ (Dip = C₆H₃-2,6-*i*-Pr₂) or the M(I) dimers [Zn₂Cp*₂]⁹ (Cp* = [η⁵-C₅Me₅]) and [Mg₂(^{Dip}Nacnac)₂]¹⁰ (^{Dip}Nacnac = [(DipNCMe₂)₂CH]⁻) with a M(I)—M(I) bond.

In the area of organometallic catalysis, the metal–metal interaction offers promising opportunities for new reactions, allowing reactions that are not known using monometallic reagents¹¹. Cooperativity and synergisms

³ a) C. Brosset, *Arkiv Kemi, Miner. Geol.* **1946**, A20 (7), A22 (11).

b) C. Brosset, *Nature*, **1935**, 135, 874.

⁴ F. A. Cotton, L. A. Murillo, R. A. Walton, *Multiple Bonds Between Metal Atoms* **2005**, 3rd edition [F. A. Cotton, R. A. Walton, in 1st (1981) and 2nd (1992) ed.], Springer, New York.

⁵ L. F. Dahl, E. Ishishi, R. E. Rundle, *J. Chem. Phys.*, **1957**, 26, 1750-1751.

⁶ a) J. F. Berry, C. C. Lu, *Inorg. Chem.*, **2017**, 56, 7577-7581.

b) C. M. Farley, C. Uyeda, *Trends Chem.*, **2019**, 1, 497-509.

⁷ F. A. Cotton, N. F. Curtis, C. B. Harris, B. F. G. Johnson, S. J. Lippard, J. T. Mague, W. R. Robinson, J. S. Wood, *Science*, **1964**, 145, 1305-1307.

⁸ T. Nguyen, A. D. Sutton, M. Brynda, J. C. Fettinger, G. J. Long, P. P. Power, *Science*, **2005**, 310, 844-847.

⁹ I. Resa, E. Carmona, E. Gutierrez-Puebla, A. Monge, *Science*, **2004**, 305, 1136-1138.

¹⁰ S. P. Green, C. Jones, A. Stasch, *Science*, **2007**, 318, 1754-1757.

¹¹ O. Kysliak, H. Görls, R. Kretschmer, *J. Am. Chem. Soc.*, **2021**, 143, 142-148.

between two metals in close proximity have tremendous utility in bond activations and catalysis¹².

A key challenge is to understand how to handle that metal–metal cooperativity to benefit catalysis.¹³ Numerous studies have been made on homodinuclear transition-metal-metal bonds, but less attention has been dedicated to heterodinuclear analogues in which unprecedented reactions (including catalytic) are likely to be found as a consequence of the synergetic effect of two transition-metal centres with contrasting features. Among heterodinuclear complexes, those containing two metals with highly dissimilar electronic affinities, that is, with contrasting Lewis character, are particularly relevant for the present doctoral Thesis and will be discussed in detail in the following section and in the context of metallic frustrated Lewis pairs (FLPs).

On the other hand, in organometallic catalytic reactions the transformation typically occurs in the centre of the metal and the ligands do not significantly change or directly participate during the reaction. However, in nature, many enzymes need a finely adjusted ligand environment that acts in cooperation with the metal and participate in the reaction. With that in mind, a relatively new approach that remain as a hot topic, known as metal–ligand cooperation (MLC), was developed and represents an important concept in catalysis with transition metals¹⁴.

¹² a) J. Campos, *Nat. Rev. Chem.*, **2020**, *4*, 696-702.

b) C. M. Farley, C. Uyeda, *Trends Chem.*, **2019**, *1*, 497–509.

c) P. Buchwalter, J. Rose, P. Braunstein, *Chem. Rev.*, **2015**, *115*, 28–126.

d) R. C. Cammarota, L. J. Clouston, C. C. Lu, *Coord. Chem. Rev.*, **2017**, *334*, 100–111.

e) D. R. Pye, N. P. Mankad, *Chem. Sci.*, **2017**, *8*, 1705–1718.

f) I. G. Powers, C. Uyeda, *ACS Catal.*, **2017**, *7*, 936–958.

g) J. Park, S. Hong, *Chem. Soc. Rev.*, **2012**, *41*, 6931–6943.

¹³ J. F. Berry, C. C. Lu, *Inorg. Chem.*, **2017**, *56*(14), 7577–7581.

¹⁴ D. Milstein, J. R. Khusnutdinova, *Angew. Chem. Int. Ed.*, **2015**, *54*, 12236 – 12273.

I.2. Frustrated Lewis Pairs

In this section, a deeper notion of the Frustrated Lewis pair (FLP) is displayed. A FLP is defined as a compound containing a Lewis acid and a Lewis base which cannot interact to form a classical adduct. It was in 1942, when Brown for the first time suggested the existence of this type of interaction between pyridines with boranes.¹⁵ Years later, Wittig and Benz reported the reaction of BPh₃ and PPh₃ with benzyne,¹⁶ and in 1966 Tochtermann described a similar addition between trityl anion and the same acid¹⁷. Also, Damico and Broadus produced an iminium cation with the same trityl anion¹⁸. In 1998, Erker reported a phosphine/borane example that gives the adduct at room temperature and afterwards exhibited an intriguing thermal rearrangement¹⁹.

¹⁵ a) H. C. Brown, H. I. Schlesinger, S. Z. Cardon. *J. Am. Chem. Soc.*, **1942**, *64*, 325–329.

b) H. C. Brown, B. Kanner. *J. Am. Chem. Soc.*, **1966**, *88*, 986–992.

¹⁶ G. Wittig, E. Benz. *Chem. Ber.*, **1959**, *92*, 1999–2013.

¹⁷ W. Tochtermann. *Angew. Chem. Int. Ed.*, **1966**, *5*, 351–371.

¹⁸ R. Damico, C. D. Broadus. *J. Org. Chem.*, **1966**, *31*, 1607–1612.

¹⁹ S. Doering, G. Erker, R. Fröhlich, O. Meyer, K. Bergander. *Organometallics*, **1998**, *17*, 2183–2187.

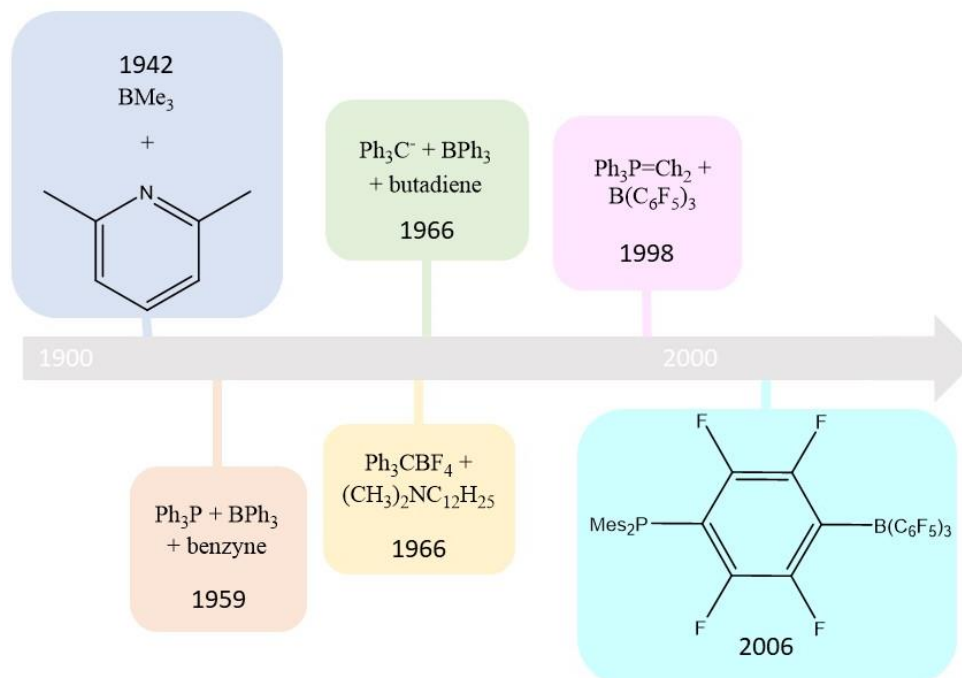


Figure 1. Line of time with the most representative examples of the examples prior to the appearance of FLP as a formal concept.

But the concept of “frustrated Lewis pair” represented a landmark discovery in the chemistry of main group elements when Stephan demonstrated in 2006 that the cooperative action of a phosphine and a borane was capable of the heterolytic cleavage of the dihydrogen molecule²⁰.

This achievement parallels in time the independent work of Power²¹ and Bertrand²² on multiply-bonded and sub-valent main group compounds

²⁰ a) G. C. Welch, R. R. San Juan, J. D. Masuda, D.W. Stephan, *Science*, **2006**, *314*, 1124–1128.

b) G. C. Welch, D. W. Stephan. *J. Am. Chem. Soc.*, **2007**, *129*, 1880–1881.

²¹ G. H. Spikes, J. C. Fettinger, P. P. Power, *J Am Chem Soc*, **2005**, *127*, 12232–12233.

²² G. D. Frey, B. Lavallo, B. Donnadiu, W. W. Schoeller, G. Bertrand, *Science*, **2007**, *316*, 439–441.

that also accomplished dihydrogen splitting. Altogether, these and related findings have revolutionized the way by which chemists look at the *p*-block. It has now become clear that main group elements can behave as transition metals under certain conditions, and this also applies to their reactivity towards small molecules²³. In fact, the mechanism followed by transition metals, sub-valent and multiply bonded main group systems or FLPs to activate small molecules is the result of a precise orbital cooperation. Oxidative addition of dihydrogen over transition metals can be rationalized by the Dewar–Chatt–Duncanson model in terms of σ -donation from H₂ to an empty metallic *d*-orbital and metal-to-ligand π -backbonding²⁴ (Figure 2). Related to this, the addition of H₂ over multiply-bonded and sub-valent main group systems also entails a synergistic interaction of frontier orbitals²⁵. In the case of FLPs, although dihydrogen splitting is heterolytic (i.e. R₃P–H⁺ / Ar₃B–H⁻), the initial step likewise involves the synergic donation from the lone pair of the (phosphine) base to the H₂ σ^* -orbital along with donation from the σ -H₂ to the empty (borane) acid orbital (Figure 1). Thus, a connection between the three modes of dihydrogen cleavage can be clearly delineated.

²³ P. P. Power, *Nature*, **2010**, *463*, 171–177.

²⁴ J. Chatt, L. A. Duncanson, *J. Chem. Soc.*, **1953**, *586*, 2939–2947.

²⁵ Y. Peng, M. Brynda, B. D. Ellis, J. C. Fettinger, E. Rivarda, P. P. Power, *Chem. Commun.*, **2008**, *45*, 6042–6044.

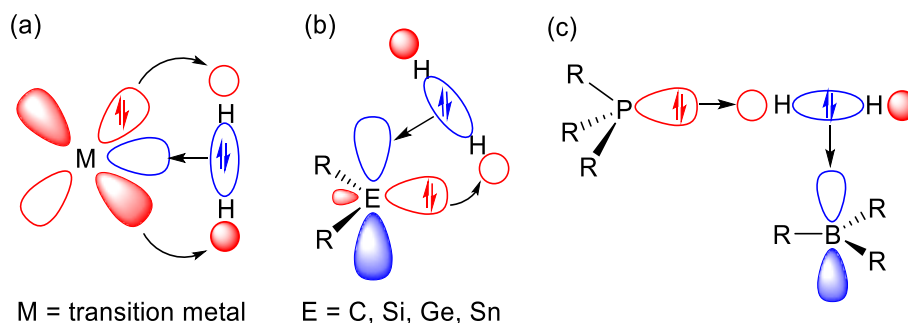


Figure 2. Frontier molecular orbital interactions for the splitting of dihydrogen by (a) transition metals; (b) sub-valent group-14 elements (tetrylenes); and (c) P/B frustrated Lewis pairs.

Much of the widespread interest in FLP systems derives from their proved proficiency as metal-free hydrogenation catalysts²⁶. This has led to a frenetic development of the field over the last decade that continuously expands to a range of related areas. A brief review of the most representative examples of that metal-free hydrogenation activation is summarized below. In 2008, Erker²⁷ described a phosphine borane system with an ethylene-bridged similar to Stephan's, who reported a system with lutidine or N heterocyclic and a borane in 2009²⁸. One year before Klankermayer's had published the first FLP-catalyzed asymmetric hydrogenation of an imine using a chiral borane²⁹ which was also carried out by Repo's group in 2011 using ansa-ammonium borates³⁰ (Figure 3, green).

²⁶ a) D. W. Stephan, *Org. Biomol. Chem.*, **2012**, *10*, 5740–5746.

b) D. J. Scott, M. J. Fuchter, A. E. Ashley, *Chem. Soc. Rev.*, **2017**, *46*, 5689–5700.

²⁷ P. Spies, G. Erker, G. Kehr, K. Bergander, R. Fröhlich, S. Grimme, D. W. Stephan, *Chem. Commun.*, **2007**, *47*, 5072–5074.

²⁸ a) S. J. Geier, A. L. Gille, T. M. Gilbert, D. W. Stephan, *Inorg. Chem.*, **2009**, *48*, 10466–10474.

b) S. J. Geier, D. W. Stephan, *J. Am. Chem. Soc.*, **2009**, *131*, 3476–3477.

²⁹ a) D. Chen, J. Klankermayer, *Chem. Comm.*, **2008**, *18*, 2130–2131.

b) D. Chen, Y. Wang, J. Klankermayer, *Angew. Chem. Int. Ed.*, **2010**, *49*, 9475–9478.

³⁰ V. Sumerin, K. Chernichenko, M. Nieger, M. Leskelä, B. Rieger, T. Repo, *Adv. Synth. Catal.*, **2011**, *353*, 2093–2110.

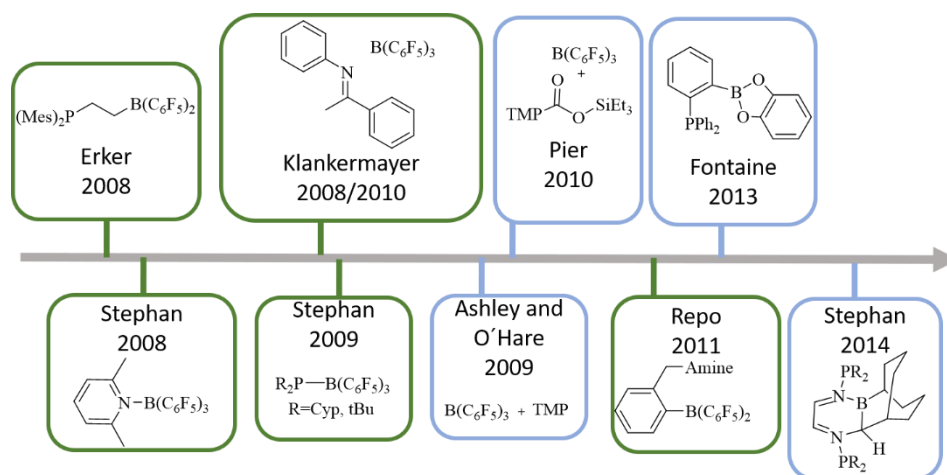


Figure 3. Representative examples of FLP systems active in catalytic hydrogenation (green) and carbon dioxide functionalization (blue).

These kind of FLP systems have also shown application in the functionalization of carbon dioxide. In 2009, Ashley and O'Hare reported the reduction to CO₂ with a system based in piperidine and borane³¹ and, a year later, Pier's group employed a silane and borane³². Other interesting reaction was the hydroboration of CO₂ with a phosphine-borane system³³ reported by Fontaine's group and replicated by Stephan employing a N-heterocycle-borane system³⁴ (Figure 3, blue)

The reactivity observed with these traditional FLPs revealed that the combination of main group elements may behave as transition metals. Nonetheless, it soon became obvious that the incorporation of transition metal centers as components of FLP systems could raise a new field to

³¹ A. E. Ashley, A. L. Thompson, D. O'Hare, *Angew. Chem. Int. Ed.*, **2009**, *48*, 9839–9843.

³² A. Berkefeld, W. E. Piers, M. Parvez, *J. Am. Chem. Soc.*, **2010**, *132*, 10660–10661.

³³ M. A. Courtemanche, M. A. Legare, L. Maron, F. G. Fontaine, *J. Am. Chem. Soc.*, **2013**, *135*, 9326–9329.

³⁴ T. Wang, D. W. Stephan, *Chem. Eur. J.*, **2014**, *20*, 3035–3039.

explore, with new chemical possibilities. In 2011, Wass³⁵ and Erker's³⁶ groups reported pioneering work on TM-based FLPs on zirconium/phosphine pairs.

Introducing transition metals into FLP architectures might seem to arguably undermine the utmost benefit of the original systems, namely, their capacity to mediate catalytic transformations in the absence of transition metals. However, there are a number of rewards that largely justify intense research in this direction, apart from the obvious enormous rise of combinatorial possibilities derived from introducing three series of transition metals (even more if lanthanides and actinides are to be considered). Among the main advantages of introducing transition metals into FLP structures the following should be had in mind:

- **Rich reactivity.** Due to the presence of partly occupied d orbitals with energies that make them suitable to participate in elementary reactions (e.g. oxidative addition, migratory insertion, reductive elimination...).
- **Structural diversity.** due to the different coordination numbers that present transition metals in comparison with the main group series.
- **Tunable properties.** due to the large number of existing ligands with different stereoelectronic properties and also the versatility of transition metals to act as Lewis bases or acids.

³⁵ a) A. M. Chapman, M. F. Haddow, D. F. Wass, *J. Am. Chem. Soc.*, **2011**, *133*, 8826–8829.

b) A. M. Chapman, M. F. Haddow, D. F. Wass, *J. Am. Chem. Soc.*, **2011**, *133*, 18463–18478.

c) A. M. Chapman, M. F. Haddow, D. F. Wass, *Eur. J. Inorg. Chem.*, **2012**, *9*, 1546–1554.

³⁶ a) X. Xu, R. Fröhlich, C. G. Daniliuc, G. Kehr, G. Erker, *Chem. Commun.*, **2012**, *48*, 6109–6111.

b) X. Xu, G. Kehr, C. G. Daniliuc, G. Erker, *J. Am. Chem. Soc.*, **2013**, *135*, 6465–6476.

- **Synthetic amenability.** The methods to prepare transition metal complexes have been developed over the last decades and in many occasions synthetic protocols are relatively simple and expeditious.
- **Broad spectra of affinities.** Transition metals exhibit a broader diversity interactions and affinities towards specific elements than main group compounds.

I.2.1. Transition Metal Frustrated Lewis Pairs (TMFLPs) with a single transition metal element

This section covers TMFLPs in which one of the two components (acid or basic) is a transition metal, which comprises the majority of the reported systems. In this Thesis, we focus on the late transition metals, and thus we will discuss the background of these in more detail, although some prominent examples of early and mid-transition metals and more recent systems based on rare-earth elements are briefly commented in the following section.

I.2.1.1 Early and mid-transition metals and rare-earth elements

Electron deficient early transition metal complexes, particularly those in high oxidation states, have been widely used as Lewis acid catalysts for a number of transformations³⁷. In an early example, prior to coining the term ‘Frustrated Lewis Pair’³⁸, Stephan demonstrated that combining the acidic titanium compound $[\text{CpTi}(\text{N}=\text{P}^t\text{Bu}_3)][\text{B}(\text{C}_6\text{F}_5)_4]$, with the sterically demanding $\text{P}(o\text{-MeC}_6\text{H}_4)_3$ phosphine, did not lead to ligand coordination

³⁷ H. Yamamoto (ed) (2000) *Lewis acids in organic synthesis*. Wiley-VCH, Weinheim.

³⁸ J. S. J. McCahill, G. C. Welch, D. W. Stephan, *Angew Chem Int Ed*, **2007**, *46*, 4968–4971.

due to steric clash providing instead cooperative cleavage of a C–Cl bond of a dichloromethane solvent molecule.

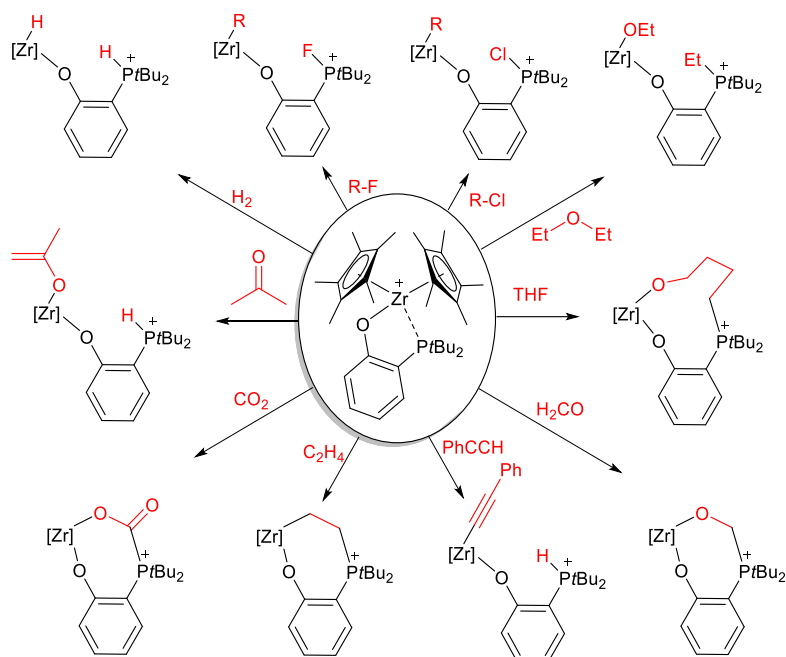
However, it was the group of Wass the first who investigated the reactivity of a TMFLP in a systematic manner. To do so, he designed a TMFLP based on a zirconium- phosphinoaroxide complex that is capable of activating a wide range of small molecules, not only H₂, but also CO₂, C₂H₄, formaldehyde and breaking C–halide or C–O bonds of different substrates (Scheme 1). These studies inspired many other groups³⁹, including ours, and it was followed by many examples on other early-TM based systems.

³⁹ See for example: a) A. T. Normand, P. Richard, C. Balan, C. G. Daniliuc, G. Kehr, G. Erker, P. L. Gendre, *Organometallics*, **2015**, *34*, 2000–2011.

b) A. T. Normand, Q. Bonnin, S. Brandès, P. Richard, P. Fleurat-Lessard, C. H. Devillers, C. Balan, P. L. Gendre, G. Kehr, *Chem. Eur. J.*, **2019**, *25*, 2803–2815.

c) M. Fischer, D. Barbul, M. Schmidtman, R. Beckhaus, *Organometallics*, **2018**, *37*, 1979–1991.

d) M. Fischer, K. Schwitalla, S. Baues, M. Schmidtman, R. Beckhaus, *Dalton Trans.*, **2019**, *48*, 1516–1523.



Scheme 1. Reactivity of the first³⁵ TMFLP complex reported by Wass.

Moving forward to group 6 of the periodic table, Bullock explored the reversible and heterolytic cleavage of the H–H bond (Scheme 2) in a series of molybdenum⁴⁰, manganese⁴¹ and iron⁴² complexes containing a pendant amine. The latter systems are particularly attractive since they serve as synthetic models of the [FeFe] —hydrogenase and [NiFe] —hydrogenases⁴³. In the case of molybdenum, it becomes clear that the

⁴⁰ S. Zhang, A. M. Appel, R. M. Bullock, *J. Am. Chem. Soc.*, **2017**, *139*, 7376–7387.

⁴¹ a) E. B. Hulley, K. D. Welch, A. M. Appel, D. L. DuBois, R. M. Bullock, *J. Am. Chem. Soc.*, **2013**, *135*, 11736–11739.

b) E. B. Hulley, M. L. Helm, R. M. Bullock, *Chem. Sci.*, **2014**, *5*, 4729–4741.

⁴² a) T. Liu, D. L. DuBois, R. M. Bullock, *Nat. Chem.*, **2013**, *5*, 228–233.

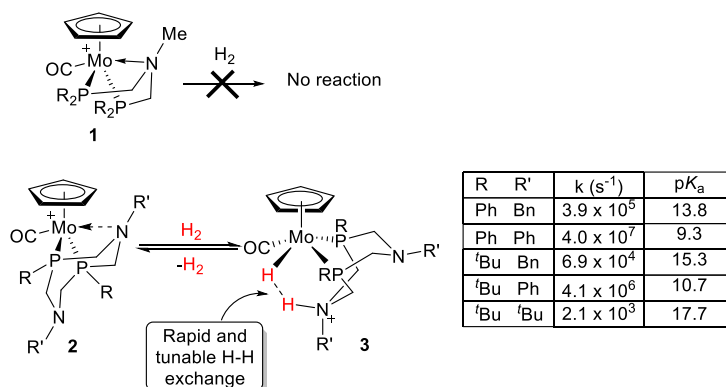
b) T. Liu, X. Wang, C. Hoffmann, D. L. DuBois, R. M. Bullock, *Angew. Chem. Int. Ed.*, **2014**, *53*, 5300–5304.

c) T. Liu, Q. Liao, M. O. Hagan, E. B. Hulley, D. L. DuBois, R. M. Bullock, *Organometallics*, **2015**, *34*, 2747–2764.

⁴³ a) J. C. Fontecilla-Camps, A. Volbeda, C. Cavazza, Y. Nicolet, *Chem. Rev.*, **2007**, *107*, 4273–4303.

b) W. Lubitz, H. Ogata, O. Rüdiger, E. Reijerse, *Chem. Rev.*, **2014**, *114*, 4081–4148.

strength of the interaction between the pendant amine and the acidic molybdenum center is crucial to achieve H₂ splitting. Thus, while compounds **1** are unable to attain this activation⁴⁴, introducing ring strain to destabilize the Mo–N interaction in **2** permits rapid cleavage of the H–H bond.



Scheme 2. Reversible activation of dihydrogen by molybdenum complexes with a pendant amine base. (Counteranions have been omitted for clarity.)

The potential of metal-free FLP systems to activate dinitrogen, a great chemical challenge owing to the strength of the N≡N triple bond, has been recently highlighted⁴⁵. First insights into this Holy Grail process were delivered by Stephan in 2017⁴⁶. During the same year Szymczak⁴⁷ and Simonneau⁴⁸ independently reported the activation of N₂ by a TMFLP approach based on iron (**4**) and molybdenum/tungsten (**5**) complexes, respectively (Scheme 3).

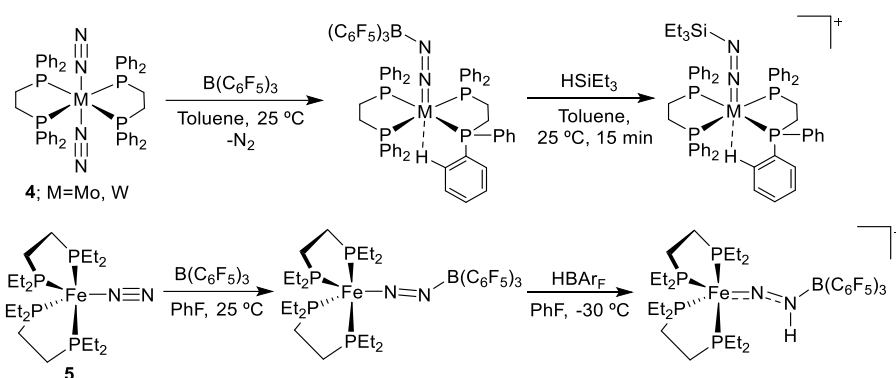
⁴⁴S. Zhang, R. M. Bullock, *Inorg. Chem.*, **2015**, *54*, 6397–6409.

⁴⁵R. L. Melen, *Angew Chem Int Ed*, **2018**, *57*, 880–882.

⁴⁶C. Tang, Q. Liang, A. R. Jupp, T. C. Johnstone, R. C. Neu, D. Song, S. Grimme, D. W. Stephan, *Angew. Chem. Int. Ed.*, **2017**, *56*, 16588–16592.

⁴⁷J. B. Geri, J. P. Shanahan, N. K. Szymczak, *J. Am. Chem. Soc.*, **2017**, *139*, 5952–5956.

⁴⁸A. Simonneau, R. Turrel, L. Vendier, M. Etienne, *Angew. Chem. Int. Ed.*, **2017**, *56*, 12268–12272.



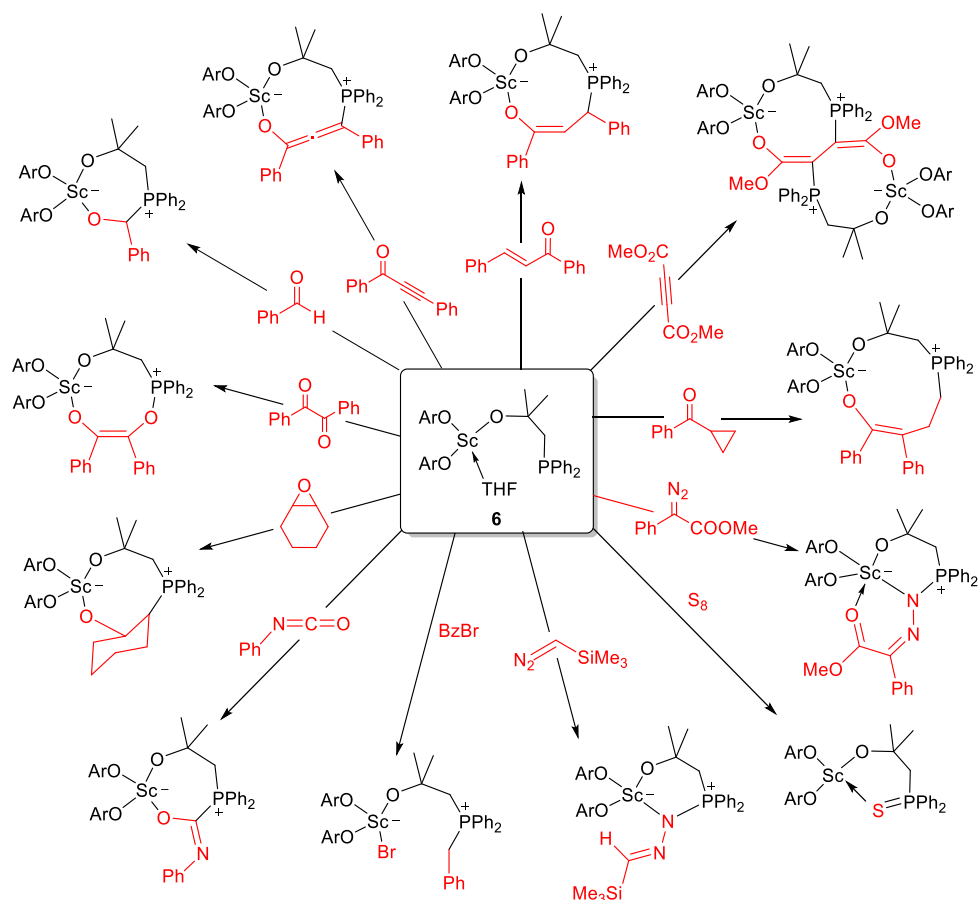
Scheme 3. Dinitrogen activation and functionalization by combining transition metal Lewis bases with $B(C_6F_5)_3$.

Despite being less explored than transition metals, the choice of rare-earth (RE) metal complexes as acids to build TMFLPs becomes evident considering their widespread use as Lewis acids in catalysis⁴⁹. Piers and Eisenstein exploited the electrophilicity of the decamethylscandocinium cation $[Cp^*_2Sc]^+$ in combination with the hydrido-(perfluorophenyl)-borate anion $[HB(C_6F_5)_3]^-$ ⁵⁰. This pair acts as an ionic FLP in which small molecules such as CO or CO₂ can be trapped in the polarized Sc^+/HB pocket and subsequently activated by hydride transfer from the borate anion. This approach allowed the developing of an efficient cooperative method for the deoxygenative hydrosilylation of CO₂. As in the case of Wass' system, these TMFLPs are also active for the activation of a broad variety of small molecules, as depicted for a representative example in Scheme 4.

⁴⁹ R. Anwander, S. Kobayashi (1999). S. Kobayashi (Eds), *Lanthanides: chemistry and use in organic synthesis*, Springer, Berlin, Heidelberg

⁵⁰ a) A. Berkefeld, W. E. Piers, M. Parvez, L. Castro, L. Maron, O. Eisenstein, *J. Am. Chem. Soc.*, **2012**, *134*, 10843–10851.

b) A. Berkefeld, W. E. Piers, M. Parvez, L. Castro, L. Maron, O. Eisenstein, *Chem. Sci.*, **2013**, *4*, 2152–2162.



Scheme 4. Small molecule activation pinwheel of a bisaryloxy scandium complex containing a bifunctional alkoxide-phosphine ligand.

I.2.1.2. Late Transition Metals

The Lewis acidity or basicity of a late transition metal can be rationally tuned by ligand and oxidation state modification. In most cases the metal has been employed as the acidic component of the FLP system, which parallels traditional bifunctional catalysts with pendant bases. However, the use of late transition metals as Lewis bases has also been contemplated. In a paramount example, Szymczak⁴⁷ exploited the $[\text{Fe}(0)(\text{depe})_2]/\text{B}(\text{C}_6\text{F}_5)_3$ (depe = 1,2-bis(diethylphosphino)ethane) pair for the activation of N_2 . Our group has more recently exploited the same

metallic Lewis base for the divergent activation of CO₂ with a variety of metallic Lewis acids⁵¹. Also working with iron complexes, Poater and Renaud have found inspiration in the FLP concept to exploit a family of iron carbonyl compounds stabilized by non-innocent functionalized cyclopentadiene fragments (Scheme 5)⁵². These bifunctional complexes, highly reminiscent of the prominent Shvo catalyst⁵³, efficiently promoted reductive amine alkylation^{52a,52c} and ketone alkylation.^{52b} Carbon monoxide abstraction with Me₃NO provides a vacant site on the electrophilic iron center where H₂ is coordinated. Computational studies revealed that substituting the cyclopentadienone in **7** by a cyclopentadienyl with a pendant amine group in **8** has an impact on the mechanism of H₂ splitting. While in the former case dihydrogen splitting is mediated by direct action of the oxygen center, in compound **8** the lower energy pathway involves the action of an external amine. Although this may not be strictly considered a TMFLP, the authors highlighted the importance of applying the concepts derived from the field of frustrated systems to the area of cooperative catalysis with transition metals.

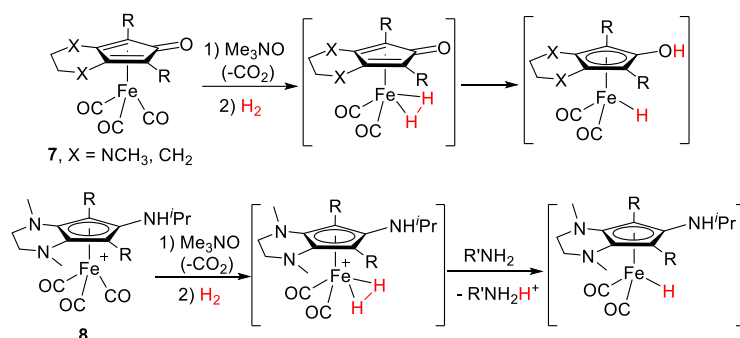
⁵¹ H. Corona, M. Pérez-Jiménez, F. de la Cruz-Martínez, I. Fernández, J. Campos, *Angew. Chem. Int. Ed.*, **2022**, DOI: 10.1002/anie.202207581.

^{52a)} T. Thai, D. S. Mérel, A. Poater, S. Gaillard, J. L. Renaud, *Chem. Eur. J.*, **2015**, *21*, 7066–7070.

b) C. Seck, M. D. Mbaye, S. Coufourier, A. Lator, J. F. Lohier, A. Poater, T. R. Ward, S. Gaillard, J. L. Renaud, *ChemCatChem*, **2017**, *9*, 4410–4416.

c) A. Lator, Q. G. Gaillard, D. S. Mérel, J. F. Lohier, S. Gaillard, A. Poater, J. L. Renaud, *J. Org. Chem.*, **2019**, *84*, 6813–6829.

⁵³ B. L. Conley, M. K. Pennington-Boggio, E. Boz, T. J. Williams, *Chem. Rev.*, **2010**, *110*, 2294–2312.



Scheme 5. Dihydrogen activation by intra- (**7**) and intermolecular (**8**) cooperative systems with mechanisms reminiscent of FLPs. Counteranions have been omitted for clarity.

In another cooperative example that somehow resembles the chemistry of FLPs, the group of Oestreich investigated in detail the tethered ruthenium (II) thiolate complex **9**, whose Ru–S bond facilitates the cooperative activation of Si–H bonds to yield a terminal ruthenium hydride and an acidic silicon fragment (stabilized by sulfur) that behaves as a silylium cation (**10**, Scheme 6). The electrophilic nature of the latter has been exploited for a number of catalytic applications⁵⁴, including the enantioselective reduction of imines after introducing axial chirality at the sulfur ligand⁵⁵. At variance with other examples of cooperative activation across metal-ligand bonds, the Ru–S bond remains virtually intact after Si–H cleavage (**9**, $d_{\text{RuS}} = 2.21$; **10** $d_{\text{RuS}} = 2.39$ Å). A detailed mechanistic

⁵⁴ a) H. F. T. Klare, M. Oestreich, J.-I. Ito, H. Nishiyama, Y. Ohki, K. Tatsumi, *J. Am. Chem. Soc.*, **2011**, *133*, 3312–3315.

b) C. D. F. Königs, H. F. T. Klare, Y. Ohki, K. Tatsumi, M. Oestreich, *Org. Lett.*, **2012**, *14*, 2842–2845.

c) J. Hermeke, H. F. T. Klare, M. Oestreich, *Chem. Eur. J.*, **2014**, *20*, 9250–9254.

d) C. D. F. Königs, M. F. Müller, N. Aiguabella, H. F. T. Klare, M. Oestreich, *Chem. Commun.*, **2013**, *49*, 1506–1508.

e) C. D. F. Königs, H. F. T. Klare, M. Oestreich, *Angew. Chem. Int. Ed.*, **2013**, *52*, 10076–10079.

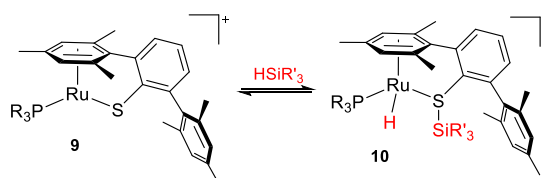
f) T. T. Metsänen, M. Oestreich, *Organometallics*, **2015**, *34*, 543–546.

g) T. Stahl, H. F. T. Klare, M. Oestreich, *J. Am. Chem. Soc.*, **2013**, *135*, 1248–1251.

h) S. Bähr, M. Oestreich, *Organometallics*, **2017**, *36*, 935–943.

⁵⁵ S. Webbolt, M. S. Maji, E. Irran, M. Oestreich, *Chem. Eur. J.*, **2017**, *23*, 6213–6219.

investigation into this activation event by a joint experimental/computational effort was also undertaken⁵⁶. A concerted σ -bond metathesis pathway across the Ru–S bond was proposed which, although conceptually differs from the mode of action of FLPs, shares some common features with the latter such as the polarized landscape between the two intervening nuclei and the heterolytic nature of the splitting. Related work by Tatsumi and Sakaki on a hydroxo-/sulfido-bridged ruthenium–germanium complex also draws the analogy with the heterolytic mode of activation of FLPs⁵⁷.



Scheme 6. Cooperative Si–H bond activation at a Ru–S bond. Counteranions have been omitted for clarity.

In the group 9 a very recent study by Carmona and Rodríguez demonstrated that a thermally induced⁵⁸ rhodium FLP constructed around a tridentate guanidine-phosphine ligand (**11**) was effective for FLP-like activation of dihydrogen and the O–H bond of water (Scheme 7). The lability of one of the Rh–N bond of **11** results from strong ring strain within the Rh–N–C–N moiety and gives access to a vacant coordination site at the acidic Rh (III) center. This vacant is in close proximity to the basic imine and as such, it shows potential for FLP-like activation. Heterolytic dihydrogen

⁵⁶ T. Stahl, P. Hrobárik, C. D. F. Königs, Y. Ohki, K. Tatsumi, S. Kemper, M. Kaupp, H. F. T. Klare, M. Oestreich, *Chem Sci*, **2015**, *6*, 4324–4334.

⁵⁷ a) N. Ochi, T. Matsumoto, T. Dei, Y. Nakao, H. Sato, K. Tatsumi, S. Sakaki, *Inorg. Chem.*, **2015**, *54*, 576–585.

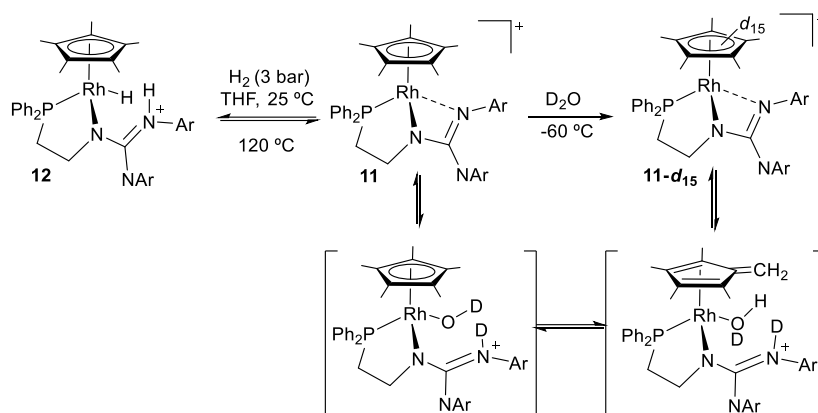
b) T. Matsumoto, Y. Nakaya, N. Itakura, K. Tatsumi, *J. Am. Chem. Soc.*, **2008**, *130*, 2458–2459.

⁵⁸ T. A. Rokob, A. Hamza, A. Stirling, I. Pápai, *J. Am. Chem. Soc.*, **2009**, *131*, 2029–2036.

splitting takes place under relatively mild conditions to yield a rhodium hydride fragment and a pendant iminium ion (**11-H₂**), as corroborated by X-ray diffraction studies. Partial reversibility was accomplished (*ca.* 30%) by heating the hydrogenated sample at 120 °C for 30 min. More interesting is the reaction with deuterated water, which results in rapid H/D scrambling in all the methyl positions at the cyclopentadienyl fragment. Although the authors could not detect any intermediate for such a process, computational investigations support the notion of an initial FLP activation of the O–H bond by the cooperative action of the acidic Rh (III) center and the basic role played by the pendant imine, followed by methyl deprotonation by the newly formed metal-hydroxide to produce a transient fulvene. Rapid equilibration among all proposed intermediates results in full deuteration of the cyclopentadienyl ring. Recently Carmona reported similar Rh complex but change the PPh₂ to pyridinyl-guanidine⁵⁹ compound, the group described these reactivity that behave like masked TMFLPs but in her last paper she described a “unmasked” TMFLP which is also capable to dehydrogenate alcohols affording metal hydrido derivatives via a concerted transition state involving simultaneously the acidic and the basic sites⁶⁰.

⁵⁹ C. Ferrer, J. Ferrer, V. Passarelli, F. J. Lahoz, P. García-Orduña, D. Carmona, *Organometallics*, **2022**, *41*, 1445–1453.

⁶⁰ M. Carmona, R. Pérez, J. Ferrer, R. Rodríguez, V. Passarelli, F. J. Lahoz, P. García-Orduña, D. Carmona, *Inorg. Chem.*, **2022**, *61*, 13149–13164.



Scheme 7. Dihydrogen and D₂O heterolytic activation by an intramolecular rhodium/imine frustrated Lewis pair, including subsequent H/D scrambling at the cyclopentadienyl ring.

The use of ligands with pendant boranes has been successful for designing efficient cooperative catalysts, particularly those involving hydrogen transfer between the metal center and the boron atom⁶¹. The cooperative mechanism by which these complexes activate E–H (E = H, Si, C, O, N...) bonds is reminiscent of frustrated systems. This analogy was drawn by Peters regarding the study of a nickel metalloborane bearing a diphosphine-borane ligand which turned out to be an efficient hydrogenation catalyst⁶². The same group has made extensive use of diphosphine-borane ligands to impart cooperative reactivity to first-row transition metals⁶³. In a recent study, the bond activation capacity of iron and cobalt metalloborane complexes was tested⁶⁴. Compounds of type **13** permit rapid activation of a series of substrates containing E–H (E = O, S, N, C, Si) bonds (Scheme 8). Interestingly, the activation of a hydrosilane (Ph₂SiH₂) was found to be

⁶¹ R. Gareth, *Chem. Soc. Rev.*, **2012**, *41*, 3535–3546.

⁶² W. H. Harman, J. C. Peters, *J. Am. Chem. Soc.*, **2012**, *134*, 5080–5082.

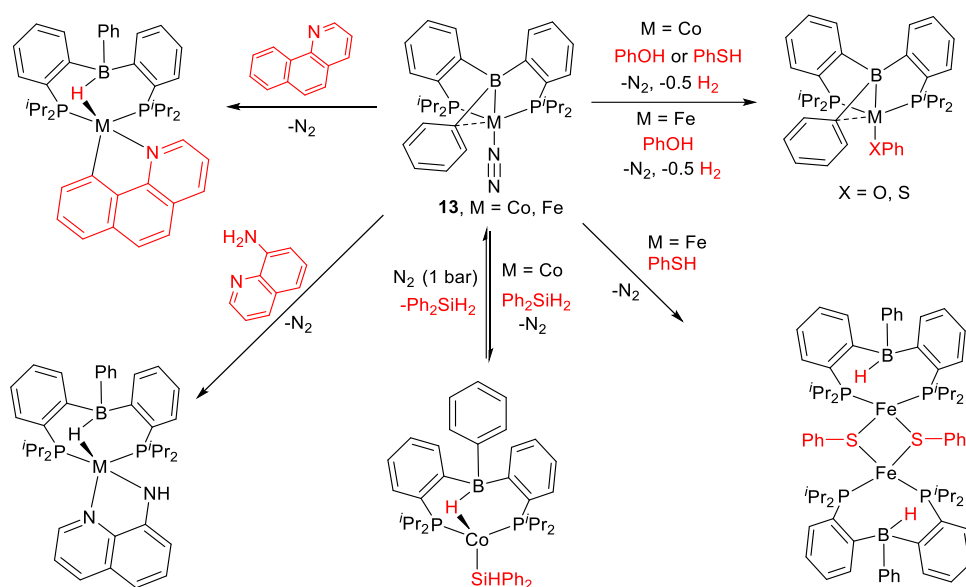
⁶³ a) H. Fong, M-E. Moret, Y. Lee, J. C. Peters, *Organometallics*, **2013**, *32*, 3053–3062.

b) S. N. MacMillan, W. Hill Harman, J. C. Peters, *Chem. Sci.*, **2014**, *5*, 590–597.

c) W. H. Harman, T-P. Lin, J. C. Peters, *Angew. Chem. Int. Ed.*, **2014**, *53*, 1081–1086.

⁶⁴ M. A. Nesbit, D. L. M. Suess, J. C. Peters, *Organometallics*, **2015**, *34*, 4741–4752.

reversible for the cobalt system. This result prompted the authors to investigate the role of these compounds as hydrosilylation catalysts. In fact, cobalt compound **13** is remarkably efficient in the hydrosilylation of ketones and aldehydes. Recently Fillol group reported a similar complex with Ni (II) that is stable to oxygen and are catalytically active for the hydrogenation of N-heteroarenes under mild conditions⁶⁵.

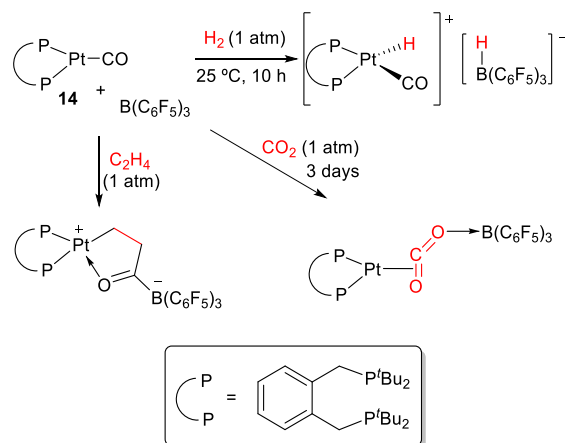


Scheme 8. Cooperative E—H bond activation using metalloborane iron and cobalt complexes.

The use of a bisphosphine Pt (0) complex (**14**) as a transition metal Lewis base in combination with a fluorinated borane as the acid allowed Wass to unveil an apparently simple TMFLP. This system perfectly emulates the behavior of main group frustrated systems and, in the case of ethylene activation, even revealed a novel and unexpected reactivity involving its coupling with carbon monoxide to yield a five-membered

⁶⁵ K. Michaliszyn, E. S. Smirnova, A. Bucci, V. Martin-Diaconescu, J. Lloret Fillol, *ChemCatChem*, **2022**, *14*, e202200039.

metallacycle (Scheme 9)⁶⁶. Mixing compound **14** with B(C₆F₅)₃ provided no spectroscopic hint of adduct formation, though broadening of ³¹P{¹H} NMR signal of **14** was discernible in chlorobenzene. This was attributed to the presence of weak Lewis acid-base interactions in solution (i.e. Pt→CO→B or Pt→B). Beyond the intriguing formation of the metallacycle derived from ethylene/CO coupling, the reactivity with CO₂ is rather interesting since it involves CO displacement by a considerably poorer ligand such as CO₂. As expected, **14** does not react with CO₂ by itself, but in the presence of B(C₆F₅)₃ the corresponding CO₂ adduct is quantitatively formed after three days as a result of push-pull stabilization. These results were later extended to other related bisphosphine ligands and the products derived from the activation of small molecules analyzed with regards to ligand modification⁶⁷.



Scheme 9. Small molecule FLP activation by a Pt(0)/B(C₆F₅)₃ pair.

An intramolecular Pt(0)/borane pair (**15**) has also been disclosed by Figueroa after hydroboration of a *bis*-isonitrile Pt(0) compound that enables

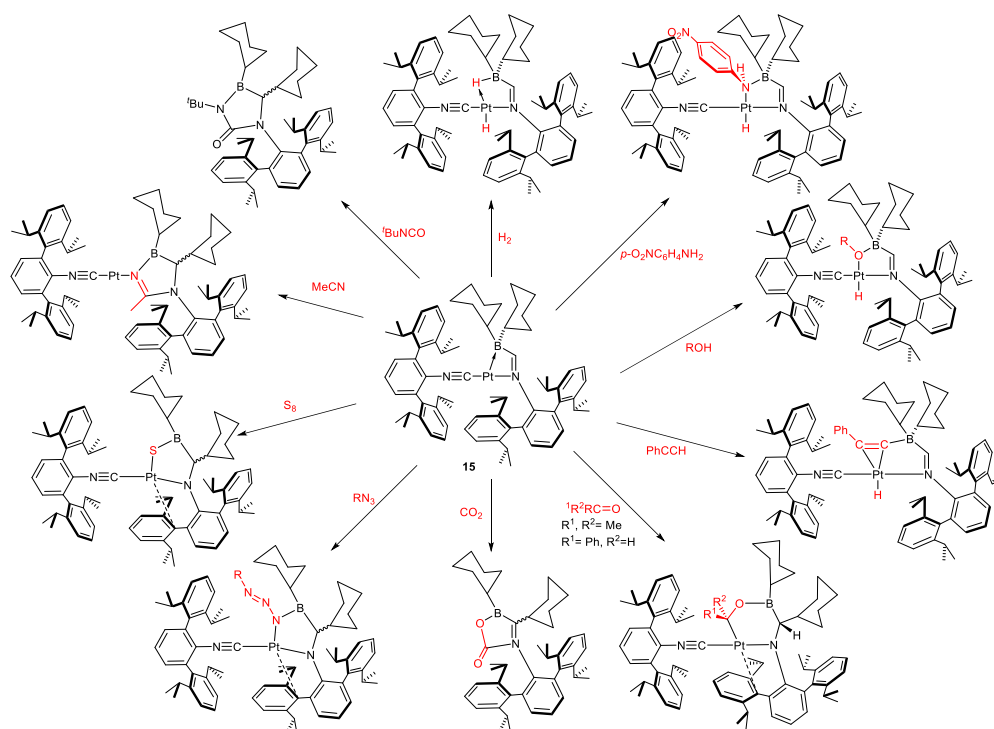
⁶⁶ S. J. K. Forrest, J. Clifton, N. Fey, P. G. Pringle, H. A. Sparkes, D. F. Wass, *Angew. Chem. Int. Ed.*, **2015**, *54*, 2223–2227.

⁶⁷ K. Mistry, P. G. Pringle, H. A. Sparkes, D. F. Wass, *Organometallics*, **2020**, *39*, 468–477.

the formation of a chelating (boryl)iminomethane ligand⁶⁸. The small bite angle of the latter framework seems to facilitate small molecule activation across the Pt→B bond in an FLP manner with a wide range of substrates (Scheme 10). For instance, compound **15** reacts with dihydrogen to produce the expected hydride/borohydride complex. Cleavage of polar E–H (O, N, C) bonds is also easily achieved for amines, alcohols and a terminal alkyne. Ketones and aldehydes react in the same fashion as main group FLPs, namely with the nucleophilic platinum center coordinated to the carbon atom and the electrophilic boron to the carbonylic oxygen. Contrarily, reaction with CO₂ produces a metal-free boracarbamate with concomitant release of the parent *bis*-isonitrile Pt(0) from which compound **15** is prepared. The reaction with *tert*-butylisocyanate to generate a boraurea proceeds in a similar fashion. These two metal-free species are alternatively prepared by the free ambiphilic (boryl)iminomethane ligand whose FLP behavior was also explored. Other unsaturated substrates such as azides or acetonitrile also provided the corresponding FLP-like activation products, while addition of elemental sulfur (S₈) yielded the formal insertion of a sulfur atom into the Pt→B dative bond.

⁶⁸ a) B. R. Barnett, C. E. Moore, A. L. Rheingold, J. S. Figueroa, *J. Am. Chem. Soc.*, **2014**, *136*, 10262–10265.

b) B. R. Barnett, M. L. Neville, C. E. Moore, A. L. Rheingold, J. S. Figueroa, *Angew. Chem. Int. Ed.*, **2017**, *56*, 7195-7199.



Scheme 10. Cooperative small molecule activation pinwheel for the geometrically constrained (boryl)iminomethane platinum compound **15**.

In the same series as platinum, gold became an obvious target to develop late transition metal FLPs due to the well-known electrophilicity of the $[LAu(I)]^+$ fragment, where L is a two electron donor ligand, typically a phosphine or a N-heterocyclic carbene (NHC)⁶⁹. In a recent attempt to design a frustrated Au(I)/Phosphine pair Hashmi combined a cationic Au(I) fragment stabilized by an extremely bulky NHC ligand (IPr^{**})⁷⁰ with the sterically hindered phosphine PMes₃ (Mes = 2,4,6-Me₃-C₆H₂). Despite the

⁶⁹ a) C. M. Friend, A. S. K. Hashmi, *Acc. Chem. Res.*, **2014**, *47*, 729–730.

b) I. Braun, A. M. Asiri, A. S. K. Hashmi, *ACS Catal.*, **2013**, *3*, 1902–1907.

c) M. Rudolph, A. S. Hashmi, *Chem. Soc. Rev.*, **2012**, *41*, 2448–2462.

d) N. Krause, C. Winter, *Chem. Rev.*, **2011**, *111*, 1994–2009.

e) A. Corma, A. Leyva-Pérez, M. J. Sabater, *Chem. Rev.*, **2011**, *111*, 1657–1712.

f) A. Firstner, *Chem. Soc. Rev.*, **2009**, *38*, 3208–3221.

g) C. Obradors, A. M. Echavarren, *Chem. Commun.*, **2014**, *50*, 16–28.

⁷⁰ S. G. Weber, C. Loos, F. Rominger, B. F. Straub, *ARKIVOC*, **2012**, *3*, 226–242.

bulkiness of the two ligands, the corresponding cationic complex [(NHC)Au(PMes₃)]⁺ was readily formed⁷¹, which illustrates the hurdle of achieving metallic frustration with a linear complex.

The group of Zhang explored the possibility of geometric frustration by developing a bifunctional phosphine ligand that incorporates a pendant tertiary amine unavailable to intramolecular interaction with gold due to geometric constraints⁷². As a soft Lewis acid, the Au(I) site in complex **16** (Scheme 11) readily coordinates C≡C bonds with simultaneous weakening of the α-C–H bond, which is profited by the lateral amine to abstract the proton despite being a rather weak base ($pK_a \approx 4$; *c.f.* R₂C(H)C≡CR': $pK_a > 30$). Conformational rigidity proved to be key for efficient isomerization, since substituting the adamantyl moieties bound to phosphorus considerably decreased the rate of catalysis. Based on this approach, a number of related studies were conducted to exploit the catalytic potential of gold compounds bearing this type of bifunctional PN ligands⁷³. The key feature in all cases is to maintain a geometry that avoids gold-amine adduct formation while forcing conformational constraints that facilitate activation of the organic substrate by the cooperative action of the two active sites.

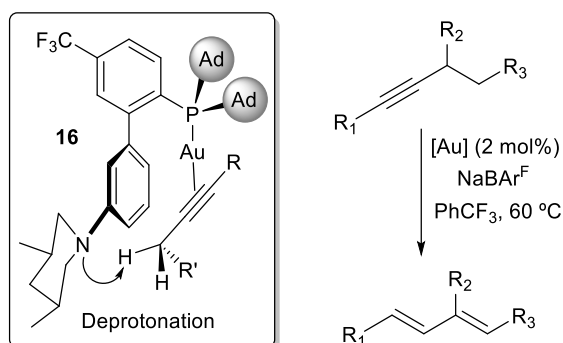
⁷¹ S. Arndt, M. M. Hansmann, P. Motloch, M. Rudolph, F. Rominger, A. S. K. Hashmi, *Chem. Eur. J.*, **2017**, *23*, 2542–2547.

⁷² Z. Wang, Y. Wang, L. Zhang, *J. Am. Chem. Soc.*, **2014**, *136*, 8887–8890.

⁷³ a) Z. Wang, A. Ying, Z. Fan, C. Hervieu, L. Zhang, *ACS Catal.*, **2017**, *5*, 3676–3680.

b) X. Li, X. Ma, Z. Wang, P-N. Liu, L. Zhang, *Angew. Chem. Int. Ed.*, **2019**, *58*, 17180–17184.

c) X. Cheng, Z. Wang, C. D. Quintanilla, L. Zhang, *J. Am. Chem. Soc.*, **2019**, *141*, 3787–3791.



Scheme 11. Catalytic isomerization of alkynes to 1,3-dienes by a bifunctional FLP-like Au(I)/NR₃ complex (**16**) that accelerates propargylic deprotonation.

I.2.2. Frustrated Lewis Pairs and Related Systems based on Two Transition Metals

In the second subsection, transition metal-only frustrated Lewis pairs (TMOFLP) in which the two components are based on transition metal fragments are described. Explicit mention to polarized heterobimetallic systems whose behavior could be understood in terms of FLP-like reactivity, and which hold great resemblance to the systems investigated in this Thesis, will also be covered.

Systems in which the two components are based on transition metals are rather rare, despite the fact that, as aforesaid, many polarized heterobimetallic complexes exhibit cooperative reactivity that is reminiscent of FLPs⁷⁴. In this section, we will first focus on the first proven example of a genuine TMOFLP and its reactivity towards small molecules to later examine recent results on polarized heterobimetallic species and their connection to the field of FLPs.

⁷⁴ a) D. W. Stephan, *Coordination Chemistry Reviews*, **1989**, 95, 41–107.

b) N. Wheatley, P. Kalck, *Chem. Rev.*, **1999**, 99, 3379–3420.

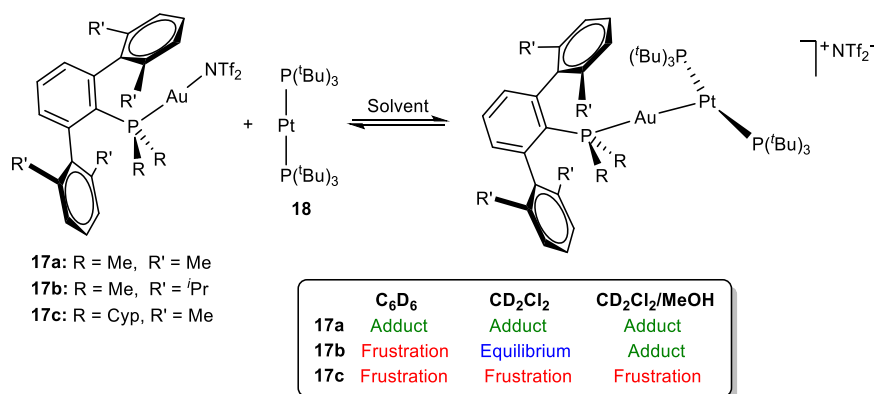
c) L. H. Gade, *Angew. Chem. Int. Ed.*, **2000**, 39, 2658–2678.

d) B. G. Cooper, J. W. Napoline, C. M. Thomas, *Catalysis Reviews*, **2012**, 54, 1–40.

e) M. Herberhold, G-X. Jin, *Angew. Chem. Int. Ed.*, **1994**, 33, 964–966.

1.2.2.1. Transition Metal Only Frustrated Lewis Pairs (TMOFLPs)

In a first attempt towards an all-transition metal FLP, the group of Wass anticipated the use of a phosphinoaryloxide zirconocene as a suitable framework to coordinate an electron rich Pt(0) center through its pendant phosphine. Contrary to the expected Zr(IV)/Pt(0) FLP, a new heterobimetallic compound is formed instead by formal insertion of the platinum center into a Zr–C bond⁷⁵. Shortly after, Campos described the first TMOFLP by combining [(PMe₂Ar^{Dipp2})Au(I)]NTf₂ (**17b**; Ar^{Dipp2} = C₆H₃-2,6-(C₆H₃-2,6-ⁱPr₂)₂; NTf₂⁻ = [N(SO₂CF₃)₂]⁻) and [Pt(P^{*t*}Bu₃)₂] (**18**), motivated by their proven Lewis acidic and basic character, respectively⁷⁶.



Scheme 12. Metal adduct formation vs full frustration in solution as a function of ligand steric and solvent conditions.

In these studies, the choice of rather bulky phosphine ligands was essential to avoid the formation of a metal-only Lewis pair (MOLP)⁷⁷. This was investigated in detail by modifying the substituents of the terphenyl phosphine ligand that binds the Au(I) fragment, more precisely by

⁷⁵ A. M. Chapman, S. R. Flynn, D. F. Wass, *Inorg. Chem.*, **2016**, 55, 1017–1021.

⁷⁶ J. Campos, *J. Am. Chem. Soc.*, **2017**, 139, 2944–2947.

⁷⁷ J. Bauer, H. Braunschweig, R. D. Dewhurst, *Chem. Rev.*, **2012**, 112, 4329–4346.

incorporating $\text{PMe}_2\text{Ar}^{\text{Xyl}_2}$ and $\text{PCyp}_2\text{Ar}^{\text{Xyl}_2}$ ($\text{Ar}^{\text{Xyl}_2} = \text{C}_6\text{H}_3\text{-2,6-(C}_6\text{H}_3\text{-2,6-Me)}_2$) ligands⁷⁸. The steric shielding provided by the three investigated phosphines follows the order $\text{PCyp}_2\text{Ar}^{\text{Xyl}_2} > \text{PMe}_2\text{Ar}^{\text{Dipp}_2} > \text{PMe}_2\text{Ar}^{\text{Xyl}_2}$, which has a direct impact on the equilibrium between metal adduct formation and complete frustration (Scheme 12). This solution equilibria are deeply affected by solvent conditions as well, in analogy to traditional FLPs⁷⁹. Thus, while the least congested system **17a** yields exclusively the corresponding metal adduct under all attempted conditions, the more hindered **17c** shifts to the opposite end. Interestingly, the system with the intermediate size phosphine $\text{PMe}_2\text{Ar}^{\text{Dipp}_2}$ presents an in-between situation in which the two extreme scenarios are modulated depending on experimental conditions^{75,80}.

Reactivity studies towards dihydrogen^{73,75} and acetylene^{73,81} revealed a strong influence of the equilibrium depicted in Scheme 12 on the activity of the bimetallic pairs. In the case of dihydrogen, it is necessary to remark that neither gold nor platinum precursors react with H_2 by themselves even under more forcing conditions. However, the bimetallic system involving the medium-sized phosphine (**17b**) was highly active, as evinced by the immediate splitting of H_2 even at $-20\text{ }^\circ\text{C}$. Full conversion of the gold precursor in the bulkier system (**17c**) required longer reaction times, though the least active pair was clearly the one based on **17a**, in which formation of the bimetallic Lewis adduct hampers H_2 activation. A joint experimental/computational effort revealed that the latter system acts as a

⁷⁸ N. Hidalgo, J. J. Moreno, M. Pérez-Jiménez, C. Maya, J. López-Serrano, J. Campos, *Chem. Eur. J.*, **2020**, *26*, 5982-5993.

⁷⁹ L. X. Dang, G. K. Schenter, T-M. Chang, S. M. Kathmann, T. Autrey, *J. Phys. Chem. Lett.*, **2012**, *3*, 3312–3319.

⁸⁰ N. Hidalgo, S. Bajo, J. J. Moreno, C. Navarro-Gilabert, B. Q. Mercado, J. Campos, *Dalton trans.*, **2019**, *48*, 9127–9138.

⁸¹ N. Hidalgo, J. J. Moreno, M. Pérez-Jiménez, C. Maya, J. López-Serrano, J. Campos, *Organometallics*, **2020**, *39*, 2534-2544.

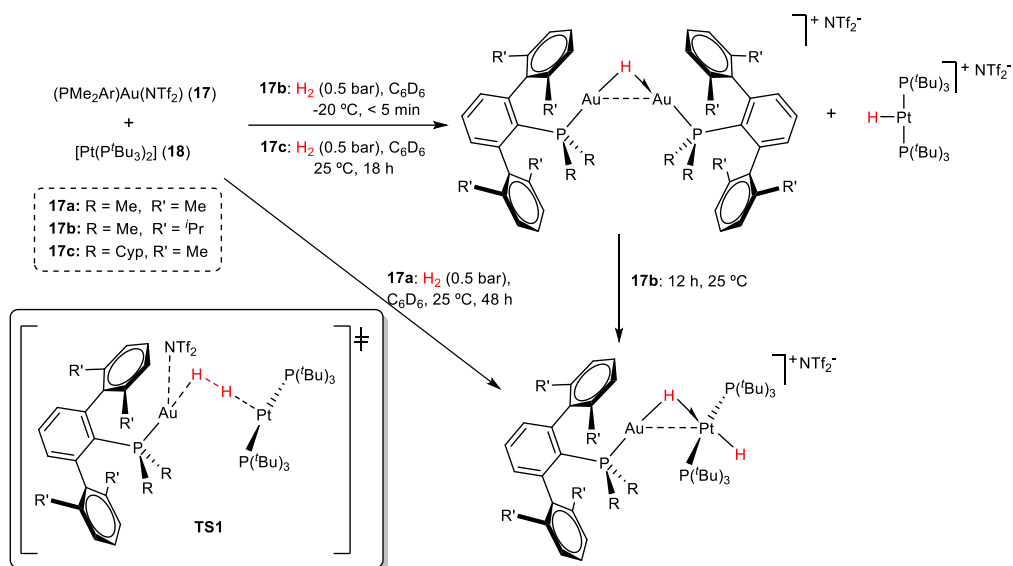
thermally induced FLP⁵⁵, in which generation of the individual monometallic fragments is a prerequisite for dihydrogen splitting to occur, thus ruling out more traditional heterobimetallic activation mechanisms.⁷⁵ A key termolecular transition state (**TS1** in Scheme 13) that parallels those proposed for main group FLPs⁸² was inferred from computational investigations. In addition, a rather strong inverse kinetic isotopic effect of 0.4-0.5 was recorded, for which a non-conventional origin was outlined. In a later study in which the ligands of Pt(0) Lewis base were substituted as well by terphenyl phosphines, our group observed the same kind of strong inverse KIE⁸³. Once more we attributed this effect to FLP-type mechanisms of H₂ activation. However, at variance with the results depicted in Scheme 13, in this later study a rare *cis*-dihydride intermediate could be trapped by the cooperation of the two metals.

⁸² a) T. A. Rokob, I. Pápai I (2013) *Hydrogen activation by frustrated Lewis pairs: Insights from computational studies*. In: G. Erker, D. Stephan (eds) *Frustrated Lewis Pairs I. Topics in Current Chemistry*. Springer, Berlin, Heidelberg, p 157–212.

b) J. Paradies, *Eur. J. Org. Chem.*, **2019**, 2-3, 283–294.

c) L. Rocchigiani, *Isr. J. Chem.*, **2015**, 55, 134–149.

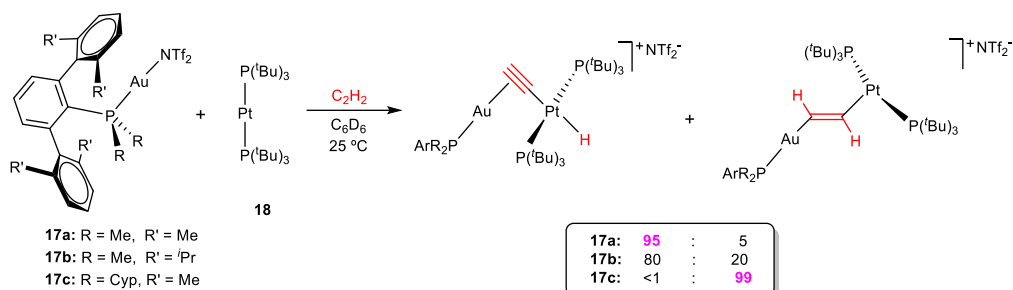
⁸³ N. Hidalgo, F. de la Cruz-Martínez, M. T. Martín, M. C. Nicasio, J. Campos, *Chem. Commun.*, **2022**, 58, 9144-9147.



Scheme 13. Heterolytic dihydrogen activation by Au(I)/Pt(0) pairs highlighting the modelled FLP-type transition state (**TS1**).

While the activation of dihydrogen by these Au(I)/Pt(0) pairs resulted in different product distributions, exposure of **17:18** to acetylene atmosphere evidenced strong selectivity effects derived from subtle modifications of the substituents of the phosphine ligands (Scheme 14)⁷⁸. For instance, the medium size phosphine in **17b** yielded a 4:1 mixture of a bridging heterobimetallic σ,π -acetylide and a rare vinylene ($-\text{CH}=\text{CH}-$) structure. In turn, reducing the steric pressure around the gold center increases the ratio of σ,π -acetylide/vinylene up to 95:5, while moving towards the fully frustrated system accomplished exactly the opposite, that is, quantitative formation of the heterobimetallic vinylene. It is worth noting that the two heterobimetallic products derived from acetylene activation highly resemble those obtained in the area of main group FLPs, where a competition between deprotonation and addition mechanisms usually takes place⁸⁴.

⁸⁴ M. A. Dureen, D. W. Stephan, *J. Am. Chem. Soc.*, **2009**, *131*, 8396–8397.



Scheme 14. Regioselectivity effects during acetylene activation by Au(I)/Pt(0) FLPs.

I.2.2.2. Polarized heterobimetallic compounds

A fascinating class of metal-metal bonded complexes that is receiving growing attention are those with M→M dative bonds, also referred as metal-only Lewis pairs (MOLPs)⁸⁵. Although noticed earlier⁸⁶, the first authoritative report on such a species dates back to 1967, when Nowell and Russell elucidated the solid-state structure of $[(\eta^5\text{-C}_5\text{H}_5)(\text{CO})_2\text{Co}\rightarrow\text{HgCl}_2]$ ⁸⁷. Numerous studies based on a wide variety of transition metals were later disclosed, particularly during the last decade⁸⁸. Apart from the fundamental appeal of these species, the interest on their study is at the heart of transition metal reactivity. The basicity of a transition

⁸⁵ J. Bauer, H. Braunschweig, R. D. Dewhurst, *Chem. Rev.*, **2012**, *112*, 4329-4346.

⁸⁶ C. E. Coffey, J. Lewis, R. S. Nyholm, *J. Chem. Soc.*, **1964**, 1741-1749.

⁸⁷ I. N. Nowell, D. R. Russell, *Chem. Commun.*, **1967**, 817-817.

⁸⁸ For selected recent MOLPs see: a) M. Ma, A. Sidiropoulos, L. Ralte, A. Stasch, C. Jones, *Chem. Commun.*, **2013**, *49*, 48-50; b) S. Bertsch, H. Braunschweig, R. D. Dewhurst, K. Radacki, C. Saalfrank, B. Wennemann, Q. Ye, *Organometallics* **2014**, *33*, 3649-3651; c) N. Arnold, H. Braunschweig, P. B. Brenner, M. A. Celik, R. D. Dewhurst, M. Haehnel, T. Kramer, I. Krummenacher, T. B. Marder, *Chem. Eur. J.* **2015**, *21*, 12357-12362; d) R. Bertermann, J. Böhnke, H. Braunschweig, R. D. Dewhurst, T. Kupfer, J. H. Muessig, L. Pentecost, K. Radacki, S. S. Sen, A. Vargas, *J. Am. Chem. Soc.* **2016**, *138*, 16140-16147; e) G. Wang, Y. S. Ceylan, T. R. Cundari, H. V. R. Dias, *J. Am. Chem. Soc.* **2017**, *139*, 14292-14301; f) J. K. Schuster, J. H. Muessig, R. D. Dewhurst, H. Braunschweig, *Chem. Eur. J.* **2018**, *24*, 9692-9697; g) L. D. Ernst, K. Koessler, A. Peter, D. Kratzert, H. Scherer, B. Butschke *Chem. Commun.* **2020**, *56*, 5350-5353.

metal site is important for small molecule coordination (e. g. borane binding in borylation processes)⁸⁹, as well as during oxidative addition reactions. In turn, the latter are elementary steps present in most catalytic cycles, as noticed from early reports⁹⁰. Thus, a better understanding of transition metal basicity (i.e. through the examination of metal-only Lewis pairs)⁹¹ may provide important information to be assimilated by bond activation and catalysis research.

In some cases, polar M–M bonds exhibit reactivity that is reminiscent of FLP systems. At variance with main group frustrated pairs, the integrity of the M–M bond may remain virtually intact during small molecule activation events, in a manner that could be understood as traditional heterobimetallic activation. However, it is also possible that the monometallic fragments may coexist in solution due to the lability of the M–M bond, thus enabling FLP-type activation pathways in the same fashion as thermally induced FLPs⁵⁵. The latter situation is more facile in unsupported heterobimetallic compounds, that is, those in which the M–M bond is the sole interaction holding the two metallic fragments together. Thus, apart from some selected examples, we will here focus on unsupported polarized heterobimetallic entities, while other bimetallic species containing bridging

⁸⁹ A. Y. Khalimon, P. Farha, L. G. Kuzminab, G. I. Nikonov, *Chem. Commun.*, **2012**, 48, 455-457.

⁹⁰ a) L. Vaska, *Acc. Chem. Res.*, **1968**, 1, 335-344.

b) J. P. Collman, W. R. Roper, *Adv. Organomet. Chem.*, **1968**, 7, 53-94.

c) D. F. Shriver, *Acc. Chem. Res.* **1970**, 3, 231-238.

d) L. Vaska, *Inorg. Chim. Acta*, **1971**, 5, 295-300.

e) H. Werner, *Pure & Appl. Chem.*, **1982**, 54, 177-188.

f) H. Werner, *Angew. Chem. Int. Ed.*, **1983**, 22, 927-949.

⁹¹ a) R. Bissert, H. Braunschweig, R. D. Dewhurst, C. Schneider, *Organometallics*, **2016**, 35, 2567-2573.

b) H. Braunschweig, C. Brunecker, R. D. Dewhurst, C. Schneider, B. Wennemann, *Chem. Eur. J.*, **2015**, 21, 19195-19201.

c) H. Braunschweig, R. D. Dewhurst, F. Hupp, C. Kaufmann, A. K. Phukan, C. Schneider, Q. Ye, *Chem. Sci.*, **2014**, 5, 4099-4104.

ligands will not be discussed. Moreover, the presence of bridging ligands usually entails additional complications regarding mechanistic aspects during small molecule activation that blurs the connection with FLPs.

The analogous reactivity between FLPs and polarized heterobimetallic complexes can be drawn by looking at early examples of unsupported systems. In a paradigmatic example, Cutler showed that complexes $[\text{Cp}(\text{CO})_2\text{M}-\text{Zr}(\text{Cl})\text{Cp}_2]$ ($\text{M} = \text{Fe}, \text{Ru}$) react with CO_2 to yield the corresponding bimetalloxy-carboxylates $[\text{Cp}(\text{CO})_2\text{M}(\mu-\eta^1-\text{C}:\eta^2-\text{O},\text{O}')\text{Zr}(\text{Cl})\text{Cp}_2]$. The resemblance to FLP systems is obvious, although the analogy could not be delineated at that time. The bimetalloxy-carboxylates are stabilized by push-pull interactions derived from the Lewis basic group 8 compound and the electrophilic zirconium fragment⁹². Although a traditional bimetallic mechanism involving the insertion of CO_2 into the M–M bond was favored, an alternative pathway through dissociation of the bimetallic compound into monometallic fragments followed by concerted trapping of CO_2 –as a thermally induced TMFLP– could not be ruled out. Subsequent reports further support the aforementioned analogy of the reactivity between polar M–M bonds and FLPs⁹³.

⁹² J. R. Pinkes, B. D. Steffey, J. C. Vites, A. R. Cutler, *Organometallics*, **1994**, *13*, 21–23.

⁹³ a) T. A. Hanna, A. M. Baranger, R. G. Bergman, *J. Am. Chem. Soc.*, **1995**, *117*, 11363–11364.

b) A. M. Baranger, R. G. Bergman, *J. Am. Chem. Soc.*, **1994**, *116*, 3822–3835.

c) H. Memmler, U. Kauper, L. H. Gade, I. J. Scowen, M. McPartlin, *Chem. Commun.*, **1996**, *15*, 1751–1752.

d) A. Schneider, L. H. Gade, M. Breuning, G. Bringmann, I. J. Scowen, M. McPartlin, *Organometallics*, **1998**, *17*, 1643–1645.

e) L. H. Gade, H. Memmler, U. Kauper, A. Schneider, S. Fabre, I. Bezougli, M. Lutz, C. Galka, I. J. Scowen, M. McPartlin, *Chem. Eur. J.*, **2000**, *6*, 692–708.

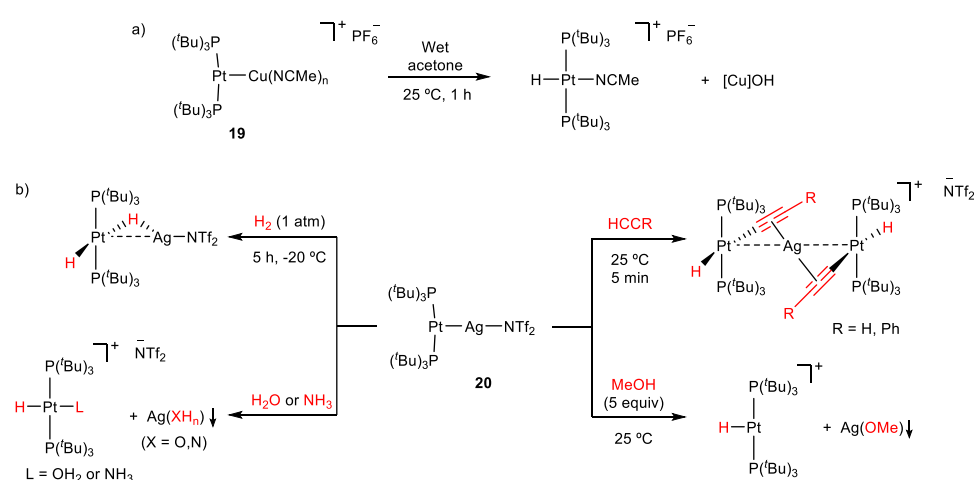
f) B. Findeis, M. Schubart, C. Platzek, L. H. Gade, I. Scowen, M. McPartlin, *Chem. Commun.*, **1996**, *2*, 219–220.

g) J. R. Pinkes, S. M. Tetrick, B. E. Landrum, A. R. Cutler, *Journal of Organometallic Chemistry*, **1998**, *556*, 1–7.

h) A. Sisak, E. Halmos, *J. Organomet. Chem.*, **2007**, *92*, 1817–1824.

i) K. Uehara, S. Hikichi, A. Inagaki, M. Akita, *Chem. Eur. J.*, **2005**, *11*, 2788–2809.

More recently the use of metal-only Lewis adducts of $[\text{Pt}(\text{P}'\text{Bu}_3)_2]$ (**18**) has been described in the context of bond activation (Scheme 15). In a first report, Jamali demonstrated the capacity of $[(\text{P}'\text{Bu}_3)_2\text{Pt}\rightarrow\text{Cu}(\text{NCMe})_n]$ (**19**) to activate an O–H bond of water (by using wet acetone as a solvent) to generate a cationic Pt(II) hydride and copper hydroxide (Scheme 15a)⁹⁴.



Scheme 15. Bond activation by metal-only Lewis pairs based on $[\text{Pt}(\text{P}'\text{Bu}_3)_2]$ (**18**).

The origin of the hydride ligand was corroborated by using D_2O . Although the mechanism could not be unambiguously determined, a cooperative pathway that implies the bimetallic adduct seems more likely. In the same vein, the group of Campos demonstrated that a similar architecture based on silver, more precisely $[(\text{P}'\text{Bu}_3)_2\text{Pt}\rightarrow\text{AgNTf}_2]$ (**20**), which revealed a rich

j) J. A. R. Schmidt, E. B. Lobkovsky, G. W. Coates, *J. Am. Chem. Soc.*, **2005**, *127*, 11426–11435.

k) J. P. Krogman, B. M. Foxman, C. M. Thomas, *J. Am. Chem. Soc.*, **2011**, *133*, 14582–14585.

l) B. G. Cooper, C. M. Fafard, B. M. Foxman, C. M. Thomas, *Organometallics*, **2010**, *29*, 5179–5186.

m) I. M. Riddlestone, N. A. Rajabi, J. P. Lowe, M. F. Mahon, S. A. Macgregor, *J. Am. Chem. Soc.*, **2010**, *35*, 11081–11084. doi:10.1021/jacs.6b05243

⁹⁴S. Jamali, S. Abedanzadeh, N. K. Khaledi, H. Samouei, Z. Hendi, S. Zacchini, R. Kia, H. R. Shahsavari, *Dalton Trans.*, **2016**, *45*, 17644–17651.

reactivity towards the activation of X–H (X = H, C, N, O) bonds (Scheme 15b)⁹⁵. The metal-only Lewis pair **20** can be easily prepared by dissolving an equimolar mixture of its parent monometallic precursors ([Pt(P'Bu₃)₂] (**18**) and AgNTf₂) in common organic solvents. The cooperative reactivity of this pair strikingly contrasts that of its monometallic fragments. For instance, while neither [Pt(P'Bu₃)₂] (**18**) nor AgNTf₂ react with H₂, compound **20** produces a Pt(II)/Ag(I) heterobimetallic dihydride under mild conditions. Similarly, while the two monometallic species do not exhibit any reactivity towards phenylacetylene, compound **20** converts into an uncommon heterobimetallic dibridged bisacetylide. The reactivity towards polar X–H (X = O, N) bonds in water, methanol and ammonia was additionally investigated. Particularly interesting is the effective cooperative cleavage of the N–H bond in ammonia, which remains an important challenge in transition metal chemistry⁹⁶.

The group of Mankad has intensively explored a variety of unbridged polarized heterobimetallic systems in recent years (Scheme 16)⁹⁷, highlighting in many occasions the analogy with frustrated Lewis pairs. As a representative example, compound **21**[CuFe] reacts with carbon disulfide⁹⁸, iodomethane^{97a}, benzyl chlorides⁹⁹, and dihydrogen¹⁰⁰ in a way

⁹⁵ N. Hidalgo, C. Maya, J. Campos, *Chem. commun.*, **2019**, 55, 8812–8815.

⁹⁶ a) J. Zhao, A. S. Goldman, J. F. Hartwig, *Science*, **2005**, 307, 1080–1082.

b) C. M. Fafard, D. Adhikari, B. M. Foxman, J. Mindiola, O. V. Ozerov, *J. Am. Chem. Soc.*, **2007**, 129, 10318–10319.

^{97a}) U. Jayarathne, T. J. Mazzacano, S. Bagherzadeh, N. P. Mankad, *Organometallic*, **2013**, 32, 3986–3992.

b) S. Banerjee, M. K. Karunananda, S. Bagherzadeh, U. Jayarathne, S. R. Parmelee, G. W. Waldhart, N. P. Mankad, *Inorg. Chem.*, **2014**, 53, 11307–11315.

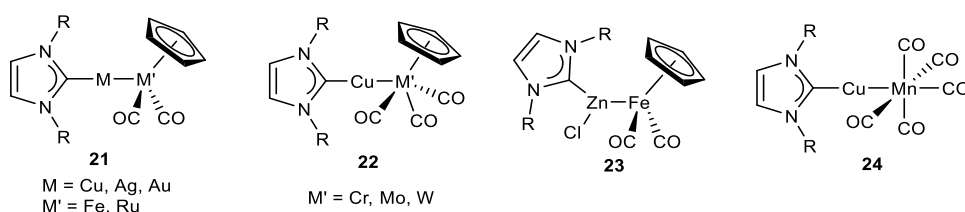
c) M. K. Karunananda, F. X. Vázquez, E. E. Alp, W. Bi, S. Chattopadhyay, T. Shibata, N. P. Mankad, *Dalton Trans.*, **2014**, 43, 13661–13671. doi:10.1039/C4DT01841A

⁹⁸ U. Jayarathne, S. R. Parmelee, N. P. Mankad, *Inorg. Chem.*, **2014**, 53, 7730–7737.

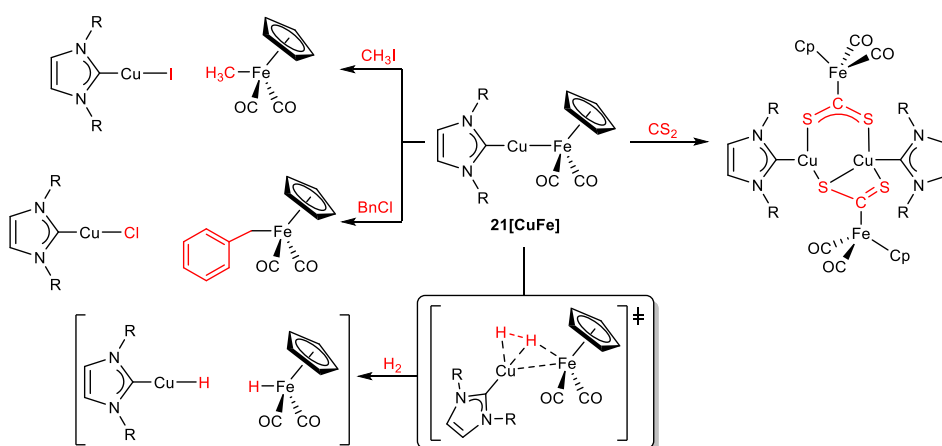
⁹⁹ M. K. Karunananda, S. R. Parmelee, G. W. Waldhart, N. P. Mankad, *Organometallics*, **2015**, 34, 3857–3864.

¹⁰⁰ M. K. Karunananda, N. P. Mankad, *Organometallics*, **2017**, 36, 220–227.

that is highly reminiscent of main group FLPs (Scheme 17). The mechanism for dihydrogen splitting has been thoroughly investigated with several metal combinations. Computational analysis revealed key orbital interactions involved in dihydrogen splitting that resemble classic FLPs. Hence, there is donation from the σ_{HH} orbital to a copper valence orbital, with concerted back-donation from the Cu–Fe bond towards the σ^*_{HH} orbital. At variance with the aforementioned **17:18** pair (Scheme 13) there is no need of M–M dissociation for H_2 activation to take place. However, the process requires high temperatures (*ca.* 150 °C) while the related fully frustrated Au(I)/Pt(0) system readily activates dihydrogen at temperatures as low as -20 °C, which might be attributed to higher activities associated to frustration⁷⁸.



Scheme 16. Selected examples of Mankad's metal-only Lewis pairs (R = Mes, Dipp).



Scheme 17. Heterobimetallic activation of small molecules by **21**[CuFe], highlighting a proposed key transition state for dihydrogen cleavage.

Nevertheless, experimental observations evinced that Mankad's heterobimetallic systems display dynamic equilibrium in solution towards the individual monometallic fragments, albeit small molecule activation seems to proceed through the M–M bound frameworks¹⁰¹. These combined results suggest that modulating the degree of frustration vs M–M interaction may be important to tune the activity of polarized heterobimetallic systems. In addition, the two approaches share an additional uncommon feature, that is, a strong inverse kinetic isotopic effect associated to dihydrogen cleavage, though the likely origin in both cases differs to some extent^{78,102}.

The heterobimetallic compounds depicted in Scheme 16 revealed important applications in catalysis that capitalize on the cooperative reactivity of the two metals in close proximity. Accordingly, highly efficient processes for *E*-selective alkyne semi-hydrogenation¹⁰³, C–H borylation¹⁰⁴, or regioselective alkyne hydrostannylation¹⁰⁵ were recently disclosed. As an archetypal example, the proposed mechanism for catalytic C–H borylation mediated by **21**[CuFe] is depicted in Scheme 18^{104b}. A comprehensive computational analysis revealed two bimetallic transition states that are crucial for catalytic turnover, agreeing with experimental observations. In the first, a bimetallic oxidative addition is proposed to occur along the Cu–Fe bond, reminiscent of heterolytic bond cleavage by FLPs. Moreover, the terminal iron hydride that emerges after C–H borylation is proposed to be intercepted by the previously formed copper hydride, regenerating

¹⁰¹ N. P. Mankad, *Chem. comm.*, **2018**, 54, 1291–1302.

¹⁰² Y. Zhang, M. K. Karunananda, H. C. Yu, K. J. Clark, W. Williams, N. P. Mankad, D. H. Ess, *ACS Catal.*, **2019**, 9, 2657–2663.

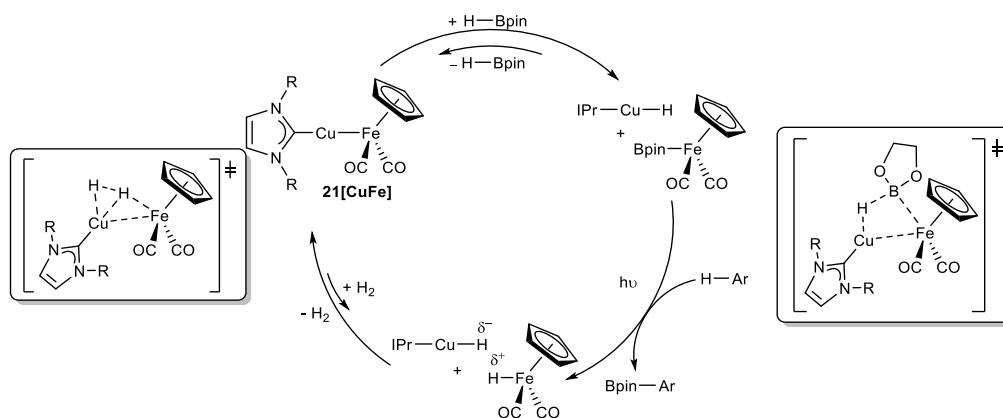
¹⁰³ M. K. Karunananda, N. P. Mankad, *J. Am. Chem. Soc.*, **2015**, 137, 14598–14601.

¹⁰⁴a) T. J. Mazzacano, N. P. Mankad, *J. Am. Chem. Soc.*, **2013**, 135, 17258–17261.

b) S. R. Parmelee, T. J. Mazzacano, Y. Zhu, N. P. Mankad, J. A. Keith, *ACS Catal.*, **2015**, 5, 3689–3699.

¹⁰⁵ L. J. Cheng, N. P. Mankad, *J. Am. Chem. Soc.*, **2019**, 141, 3710–3716.

21[CuFe] after a bimolecular reductive elimination of H₂ involving an FLP-like transition state (identical to the one shown in Scheme 17).

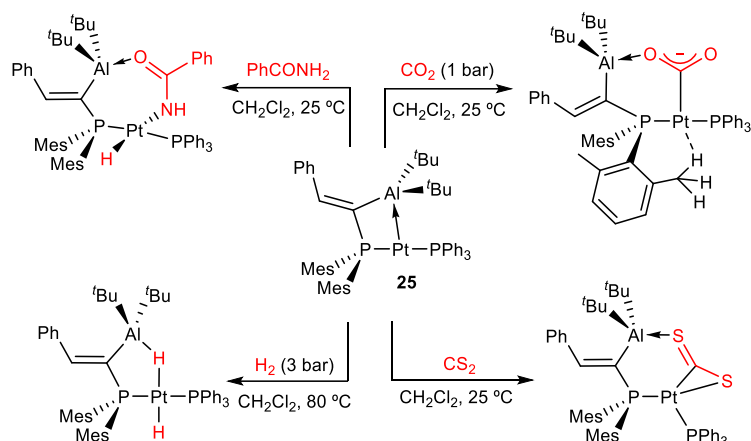


Scheme 18. Proposed catalytic cycle for C–H borylation mediated by polar heterobimetallic compound **21[CuFe]** highlighting key cooperative transition states.

It is also possible to access bimetallic FLPs in which only one of the components is based on a transition metal, while the other corresponds to a main group metal. Compound **25** in Scheme 19, comprised of a basic platinum site and an acidic aluminum partner, constitutes a representative example¹⁰⁶. The presence of a Pt→Al dative bond was confirmed by X-ray diffraction studies and computational analysis. However, the strain associated to the four-membered metallacycle facilitates the insertion of several small molecules along the Pt–Al bond in an FLP-manner. Thus, this pair reacts with CO₂ and CS₂ to provide the corresponding adducts stabilized by push-pull forces, while oxidative addition of N–H and H–H bonds is found after addition of an amide or dihydrogen, respectively. Theoretical studies on the mechanism of H₂ activation provided evidence of an FLP-like

¹⁰⁶ M. Devillard, R. Declercq, E. Nicolas, A. W. Ehlers, J. Backs, N. Saffon-Merceron, G. Bouhadir, J. C. Sloatweg, W. Uhl, D. Bourissou, *J. Am. Chem. Soc.*, **2016**, *138*, 4917–4926.

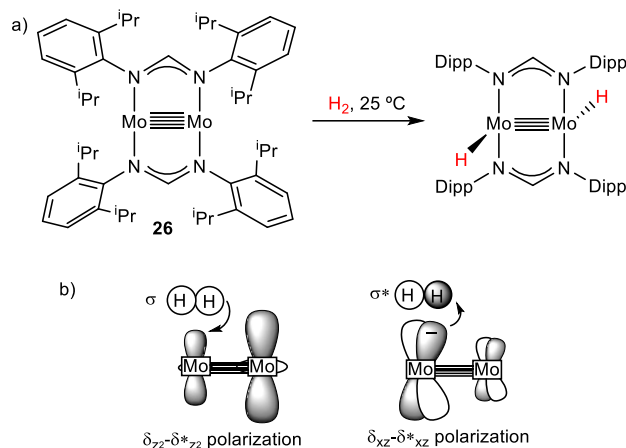
transition state in which dihydrogen coordinates side-on to the acidic Al center and end-on to the basic Pt nucleus.



Scheme 19. FLP-like small molecule activation along a constraint Pt→Al bond.

In an interesting study, Sakaki extended the idea of TMFLPs to multiply bonded complexes¹⁰⁷, for which a polarization of the M–M multiple bond is proposed to parallel the polarization found in encounter complexes of FLP systems. The group focused, from a computational perspective, on the oxidative addition of H–H, C–H and O–H bonds over the quintuply bonded compound **26** (Scheme 20). The key orbitals involved in σ -bond cleavage get polarized in the transition state (Scheme 20b) facilitating charge transfer from the M–M bond to the σ^*_{HH} orbital, while weakening the exchange repulsion between the multiple M–M bond and the E–H (E = H, C, O) substrate. This study provides encouragement to investigate other multiply bonded bimetallic compounds that can somehow behave as FLP-like entities due to facile M–M bond polarization.

¹⁰⁷ Y. Chen, S. Sakaki, *Inorg. Chem.*, **2017**, *56*, 4011–4020.



Scheme 20. a) Addition of dihydrogen over the quintuple bonded Mo₂ complex **26**; b) Simplified representation of the polarized δ_{Mo_2} orbitals participating in H₂ cleavage reminiscent of FLPs.

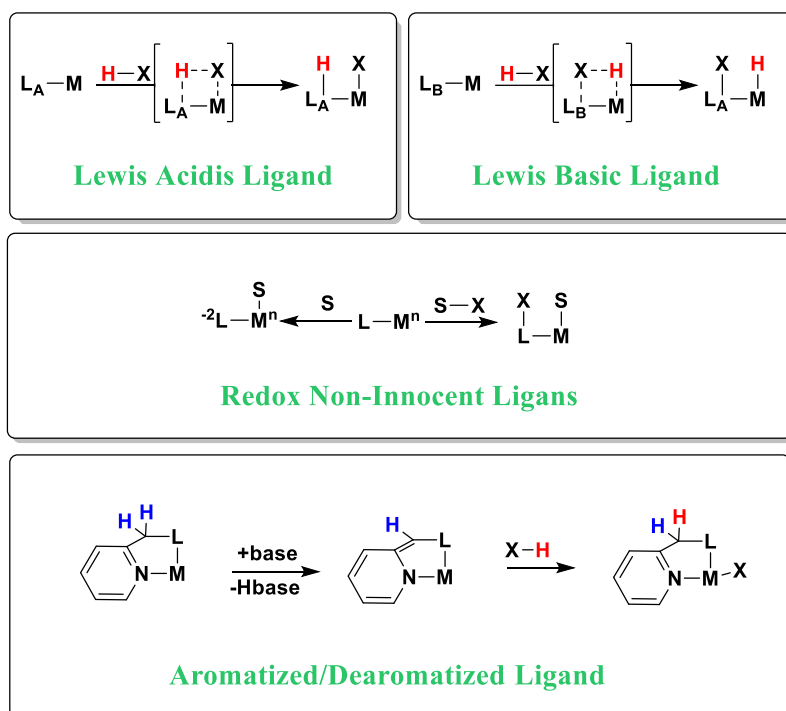
In summary, the introduction of transition metals into FLPs, an area that rapidly became an emblem of metal-free catalysis, is somehow serving to reconnect main group and transition metal chemistry research, sometimes oddly segmented. Advanced computational work has proved essential to delineate a more solid analogy between frustrated Lewis pairs and cooperative transition metal systems whose reactivity can easily be understood in terms of ‘frustration’. The barrier between TMFLPs and the broader area of transition metal cooperative systems has become rather diffuse, even more if we assume a definition of an FLP as a *combination of a Lewis acid and a base that exhibits FLP chemistry*¹⁰⁸. The identification of key transition states by computational means is rendering insightful information that will be decisive to develop novel architectures with desired properties.

I.3. Metal- Ligand Cooperation

¹⁰⁸ F. G. Fontaine, D. W. Stephan, *Phil. Trans. R. Soc. A.*, **2017**, 375, 20170004.

In conventional homogeneous catalysis the role of the ligands was assumed to be only as spectators that do not interact with substrates during the course of a reaction. But this paradigm did not hold, for instance, in many enzymes in which the ligands often act in cooperation with a metal center to perform bond activation reactions. The knowledge and understanding of such biological examples have inspired advances in ligand design and in catalytic reactions in which the metal center and the ligand of a complex are both modified. During the last decade, a trend appears in catalysis by transition metal complexes based on the concept of the metal-ligand cooperation (MLC). In 2015, Milstein¹⁴ reviewed works focused on diverse modes of MLC in bond formation or bond cleavage reactions in which ligands directly bound to the metal are chemically modified.

The more usual type of MLC involves a ligand that can behave as a Lewis acidic or basic fragment to cooperate with the metal. Besides, there are other types of cooperation that include, for instance, the use of redox non-innocent ligands and the aromatization/dearomatization of rings, which is more typical in pincer-type complexes and has been widely investigated by the group of Milstein. Scheme 21 includes a general representation of these types of MLC processes.



Scheme 21. General representation of the concept of metal-ligand cooperation (MLC).

In terms of the atoms involved in the cooperation, there are plenty of possibilities. Nonetheless, most examples are based on bond activation

events across M—L bonds where the donor atoms are N¹⁰⁹, O¹¹⁰, S¹¹¹, B¹¹², or C¹¹³. In this Thesis we have developed several systems in which we have

-
- ¹⁰⁹ a) R. Noyori, S. Hashiguchi, *Acc. Chem. Res.*, **1997**, *30*, 97-102.
b) R. Noyori, T. Okhuma, *Angew. Chem. Int. Ed.*, **2001**, *40*, 40-73.
c) R. Noyori, M. Koizumi, D. Ishii, T. Ohkuma, *Pure Appl. Chem.*, **2001**, *73*, 227-232.
d) R. Noyori, M. Kitamura, T. Ohkuma, *Proc. Natl. Acad. Sci. USA*, **2004**, *101*, 5356-5362.
e) T. Ohkuma, H. Ooka, S. Hashiguchi, T. Ikariya, R. Noyori, *J. Am. Chem. Soc.*, **1995**, *117*, 2675-2676.
f) C. A. Sandoval, T. Ohkuma, K. Muniz, R. Noyori, *J. Am. Chem. Soc.*, **2003**, *125*, 13490-13503.
g) T. Ikariya, A. J. Blacker, *Acc. Chem. Res.*, **2007**, *40*, 1300-1308.
h) T. Ikariya, I. D. Gridnev, *Top. Catal.*, **2010**, *53*, 894-901.
i) T. Ikariya, *Bull. Chem. Soc. Jpn.*, **2011**, *84*, 1-16.
j) P. A. Dub, T. Ikariya, *ACS Catal.*, **2012**, *2*, 1718-1741.
k) L. A. Berben, *Chem. Eur. J.*, **2015**, *21*, 2734-2742.
l) H. Grützmaier, *Angew. Chem. Int. Ed.*, **2008**, *47*, 1814-1818.
m) P. E. Sues, K. Z. Demmans, R. H. Morris, *Dalton Trans.*, **2014**, *43*, 7650-7667.
n) R. H. Morris, *Acc. Chem. Res.*, **2015**, *48*, 1494-1502.
¹¹⁰ L. E. Doyle, W. E. Piers, J. Borau-Garcia, *J. Am. Chem. Soc.*, **2015**, *137*(6), 2187-2190.
¹¹¹ a) Z. K. Sweeney, J. L. Polse, R. G. Bergman, R. A. Andersen, *Organometallics*, **1999**, *18*, 5502-5510.
b) R. C. Linck, R. J. Pafford, T. B. Rauchfuss, *J. Am. Chem. Soc.*, **2001**, *123*, 8856-8857.
c) A. Ienco, M. J. Calhorda, J. Reinhold, F. Reineri, C. Bianchini, M. Peruzzini, F. Vizza, C. Mealli, *J. Am. Chem. Soc.*, **2004**, *126*, 11954-11965.
d) K. D. Hesp, R. McDonald, M. J. Ferguson, M. Stradiotto, *J. Am. Chem. Soc.*, **2008**, *130*, 16394-16406.
e) Y. Ohki, M. Sakamoto, K. Tatsumi, *J. Am. Chem. Soc.*, **2008**, *130*, 11610-11611.
f) M. Sakamoto, Y. Ohki, G. Kehr, G. Erker, K. Tatsumi, *J. Organomet. Chem.*, **2009**, *694*, 2820-2824.
g) Y. Ohki, Y. Takikawa, H. Sadohara, C. Kesenheimer, B. Engendahl, E. Kapatina, K. Tatsumi, *Chem. Asian J.*, **2008**, *3*, 1625-1635.
h) T. Stahl, K. Mithler, Y. Ohki, K. Tatsumi, M. Oestreich, *J. Am. Chem. Soc.*, **2013**, *135*, 10978-10981.
¹¹² G. R. Owen, *Chem. Soc. Rev.*, **2012**, *41*, 3535-3546.
¹¹³ a) H. D. Empsall, E. M. Hyde, R. Markham, W. S. McDonald, M. C. Norton, B. L. Shaw, B. Weeks, *J. Chem. Soc. Chem. Commun.*, **1977**, 589-590.
b) C. Crocker, R. J. Errington, R. Markham, C. J. Moulton, K. J. Odell, B. L. Shaw, *J. Am. Chem. Soc.*, **1980**, *102*, 4373-4379.
c) C. Crocker, R. J. Errington, R. Markham, C. J. Moulton, B. L. Shaw, *J. Chem. Soc. Dalton Trans.*, **1982**, 387-395.
d) C. Crocker, H. D. Empsall, R. J. Errington, E. M. Hyde, W. S. McDonald, R. Markham, M. C. Norton, B. L. Shaw, B. Weeks, *J. Chem. Soc. Dalton Trans.*, **1982**, 1217-1224.
e) C. Crocker, R. J. Errington, W. S. McDonald, K. J. Odell, B. L. Shaw, R. J. Goodfellow, *J. Chem. Soc. Chem. Commun.*, **1979**, 498-499.
f) D. Gelman, S. Musa, *ACS Catal.*, **2012**, *2*, 2456-2466.
g) D. G. Gusev, A. J. Lough, *Organometallics*, **2002**, *21*, 2601-2603.
h) R. J. Burford, W. E. Piers, M. Parvez, *Organometallics*, **2012**, *31*, 2949-2952.

investigated cooperative effects between a rhodium center and a boron functionality. Also, we have examined the non-innocent behavior of cyclopentadienyl [Cp, (C₅R₅)] and indenyl [Ind, (C₉H₇)] ligands, which can also participate in MLC events. Thus, in the following two sub-sections, we will only focus on previous MLC examples on the cooperative behavior of either boron-based moieties or Cp and Ind ligands.

I.3.1. Metal-ligand cooperation involving boron-based moieties

The presence of boron-functionalities in ligands of transition metal complexes is highly related to the area of hydrogen atom transfer and storage. This still nascent field is vastly dominated by borohydride and borane moieties as reversible hydrogen atom shuttles and stores. In the following lines we will discuss these hydrogen transfer reactions and the transformations that involve metals and borohydride and borane functions.

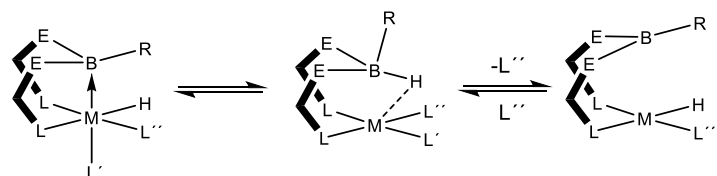
In 1999 Hill reported the first example of hydrogen atom transfer from a borohydride unit to a transition metal centre forming a new metal hydride species within a ruthenium complex.¹¹⁴ Afterwards, many more examples have appeared in the literature with unprecedented reactivity, and only a few selected examples and general aspects will be discussed herein.

In general terms, in the majority of the systems that participate in the process of transferring a hydrogen atom from the boron center to the metal, and *vice versa*, an interaction between the metal and the boron atom is observed. A general process is depicted in Scheme 22, where the aforesaid interaction may or may not disappear upon hydrogen transfer.

i) D. V. Gutsulyak, W. E. Piers, J. Borau-Garcia, M. Parvez, *J. Am. Chem. Soc.*, **2013**, *135*, 11776-11779.

j) C. C. Comanescu, V. M. Iluc, *Organometallics*, **2014**, *33*, 6059-6064.

¹¹⁴ A. F. Hill, G. R. Owen, A. J. P. White, D. J. Williams, *Angew. Chem. Int. Ed.*, **1999**, *38*, 2759-2761.



Scheme 22. A representative mechanism for metal-ligand-cooperation involving the transformation between borane and borohydride ($E^{\wedge}L$ represents a bridging supporting group).

The metal borane dative interaction represented in the left structure of Scheme 22 involves an empty orbital in the Lewis acidic borane and a filled orbital in the metal centre that overlaps. Thus, this interaction contrasts with the traditional view of ligands as donor fragments towards Lewis acidic metals. In this case, the borane atom acts as a σ -acceptor ligand, known as Z-type ligand. This class of ligands has attracted continuously growing attention due to its flexibility (as seen in Scheme 22) and the capacity to tune the electronic properties of the transition metal¹¹⁵. There have been many studies discussing the properties of this dative bonding with Z-type borane ligands. Braunschweig reported a prominent example including two related platinum-borane complexes where the Pt—B distances supported the presence of a dative bond¹¹⁶. Also, highly interesting are the independent studies from Bourissou¹¹⁷ and Mösch-Zanetti¹¹⁸ on related copper structures with tetradentate ligands. In those, the donor atoms occupy the three

¹¹⁵ a) A. Amgoune, D. Bourissou, *Chem. Commun.*, **2011**, 47, 859-871.

b) G. Bouhadir, D. Bourissou, *Chem. Soc. Rev.*, **2016**, 45, 1065-1079.

c) D. You, F. P. Gabbaï, *Trends in Chemistry*, **2019**, 1(5), 485-496.

¹¹⁶ H. Braunschweig, A. Damme, T. Kupfer, *Angew. Chem., Int. Ed.*, **2011**, 50, 7179-7182.

¹¹⁷ M. Sircoglou, S. Bontemps, G. Bouhadir, N. Saffon, K. Miqueu, W. Gu, M. Mercy, C.-H. Chen, B. M. Foxman, L. Maron, O. V. Ozerov, D. Bourissou, *J. Am. Chem. Soc.*, **2008**, 130, 16729-16738.

¹¹⁸ G. Nuss, G. Saischek, B. N. Harum, M. Volpe, F. Belaj, N. C. Mösch-Zanetti, *Inorg. Chem.*, **2011**, 50, 12632-12640.

equatorial sites of a trigonal bipyramidal copper centre and the borane functional group the axial positions. Although all reported the complexes have similar structures, it is interesting the study of the boron-copper distance, which is consistent with the pyramidalization and the degree of interaction between these centres.

From a structural point of view, a wide variety of metal borane complexes have been developed using a number of different E^ΛL supporting groups. Usually, these supporting groups have three-atom bridges, thus providing a stable triple five-membered rings. There has been a rapid expansion in the development of these frontier supporting groups, which a wide variety of structures, being very common the use of heterocycles. For instance, Bourissou¹¹⁹ reported the first complex that contain phosphorous and Owen the first containing a nitrogen heterocycle, but the structural variety is wide, including also heterocycles that present sulphur atoms to bind the metal and nitrogen atoms to bind the boron centre, among others.

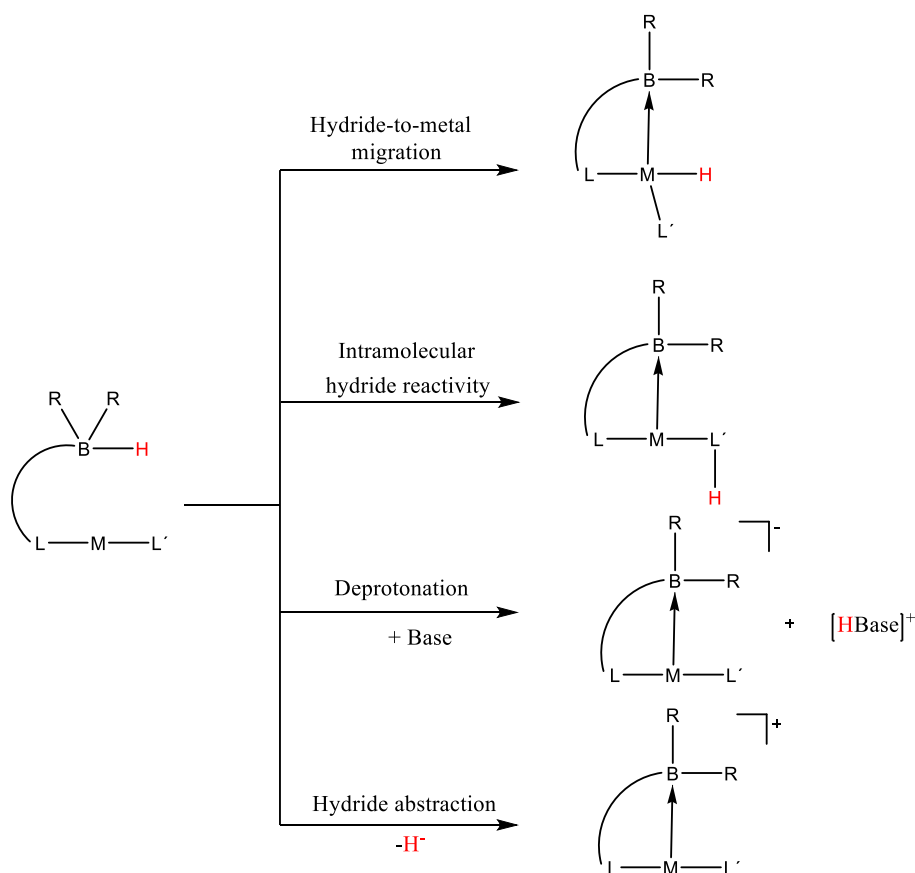
Synthetically, there are different routes to synthesize metal-borane complexes. The first synthetic route derived from the classic scorpionate ligands reported by Trofimenko¹²⁰ and involve the transformation of a boron-hydride moiety to a borane. Variations of this original approach are yet the most useful strategy. In fact, the use of a borohydride moiety is common to most synthetic approaches, whose general representation is depicted in Scheme 23. From that moiety, a hydride can migrate to the transition metal allowing the subsequent formation of a M—B bond, with the only requirement being a coordination site available at the metal centre. Alternatively, the hydride can react with a ligand already coordinated to the

¹¹⁹ a) A. Amgoune, D. Bourissou, *Chem. Commun.*, **2011**, 47, 8163-8165.

b) G. Bouhadir, A. Amgoune, D. Bourissou, *Adv. Organomet. Chem.*, **2011**, 58,1-106

¹²⁰ C. Pettinari, in *Scorpionates II: Chelating Borate Ligands*, Imperial College Press, London, **2008**.

metal, typically an unsaturated C-based nucleophile. the deprotonation of the borohydride by addition of an external base in the presence of an oxidizing agent has also been documented by Connelly¹²¹. Finally, the abstraction of a hydride has been described by Rabinovich¹²² to access the first metal-borane complex based on cobalt.



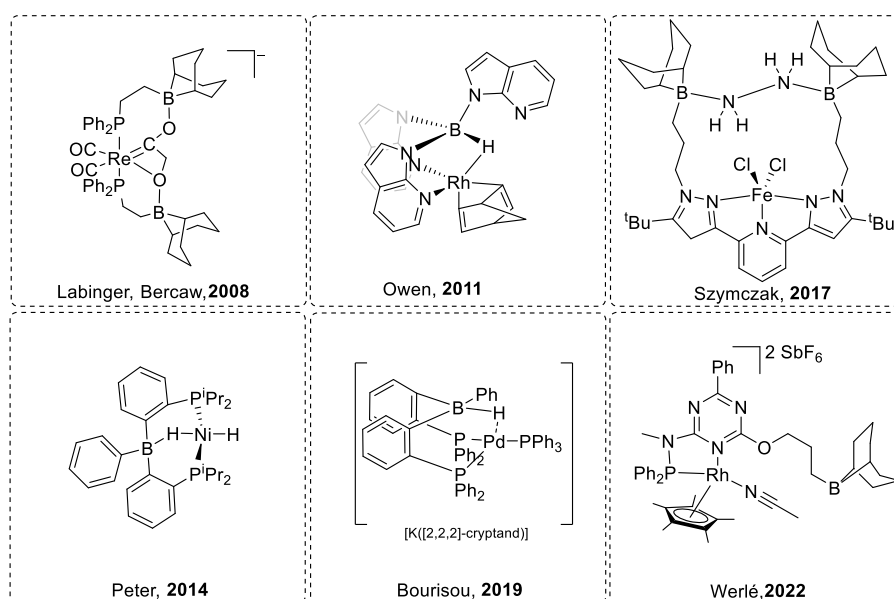
Scheme 23. Representation of the most common synthetic pathways to access metal-borane complexes from borohydride functionalities.

¹²¹a) R. J. Blagg, C. J. Adams, J. P. H. Charmant, N. G. Connelly, M. F. Haddow, A. Hamilton, J. Knight, A. G. Orpen, B. M. Ridgway, *Dalton Trans.*, **2009**, 8724-8736.

b) M. J. López-Gómez, N. G. Connelly, M. F. Haddow, A. Hamilton, A. G. Orpen, *Dalton Trans.*, **2010**, 39, 5221-5230.

¹²² D. J. Mihalcik, J. L. White, J. M. Tanski, L. N. Zakharov, G. P. A. Yap, C. D. Incarvito, A. L. Rheingold and D. Rabinovich, *Dalton Trans.*, **2004**, 1626-1634.

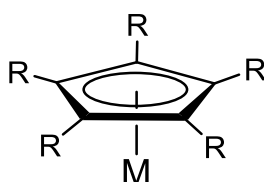
Beyond bonding and structure, a highly distinctive feature of boron-containing ligands is their reactivity. These complexes can carry out different reactions that rely on the cooperation between the metal and the boron atom. Those include, but are not restricted to, reversible hydride migration between the metal and the boron, cooperative reactivity with oxidizing agents or FLP-type behaviour in which the boron act as the acid in cooperation with a Lewis basic transition metal. Besides, the last years have witnessed a rapid evolution on the use of boron functionalities in the second coordination sphere of the metals for a variety of bond activation processes and catalytic applications. Scheme 24 includes a collection of recent representative examples in which metal-boron cooperation for bond activation and/or catalysis has been demonstrated.



Scheme 24. Representative boron-containing transition metal compounds that perform cooperative bond activation and/or catalysis.

I.3.2. Metal-ligand cooperation involving cyclopentadienyl ligands

The cyclopentadienyl ligands ($C_5R_5^-$) (Figure 4), abbreviated in general as Cp, are undoubtedly among the most widely used stabilizing fragments in organometallic chemistry and homogeneous catalysis¹²³. They exhibit variable hapticity (ranging from η^1 to η^5)¹²⁴ and have a rich capacity to bind, in essence, any metallic element across the periodic table¹²⁵. Their ubiquity is largely related to their reliability as robust spectator ligands. The widespread utility of the Cp ligands is enhanced by the versatility of this motif to be functionalized in a variety of ways. Among those, its pentamethyl version, ($C_5Me_5^-$), abbreviated as Cp*, is likely among the most amply used moieties rivalling the original ($C_5H_5^-$) unit.



M = s, p, d and f-block

Figure 4. General representation of the widespread cyclopentadienyl ligands.

¹²³ a) R. H. Crabtree, *J. Organomet. Chem.*, **2005**, 690, 5451-5457.

b) R. H. Crabtree, *The Organometallic Chemistry of the Transition Metals*, (John Wiley & Sons) 7th ed, NY, **2019**.

¹²⁴ a) J. M. O'Connor, C. P. Casey, *Chem. Rev.*, **1987**, 87, 307-318.

b) L. F. Veiros, *Organometallics*, **2000**, 19, 5549-5558.

¹²⁵ a) R. Poli, *Chem. Rev.*, **1991**, 91, 509-551.

b) P. H. Budzelaar, J. J. Engelberts, J. H. van Lenthe, *Organometallics*, **2003**, 22, 1562-1576.

c) P. A. Deck, *Coord. Chem. Rev.*, **2006**, 250, 1032-1055.

d) W. J. Evans, *Organometallics*, **2016**, 35, 3088-3100.

Although Cp ligands have been generally considered as robust and spectator fragments, there is increased interest in their utility as non-innocent motifs. This is propelled by rapid progress in the broad field of cooperative chemistry¹²⁶. For example, protonation of (C₅R₅)M fragments can take place either at the metal centre¹²⁷ or on the Cp ring¹²⁸, with formal proton migration¹²⁹ permitting the two structures to interconvert (Figure 5A)¹³⁰. This has been recently exploited¹³¹ to design proton-coupled-electron-transfer (PCET) processes applied to hydrogen evolution¹³² or dinitrogen reduction¹³³ reactions.

¹²⁶ Cooperative Catalysis (Ed. Peters, R.), Wiley-VCH, Weinheim, **2015**.

¹²⁷ a) T. J. Curphey, J. O. Santer, M. Rosenblum, J. H. Richards, *J. Am. Chem. Soc.*, **1960**, *82*, 5249-5250.

b) D. C. Liles, A. Shaver, E. Singleton, M. B. Wiege, *J. Organomet. Chem.*, **1985**, C33-C36.

c) M. Malischewski, K. Seppelt, J. Sutter, F. W. Heinemann, B. Dittrich, K. Meyer, *Angew. Chem. Int. Ed.*, **2017**, *56*, 13372-13376.

¹²⁸ a) T. L. Court, H. Werner, *J. Organomet. Chem.*, **1974**, *65*, 245-251.

b) U. Koelle, F. Khouzami, *Angew. Chem. Int. Ed. Engl.*, **1980**, *19*, 640-641.

c) Y. Peng, M. V. Ramos-Garcés, D. Lionetti, J. D. Blakemore, *Inorg. Chem.*, **2017**, *56*, 10824-10831.

¹²⁹ M. Paneque, P. M. Maitlis, *J. Chem. Soc., Chem. Commun.*, **1989**, *2*, 105-106.

¹³⁰ a) W. D. Jones, V. L. Kuykendall, A. D. Selmecky, *Organometallics*, **1991**, *10*(2), 1568-1577.

b) A. Zamorano, N. Rendon, J. E. V. Valpuesta, E. Álvarez, E. Carmona, *Inorg. Chem.*, **2015**, *54*(13), 6573-6581.

c) M. W. Drover, D. J. Schild, P. H. Oyala, J. C. Peters, *Angew. Chem. Int. Ed.*, **2019**, *58*, 15504-15511.

d) S. I. Johnson, H. B. Gray, J. D. Blakemore, W. A. Goddard III, *Inorg. Chem.*, **2017**, *56*, 11375-11386.

¹³¹ C. E. Kefalidis, L. Perrin, C. J. Burns, D. J. Berg, L. Maron, R. A. Andersen, *Dalton Trans.*, **2015**, *44*, 2575-2587.

¹³² a) L. M. A. Quintana, S. I. Johnson, S. L. Corona, W. Villatoro, W. A. Goddard III, M. K. Takase, D. G. VanderVelde, J. R. Winkler, H. B. Gray, J. D. Blakemore, *Proc. Natl. Acad. Sci. USA* **2016**, *113*, 6409-6414.

b) C. L. Pitman, O. N. L. Finster, A. J. M. Miller, *Chem. Commun.*, **2016**, *52*, 9105-9108.

c) S. Pal, S. Kusumoto, K. Nozaki, *Organometallics*, **2018**, *37*, 906-914.

¹³³ a) M. J. Chalkley, T. J. Del Castillo, B. D. Matson, J. P. Roddy, J. C. Peters, *ACS Cent. Sci.* **2017**, *3*, 217-223.

b) M. J. Chalkley, T. J. Del Castillo, B. D. Matson, J. C. Peters, *J. Am. Chem. Soc.* **2018**, *140*, 6122-6129.

c) M. J. Chalkley, P. H. Oyala, J. C. Peters, *J. Am. Chem. Soc.* **2019**, *141*, 4721-4729.

The aforesaid permethylated cyclopentadienyl ligand ((C₅Me₅)⁻. Cp*) enables additional activation at the CH₃ units (Figure 5A). Deprotonation involving a redox event at the metal by treatment with an external base or through an intramolecular pathway by means of a basic anchoring ligand is well documented¹³⁴, forming tuck-in complexes¹³⁵ and, in some cases, leading to stable fulvene-containing structures¹³⁶. Hydride abstraction has also been demonstrated, proceeding in two steps through one-electron oxidation followed by hydrogen atom abstraction¹³⁷. Direct hydride migration from a methyl group to the metal was soon recognized for

-
- ¹³⁴ a) H. Caldwell, P. S. Pregosin, *Organometallics*, **2008**, *27*, 1591-1595.
 b) S. Takemoto, H. Morita, K. Karitani, H. Fujiwara, H. Matsuzaka, *J. Am. Chem. Soc.*, **2009**, *131*, 18026-18027.
 c) M. Bernechea, J. R. Berenguer, E. Lalinde, J. Torroba, *Organometallics*, **2009**, *28*, 312-320.
 d) J. J. Moreno, M. F. Espada, J. Campos, J. Lopez-Serrano, S. A. Macgregor, E. Carmona, *J. Am. Chem. Soc.* **2019**, *141*, 2205-2210.
¹³⁵ a) F. G. N. Cloke, J. C. Green, M. L. H. Green, C. P. Morley, *J. Chem. Soc., Chem. Commun.*, **1985**, 945-946.
 b) P. N. Riley, J. R. Parker, P. E. Fanwick, I. P. Rothwell, *Organometallics*, **1999**, *18*, 3579-3583.
 c) V. Kupfer, U. Thewalt, I. Tišlerová, P. Štěpnička, R. Gyepes, J. Kubišta, M. Horáček, K. Mach, *J. Organomet. Chem.*, **2001**, *620*, 39-50.
 d) Y. Sun, R. E. v. H. Spence, W. E. Piers, M. Parvez, G. P. A. Yap, *J. Am. Chem. Soc.*, **1997**, *119* (22), 5132-5143.
¹³⁶ a) D. S. Glueck, R. G. Bergman, *Organometallics*, **1990**, *9*, 2862-2863.
 b) L. Fan, C. Wei, F. I. Aigbirhio, M. L. Turner, O. V. Gusev, L. N. Morozova, D. R. T. Knowles, P. M. Maitlis, *Organometallics*, **1996**, *15*, 98-104.
 c) P. L. Holland, R. A. Andersen, R. G. Bergman, J. Huang, S. P. Nolan, *J. Am. Chem. Soc.*, **1997**, *119*, 12800-12814.
 d) E. Rüba, K. Mereiter, R. Schmid, K. Kirchner, E. Bustelo, M. C. Puerta, P. Valerga, *Organometallics*, **2002**, *21*, 2912-2920.
 e) A. Rodríguez-Bárcano, A. J. Blacker, P. C. McGowan, *Dalton Trans.*, **2013**, *42*, 16669-16671.
 f) Y. Mori, T. Ando, T. Matsumoto, T. Yatabe, M. Kikkawa, K.-S. Yoon, *Angew. Chem. Int. Ed.* **2018**, *57*, 15792-15796.
¹³⁷ a) J. M. Meredith, K. I. Goldberg, W. Kaminsky, D. M. Heinekey, *Organometallics*, **2012**, *31*, 8459-8462.
 b) S. Li, X. Wang, Z. Zhang, Y. Zhao, X. Wang, *Dalton Trans.*, **2015**, *44*, 19754-19757.
 c) R. C. Klet, D. M. Kaphan, C. Liu, C. Yang, A. J. Kropf, F. A. Perras, M. Pruski, A. S. Hock, M. Delferro, *J. Am. Chem. Soc.*, **2018**, *140*, 6308-6316.

early transition metals¹³⁸. Alternatively, the incorporation of a second metal centre in close proximity (i.e. in cluster structures) allows for C—H bond activation of one methyl terminus (Figure 5B) to form tuck-over complexes¹³⁹, with reversibility being documented in some cases¹⁴⁰.

-
- ¹³⁸ a) J. E. Bercaw, *J. Am. Chem. Soc.*, **1974**, *96*, 5087-5094.
b) C. McDade, J.C. Green, J. E. Bercaw, *Organometallics*, **1982**, *1*, 1629-1634.
c) A. R. Bulls, W. P. Schaefer, M. Serfas, J. E. Bercaw, *Organometallics*, **1987**, *6*, 1219-1226.
d) F. G. N. Cloke, J. P. Day, J. C. Green, C. P. Morley, A.C. Swain, *J. Chem. Soc. Dalton Trans.*, **1991**, 789-796.
e) A. Nutton, P. M. Maitlis, *Dalton Trans.*, **1981**, 2335-2338.
f) H. J. Kraus, H. Werner, *Angew. Chem. Int. Ed. Engl.*, **1982**, *21*, 866-867.
g) H. Werner, G. T. Crisp, P. W. Jolly, H.-J. Kraus, C. Krüger, *Organometallics*, **1983**, *2*, 1369-1377.
h) C. P. Lenges, P. S. White, M. Brookhart, *J. Am. Chem. Soc.*, **1999**, *121*, 4385-4396.
- ¹³⁹ a) F. Bottomley, I. J. B. Lin, P. S. White, *J. Am. Chem. Soc.*, **1981**, *103*, 703-704.
b) F. W. B. Einstein, R.H. Jones, X. Zhang, X. Yan, R. Nagelkerke, D. Sutton, *J. Chem. Soc., Chem. Commun.*, **1989** 1424-1426.
c) W. Wang, H. B. Davis, F. W. B. Einstein, R. K. Pomeroy, *Organometallics*, **1994**, *13*, 5113-5121.
d) M. I. Bruce, P. A. Humphrey, B. W. Skelton, A. H. White, *J. Organomet. Chem.*, **1996**, *522*, 259-263.
e) W. J. Evans, J. M. Perotti, J. W. Ziller, *Inorg. Chem.*, **2005**, *44*(16), 5820-5825.
f) Y. Takahashi, K.-I. Fujita, R. Yamaguchi, *Eur. J. Inorg. Chem.*, **2008**, 4360-4368.
g) J. J. Carbó, D. García-López, M. Gómez-Pantoja, J. I. González-Pérez, A. Martín, M. Mena, C. Santamaría, *Organometallics*, **2017**, *36*, 3076-3083.
- ¹⁴⁰ a) C. Chung, W.-C. Tseng, Y. Chi, S.-M. Peng, G.-H. Lee, *Organometallics*, **1998**, *17*, 2207-2214.
b) T. Shima, Z. Hou, *Organometallics*, **2009**, *28*, 2244-2252.

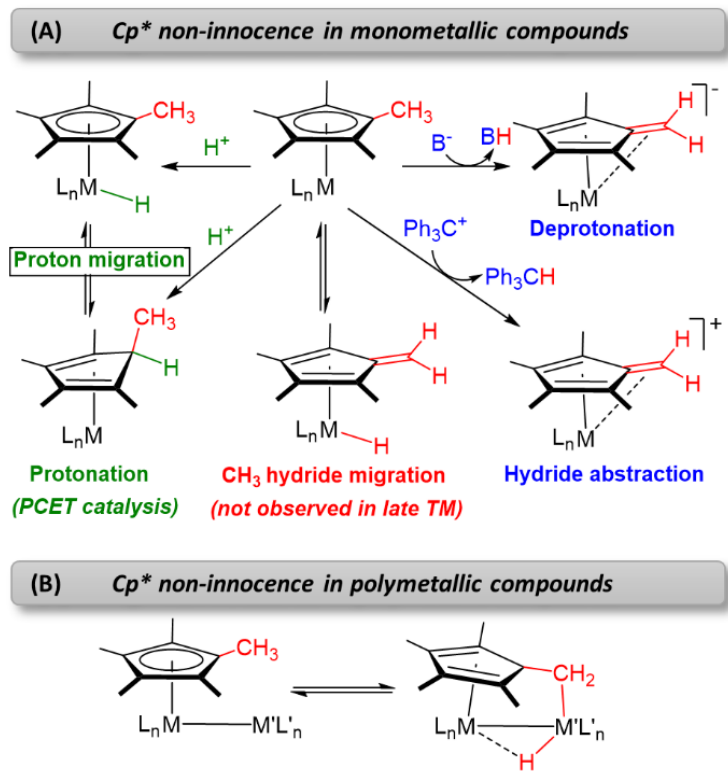


Figure 5. Previous routes for the activation of Cp* (and related) ligands in (A) mononuclear compounds and (B) polymetallic species.

I.4. References

1. A. Werner, On the constitution and configuration of higher-order compounds. Nobel Lecture, December 11, 1913. The Nobel Prize <https://www.nobelprize.org/prizes/chemistry/1913/werner/lecture>.
- 2.a) S. Kirschner, *Coordination Chemistry*, Springer New York, NY, **1969**, <https://doi.org/10.1007/978-1-4899-6555-4>.
b) *Comprehensive Coordination Chemistry II* (Elsevier, 2004).
3. a) C. Brosset, *Arkiv Kemi, Miner. Geol.* **1946**, A20 (7), A22 (11).
b) C. Brosset, *Nature*, **1935**, 135, 874.
4. F. A. Cotton, L. A. Murillo, R. A. Walton, *Multiple Bonds Between Metal Atoms* **2005**, 3rd edition [F. A. Cotton, R. A. Walton, in 1st (**1981**) and 2nd (**1992**) ed.], Springer, New York.
5. L. F. Dahl, E. Ishishi, R. E. Rundle, *J. Chem. Phys.*, **1957**, 26, 1750-1751.
6. a) J. F. Berry, C. C. Lu, *Inorg. Chem.*, **2017**, 56, 7577-7581.
b) C. M. Farley, C. Uyeda, *Trends Chem.*, **2019**, 1, 497-509.
7. F. A. Cotton, N. F. Curtis, C. B. Harris, B. F. G. Johnson, S. J. Lippard, J. T. Mague, W. R. Robinson, J. S. Wood, *Science*, **1964**, 145, 1305-1307.
8. T. Nguyen, A. D. Sutton, M. Brynda, J. C. Fettinger, G. J. Long, P. P. Power, *Science*, **2005**, 310, 844-847.
9. I. Resa, E. Carmona, E. Gutierrez-Puebla, A. Monge, *Science*, **2004**, 305, 1136-1138.
10. S. P. Green, C. Jones, A. Stasch, *Science*, **2007**, 318, 1754-1757.
11. O. Kysliak, H. Görls, R. Kretschmer, *J. Am. Chem. Soc.*, **2021**, 143, 142-148.
12. a) J. Campos, *Nat. Rev. Chem.*, **2020**, 4, 696-702.
b) C. M. Farley, C. Uyeda, *Trends Chem.*, **2019**, 1, 497-509.
c) P. Buchwalter, J. Rose, P. Braunstein, *Chem. Rev.*, **2015**, 115, 28-126.
d) R. C. Cammarota, L. J. Clouston, C. C. Lu, *Coord. Chem. Rev.*, **2017**, 334, 100-111.
e) D. R. Pye, N. P. Mankad, *Chem. Sci.*, **2017**, 8, 1705-1718.
f) I. G. Powers, C. Uyeda, *ACS Catal.*, **2017**, 7, 936-958.
g) J. Park, S. Hong, *Chem. Soc. Rev.*, **2012**, 41, 6931-6943.

13. J. F. Berry, C. C. Lu, *Inorg. Chem.*, **2017**, *56*(14), 7577–7581.
14. D. Milstein, J. R. Khusnutdinova, *Angew. Chem. Int. Ed.*, **2015**, *54*, 12236 – 12273.
15. a) H. C. Brown, H. I. Schlesinger, S. Z. Cardon. *J. Am. Chem. Soc.*, **1942**, *64*, 325–329. b) H. C. Brown, B. Kanner. *J. Am. Chem. Soc.*, **1966**, *88*, 986–992.
16. G. Wittig, E. Benz. *Chem. Ber.*, **1959**, *92*, 1999–2013.
17. W. Tochtermann. *Angew. Chem. Int. Ed.*, **1966**, *5*, 351–371.
18. R. Damico, C. D. Broadus. *J. Org. Chem.*, **1966**, *31*, 1607–1612.
19. S. Doering, G. Erker, R. Fröhlich, O. Meyer, K. Bergander, *Organometallics*, **1998**, *17*, 2183–2187.
20. a) G. C. Welch, R. R. San Juan, J. D. Masuda, D.W. Stephan, *Science*, **2006**, *314*, 1124–1128.
b) G. C. Welch, D. W. Stephan. *J. Am. Chem. Soc.*, **2007**, *129*, 1880–1881.
21. G. H. Spikes, J. C. Fettinger, P. P. Power, *J Am Chem Soc*, **2005**, *127*, 12232–12233.
22. G. D. Frey, B. Lavallo, B. Donnadiou, W. W. Schoeller, G. Bertrand, *Science*, **2007**, *316*, 439–441.
23. P. P. Power, *Nature*, **2010**, *463*, 171–177.
24. J. Chatt, L. A. Duncanson, *J. Chem. Soc.*, **1953**, *586*, 2939–2947.
25. Y. Peng, M. Brynda, B. D. Ellis, J. C. Fettinger, E. Rivarda, P. P. Power, *Chem. Commun.*, **2008**, *45*, 6042–6044.
26. a) D. W. Stephan, *Org. Biomol. Chem.*, **2012**, *10*, 5740–5746.
b) D. J. Scott, M. J. Fuchter, A. E. Ashley, *Chem. Soc. Rev.*, **2017**, *46*, 5689–5700.
27. P. Spies, G. Erker, G. Kehr, K. Bergander, R. Fröhlich, S. Grimme, D. W. Stephan, *Chem. Commun.*, **2007**, *47*, 5072–5074.
28. a) S. J. Geier, A. L. Gille, T. M. Gilbert, D. W. Stephan, *Inorg. Chem.*, **2009**, *48*, 10466–10474.
b) S. J. Geier, D. W. Stephan, *J. Am. Chem. Soc.*, **2009**, *131*, 3476–3477.
29. a) D. Chen, J. Klankermayer, *Chem. Comm.*, **2008**, *18*, 2130–2131.
b) D. Chen, Y. Wang, J. Klankermayer, *Angew. Chem. Int. Ed.*, **2010**, *49*, 9475–9478.

30. V. Sumerin, K. Chernichenko, M. Nieger, M. Leskelä, B. Rieger, T. Repo, *Adv. Synth. Catal.*, **2011**, 353, 2093–2110.
31. A. E. Ashley, A. L. Thompson, D. O'Hare, *Angew. Chem. Int. Ed.*, **2009**, 48, 9839–9843.
32. A. Berkefeld, W. E. Piers, M. Parvez, *J. Am. Chem. Soc.*, **2010**, 132, 10660–10661.
33. M. A. Courtemanche, M. A. Legare, L. Maron, F. G. Fontaine, *J. Am. Chem. Soc.*, **2013**, 135, 9326–9329.
34. T. Wang, D. W. Stephan, *Chem. Eur. J.*, **2014**, 20, 3035–3039.
35. a) A. M. Chapman, M. F. Haddow, D. F. Wass, *J. Am. Chem. Soc.*, **2011**, 133, 8826–8829.
- b) A. M. Chapman, M. F. Haddow, D. F. Wass, *J. Am. Chem. Soc.*, **2011**, 133, 18463–18478.
- c) A. M. Chapman, M. F. Haddow, D. F. Wass, *Eur. J. Inorg. Chem.*, **2012**, 9, 1546–1554.
36. a) X. Xu, R. Fröhlich, C. G. Daniliuc, G. Kehr, G. Erker, *Chem. Commun.*, **2012**, 48, 6109–6111.
- b) X. Xu, G. Kehr, C. G. Daniliuc, G. Erker, *J. Am. Chem. Soc.*, **2013**, 135, 6465–6476.
37. H. Yamamoto (ed) (**2000**) *Lewis acids in organic synthesis*. Wiley-VCH, Weinheim.
38. J. S. J. McCahill, G. C. Welch, D. W. Stephan, *Angew Chem Int Ed*, **2007**, 46, 4968–4971.
39. See for example: a) A. T. Normand, P. Richard, C. Balan, C. G. Daniliuc, G. Kehr, G. Erker, P. L. Gendre, *Organometallics*, **2015**, 34, 2000–2011.
- b) A. T. Normand, Q. Bonnin, S. Brandès, P. Richard, P. Fleurat-Lessard, C. H. Devillers, C. Balan, P. L. Gendre, G. Kehr, *Chem. Eur. J.*, **2019**, 25, 2803–2815.
- c) M. Fischer, D. Barbul, M. Schmidtman, R. Beckhaus, *Organometallics*, **2018**, 37, 1979–1991.
- d) M. Fischer, K. Schwitalla, S. Baues, M. Schmidtman, R. Beckhaus, *Dalton Trans.*, **2019**, 48, 1516–1523.

40. S. Zhang, A. M. Appel, R. M. Bullock, *J. Am. Chem. Soc.*, **2017**, *139*, 7376–7387.
41. a) E. B. Hulley, K. D. Welch, A. M. Appel, D. L. DuBois, R. M. Bullock, *J. Am. Chem. Soc.*, **2013**, *135*, 11736–11739.
b) E. B. Hulley, M. L. Helm, R. M. Bullock, *Chem. Sci.*, **2014**, *5*, 4729–4741.
42. a) T. Liu, D. L. DuBois, R. M. Bullock, *Nat. Chem.*, **2013**, *5*, 228–233.
b) T. Liu, X. Wang, C. Hoffmann, D. L. DuBois, R. M. Bullock, *Angew. Chem. Int. Ed.*, **2014**, *53*, 5300–5304.
c) T. Liu, Q. Liao, M. O. Hagan, E. B. Hulley, D. L. DuBois, R. M. Bullock, *Organometallics*, **2015**, *34*, 2747–2764.
43. a) J. C. Fontecilla-Camps, A. Volbeda, C. Cavazza, Y. Nicolet, *Chem. Rev.*, **2007**, *107*, 4273–4303.
b) W. Lubitz, H. Ogata, O. Rüdiger, E. Reijerse, *Chem. Rev.*, **2014**, *114*, 4081–4148.
44. S. Zhang, R. M. Bullock, *Inorg. Chem.*, **2015**, *54*, 6397–6409.
45. R. L. Melen, *Angew Chem Int Ed*, **2018**, *57*, 880–882.
46. C. Tang, Q. Liang, A. R. Jupp, T. C. Johnstone, R. C. Neu, D. Song, S. Grimme, D. W. Stephan, *Angew. Chem. Int. Ed.*, **2017**, *56*, 16588–16592.
47. J. B. Geri, J. P. Shanahan, N. K. Szymczak, *J. Am. Chem. Soc.*, **2017**, *139*, 5952–5956.
48. A. Simonneau, R. Turrel, L. Vendier, M. Etienne, *Angew. Chem. Int. Ed.*, **2017**, *56*, 12268–12272.
49. R. Anwander, S. Kobayashi (1999). S. Kobayashi (Eds), *Lanthanides: chemistry and use in organic synthesis*, Springer, Berlin, Heidelberg
50. a) A. Berkefeld, W. E. Piers, M. Parvez, L. Castro, L. Maron, O. Eisenstein, *J. Am. Chem. Soc.*, **2012**, *134*, 10843–10851.
b) A. Berkefeld, W. E. Piers, M. Parvez, L. Castro, L. Maron, O. Eisenstein, *Chem. Sci.*, **2013**, *4*, 2152–2162.
51. H. Corona, M. Pérez-Jiménez, F. de la Cruz-Martínez, I. Fernández, J. Campos, *Angew. Chem. Int. Ed.*, **2022**, DOI: 10.1002/anie.202207581.

52. a) T. Thai, D. S. Mérel, A. Poater, S. Gaillard, J. L. Renaud, *Chem. Eur. J.*, **2015**, *21*, 7066–7070.
- b) C. Seck, M. D. Mbaye, S. Coufourier, A. Lator, J. F. Lohier, A. Poater, T. R. Ward, S. Gaillard, J. L. Renaud, *ChemCatChem*, **2017**, *9*, 4410–4416.
- c) A. Lator, Q. G. Gaillard, D. S. Mérel, J. F. Lohier, S. Gaillard, A. Poater, J. L. Renaud, *J. Org. Chem.*, **2019**, *84*, 6813–6829.
53. B. L. Conley, M. K. Pennington-Boggio, E. Boz, T. J. Williams, *Chem. Rev.*, **2010**, *110*, 2294–2312.
54. a) H. F. T. Klare, M. Oestreich, J.-I. Ito, H. Nishiyama, Y. Ohki, K. Tatsumi, *J. Am. Chem. Soc.*, **2011**, *133*, 3312–3315.
- b) C. D. F. Königs, H. F. T. Klare, Y. Ohki, K. Tatsumi, M. Oestreich, *Org. Lett.*, **2012**, *14*, 2842–2845.
- c) J. Hermeke, H. F. T. Klare, M. Oestreich, *Chem. Eur. J.*, **2014**, *20*, 9250–9254.
- d) C. D. F. Königs, M. F. Müller, N. Aiguabella, H. F. T. Klare, M. Oestreich, *Chem. Commun.*, **2013**, *49*, 1506–1508.
- e) C. D. F. Königs, H. F. T. Klare, M. Oestreich, *Angew. Chem. Int. Ed.*, **2013**, *52*, 10076–10079.
- f) T. T. Metsänen, M. Oestreich, *Organometallics*, **2015**, *34*, 543–546.
- g) T. Stahl, H. F. T. Klare, M. Oestreich, *J. Am. Chem. Soc.*, **2013**, *135*, 1248–1251.
- h) S. Bähr, M. Oestreich, *Organometallics*, **2017**, *36*, 935–943.
55. S. Webbolt, M. S. Maji, E. Irran, M. Oestreich, *Chem. Eur. J.*, **2017**, *23*, 6213–6219.
56. T. Stahl, P. Hrobárik, C. D. F. Königs, Y. Ohki, K. Tatsumi, S. Kemper, M. Kaupp, H. F. T. Klare, M. Oestreich, *Chem Sci*, **2015**, *6*, 4324–4334.
57. a) N. Ochi, T. Matsumoto, T. Dei, Y. Nakao, H. Sato, K. Tatsumi, S. Sakaki, *Inorg. Chem.*, **2015**, *54*, 576–585.
- b) T. Matsumoto, Y. Nakaya, N. Itakura, K. Tatsumi, *J. Am. Chem. Soc.*, **2008**, *130*, 2458–2459.
58. T. A. Rokob, A. Hamza, A. Stirling, I. Pápai, *J. Am. Chem. Soc.*, **2009**, *131*, 2029–2036.

59. C. Ferrer, J. Ferrer, V. Passarelli, F. J. Lahoz, P. García-Orduña, D. Carmona, *Organometallics*, **2022**, *41*, 1445–1453.
60. M. Carmona, R. Pérez, J. Ferrer, R. Rodríguez, V. Passarelli, F. J. Lahoz, P. García-Orduña, D. Carmona, *Inorg. Chem.*, **2022**, *61*, 13149–13164.
61. R. Gareth, *Chem. Soc. Rev.*, **2012**, *41*, 3535–3546.
62. W. H. Harman, J. C. Peters, *J. Am. Chem. Soc.*, **2012**, *134*, 5080–5082.
63. a) H. Fong, M-E. Moret, Y. Lee, J. C. Peters, *Organometallics*, **2013**, *32*, 3053–3062.
- b) S. N. MacMillan, W. Hill Harman, J. C. Peters, *Chem. Sci.*, **2014**, *5*, 590–597.
- c) W. H. Harman, T-P. Lin, J. C. Peters, *Angew. Chem. Int. Ed.*, **2014**, *53*, 1081–1086.
64. M. A. Nesbit, D. L. M. Suess, J. C. Peters, *Organometallics*, **2015**, *34*, 4741–4752.
65. K. Michaliszyn, E. S. Smirnova, A. Bucci, V. Martin-Diaconescu, J. Lloret Fillol, *ChemCatChem*, **2022**, *14*, e202200039.
66. S. J. K. Forrest, J. Clifton, N. Fey, P. G. Pringle, H. A. Sparkes, D. F. Wass, *Angew. Chem. Int. Ed.*, **2015**, *54*, 2223–2227.
67. K. Mistry, P. G. Pringle, H. A. Sparkes, D. F. Wass, *Organometallics*, **2020**, *39*, 468–477
68. a) B. R. Barnett, C. E. Moore, A. L. Rheingold, J. S. Figueroa, *J. Am. Chem. Soc.*, **2014**, *136*, 10262–10265.
- b) B. R. Barnett, M. L. Neville, C. E. Moore, A. L. Rheingold, J. S. Figueroa, *Angew. Chem. Int. Ed.*, **2017**, *56*, 7195–7199.
69. a) C. M. Friend, A. S. K. Hashmi, *Acc. Chem. Res.*, **2014**, *47*, 729–730.
- b) I. Braun, A. M. Asiri, A. S. K. Hashmi, *ACS Catal.*, **2013**, *3*, 1902–1907.
- c) M. Rudolph, A. S. Hashmi, *Chem. Soc. Rev.*, **2012**, *41*, 2448–2462.
- d) N. Krause, C. Winter, *Chem. Rev.*, **2011**, *111*, 1994–2009.
- e) A. Corma, A. Leyva-Pérez, M. J. Sabater, *Chem. Rev.*, **2011**, *111*, 1657–1712.
- f) A. Ffirstner, *Chem. Soc. Rev.*, **2009**, *38*, 3208–3221.
- g) C. Obradors, A. M. Echavarren, *Chem. Commun.*, **2014**, *50*, 16–28.
70. S. G. Weber, C. Loos, F. Rominger, B. F. Straub, *ARKIVOC*, **2012**, *3*, 226–242.

71. S. Arndt, M. M. Hansmann, P. Motloch, M. Rudolph, F. Rominger, A. S. K. Hashmi, *Chem. Eur. J.*, **2017**, *23*, 2542–2547.
72. Z. Wang, Y. Wang, L. Zhang, *J. Am. Chem. Soc.*, **2014**, *136*, 8887–8890.
73. a) Z. Wang, A. Ying, Z. Fan, C. Hervieu, L. Zhang, *ACS Catal.*, **2017**, *5*, 3676–3680.
- b) X. Li, X. Ma, Z. Wang, P-N. Liu, L. Zhang, *Angew. Chem. Int. Ed.*, **2019**, *58*, 17180–17184.
- c) X. Cheng, Z. Wang, C. D. Quintanilla, L. Zhang, *J. Am. Chem. Soc.*, **2019**, *141*, 3787–3791.
74. a) D. W. Stephan, *Coordination Chemistry Reviews*, **1989**, *95*, 41–107.
- b) N. Wheatley, P. Kalck, *Chem. Rev.*, **1999**, *99*, 3379–3420.
- c) L. H. Gade, *Angew. Chem. Int. Ed.*, **2000**, *39*, 2658–2678.
- d) B. G. Cooper, J. W. Napoline, C. M. Thomas, *Catalysis Reviews*, **2012**, *54*, 1–40.
- e) M. Herberhold, G-X. Jin, *Angew. Chem. Int. Ed.*, **1994**, *33*, 964–966.
75. A. M. Chapman, S. R. Flynn, D. F. Wass, *Inorg. Chem.*, **2016**, *55*, 1017–1021.
76. J. Campos, *J. Am. Chem. Soc.*, **2017**, *139*, 2944–2947.
77. J. Bauer, H. Braunschweig, R. D. Dewhurst, *Chem. Rev.*, **2012**, *112*, 4329–4346
78. N. Hidalgo, J. J. Moreno, M. Pérez-Jiménez, C. Maya, J. López-Serrano, J. Campos, *Chem. Eur. J.*, **2020**, *26*, 5982–5993.
79. L. X. Dang, G. K. Schenter, T-M. Chang, S. M. Kathmann, T. Autrey, *J. Phys. Chem. Lett.*, **2012**, *3*, 3312–3319.
80. N. Hidalgo, S. Bajo, J. J. Moreno, C. Navarro-Gilabert, B. Q. Mercado, J. Campos, *Dalton trans.*, **2019**, *48*, 9127–9138.
81. N. Hidalgo, J. J. Moreno, M. Pérez-Jiménez, C. Maya, J. López-Serrano, J. Campos, *Organometallics*, **2020**, *39*, 2534–2544.
82. a) T. A. Rokob, I. Pápai I (2013) *Hydrogen activation by frustrated Lewis pairs: Insights from computational studies*. In: G. Erker, D. Stephan (eds) *Frustrated Lewis Pairs I. Topics in Current Chemistry*. Springer, Berlin, Heidelberg, p 157–212.
- b) J. Paradies, *Eur. J. Org. Chem.*, **2019**, 2-3, 283–294.

- c) L. Rocchigiani, *Isr. J. Chem.*, **2015**, *55*, 134–149.
83. N. Hidalgo, F. de la Cruz-Martínez, M. T. Martín, M. C. Nicasio, J. Campos, *Chem. Commun.*, **2022**, *58*, 9144-9147.
84. M. A. Dureen, D. W. Stephan, *J. Am. Chem. Soc.*, **2009**, *131*, 8396–8397.
85. J. Bauer, H. Braunschweig, R. D. Dewhurst, *Chem. Rev.*, **2012**, *112*, 4329-4346.
86. C. E. Coffey, J. Lewis, R. S. Nyholm, *J. Chem. Soc.*, **1964**, 1741-1749.
87. I. N. Nowell, D. R. Russell, *Chem. Commun.*, **1967**, 817-817.
88. For selected recent MOLPs see: a) M. Ma, A. Sidiropoulos, L. Ralte, A. Stasch, C. Jones, *Chem. Commun.*, **2013**, *49*, 48-50.
- b) S. Bertsch, H. Braunschweig, R. D. Dewhurst, K. Radacki, C. Saalfrank, B. Wennemann, Q. Ye, *Organometallics* **2014**, *33*, 3649-3651.
- c) N. Arnold, H. Braunschweig, P. B. Brenner, M. A. Celik, R. D. Dewhurst, M. Haehnel, T. Kramer, I. Krummenacher, T. B. Marder, *Chem. Eur. J.* **2015**, *21*, 12357-12362.
- d) R. Bertermann, J. Böhnke, H. Braunschweig, R. D. Dewhurst, T. Kupfer, J. H. Muessig, L. Pentecost, K. Radacki, S. S. Sen, A. Vargas, *J. Am. Chem. Soc.* **2016**, *138*, 16140-16147.
- e) G. Wang, Y. S. Ceylan, T. R. Cundari, H. V. R. Dias, *J. Am. Chem. Soc.* **2017**, *139*, 14292–14301.
- f) J. K. Schuster, J. H. Muessig, R. D. Dewhurst, H. Braunschweig, *Chem. Eur. J.* **2018**, *24*, 9692-9697.
- g) L. D. Ernst, K. Koessler, A. Peter, D. Kratzert, H. Scherer, B. Butschke *Chem. Commun.* **2020**, *56*, 5350-5353.
89. A. Y. Khalimon, P. Farha, L. G. Kuzminab, G. I. Nikonov, *Chem. Commun.*, **2012**, *48*, 455-457.
90. a) L. Vaska, *Acc. Chem. Res.*, **1968**, *1*, 335-344.
- b) J. P. Collman, W. R. Roper, *Adv. Organomet. Chem.*, **1968**, *7*, 53-94.
- c) D. F. Shriver, *Acc. Chem. Res.* **1970**, *3*, 231-238.
- d) L. Vaska, *Inorg. Chim. Acta*, **1971**, *5*, 295-300.
- e) H. Werner, *Pure & Appl. Chem.*, **1982**, *54*, 177-188.
- f) H. Werner, *Angew. Chem. Int. Ed.*, **1983**, *22*, 927-949.

91. a) R. Bissert, H. Braunschweig, R. D. Dewhurst, C. Schneider, *Organometallics*, **2016**, *35*, 2567-2573.
- b) H. Braunschweig, C. Brunecker, R. D. Dewhurst, C. Schneider, B. Wennemann, *Chem. Eur. J.*, **2015**, *21*, 19195-19201.
- c) H. Braunschweig, R. D. Dewhurst, F. Hupp, C. Kaufmann, A. K. Phukan, C. Schneider, Q. Ye, *Chem. Sci.*, **2014**, *5*, 4099-4104.
92. J. R. Pinkes, B. D. Steffey, J. C. Vites, A. R. Cutler, *Organometallics*, **1994**, *13*, 21-23.
93. a) T. A. Hanna, A. M. Baranger, R. G. Bergman, *J. Am. Chem. Soc.*, **1995**, *117*, 11363-11364.
- b) A. M. Baranger, R. G. Bergman, *J. Am. Chem. Soc.*, **1994**, *116*, 3822-3835.
- c) H. Memmler, U. Kauper, L. H. Gade, I. J. Scowen, M. McPartlin, *Chem. Commun.*, **1996**, *15*, 1751-1752.
- d) A. Schneider, L. H. Gade, M. Breuning, G. Bringmann, I. J. Scowen, M. McPartlin, *Organometallics*, **1998**, *17*, 1643-1645.
- e) L. H. Gade, H. Memmler, U. Kauper, A. Schneider, S. Fabre, I. Bezougli, M. Lutz, C. Galka, I. J. Scowen, M. McPartlin, *Chem. Eur. J.*, **2000**, *6*, 692-708.
- f) B. Findeis, M. Schubart, C. Platzek, L. H. Gade, I. Scowen, M. McPartlin, *Chem. Commun.*, **1996**, *2*, 219-220.
- g) J. R. Pinkes, S. M. Tetrick, B. E. Landrum, A. R. Cutler, *Journal of Organometallic Chemistry*, **1998**, *556*, 1-7.
- h) A. Sisak, E. Halmos, *J. Organomet. Chem.*, **2007**, *92*, 1817-1824.
- i) K. Uehara, S. Hikichi, A. Inagaki, M. Akita, *Chem. Eur. J.*, **2005**, *11*, 2788-2809.
- j) J. A. R. Schmidt, E. B. Lobkovsky, G. W. Coates, *J. Am. Chem. Soc.*, **2005**, *127*, 11426-11435.
- k) J. P. Krogman, B. M. Foxman, C. M. Thomas, *J. Am. Chem. Soc.*, **2011**, *133*, 14582-14585.
- l) B. G. Cooper, C. M. Fafard, B. M. Foxman, C. M. Thomas, *Organometallics*, **2010**, *29*, 5179-5186.
- m) I. M. Riddlestone, N. A. Rajabi, J. P. Lowe, M. F. Mahon, S. A. Macgregor, *J. Am. Chem. Soc.*, **2010**, *35*, 11081-11084. doi:10.1021/jacs.6b05243

94. S. Jamali, S. Abedanzadeh, N. K. Khaledi, H. Samouei, Z. Hendi, S. Zacchini, R. Kia, H. R. Shahsavari, *Dalton Trans.*, **2016**, 45, 17644–17651.
95. N. Hidalgo, C. Maya, J. Campos, *Chem. commun.*, **2019**, 55, 8812–8815.
96. a) J. Zhao, A. S. Goldman, J. F. Hartwig, *Science*, **2005**, 307, 1080–1082.
b) C. M. Fafard, D. Adhikari, B. M. Foxman, J. Mindiola, O. V. Ozerov, *J. Am. Chem. Soc.*, **2007**, 129, 10318–10319.
97. a) U. Jayarathne, T. J. Mazzacano, S. Bagherzadeh, N. P. Mankad, *Organometallic*, **2013**, 32, 3986–3992.
b) S. Banerjee, M. K. Karunananda, S. Bagherzadeh, U. Jayarathne, S. R. Parmelee, G. W. Waldhart, N. P. Mankad, *Inorg. Chem.*, **2014**, 53, 11307–11315.
c) M. K. Karunananda, F. X. Vázquez, E. E. Alp, W. Bi, S. Chattopadhyay, T. Shibatade, N. P. Mankad, *Dalton Trans.*, **2014**, 43, 13661–13671.
98. U. Jayarathne, S. R. Parmelee, N. P. Mankad, *Inorg. Chem.*, **2014**, 53, 7730–7737.
99. M. K. Karunananda, S. R. Parmelee, G. W. Waldhart, N. P. Mankad, *Organometallics*, **2015**, 34, 3857–3864.
100. M. K. Karunananda, N. P. Mankad, *Organometallics*, **2017**, 36, 220–227.
101. N. P. Mankad, *Chem. comm.*, **2018**, 54, 1291–1302.
102. Y. Zhang, M. K. Karunananda, H. C. Yu, K. J. Clark, W. Williams, N. P. Mankad, D. H. Ess, *ACS Catal.*, **2019**, 9, 2657–2663.
103. M. K. Karunananda, N. P. Mankad, *J. Am. Chem. Soc.*, **2015**, 137, 14598–14601.
104. a) T. J. Mazzacano, N. P. Mankad, *J. Am. Chem. Soc.*, **2013**, 135, 17258–17261.
b) S. R. Parmelee, T. J. Mazzacano, Y. Zhu, N. P. Mankad, J. A. Keith, *ACS Catal.*, **2015**, 5, 3689–3699.
105. L. J. Cheng, N. P. Mankad, *J. Am. Chem. Soc.*, **2019**, 141, 3710–3716.
106. M. Devillard, R. Declercq, E. Nicolas, A. W. Ehlers, J. Backs, N. Saffon-Merceron, G. Bouhadir, J. C. Slootweg, W. Uhl, D. Bourissou, *J. Am. Chem. Soc.*, **2016**, 138, 4917–4926.
107. Y. Chen, S. Sakaki, *Inorg. Chem.*, **2017**, 56, 4011–4020.

108. F. G. Fontaine, D. W. Stephan, *Phil. Trans. R. Soc. A.*, **2017**, 375, 20170004.
109. a) R. Noyori, S. Hashiguchi, *Acc. Chem. Res.*, **1997**, 30, 97-102.
b) R. Noyori, T. Ohkuma, *Angew. Chem. Int. Ed.*, **2001**, 40, 40-73.
c) R. Noyori, M. Koizumi, D. Ishii, T. Ohkuma, *Pure Appl. Chem.*, **2001**, 73, 227-232.
d) R. Noyori, M. Kitamura, T. Ohkuma, *Proc. Natl. Acad. Sci. USA*, **2004**, 101, 5356-5362.
e) T. Ohkuma, H. Ooka, S. Hashiguchi, T. Ikariya, R. Noyori, *J. Am. Chem. Soc.*, **1995**, 117, 2675-2676.
f) C. A. Sandoval, T. Ohkuma, K. Muniz, R. Noyori, *J. Am. Chem. Soc.*, **2003**, 125, 13490-13503.
g) T. Ikariya, A. J. Blacker, *Acc. Chem. Res.*, **2007**, 40, 1300-1308.
h) T. Ikariya, I. D. Gridnev, *Top. Catal.*, **2010**, 53, 894-901.
i) T. Ikariya, *Bull. Chem. Soc. Jpn.*, **2011**, 84, 1-16.
j) P. A. Dub, T. Ikariya, *ACS Catal.*, **2012**, 2, 1718-1741.
k) L. A. Berben, *Chem. Eur. J.*, **2015**, 21, 2734-2742.
l) H. Grtzmacher, *Angew. Chem. Int. Ed.*, **2008**, 47, 1814-1818.
m) P. E. Sues, K. Z. Demmans, R. H. Morris, *Dalton Trans.*, **2014**, 43, 7650-7667.
n) R. H. Morris, *Acc. Chem. Res.*, **2015**, 48, 1494-1502.
110. L. E. Doyle, W. E. Piers, J. Borau-Garcia, *J. Am. Chem. Soc.*, **2015**, 137(6), 2187-2190.
111. a) Z. K. Sweeney, J. L. Polse, R. G. Bergman, R. A. Andersen, *Organometallics*, **1999**, 18, 5502-5510.
b) R. C. Linck, R. J. Pafford, T. B. Rauchfuss, *J. Am. Chem. Soc.*, **2001**, 123, 8856-8857.
c) A. Ienco, M. J. Calhorda, J. Reinhold, F. Reineri, C. Bianchini, M. Peruzzini, F. Vizza, C. Mealli, *J. Am. Chem. Soc.*, **2004**, 126, 11954-11965.
d) K. D. Hesp, R. McDonald, M. J. Ferguson, M. Stradiotto, *J. Am. Chem. Soc.*, **2008**, 130, 16394-16406.
e) Y. Ohki, M. Sakamoto, K. Tatsumi, *J. Am. Chem. Soc.*, **2008**, 130, 11610-11611.

- f) M. Sakamoto, Y. Ohki, G. Kehr, G. Erker, K. Tatsumi, *J. Organomet. Chem.*, **2009**, *694*, 2820-2824.
- g) Y. Ohki, Y. Takikawa, H. Sadohara, C. Kesenheimer, B. Engendahl, E. Kapatina, K. Tatsumi, *Chem. Asian J.*, **2008**, *3*, 1625-1635.
- h) T. Stahl, K. Mîther, Y. Ohki, K. Tatsumi, M. Oestreich, *J. Am. Chem. Soc.*, **2013**, *135*, 10978-10981.
112. G. R. Owen, *Chem. Soc. Rev.*, **2012**, *41*, 3535–3546.
113. a) H. D. Empsall, E. M. Hyde, R. Markham, W. S. McDonald, M. C. Norton, B. L. Shaw, B. Weeks, *J. Chem. Soc. Chem. Commun.*, **1977**, 589-590.
- b) C. Crocker, R. J. Errington, R. Markham, C. J. Moulton, K. J. Odell, B. L. Shaw, *J. Am. Chem. Soc.*, **1980**, *102*, 4373-4379.
- c) C. Crocker, R. J. Errington, R. Markham, C. J. Moulton, B. L. Shaw, *J. Chem. Soc. Dalton Trans.*, **1982**, 387-395.
- d) C. Crocker, H. D. Empsall, R. J. Errington, E. M. Hyde, W. S. McDonald, R. Markham, M. C. Norton, B. L. Shaw, B. Weeks, *J. Chem. Soc. Dalton Trans.*, **1982**, 1217-1224.
- e) C. Crocker, R. J. Errington, W. S. McDonald, K. J. Odell, B. L. Shaw, R. J. Goodfellow, *J. Chem. Soc. Chem. Commun.*, **1979**, 498-499.
- f) D. Gelman, S. Musa, *ACS Catal.*, **2012**, *2*, 2456-2466.
- g) D. G. Gusev, A. J. Lough, *Organometallics*, **2002**, *21*, 2601-2603.
- h) R. J. Burford, W. E. Piers, M. Parvez, *Organometallics*, **2012**, *31*, 2949-2952
- i) D. V. Gutsulyak, W. E. Piers, J. Borau-Garcia, M. Parvez, *J. Am. Chem. Soc.*, **2013**, *135*, 11776-11779.
- j) C. C. Comanescu, V. M. Iluc, *Organometallics*, **2014**, *33*, 6059-6064.
114. A. F. Hill, G. R. Owen, A. J. P. White, D. J. Williams, *Angew. Chem. Int. Ed.*, **1999**, *38*, 2759-2761.
115. a) A. Amgoune, D. Bourissou, *Chem. Commun.*, **2011**, *47*, 859-871.
- b) G. Bouhadir, D. Bourissou, *Chem. Soc. Rev.*, **2016**, *45*, 1065-1079.
- c) D. You, F. P. Gabbaï, *Trends in Chemistry*, **2019**, *1*(5), 485-496.
116. H. Braunschweig, A. Damme, T. Kupfer, *Angew. Chem., Int. Ed.*, **2011**, *50*, 7179-7182.

117. M. Sircoglou, S. Bontemps, G. Bouhadir, N. Saffon, K. Miqueu, W. Gu, M. Mercy, C.-H. Chen, B. M. Foxman, L. Maron, O. V. Ozerov, D. Bourissou, *J. Am. Chem. Soc.*, **2008**, *130*, 16729-16738.
118. G. Nuss, G. Saischek, B. N. Harum, M. Volpe, F. Belaj, N. C. Mo'sch-Zanetti, *Inorg. Chem.*, **2011**, *50*, 12632-12640.
119. a) A. Amgoune, D. Bourissou, *Chem. Commun.*, **2011**, *47*, 8163-8165.
b) G. Bouhadir, A. Amgoune, D. Bourissou, *Adv. Organomet. Chem.*, **2011**, *58*, 1-106
120. C. Pettinari, in *Scorpionates II: Chelating Borate Ligands*, Imperial College Press, London, **2008**.
121. a) R. J. Blagg, C. J. Adams, J. P. H. Charmant, N. G. Connelly, M. F. Haddow, A. Hamilton, J. Knight, A. G. Orpen, B. M. Ridgway, *Dalton Trans.*, **2009**, 8724-8736.
b) M. J. López-Gómez, N. G. Connelly, M. F. Haddow, A. Hamilton, A. G. Orpen, *Dalton Trans.*, **2010**, *39*, 5221-5230.
122. D. J. Mihalcik, J. L. White, J. M. Tanski, L. N. Zakharov, G. P. A. Yap, C. D. Incarvito, A. L. Rheingold and D. Rabinovich, *Dalton Trans.*, **2004**, 1626-1634.
123. a) R. H. Crabtree, *J. Organomet. Chem.*, **2005**, *690*, 5451-5457.
b) R. H. Crabtree, *The Organometallic Chemistry of the Transition Metals*, (John Wiley & Sons) 7th ed, NY, **2019**.
124. a) J. M. O'Connor, C. P. Casey, *Chem. Rev.*, **1987**, *87*, 307-318.
b) L. F. Veiros, *Organometallics*, **2000**, *19*, 5549-5558.
125. a) R. Poli, *Chem. Rev.*, **1991**, *91*, 509-551.
b) P. H. Budzelaar, J. J. Engelberts, J. H. van Lenthe, *Organometallics*, **2003**, *22*, 1562-1576.
c) P. A. Deck, *Coord. Chem. Rev.*, **2006**, *250*, 1032-1055.
d) W. J. Evans, *Organometallics*, **2016**, *35*, 3088-3100.
126. Cooperative Catalysis (Ed. Peters, R.), Wiley-VCH, Weinheim, **2015**.
127. a) T. J. Curphey, J. O. Santer, M. Rosenblum, J. H. Richards, *J. Am. Chem. Soc.*, **1960**, *82*, 5249-5250.

- b) D. C. Liles, A. Shaver, E. Singleton, M. B. Wiege, *J. Organomet. Chem.*, **1985**, C33-C36.
- c) M. Malischewski, K. Seppelt, J. Sutter, F. W. Heinemann, B. Dittrich, K. Meyer, *Angew. Chem. Int. Ed.*, **2017**, *56*, 13372-13376.
128. a) T. L. Court, H. Werner, *J. Organomet. Chem.*, **1974**, *65*, 245-251.
- b) U. Koelle, F. Khouzami, *Angew. Chem. Int. Ed. Engl.*, **1980**, *19*, 640-641.
- c) Y. Peng, M. V. Ramos-Garcés, D. Lionetti, J. D. Blakemore, *Inorg. Chem.*, **2017**, *56*, 10824-10831.
129. M. Paneque, P. M. Maitlis, *J. Chem. Soc., Chem. Commun.*, **1989**, *2*, 105-106.
130. a) W. D. Jones, V. L. Kuykendall, A. D. Selmecky, *Organometallics*, **1991**, *10*(2), 1568-1577.
- b) A. Zamorano, N. Rendon, J. E. V. Valpuesta, E. Álvarez, E. Carmona. *Inorg. Chem.*, **2015**, *54*(13), 6573-6581.
- c) M. W. Drover, D. J. Schild, P. H. Oyala, J. C. Peters, *Angew. Chem. Int. Ed.*, **2019**, *58*, 15504-15511.
- d) S. I. Johnson, H. B. Gray, J. D. Blakemore, W. A. Goddard III, *Inorg. Chem.*, **2017**, *56*, 11375-11386.
131. C. E. Kefalidis, L. Perrin, C. J. Burns, D. J. Berg, L. Maron, R. A. Andersen, *Dalton Trans.*, **2015**, *44*, 2575-2587.
132. a) L. M. A. Quintana, S. I. Johnson, S. L. Corona, W. Villatoro, W. A. Goddard III, M. K. Takase, D. G. VanderVelde, J. R. Winkler, H. B. Gray, J. D. Blakemore, *Proc. Natl. Acad. Sci. USA* **2016**, *113*, 6409-6414.
- b) C. L. Pitman, O. N. L. Finster, A. J. M. Miller, *Chem. Commun.*, **2016**, *52*, 9105-9108.
- c) S. Pal, S. Kusumoto, K. Nozaki, *Organometallics*, **2018**, *37*, 906-914.
133. a) M. J. Chalkley, T. J. Del Castillo, B. D. Matson, J. P. Roddy, J. C. Peters, *ACS Cent. Sci.* **2017**, *3*, 217-223.
- b) M. J. Chalkley, T. J. Del Castillo, B. D. Matson, J. C. Peters, *J. Am. Chem. Soc.* **2018**, *140*, 6122-6129.
- c) M. J. Chalkley, P. H. Oyala, J. C. Peters, *J. Am. Chem. Soc.* **2019**, *141*, 4721-4729.

134. a) H. Caldwell, P. S. Pregosin, *Organometallics*, **2008**, *27*, 1591-1595.
b) S. Takemoto, H. Morita, K. Karitani, H. Fujiwara, H. Matsuzaka, *J. Am. Chem. Soc.*, **2009**, *131*, 18026-18027.
c) M. Bernechea, J. R. Berenguer, E. Lalinde, J. Torroba, *Organometallics*, **2009**, *28*, 312-320.
d) J. J. Moreno, M. F. Espada, J. Campos, J. Lopez-Serrano, S. A. Macgregor, E. Carmona, *J Am. Chem. Soc.* **2019**, *141*, 2205-2210.
135. a) F. G. N. Cloke, J. C. Green, M. L. H. Green, C. P. Morley, *J. Chem. Soc., Chem. Commun.*, **1985**, 945-946.
b) P. N. Riley, J. R. Parker, P. E. Fanwick, I. P. Rothwell, *Organometallics*, **1999**, *18*, 3579-3583.
c) V. Kupfer, U. Thewalt, I. Tišlerová, P. Štěpnička, R. Gyepes, J. Kubišta, M. Horáček, K. Mach, *J. Organomet. Chem.*, **2001**, *620*, 39-50.
d) Y. Sun, R. E. v. H. Spence, W. E. Piers, M. Parvez, G. P. A. Yap, *J. Am. Chem. Soc.*, **1997**, *119* (22), 5132-5143.
136. a) D. S. Glueck, R. G. Bergman, *Organometallics*, **1990**, *9*, 2862-2863.
b) L. Fan, C. Wei, F. I. Aigbirhio, M. L. Turner, O. V. Gusev, L. N. Morozova, D. R. T. Knowles, P. M. Maitlis, *Organometallics*, **1996**, *15*, 98-104.
c) P. L. Holland, R. A. Andersen, R. G. Bergman, J. Huang, S. P. Nolan, *J. Am. Chem. Soc.*, **1997**, *119*, 12800-12814.
d) E. Rüba, K. Mereiter, R. Schmid, K. Kirchner, E. Bustelo, M. C. Puerta, P. Valerga, *Organometallics*, **2002**, *21*, 2912-2920.
e) A. Rodríguez-Bárzano, A. J. Blacker, P. C. McGowan, *Dalton Trans.*, **2013**, *42*, 16669-16671.
f) Y. Mori, T. Ando, T. Matsumoto, T. Yatabe, M. Kikkawa, K.-S. Yoon, *Angew.Chem.Int. Ed.* **2018**, *57*, 15792-15796.
137. a) J. M. Meredith, K. I. Goldberg, W. Kaminsky, D. M. Heinekey, *Organometallics*, **2012**, *31*, 8459-8462.
b) S. Li, X. Wang, Z. Zhang, Y. Zhao, X. Wang, *Dalton Trans.*, **2015**, *44*, 19754-19757.

- c) R. C. Klet, D. M. Kaphan, C. Liu, C. Yang, A. J. Kropf, F. A. Perras, M. Pruski, A. S. Hock, M. Delferro, *J. Am. Chem. Soc.*, **2018**, *140*, 6308-6316.
138. a) J. E. Bercaw, *J. Am. Chem. Soc.*, **1974**, *96*, 5087-5094.
- b) C. McDade, J.C. Green, J. E. Bercaw, *Organometallics*, **1982**, *1*, 1629-1634.
- c) A. R. Bulls, W. P. Schaefer, M. Serfas, J. E. Bercaw, *Organometallics*, **1987**, *6*, 1219-1226.
- d) F. G. N. Cloke, J. P. Day, J. C. Green, C. P. Morley, A.C. Swain, *J. Chem. Soc. Dalton Trans.*, **1991**, 789-796.
- e) A. Nutton, P. M. Maitlis, *Dalton Trans.*, **1981**, 2335-2338.
- f) H. J. Kraus, H. Werner, *Angew. Chem. Int. Ed. Engl.*, **1982**, *21*, 866-867.
- g) H. Werner, G. T. Crisp, P. W. Jolly, H.-J. Kraus, C. Krüger, *Organometallics*, **1983**, *2*, 1369-1377.
- h) C. P. Lenges, P. S. White, M. Brookhart, *J. Am. Chem. Soc.*, **1999**, *121*, 4385-4396.
139. a) F. Bottomley, I. J. B. Lin, P. S. White, *J. Am. Chem. Soc.*, **1981**, *103*, 703-704.
- b) F. W. B. Einstein, R.H. Jones, X. Zhang, X.Yan, R. Nagelkerke, D. Sutton, *J. Chem. Soc., Chem. Commun.*, **1989** 1424-1426.
- c) W. Wang, H. B. Davis, F. W. B. Einstein, R. K. Pomeroy, *Organometallics*, **1994**, *13*, 5113-5121.
- d) M. I. Bruce, P. A. Humphrey, B. W. Skelton, A. H. White, *J. Organomet. Chem.*, **1996**, *522*, 259-263.
- e) W. J. Evans, J. M. Perotti, J. W. Ziller, *Inorg. Chem.*, **2005**, *44*(16), 5820-5825.
- f) Y. Takahashi, K.-I. Fujita, R. Yamaguchi, *Eur. J. Inorg. Chem.*, **2008**, 4360-4368.
- g) J. J. Carbó, D. García-López, M. Gómez-Pantoja, J. I. González-Pérez, A. Martín, M. Mena, C. Santamaría, *Organometallics*, **2017**, *36*, 3076-3083.
140. a) C. Chung, W.-C. Tseng, Y. Chi, S.-M. Peng, G.-H. Lee, *Organometallics*, **1998**, *17*, 2207-2214.
- b) T. Shima, Z. Hou, *Organometallics*, **2009**, *28*, 2244-2252.

CHAPTER II

II.1. Introductory comments

The development on the study of metal-metal bonds has been summarized in chapter I, highlighting the importance of M→M dative bonds in metal-only Lewis pairs (MOLPs) and the growing interest on investigating this type of compounds. Nonetheless, some additional comments on this matter are in order before discussing the results obtained in this Thesis.

Bimetallic dative bonding has implications in many catalytic processes that involve the participation of two metal fragments of contrasting electronic nature. For instance, a series of studies on Pd-catalyzed Negishi and Sonogashira cross-coupling reactions revealed the impact on catalytic performance of bimetallic Lewis acid-base interactions between an electron rich Pd(II) center and acidic Zn(II) or Cu(I) fragments¹. Unsupported MOLP compounds have also proved competent in the activation of a variety of E—H bonds (E = H, X, N, O) where their individual monometallic constituents revealed themselves inactive². The incorporation of acidic metals or metalloids as σ -acceptors Z-type ligands in MOLP-type structures permits structural and electronic modulation of the basic metal

¹ a) B. Fuentes, M. García-Melchor, A. Lledós, F. Maseras, J. A. Casares, G. Ujaque, P. Espinet, *Chem. Eur. J.*, **2010**, *16*, 8596-8599.

b) M. García-Melchor, B. Fuentes, A. Lledós, J. A. Casares, G. Ujaque, P. Espinet, *J. Am. Chem. Soc.*, **2011**, *133*, 13519–13526.

c) J. del Pozo, G. Salas, R. Álvarez, J. A. Casares, P. Espinet, *Organometallics*, **2016**, *35*, 3604-3611; d) R. J. Oeschger, D. H. Ringger, P. Chen, *Organometallics*, **2015**, *34*, 3888-3892.

² a) N. Hidalgo, C. Maya, J. Campos, *Chem. Commun.*, **2019**, *55*, 8812-8815.

b) S. Jamali, S. Abedanzadeh, N. K. Khaledi, H. Samouei, Z. Hendi, S. Zacchini, R. Kiaa, H. R. Shahsavari, *Dalton Trans.*, **2016**, *45*, 17644-17651.

c) M. K. Karunananda, N. P. Mankad NP *Organometallics*, **2017**, *36*, 220–227.

d) N. P. Mankad *Chem Comm.*, **2018**, *54*, 1291–1302.

e) Y. Zhang, M. K. Karunananda, H. –C. Yu, K. J. Clark, W. Williams, N. P. Mankad, D. H. Ess, D. H. *ACS Catal.*, **2019**, *9*, 2657-2663.

site³, while the strength of the M→M dative bonding in thermally induced⁴ metal-only frustrated Lewis pairs, broadly discussed in Chapter I, deeply impacts the reactivity and catalytic performance of the latter systems⁵. In addition, metal-to-metal dative bonding has important implications in supramolecular and molecular engineering⁶, as well as in host-guest chemistry⁷.

With all this in mind, it becomes obvious that a deep understanding of the nature of metal-to-metal bond in these molecular compounds and supramolecular aggregations will have an important impact in a range of areas. In fact, this has been a matter of intense debate, which is not surprising considering the set of bonding components that may be involved (i.e. ionic, covalent, dative, dispersion...). As such, unsupported systems in which the bond between the two metals is the sole force holding the two fragments together constitute ideal motifs to study since other factors that may obscure bonding analysis are excluded. In their original report, Nowell and Russell postulated that $[(\eta^5\text{-C}_5\text{H}_5)(\text{CO})_2\text{Co}\rightarrow\text{HgCl}_2]$ could be considered a metallic Lewis acid-base adduct⁹, as lately proposed for many other systems^{5a,8},

³ a) B. R. Barnett, C. E. Moore, P. Chandrasekaran, S. Sproules, A. L. Rheingold, S. DeBeerde, J. S. Figueroa, *Chem. Sci.*, **2015**, *6*, 7169-7178.

b) H. Yang, F. P. Gabbaï, *J. Am. Chem. Soc.*, **2015**, *137*, 13425-13432.

c) S. Sen, I.-S. Ke, F. P. Gabbaï, *Organometallics*, **2017**, *36*, 4224-4230.

⁴ T. A. Rokob, A. Hamza, A. Stirling, I. Pápai, *J. Am. Chem. Soc.*, **2009**, *131*, 2029-2036.

⁵ a) M. Devillard, R. Declercq, E. Nicolas, A. W. Ehlers, J. Backs, N. Saffon-Merceron, G. Bouhadir, J. C. Slootweg, W. Uhl, D. Bourissou, *J. Am. Chem. Soc.*, **2016**, *138*, 4917-4926.

b) J. Campos, *J. Am. Chem. Soc.*, **2017**, *139*, 2944-2947.

c) N. Hidalgo, J. J. Moreno, M. Pérez-Jiménez, C. Maya, J. López-Serrano, J. Campos, *Chem. Eur. J.*, **2020**, *26*, 1-13.

⁶ M. J. Katz, K. Sakai, D. B. Leznoff, *Chem. Soc. Rev.*, **2008**, *37*, 1884-1895.

⁷ K. Omoto, S. Tashiro, M. Shionoya, *Z. Anorg. Allg. Chem.*, **2015**, *641*, 2056-2059.

⁸ For some recent examples see: a) H. Braunschweig, R. D. Dewhurst, F. Hupp, C. Schneider, *Chem. Commun.*, **2014**, *50*, 15685-15688.

b) H. Braunschweig, R. D. Dewhurst, F. Hupp, J. Wolf, *Chem. Eur. J.*, **2015**, *21*, 1860-1862.

c) B. R. Barnett, J. S. Figueroa, *Chem. Commun.*, **2016**, *52*, 13829-13839.

including those based on d^8-d^{10} interactions (referred to the last filled subshell of the bonding metals)⁹. An alternative description proposed by Pyykkö implies dispersion forces as the main component of the bimetallic bonding¹⁰. However, more recent computational work speaks in favor of the former assumption, revealing that dispersion forces contribute to a lesser extent in these types of systems compared to the role of electrostatic and orbital interactions¹¹.

Most studies have focused on the synthesis and structural characterization of a group of several MOLPs or on the computational analysis of previously reported bimetallic architectures of this kind. However, a more comprehensive and combined experimental/computational approach to a family of unsupported MOLPs is lacking.

This chapter contains synthetic, structural, and a brief summary of computational studies on a variety of MOLPs generated by combination of the Rh(I) precursor $[(\eta^5\text{-C}_5\text{Me}_5)\text{Rh}(\text{PMe}_3)_2]$ ¹² (**1a**) with well-known metallic and metalloid Lewis acids. The selection of **1a** as the Lewis base was made on the basis of the following features:

d) U. Jayarathne, T. J. Mazzacano, S. Bagherzadeh, N. P. Mankad, *Organometallic*, **2013**, 32, 3986–3992.

e) S. Banerjee, M. K. Karunananda, S. Bagherzadeh, U. Jayarathne, S. R. Parmelee, G. W. Waldhart, N. P. Mankad, *Inorg. Chem.*, **2014**, 53, 11307–11315.

f) M. K. Karunananda, F. X. Vázquez, E. E. Alp, W. Bi, S. Chattopadhyay, T. Shibatake, N. P. Mankad, *Dalton Trans.*, **2014**, 43, 13661–13671.

⁹ a) G. Aullón, S. Alvarez, *Inorg. Chem.*, **1996**, 35, 3137–3144.

b) M.-E. Moret in *Higher Oxidation State Organopalladium and Platinum Chemistry* (Ed.: A. J. Canty) *Topics in Organometallic Chemistry*, Springer: Berlin Heidelberg, **2011**, pp 157–184.

¹⁰ a) P. Pyykkö, J. Li, N. Runeberg, *Chem. Phys. Lett.*, **1994**, 218, 133–138.

b) P. Pyykkö, Y. Zhao, *Angew. Chem. Int. Ed. Engl.*, **1991**, 30, 604–605.

¹¹ a) R. J. Oeschger, P. Chen, *Organometallics*, **2017**, 36, 1465–1468.

b) Eno Paenurk, R. Gershoni-Poranne, P. Chen, *Organometallics*, **2017**, 36, 4854–4863.

c) G. Wang, T. T. Ponduru, Q. Wang, L. Zhao, G. Frenking, H. V. R. Dias, *Chem. Eur. J.*, **2017**, 23, 17222 – 17226.

d) M. Baya, U. Belío, D. Campillo, I. Fernández, S. Fuertes, A. Martín, *Chem. Eur. J.*, **2018**, 24, 13879–13889.

¹² B. Klingert, H. Werner, *Chem. Ber.*, **1983**, 116, 1450–1462.

- Its basic behavior has already been well established¹², in 1983 Werner reported the synthesis of this compound and different types of reactions that showed its basic nature.
- PMe₃ ligands enhance the nucleophilicity of the Rh(I) site compared to its more widely explored carbonyl analog [(η^5 -C₅Me₅)Rh(CO)₂]¹³.
- The robustness of (η^5 -C₅Me₅) ligand prevents undesired reactivity recorded for its unsubstituted (η^5 -C₅H₅) analogue¹⁴.
- As a neutral Lewis base, the combination with neutral acids will minimize the ionic and electrostatic components of the Rh(I)→M bond.
- As a pentacoordinate 18-electron species, insertion reactions into polar bonds of the Lewis acid, or the formation of intermediate alkyl or hydride bridging species¹⁵ that would cloud analysis of the Rh(I)→M bond, will be less favored.
- ¹⁰³Rh is NMR active ($I = 1/2$, 100% abundant), so reactions can be monitored by NMR.

With all this in mind, we have combined **1a** with a variety of *s*, *p*, and *d*-block metals as Lewis acids exploring the formation of new M→M bonds. With the exception of copper and silver complexes, we avoided the extensive use of transition metal electrophiles to circumvent more complex bonding pictures on grounds of their available *d* orbitals. Some of these compounds represent unique examples of bimetallic structures.

¹³ J. W. Kang, P. M. Maitlis, *J. Organomet. Chem.*, **1971**, 26, 393-399.

¹⁴ A. K. Swarnakar, M. J. Ferguson, R. McDonald, E. Rivard, *Dalton Trans.*, **2016**, 45, 6071-6078.

¹⁵ M. J. Butler, M. R. Crimmin, *Chem. Commun.*, **2017**, 53, 1348-1365.

II.2. Results and Discussion

This discussion is divided into four sections. Firstly, the synthesis and structure of the MOLPs formed with the *s*-block acids are described, later a second part is dedicated to MOLPs of metals and metalloids of the *p*-block, while a third part covers the compounds with *d*-block metals. Finally, the last section summarizes the results of the computational studies performed with all the Rh(I) MOLPs synthesized to acquire a fundamental knowledge on the nature of the Rh→M bonding.

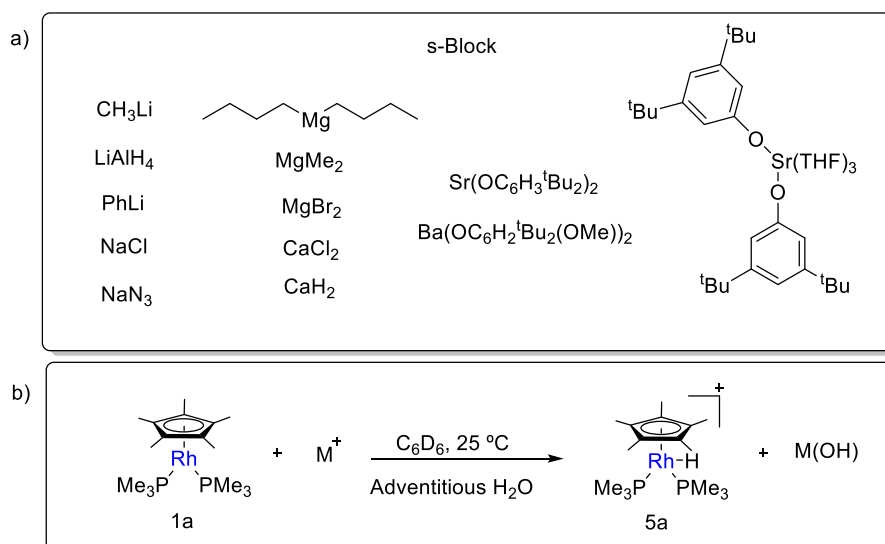
II.2.1. Synthesis of Rh(I) MOLPs with *s*-Block Acids

The number of compounds exhibiting metalphilic interactions between transition and alkali metals is abundant¹⁶. Systems that show identical or even reduced M—M bond distances compared to the sum of their corresponding covalent atomic radii¹⁷ presumably present some degree of bond covalency. We have investigated the reactions between Rh complex **1a** with alkali and alkaline compounds with lithium, sodium, strontium, barium, magnesium and calcium (scheme 1). In all these cases the only Rh-containing species that could be isolated was the Rh(III) hydride **5a**, formed due to the activation of adventitious water, not observing in any case the desired compound with M→M bond. It is assumed that in all those reactions an equivalent amount of the corresponding *s*-block metal hydroxide is formed, though we did not perform additional experiments to ascertain its nature. For further validation, compound **5a** could be independently

¹⁶ K. Jonas, C. Krüger, *Angew. Chem. Int. Ed. Engl.*, **1980**, *19*, 520-537.

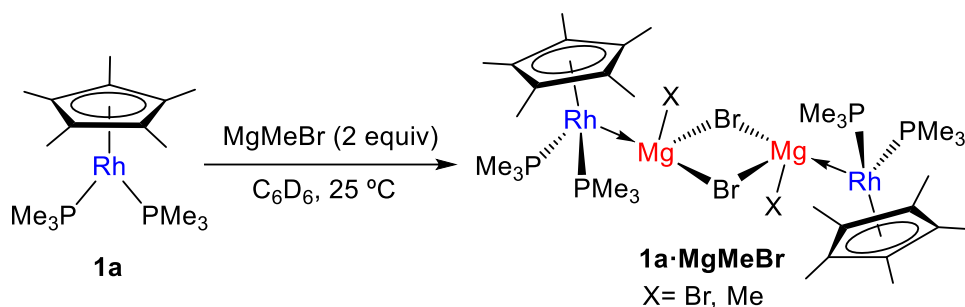
¹⁷ B. Cordero, V. Gómez, A. E. Platero-Prats, M. Revés, J. Echeverría, E. Cremades, F. Barragán, S. Alvarez, *Dalton Trans.*, **2008**, 2832-2838.

synthesized by adding equimolar amounts of ammonium salts to **1a** and it has been utilized as a benchmark species.



Scheme 1: (a) *s*-block precursors which failed to provide Rh→M MOLPs; (b) formation of compound **5a** by bimetallic adventitious water activation (M = *s*-block metal from (a)).

However, the reaction of **1a** with two equivalents of the Grignard reagent MgMeBr readily yielded a new species **1a·MgMeBr** (Scheme 2) characterized by a sharp decrease of the ¹J_{PRh} coupling constant to 172 Hz, (216 Hz for **1a**) along with shifts of the ³¹P{¹H} (δ = -10.2 ppm) and pentamethylcyclopentadienyl ¹H (δ = 1.87 ppm) NMR signals towards lower frequencies in comparison with the same parameters for complex **1a** (³¹P{¹H}, δ = -6.6 ppm and ¹H, δ = 2.17).



Scheme 2. Synthesis of metal-only Lewis pairs by combination of **1a** and *s*-block metal precursor MgMeBr.

Despite the high instability of **1a·MgMeBr**, single crystals suitable for X-ray diffraction studies were grown from diluted benzene solutions and revealed the dimeric structure $[(\eta^5\text{-C}_5\text{Me}_5)(\text{PMe}_3)_2\text{Rh}\rightarrow\text{Mg}(\text{Me}_x\text{Br}_{1-x})(\mu\text{-Br})]_2$ (Figure 1) in which the methyl group bound to magnesium is mostly exchanged by a bromide nucleus¹⁸ (Me:Br with 15:85 occupancies). Using an equimolar amount of the Grignard reagent did not provide full conversion of **1a**, while the addition of MgBr₂ or MgMe₂ to access a MOLP without substitutional disorder proved unsuccessful (see Scheme 1), partly due to solubility issues.

¹⁸ R. M. Peltzer, O. Eisenstein, A. Nova, M. Cascella, *J. Phys. Chem. B.*, **2017**, *121*, 4226-4237.

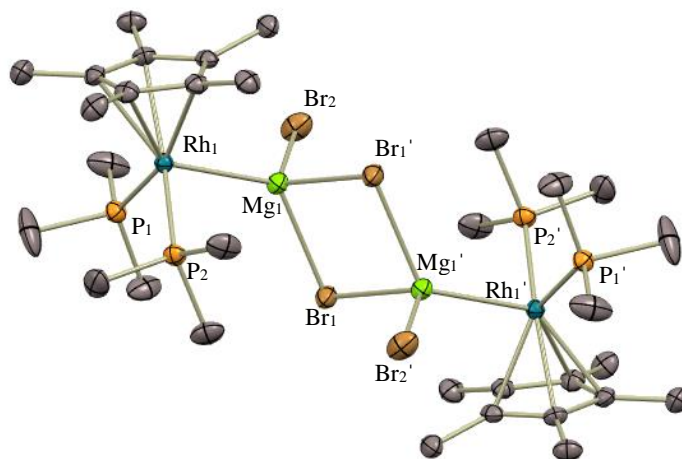


Figure 1. ORTEP diagram of compound **1a·MgMeBr**.

(Unless otherwise noted, in all ORTEPs of this Thesis, for the sake of clarity, hydrogen atoms and solvent molecules are excluded, while thermal ellipsoids are set at 50 % probability.)

As expected, MOLP **1a·MgMeBr** adopts a piano-stool conformation after coordination of the Lewis acid. The Rh→Mg bond distance accounts for 2.651(3) Å, shortened by *ca.* 0.2 Å with respect to the sum of the covalent radii (2.83Å)¹⁷, thus indicative of bond covalency (*vide infra*). Two other parameters, namely d_{rel} ⁷ (0.94) and *fsr* (formal shortness ratio)¹⁹ (1.01), defined as the ratio between the M—M bond distance and the sum of either the covalent radii or the metallic radii, respectively, underpin this assumption. The average Rh—P bond distance accounts for 2.246(2)Å, with a P-Rh-P angle of 95.09(8) and a distance between Rh and the Cp* centroid of C₅Me₅ of 1.958(7)Å, all normal values for piano-stool Rh compounds.

It is worth of note that this exotic structure is the first unambiguous example of an unsupported Rh→Mg bond, since the only prior related

¹⁹ L. Pauling, *J. Am. Chem. Soc.*, **1947**, 69, 542-553.

example, reported by Crimmin, contains a metal hydride that exhibits some degree of bridging character²⁰. Moreover, despite the extensive use of Grignard reagents in organometallic chemistry, it is surprising that compound **1a·MgMeBr** seems to be the only Mg-based MOLP comprised of neutral fragments²¹.

As stated above, the choice of rhodium as the Lewis base was in part made attending to its NMR activity. To observe chemical shifts associated to ¹⁰³Rh centers we employed a cross polarization approach by means of HMQC experiments through its coupling to ³¹P nuclei (Figure 2).

²⁰ O. Ekkert, A. J. P. White, H. Toms, M. R. Crimmin, *Chem. Sci.* **2015**, *6*, 5617-5622.

²¹ Previously reported magnesium MOLPs are based on cationic magnesium fragments. See for example:

a) M. P. Blake, N. Kaltsoyannis, P. Mountford, *J. Am. Chem. Soc.*, **2015**, *137*, 12352-12368.

b) J. Hicks, C. E. Hoyer, B. Moubaraki, G. L. Manni, E. Carter, D. M. Murphy, K. S. Murray, L. Gagliardi, C. Jones, *J. Am. Chem. Soc.*, **2014**, *136*, 5283-5286.

c) M. P. Blake, N. Kaltsoyannis, P. Mountford, *Chem. Commun.*, **2013**, *49*, 3315-3317.

d) J. T. Golden, T. H. Peterson, P. L. Holland, R. G. Bergman, R. A. Andersen, *J. Am. Chem. Soc.*, **1998**, *120*, 223-224.

e) W. Kaschube, K.-R. Pörschke, K. Angermund, C. Krüger, G. Wilke, *Chem. Ber.*, **1988**, *121*, 1921-1929.

f) M. Ohashi, K. Matsubara, T. Iizuka, H. Suzuki, *Angew. Chem., Int. Ed.*, **2003**, *42*, 937-940.

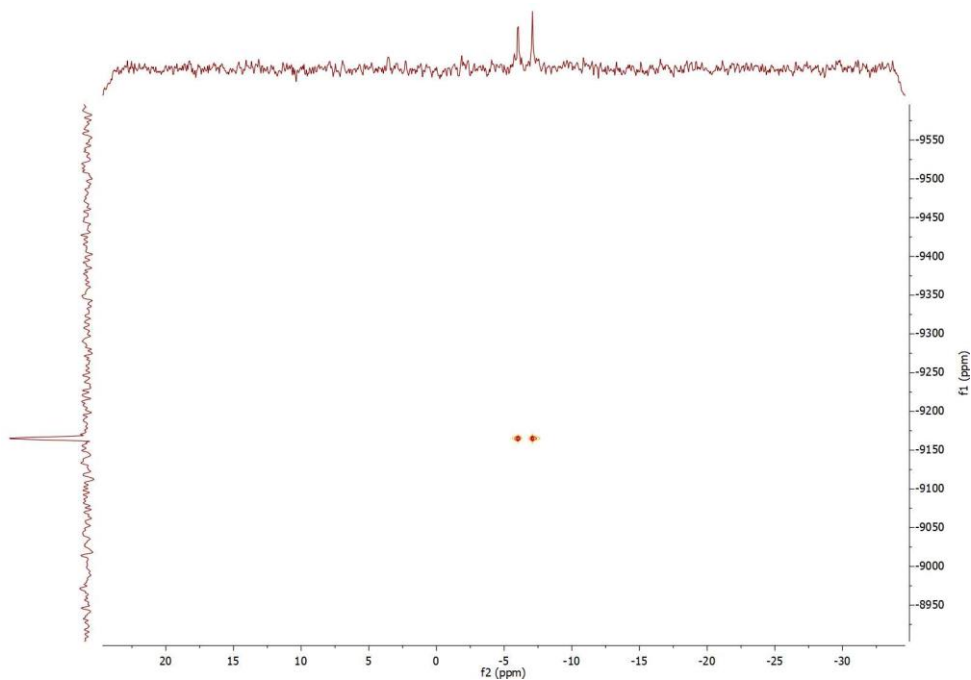


Figure 2. Cross polarization experiment (HMQC) $^{103}\text{Rh}\{^1\text{H}\}\text{-}^{31}\text{P}\{^1\text{H}\}$ NMR spectra of **1a**.

Considering its low sensitivity and rather wide chemical shift range (*ca.* 12000 ppm)²², this strategy enormously facilitates the acquisition of ^{103}Rh NMR data. The new MOLPs are characterized by $^{103}\text{Rh}\{^1\text{H}\}$ NMR resonances shifted to lower frequencies compared to precursor **1a** (-9165 ppm), with **1a**·**MgMeBr** exhibiting a signal at -9404 ppm (Figure 3).

²² N. Sheng Loong Tan, G. L. Nealon, J. M. Lynam, A. N. Sobolev, M. R. Rowles, M. I. Ogden, M. Massi, A. B. Lowe, *Dalton Trans.*, **2019**, 48, 16437-16447.

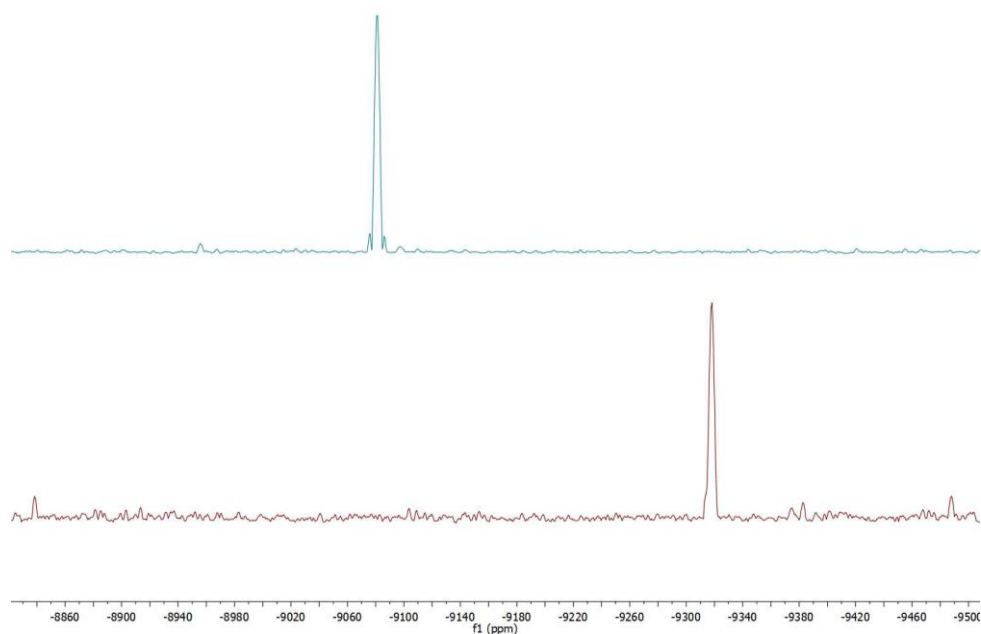


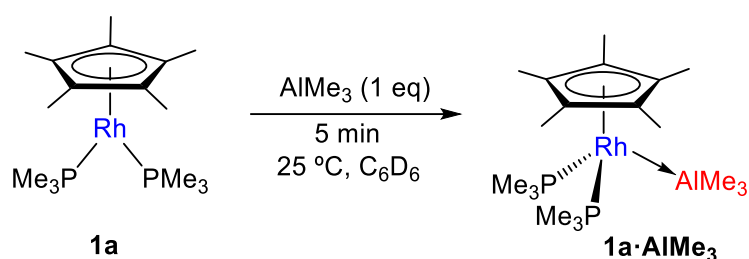
Figure 3. $^{103}\text{Rh}\{^1\text{H}\}$ NMR spectra of **1a** (green) and **1a**·**MgMeBr** (red) obtained from cross polarization experiments (HMQC).

II.2.2. Synthesis of Rh(I) MOLPs with *p*-Block Acids

Moving to the *p*-block we examined the reactivity of **1a** with widely used metalloid precursors of the group 13 and 14, more precisely AlCl_3 , AlMe_3 , GaCl_3 , GeCl_2 ·dioxane, and SnCl_2 . Tricoordinate group 14 species have been widely exploited as Lewis acids but heavier tetrylenes (i.e. $:\text{GeCl}_2$, $:\text{SnCl}_2$) exhibit ambiphilic behavior due to the joint presence of a lone electron pair that can be donated and an empty *p* orbital which can accept a pair of electrons.

The objective of this work is to obtain both types of MOLPs with the purpose of later providing a comparison of the bonding scheme between each other. The reactions of **1a** with either AlCl_3 or GaCl_3 were unsuccessful. In the case of AlCl_3 , the formation of intractable mixtures was

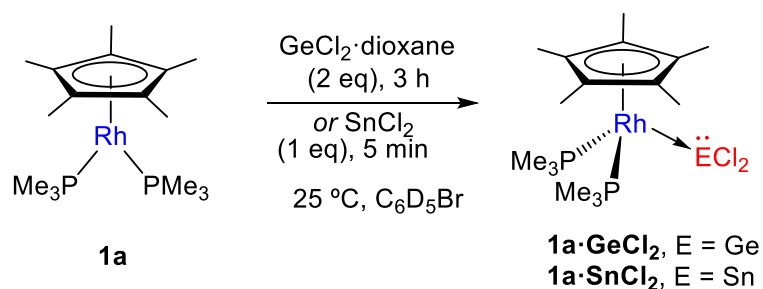
observed while the mixture with GaCl₃ resulted in the precipitation of a highly insoluble material. That is not surprising considering previously reported difficulties to access Rh-alane MOLPs by direct combination of the two metal fragments²³. However, the addition of one equivalent of AlMe₃ (toluene solution, 1M) to a benzene solution of **1a** resulted in clean formation of the corresponding **1a·AlMe₃** MOLP (Scheme 3).



Scheme 3. Synthesis of Rh(I) MOLPs with AlMe₃.

The same occurs by adding GeCl₂·dioxane or SnCl₂ to bromobenzene solutions of the rhodium precursor to yield **1a·GeCl₂** and **1a·SnCl₂**, respectively, although a longer reaction time was needed for the Ge derivate which required three hours for completion while the tin MOLP formed immediately. Another difference occurred in the reaction with germanium, two equivalents of GeCl₂·dioxane were required to achieve full consumption of **1a**, probably because the second germanium facilitates dioxane withdrawal from the coordinating GeCl₂ terminus (Scheme 4).

²³ A. Hofmann, A. Lamprecht, J. O. C. Jiménez-Halla, T. Tröster, R. D. Dewhurst, C. Lenczyk, H. Braunschweig, *Chem. Eur. J.*, **2018**, *24*, 11795-11802.



Scheme 4. Synthesis of Rh(I) MOLPs with tetrylenes dihalides and AlMe_3 .

Multinuclear NMR spectroscopic analysis illustrates the formation of the new MOLPs exhibiting the same distinctive features commented above (Table 1), that is, a marked decrease of the $^1J_{\text{PRh}}$ coupling constant of *ca.* 40 Hz and a displacement to lower frequencies of the ^1H NMR signal due to the pentamethylcyclopentadienyl ring. For the tin analogue, we could also detect a broad $^{119}\text{Sn}\{^1\text{H}\}$ NMR signal at 810.7 ppm, while $\text{1a} \cdot \text{AlMe}_3$ provides a distinctive ^1H NMR singlet at -0.1 ppm due to the Al-bound methyl termini, with a corresponding $^{13}\text{C}\{^1\text{H}\}$ NMR signal at 1.0 ppm. Interestingly, $^{103}\text{Rh}\{^1\text{H}\}$ NMR resonances due to the tetrylene MOLPs appear upshifted by *ca.* 400 ppm ($\delta = -8756$, $\text{1a} \cdot \text{GeCl}_2$; -8836 ppm, $\text{1a} \cdot \text{SnCl}_2$) compared to 1a ($\delta = -9165$ ppm), contrasting with the other main-group based MOLPs reported herein.

Table 1. Selected NMR spectroscopic data.

Compound	$^1\text{H}, \delta$ (C_5Me_5)	$^1\text{H}, \delta$ (PMe_3)	$^1J_{\text{PRh}}$ (Hz)	$^{31}\text{P}\{^1\text{H}\}, \delta$	$^{103}\text{Rh}\{^1\text{H}\},$ [a] δ
$\text{1a} \cdot \text{GeCl}_2$	1.67	1.55	171	-7.0	-8756
$\text{1a} \cdot \text{SnCl}_2$	1.67	1.56	169	-8.5	-8836
$\text{1a} \cdot \text{AlMe}_3$	1.67	1.10	181	-6.9	-9272

[a] ^{103}Rh NMR data referenced to $\text{Rh}(\text{acac})_3$

Single-crystals of compounds **1a·GeCl₂**, **1a·SnCl₂**, and **1a·AlMe₃** amenable to X-ray diffraction studies were grown by slow diffusion of pentane into their benzene or bromobenzene solutions, once more revealing the piano stool configuration around the rhodium center after coordination to the Lewis acids (Figure 4). The unsupported M—M bond distances for **1a·GeCl₂** (2.501(1) Å) and **1a·SnCl₂** (2.687(3) Å) are slightly shorter than the sum of their covalent radii ($r_{\text{Rh+Ge}} = 2.62$ Å; $r_{\text{Rh+Sn}} = 2.81$ Å)¹⁷, while that of **1a·AlMe₃** (2.635(4) Å) is identical to the expected theoretical value for a covalent interaction (2.63 Å)¹⁷. The most relevant bond distances and angles are listed in Table 2.

Table 2. X-ray data of crystal **1a·GeCl₂**, **1a·SnCl₂**, and **1a·AlMe₃**.

MOLP	d_{RhM} (Å)	$d_{\text{RhP}}^{[\text{a}]}$ (Å)	$d_{\text{RhCp}^*}^{[\text{b}]}$ (Å)	PRhP (°)
1a·GeCl₂	2.501(1)	2.268(1)	1.978(5)	94.67(6)
1a·SnCl₂	2.687(3)	2.266(1)	1.968(4)	93.72(3)
1a·AlMe₃	2.635(4)	2.244(4)	1.964(4)	95.30(2)

[a] $d_{\text{Rh—P}}$ = average Rh—P bond distance. [b] $d_{\text{Rh—Cp}^*}$ = distance between Rh and the centroid of C₅Me₅.

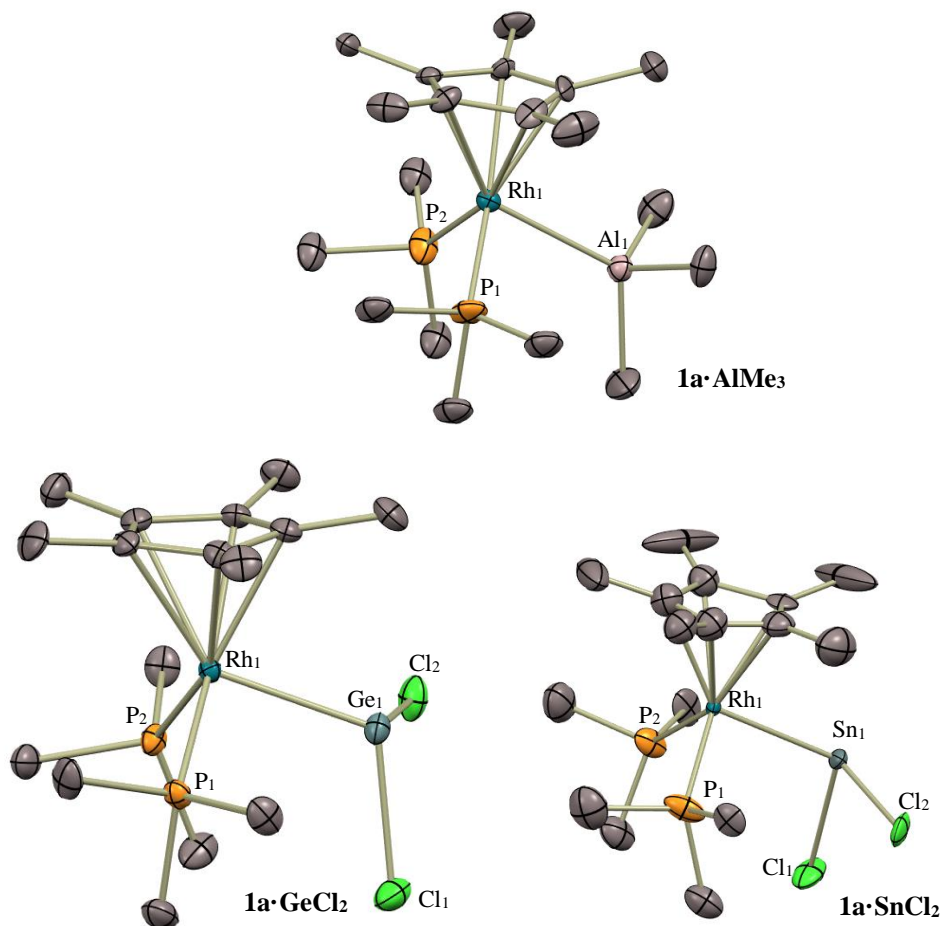


Figure 4. ORTEP diagram of compounds **1a·AlMe₃**, **1a·GeCl₂** and **1a·SnCl₂**.

The asymmetric unit of structure **1a·GeCl₂** contains four independent molecules of the MOLP, being the aforementioned Rh→Ge bond distance the average for all of them. The solid-state structures of **1a·GeCl₂** and **1a·SnCl₂** unveil a strong pyramidalization of the tetrel moiety, as seen in other related systems based on platinum²⁴. However, this

²⁴ a) A. V. Zabula, T. Pape, A. Hepp, F. E. Hahn, *Dalton Trans.*, **2008**, 5886-5890.

b) D. Heitmann, T. Pape, A. Hepp, C. Muck-Lichtenfeld, S. Grimme, F. E. Hahn, *J. Am. Chem. Soc.*, **2011**, *133*, 11118-11120.

c) H. Braunschweig, A. Damme, R. D. Dewhurst, F. Hupp, J. O. C. Jimenez- Halla, K. Radacki, *Chem. Commun.*, **2012**, *48*, 10410-10412.

is not the case in other metallic complexes with bound tetrel and a planar disposition around the group 14 element²⁵. It has been noticed that pyramidalization requires both coordination to strongly Lewis basic metals and a non-directional lone pair^{24d}, features fulfilled for **1a·ECl₂** (E = Ge, Sn). Since the lone pair on stannylene dichloride has more pronounced *s*-character than that in its germylene analogue, the directionality of the former is decreased, and as such a higher pyramidalization is anticipated for **1a·SnCl₂**. In fact, the pyramidalization angle estimated by the POAV method of Haddon²⁶ for **1a·SnCl₂** (26.2) surpasses that of **1a·GeCl₂** (24.4).

To the best of our knowledge, compounds **1a·GeCl₂** and **1a·SnCl₂** represent the first examples of rhodium-bound germylene and stannylene non-stabilized by the coordination of a base. All prior structures containing Rh—E(II) (E = Ge, Sn) bonds involve tetrel centers bearing an additional intra- or intermolecular Lewis donor²⁷.

As introduced earlier, the preparation of a Rh-alane adduct by direct combination of the two metal fragments, as reported herein, had so far been unsuccessful. The first crystallographically characterized Rh-alane adduct was reported by Braunschweig relying on the transmetalation of the alane

d) F. Hupp, M. Ma, F. Kroll, J. O. C. Jimenez-Halla, R. D. Dewhurst, K. Radacki, A. Stasch, C. Jones, H. Braunschweig *Chem. Eur. J.*, **2014**, *20*, 16888-16898.

²⁵ H. Arp, J. Baumgartner, C. Marschner, P. Zark, T. Müller, *J. Am. Chem. Soc.*, **2012**, *134*, 10864-10875.

²⁶ R. C. Haddon, *J. Phys. Chem. A.*, **2001**, *105*, 4164-4165.

²⁷ a) L. Á. Ivarez-Rodríguez, J. A. Cabeza, J. M. Fernandez-Colinas, P. García-Álvarez, D. Polo, *Organometallics*, **2016**, *35*, 2516-2523. b) D. Matioszek, N. Saffon, J.-M. Sotiropoulos, K. Miqueu, A. Castel, J. Escudie, *Inorg. Chem.*, **2012**, *51*, 11716-11721. c) J.M. García, E. Ocando-Mavárez, T. Kato, D. Santiago-Coll, A. Briceno, N. Saffon-Merceron, A. Baceiredo, *Inorg. Chem.*, **2012**, *51*, 8187-8193. d) M. Veith, A. Müller, L. Stahl, M. Nötzel, M. Jarczyk, V. Huch, *Inorg. Chem.*, **1996**, *35*, 3848-3855. e) M. L. B. Ismail, F.-Q. Liu, W.-L. Yim, R. Ganguly, Y. Li, C.-W. So, *Inorg. Chem.*, **2017**, *56*, 5402-5410. f) M. Kilian, H. Wadepohl, L. H. Gad, *Eur. J. Inorg. Chem.*, **2008**, 1892-1900. g) J. Martincová, R. Dostálová, L. Dostál, A. Růžička, R. Jambo, *Organometallics*, **2009**, *28*, 4823-4828.

from [(PCy₃)₂Pt→AlCl₃] to [(η⁵-C₅H₅)Rh(PMe₃)₂]²⁸. The Rh→Al bond distance in **1a**·AlMe₃ is considerably elongated by around 0.2 Å relative to the two previously reported Rh-alane adducts based on AlCl₃²³, as expected for the less acidic AlMe₃. This diminished acidity may explain the absence of previous unsupported transition metal MOLPs containing trimethylaluminum, being **1a**·AlMe₃ the first of its kind²⁹. Once more, this is an unexpected finding considering the extensive use of AlMe₃ as a methylating agent or in transition metal catalyzed polymerization.

II.2.3. Synthesis of Rh(I) MOLPs with *d*-Block Acids

To complete this work, MOLPs with *d*-block acids have also been investigated. In particular, we examined the equimolar combination of **1a** with commercial compounds [Cp₂ZrCl₂], Ti[OCH(CH₃)₂]₄, Y(OTf)₃ and La(OTf)₃. However, we could not obtain the targeted Rh MOLP in neither of these cases due to formation of the rhodium hydride **5a**, intractable mixture of products or complete unreactivity. Nonetheless, well-behaved bimetallic adducts of Zn and Cu were obtained and will be discussed in the following paragraphs.

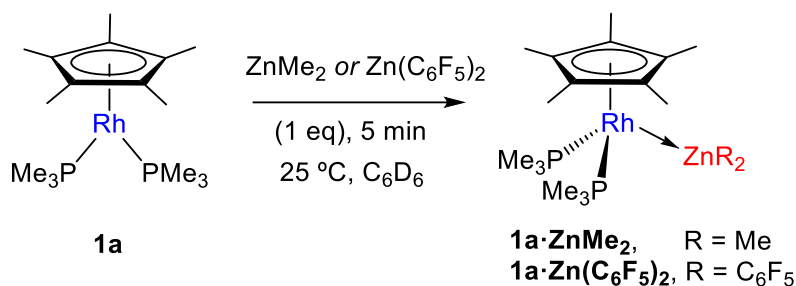
With regard to zinc, we decided to check the reactivity of **1a** with two common precursors, more precisely ZnMe₂ and Zn(C₆F₅)₂. Complexes **1a**·ZnMe₂ and **1a**·Zn(C₆F₅)₂ were immediately formed after addition of one

²⁸ a) J. Bauer, H. Braunschweig and K. Radacki, *Chem. Commun.*, **2012**, 48, 10407-10409. b) A related Rh/Al species was earlier disclosed, though the Rh—Al interaction may not be described as dative bond: J. M. Mayer and J. C. Calabrese, *Organometallics*, **1984**, 3, 1292-1298.

²⁹ Previous examples contain AlMe₃ as a bridging motif or bound to *p*-block metals and metalloids: a) Z. Weng, S. Teo, L. L. Kohb, T. S. A. Hor, *Chem. Commun.*, **2006**, 1319-1321. b) M. Oishi, M. Oshima, H. Suzukib *Inorg. Chem.*, **2014**, 53, 6634-6654. c) S. Ogoshi, M. Ueta, T. Arai, H. Kurosawa, *J. Am. Chem. Soc.*, **2005**, 127, 12810-12811. d) S. Schulz, A. Kuczkowski, M. Nieger *J. Organomet. Chem.*, **2000**, 604, 202-207. e) K. Zeckert, *Dalton Trans.*, **2012**, 41, 14101-14106.

equivalent of the organometallic zinc substrate over a benzene solution of **1a** (Scheme 4). These complexes exhibit sharp $^{31}\text{P}\{^1\text{H}\}$ NMR signals at 6.9 ($^1J_{\text{PRh}} = 192$ Hz) and -7.2 ppm ($^1J_{\text{PRh}} = 167$ Hz), respectively. The noticeable decrease of the $^1J_{\text{PRh}}$ coupling constants relative to **1a** ($^1J_{\text{PRh}} = 216$ Hz) evidences formation of Rh \rightarrow Zn MOLPs.

The pentamethylcyclopentadienyl ^1H NMR signals (1.76 ppm for **1a** \cdot ZnMe $_2$; 1.59 ppm for **1a** \cdot Zn(C $_6$ F $_5$) $_2$) are shifted towards lower frequencies in comparison with that of complex **1a** (2.17 ppm) and their corresponding $^{103}\text{Rh}\{^1\text{H}\}$ NMR resonances appear downshifted to -9212 (**1a** \cdot ZnMe $_2$) and -9355 (**1a** \cdot Zn(C $_6$ F $_5$) $_2$) ppm (-9165 ppm for **1a**).



Scheme 5. Synthesis of Rh(I) MOLPs with electrophiles ZnMe $_2$ and Zn(C $_6$ F $_5$) $_2$.

Crystals of **1a** \cdot ZnMe $_2$ and **1a** \cdot Zn(C $_6$ F $_5$) $_2$ were grown by slow diffusion of pentane into their benzene solutions. The main geometric parameters of these and prior structures already discussed within this Chapter are collected in Table 4. The larger acidity of the fluorinated zinc moiety is reflected in a shorter Rh \rightarrow Zn bond distance of 2.484(1) Å in **1a** \cdot Zn(C $_6$ F $_5$) $_2$ compared to that in **1a** \cdot ZnMe $_2$ ($d_{\text{RhZn}} = 2.618(1)$ Å), attesting as well that steric effects may be less relevant (Figure 5). Nonetheless, both Rh \rightarrow Zn distances account for less than the sum of the corresponding covalent radii (2.64 Å) 17 , suggesting a strong metal-metal interaction. These two complexes constitute the first unsupported MOLPs exhibiting a dative

Rh→Zn bond and constructed around neutral fragments^{20,30}. Structures like these are presumably relevant intermediates during Rh(I)-catalyzed Negishi coupling reactions^{30e,31}. Mechanistic studies have permitted to isolate a Rh/Zn complex derived from insertion of the rhodium center into one of the Zn—C bonds in diphenylzinc^{31b}, whose likely precursor consists in a Lewis adduct akin to **1a**·ZnMe₂ or **1a**·Zn(C₆F₅)₂.

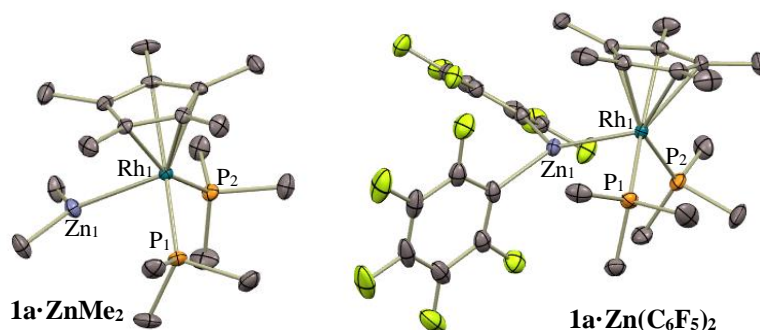


Figure 5. ORTEP diagrams of compounds **1a**·ZnMe₂ and **1a**·Zn(C₆F₅)₂.

Table 3. X-ray data of crystal **1a**·Zn(C₆F₅)₂ and **1a**·ZnMe₂.

MOLP	d_{RhM} (Å)	$d_{\text{RhP}}^{[\text{d}]}$ (Å)	$d_{\text{RhCp}^*}^{[\text{e}]}$ (Å)	PRhP (°)
1a ·Zn(C ₆ F ₅) ₂	2.484(1)	2.253(6)	1.925(4)	93.13(2)
1a ·ZnMe ₂	2.618(1)	2.234(1)	1.950(5)	93.28(6)

³⁰ a) J. J. Gair, Y. Qiu, R. L. Khade, N. H. Chan, A. S. Filatov, Y. Zhang, J. C. Lewis, *Organometallics*, **2019**, *38*, 1407-1412.

b) T. Cadenbach, T. Bollermann, C. Gemel, M. Tombul, I. Fernandez, M. V. Hopffgarten, G. Frenking, R. A. Fischer, *J. Am. Chem. Soc.*, **2009**, *131*, 16063-16077.

c) M. Molon, T. Cadenbach, T. Bollermann, C. Gemel, R. A. Fischer, *Chem. Commun.*, **2010**, *46*, 5677-5679.

d) O. Ekkert, A. J. P. White, M. R. Crimmin, *Angew. Chem.*, **2016**, *128*, 16265-16268.

e) C. J. Pell, W.-C. Shih, S. Gatard, O. V. Ozerov, *Chem. Commun.*, **2017**, *53*, 6456-6459.

f) M. D. Fryzuk, D. H. McConville, S. J. Rettig, *Organometallics*, **1990**, *9*, 1359-1360.

³¹ a) H. Takahashi, S. Inagaki, N. Yoshii, F. Gao, Y. Nishihara, K. Takagi, *J. Org. Chem.*, **2009**, *74*, 2794-2797.

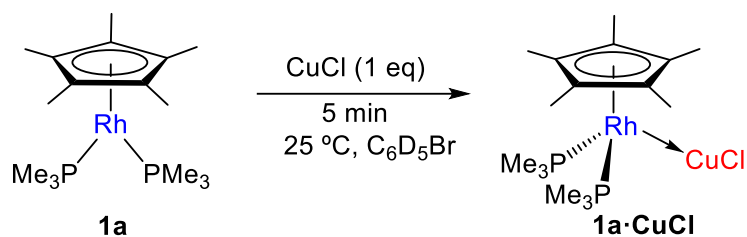
b) S. Ejiri, S. Odo, H. Takahashi, Y. Nishimura, K. Gotoh, Y. Nishihara, K. Takagi, *Org. Lett.*, **2010**, *12*, 1692-1695.

[a] $d_{\text{Rh-P}}$ = average Rh—P bond distance. [b] $d_{\text{Rh-Cp}^*}$ = distance between Rh and the centroid of C_5Me_5 .

Table 4. Main bond distances and angles for the X-ray structures presented throughout this chapter.

MOLP	<i>Centroide</i> (°)	<i>Centroide</i> (°)	PRhP (°)	PRhE (°)
1a·MgMeBr	129.4 127.10	113.40	95.10	91.71 87.33
1a·AlMe₃	127.65 127.10	118.35	95.26	87.89 88.58
1a·GeCl₂	126.84 126.54	112.78	95.15	91.85 94.71
1a·SnCl₂	127.49 126.45	112.00	95.60	95.81 90.09
1a·ZnMe₂	131.73 130.4	108.62	93.29	91.04 87.51
1a·Zn(C₆F₅)₂	128.51 129.52	114.22	93.13	95.81 90.09

Reaction with copper precursors, whose acidity is also well-recognized, proved more problematic. Reaction with CuOTf (OTf⁻ = CF₃SO₃⁻) or AgNTf₂ (NTf₂⁻ = (CF₃SO₂)₂N⁻) resulted in complex mixtures that involve a number of rhodium compounds as inferred from the presence of several doublets in the corresponding ³¹P{¹H} NMR spectra. In contrast, addition of one equivalent of CuCl over a bromobenzene solution of **1a** cleanly provided a new species (**1a·CuCl**) characterized by a ³¹P{¹H} NMR doublet at -3.0 ppm and a phosphorus-rhodium coupling constant of 144 Hz, once again suggesting the formation of a dative bond between the two metals (Scheme 6).



Scheme 6. Synthesis of Rh(I) MOLPs with the electrophile CuCl.

The corresponding $^{103}\text{Rh}\{^1\text{H}\}$ signal resonates at -8540 ppm, shifted to higher frequencies compared to **1**. This contrasts with all other MOLPs described herein except those containing ambiphilic tetrylenes, which speaks in favor of some differences in the bonding situation between the MOLPs involving purely acidic fragments and those where some degree of back-donation may be anticipated (i.e. those based on Ge, Sn, and Cu).

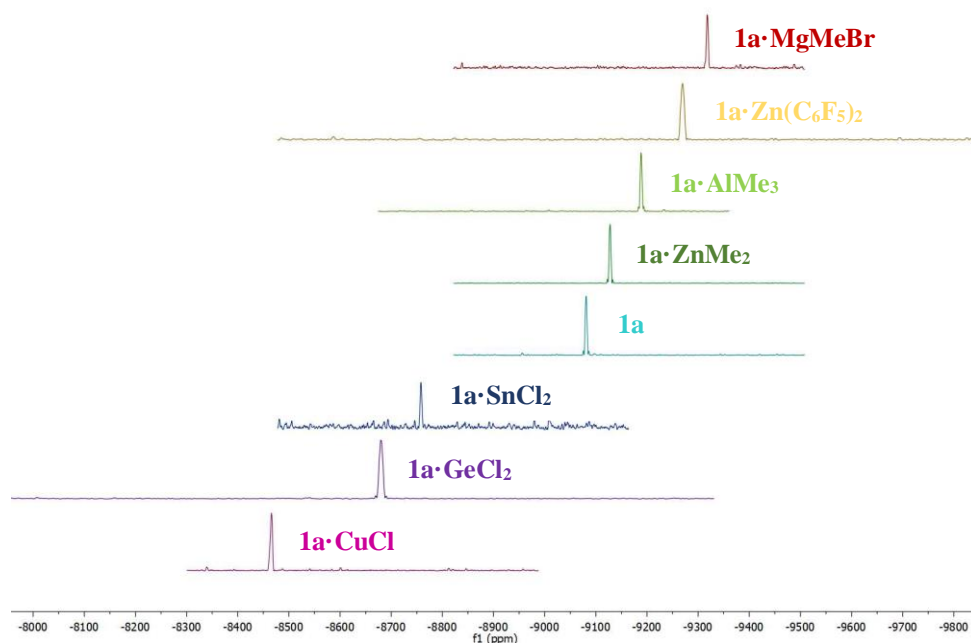


Figure 6. $^{103}\text{Rh}\{^1\text{H}\}$ NMR spectra of **1a** and Rh \rightarrow -based MOLPs obtained from cross polarization experiments (HMQC).

Regarding the copper adduct, attempts to grow single crystals of **1**·CuCl were unfruitful, partly because of the low solubility of the adduct which caused rapid precipitation in most cases. This fact, along with non-definitive diffusion spectroscopic studies, prevented us to obtain a clear picture of its molecular structure. In principle, both a monomeric or dimeric nature could be proposed. To discern between these two possibilities DFT calculations were performed as an independent work to this thesis and the main results are discussed in the following section. However, attempts to optimize a dimeric species of type $[(\eta^5\text{-C}_5\text{Me}_5)\text{Rh}(\text{PMe}_3)_2\text{Cu}(\mu\text{-Cl})]_2$ resulted in cleavage of the chloride bridges, supporting an unbridged formulation for **1a**·CuCl. It is interesting to note that this species represents a rare case of Rh→Cu MOLP, with prior complexes bearing a Rh→Cu bond typically relying on the stability conferred by bridging ligands³², the use of cationic copper fragments³³ or the coordination of the neutral copper halide as a bridging motif³⁴.

II.2.4. Computational analysis of Rh→M bonding in Rh(I) MOLPs

The nature of the Rh→M interactions in the bimetallic adducts has been investigated by DFT calculations, analysis of the calculated electron densities of the adducts within the Atoms In Molecules theory (AIM)³⁵ and

³² a) D. Schneider, H. Werne, *Organometallics*, **1993**, 12, 4420-4430.

b) H. Werner, J. Wolf, G. Müller, C. Krüger, *J. Organomet. Chem.*, **1988**, 342, 381-398.

³³ a) M. U. Pilotti, I. Topaloglu, F. G. A. Stone, *J. Chem. Soc. Dalton Trans.* **1991**, 1355-1360.

b) M. J. Fernandez, J. Modrego, L. A. Oro, M.-C. Apreda, F. H. Cano, C. Foces-Foces, *J. Chem. Soc. Dalton Trans.*, **1989**, 1249-1252.

c) C. G. Arena, F. Faraone, M. Lanfranchi, E. Rotondo, A. Tiripicchio. *Inorg. Chem.*, **1992**, 31, 4797-4802.

³⁴ G. Bruno, S. L. Schiavo, E. Rotondo, P. Piraino, F. Faraone, *Organometallics*, **1987**, 6, 2502-2507.

³⁵ R. F. W. Bader, *Atoms in Molecules: A Quantum Theory*, Oxford University Press, Oxford, **1995**.

Natural Bonding Orbitals (NBO) analysis³⁶. Although this theoretical work is independent of this Thesis, a relevant summary of the results is given below.

Optimized geometries of the adducts in bulk solvent were obtained by DFT methods (SMD- ω B97XD/6-31g(d,p)/SDD level)³⁷ with the Gaussian09 software³⁸ and in good agreement with the X-ray diffraction geometries available (RMSD for all geometries is 0.58 Å). In particular, the calculated Rh→M distances remain equal or below the sum of the covalent radii of the two atoms¹⁷. Optimized geometries for the Cu adduct was also calculated as a monomeric species and the calculations afforded a Rh→M distance of 2.37 Å ($\sum_{\text{cov radii}} = 2.74$ Å).

-
- ³⁶ a) J. P. Foster, F. Weinhold, *J. Am. Chem. Soc.*, **1980**, *102*, 7211-7218.
b) A. E. Reed, L. A. Curtiss, F. Weinhold, *Chem. Rev.*, **1988**, *88*, 899-926.
c) E. D. Glendening, C. R. Landis, F. Weinhold, *J. Comput. Chem.*, **2013**, *34*, 1429-1437.
d) E. D. Glendening, J. K. Badenhoop, A. E. Reed, J. E. Carpenter, J. A. Bohmann, C. M. Morales, C. R. Landis, F. Weinhold, NBO 6.0.; *Theoretical Chemistry Institute*, University of Wisconsin: Madison, **2013**. Available at: www.chem.wisc.edu
³⁷a) A. V. Marenich, C. J. Cramer, D. G. Truhlar, *J. Phys. Chem. B*, **2009**, *113*, 6378-6396.
b) J.-D. Chai, M. Head-Gordon, *Phys. Chem. Chem. Phys.*, **2008**, *10*, 6615-6620.
c) R. Ditchfield, W. J. Hehre, J. A. Pople, *J. Chem. Phys.*, **1971**, *54*, 724-728.
d) J.-P. Blaudeau, M. P. McGrath, L. A. Curtiss, L. Radom, *J. Chem. Phys.*, **1997**, *107*, 5016-5021.
e) M. M. Francl, W. J. Pietro, W. J. Hehre, J. S. Binkley, M. S. Gordon, D. J. DeFrees, J. A. Pople, *J. Chem. Phys.*, **1982**, *77*, 3654-3665.
f) V. A. Rassolov, J. A. Pople, M. A. Ratner, T. L. Windus, *J. Chem. Phys.*, **1998**, *109*, 1223-1229.
³⁸ Gaussian 09, Revisions B.01 and E.01, M. J. Frisch, G. W. Trucks, H. B. Schlegel, G. E. Scuseria, M. A. Robb, J. R. Cheeseman, G. Scalmani, V. Barone, G. A. Petersson, H. Nakatsuji, X. Li, M. Caricato, A. Marenich, J. Bloino, B. G. Janesko, R. Gomperts, B. Mennucci, H. P. Hratchian, J. V. Ortiz, A. F. Izmaylov, J. L. Sonnenberg, D. Williams-Young, F. Ding, F. Lipparini, F. Egidi, J. Goings, B. Peng, A. Petrone, T. Henderson, D. Ranasinghe, V. G. Zakrzewski, J. Gao, N. Rega, G. Zheng, W. Liang, M. Hada, M. Ehara, K. Toyota, R. Fukuda, J. Hasegawa, M. Ishida, T. Nakajima, Y. Honda, O. Kitao, H. Nakai, T. Vreven, K. Throssell, J. A. Montgomery, Jr., J. E. Peralta, F. Ogliaro, M. Bearpark, J. J. Heyd, E. Brothers, K. N. Kudin, V. N. Staroverov, T. Keith, R. Kobayashi, J. Normand, K. Raghavachari, A. Rendell, J. C. Burant, S. S. Iyengar, J. Tomasi, M. Cossi, J. M. Millam, M. Klene, C. Adamo, R. Cammi, J. W. Ochterski, R. L. Martin, K. Morokuma, O. Farkas, J. B. Foresman, and D. J. Fox, Gaussian, Inc., Wallingford CT, **2016**.

Topological analysis of the electron density was carried out with the AIM methods and the Multiwfn software³⁹ from wavefunctions calculated at the SMD- ω B97XD/6-311++g(2d,p)/Sapporo-TZP level⁴⁰ with the previously optimized geometries. This study located bond critical points (BCPs) in the electron density and unique bond paths connecting the Rh and M atoms for all adducts (Figure 7). The existence of BCP and bond paths between two atoms has been interpreted as the necessary condition for them to form a chemical bond and several indicators based on the electron density have been used in the literature to characterize interatomic interactions^{35,41}.

Not surprisingly, these studies suggest that the least electronegative atoms (Mg) form predominantly ionic interactions with Rh, whereas the covalent character becomes more prominent as the electronegativity of the element bound to Rh increases and their electronegativity difference decreases. Nevertheless, we have quantified some degree of electron sharing for all investigated MOLPs. Besides, Natural Bonding Orbital (NBO) analysis reveal that the NBO description of the Rh \rightarrow M bonding varied among all bimetallic structures. In general terms, the degree of interaction, based on bond order, occupancy of the donor and acceptor orbitals and donor-acceptor stabilization energies is weaker for *s*-block metals,

³⁹a) T. Lu, F. Chen, *J. Comput. Chem.*, **2012**, *33*, 580-592.

b) Multiwfn, v. 6.0. <http://sobereva.com/multiwfn/>

⁴⁰ a) A. D. McLean, G. S. Chandler, *J. Chem. Phys.*, **1980**, *72*, 5639-5648.

b) R. Krishnan, J. S. Binkley, R. Seeger, J. A. Pople, *J. Chem. Phys.*, **1980**, *72*, 650-654.

c) B. P. Pritchard, D. Altarawy, B. Didier, T. D. Gibson, T. L. Windus, *J. Chem. Inf. Model.*, **2019**, *59*, 4814-4820.

d) T. Noro, M. Sekiya, T. Koga, *Theor. Chem. Acc.*, **2012**, *131*, doi: 10.1007/s00214-012-1124-z

e) Wavefunctions were exported from Gaussian09 as extended wavefunction .wfx files with an added electron density function (EDF) field to represent inner core electrons when using ECPs.

⁴¹ P. L. A. Popelier, *The QTAIM Perspective of Chemical Bonding. In The Chemical Bond* (Eds G. Frenking and S. Shaik). **2014** doi: <https://doi.org/10.1002/9783527664696.ch8>

intermediate for the *d*-block and greater in *p*-block metals containing adducts.

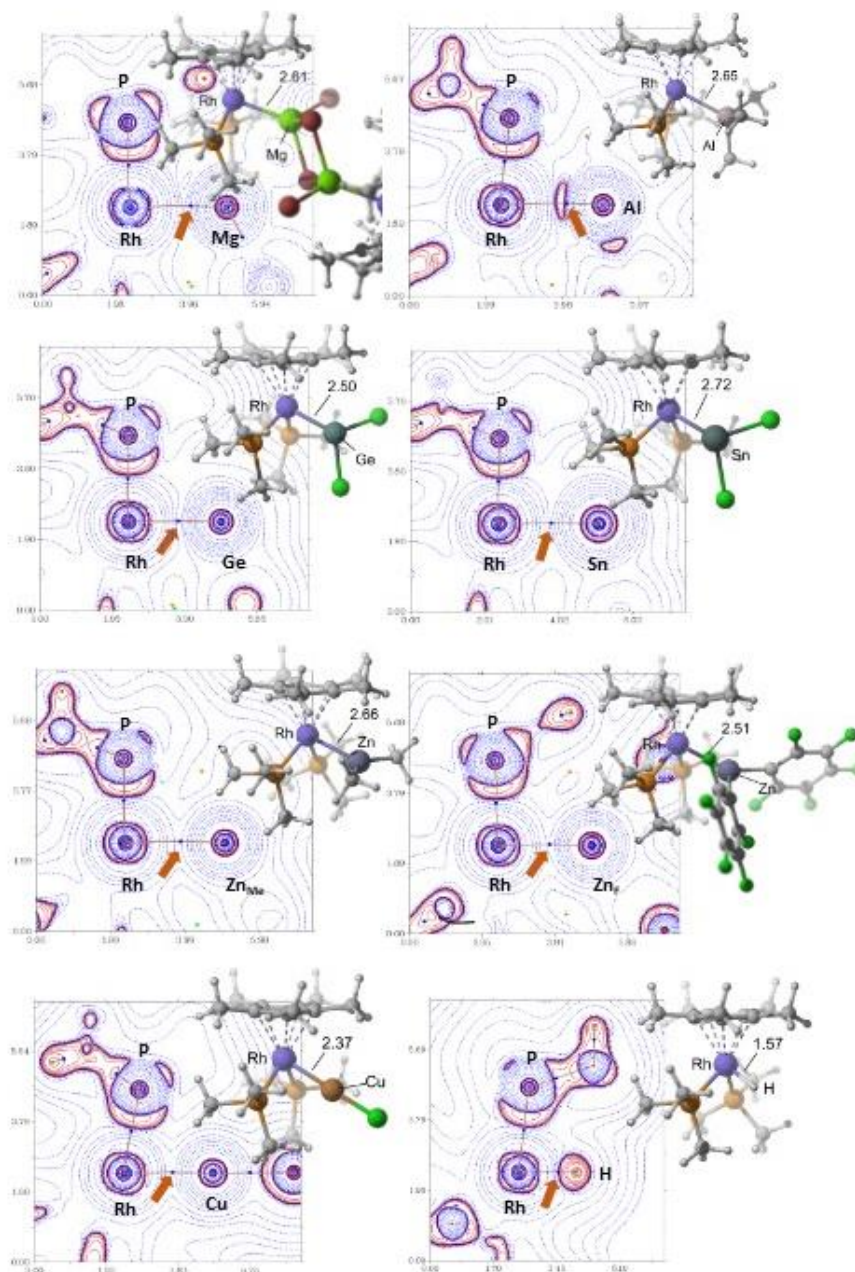


Figure 7. BCPs (blue dots) and bond paths (orange trace) of the electron density of $1 \cdot \text{MgMeBr}$, $1 \cdot \text{AlMe}_3$, $1 \cdot \text{SnCl}_2$, $1 \cdot \text{GeCl}_2$, $1 \cdot \text{ZnMe}_2$, $1 \cdot \text{Zn}(\text{C}_6\text{F}_5)_2$,

1·CuCl and **5a** in one of the M—Rh—P planes. The orange arrows point to the Rh—M BCPs. The optimized geometries of the adducts are also shown⁴². Distances are in Å.

Curiously, the Rh→M bond is dominated by electron donation from the Rh—P bonds rather than from a filled Rh *d*-orbital to the acidic site, as we initially anticipated. In particular, as the Rh(I)→M interactions become more important, there is a greater involvement of $\sigma(\text{Rh—P})$ orbitals (and in some cases weak back donation onto $\sigma^*(\text{Rh—P})$), therefore weakening the Rh—P bonds, which correlates perfectly with the corresponding experimental and computational Rh—P bond distances. This feature is particularly important for the subsequent studies that are discussed in the following Chapter, where the stability of the Rh—P bonds play an important role.

In summary, the choice of $[(\eta^5\text{-C}_5\text{Me}_5)\text{Rh}(\text{PMe}_3)]$ as a Lewis base for the synthesis of unsupported MOLPs has proved highly successful. We have prepared up to nine Rh→based bimetallic compounds of this kind, providing X-ray diffraction structures for those containing fragments MgMeBr, AlMe₃, GeCl₂, SnCl₂, Zn(C₆F₅)₂, and ZnMe₂. It is surprising that despite the wide use of some of these Lewis acidic fragments, their corresponding MOLPs represent highly unusual examples of unsupported M→M bonding, particularly in cases like those with a Rh→Mg (**1a·MgMeBr**) or a Rh→Al (**1a·AlMe₃**) dative bonds. We provide here complete spectroscopic and crystallographic data of all these Rh MOLPs, as well as a summary of the comprehensive computational investigation carried out in parallel on the Rh→M bonding with several sound correlations found for relevant parameters associated to the metal-to-metal bond. For instance, the more

⁴² Some figures have been rendered using the Cylview software. “CYLview, 1.0b; Legault, C. Y., Université de Sherbrooke, 2009 (<http://www.cylview.org>)”

electronegative atoms (Ge, Sn, Al) tend to form more covalent bonds with rhodium, whereas the ionic character becomes more prominent in the least electronegative (Mg). Interestingly, the main orbital component to the Rh→M dative bond involves donation from $\sigma(\text{Rh-P})$, which in turn weakens those bonds. These studies, which demonstrate the Lewis nature of the selected Rh(I) compound, established the ground rules over which we have constructed more congested bimetallic systems in the following Chapter.

II. 3. Experimental Section

II. 3.1. General considerations

All preparations and manipulations were carried out using standard Schlenk and glove-box techniques, under an atmosphere of argon and of high purity nitrogen, respectively. All solvents were dried, stored over 4 Å molecular sieves, and degassed prior to use. Toluene (C₇H₈) and n-pentane (C₅H₁₂) were distilled under nitrogen over sodium. Benzene-*d*⁶ was dried over molecular sieves (4 Å). Tin dichloride was dried by vigorous stirring with acetic anhydride, while copper(I) chloride was by co-evaporation with toluene and drying under vacuum. Other chemicals were commercially available and used as received. For elemental analyses, a LECO TruSpec CHN elementary analyzer was utilized.

II. 3.1.1. NMR Spectroscopy

Solution NMR spectra were recorded on Bruker AMX-300, DRX-400, and DRX-500 spectrometers. Spectra were referenced to external SiMe₄ (δ : 0 ppm) using the residual proton solvent peaks as internal standards (¹H NMR experiments), or the characteristic resonances of the solvent nuclei (¹³C NMR experiments), while ³¹P was referenced to H₃PO₄. Spectral assignments were made by routine one- and two-dimensional NMR experiments where appropriate. ¹⁰³Rh NMR was acquired at 15.9 MHz using an observed 5 mm triple resonance broadband probe (broadband inner coil and doubly tuned ¹H/³¹P outer coil) with 90° pulses of 37.5 μ s and 30.0 μ s for ¹⁰³Rh and ³¹P, respectively. ¹⁰³Rh chemical shifts, δ , are given in ppm relative to $\bar{\nu} = 3.186447^{43}$ (reference compound Rh(acac)₃, where acac

⁴³ R. K. Harris, E. D. Becker, S. M. Cabal de Menezes, P. Granger, R. E. Hoffman and K. W. Zilm, *Pure & Appl. Chem.*, **2008**, *80*, 59-84.

stands for $[\text{CH}_3\text{COCHCOCH}_3]^-$) and derived indirectly from the $^{31}\text{P}-^{103}\text{Rh}$ HMQC experiments by four pulse $^{31}\text{P}-^{103}\text{Rh}$ HMQC experiments with ^1H decoupling during acquisition. Note that despite the fact that IUPAC recommends the use of $\text{Rh}(\text{acac})_3$ as the reference, the alternative X_i value $\bar{\nu} = 3.160000$ for Rh metal has been commonly employed in the literature. The experiments were optimized using the $^1J_{\text{RhP}}$ values obtained from the corresponding $^{31}\text{P}\{^1\text{H}\}$ spectra. The transmitter frequency offset and the spectral width were varied to ensure that no signals were folded. 2D data were zero filled and processed with exponential line broadening of 10 Hz in the direct F2 dimension, and unshifted sine-bell window function in the indirect F1 dimension.

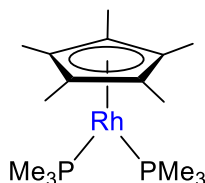
II. 3.1.2. Crystallographic details

Low-temperature diffraction data were collected either on a Bruker D8 Quest APEX-III single crystal diffractometer with a Photon III detector and a $1\mu\text{S}$ 3.0 microfocus X-ray source (**1a**·**MgMeBr**, **1a**·**GeCl₂**, **1a**·**SnCl₂**, **1a**·**AlMe₃**, **1a**·**ZnMe₂**, **1a**·**Zn(C₆F₅)₂**) or on a Bruker APEX-II CCD diffractometer (**5a**) at the Instituto de Investigaciones Químicas, Sevilla. In both cases data were collected by means of ω and φ scans using monochromatic radiation $\lambda(\text{Mo K}\alpha 1) = 0.71073 \text{ \AA}$. The diffraction images collected were processed and scaled using APEX-III or APEX-II software. The structures were solved with SHELXT and were refined against F^2 on all data by full-matrix least squares with SHELXL⁴⁴. All non-hydrogen atoms were refined anisotropically. Hydrogen atoms were included in the model at geometrically calculated positions and refined using a riding model, unless otherwise noted. The isotropic displacement parameters of all hydrogen atoms were fixed to 1.2 times the U value of the atoms to which they are

⁴⁴ G. M. Sheldrick, *Acta Cryst.*, **2008**, *A64*, 112–122.

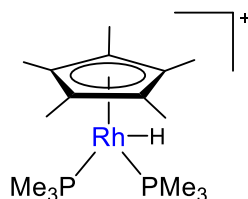
linked (1.5 times for methyl groups). **1a·GeCl₂**, **1a·ZnMe₂** and **1a·AlMe₃** were refined as inversion twins. For the latter anisotropic displacement parameters of the terminal methyl group of PMe₃ ligands were restrained to be similar to their phosphorus nuclei by using SIMU and DELU commands. Structure **1a·MgMeBr** was refined as a twinned structure with 68:32 components and present substitutional disorder between a bromide and a methyl group at the terminal Mg-X fragment (Br:Me, 74:26). Similarly, **1a·SnCl₂** was refined as two-component twin with (80:20). Besides, it presents positional disorder of the bound SnCl₂ unit (67:33). Bond distances and angles for the two SnCl₂ components were restrained to be similar using SADI, while their corresponding anisotropic displacement parameters were restrained with SIMU and DELU instructions. The reduced quality of the crystal also forced us to introduce several restraints for the highly librating carbon atoms. In structure **5a** the position of the hydride ligand was located at the Fourier electron density map and its Rh—H bond distance and geometry around the metal restrained. The whole Cp* ligand appears disordered over two positions with occupancies of 67:33, their geometry constrained with AFIX instructions and their anisotropic displacement parameters restrained with SIMU and DELU instructions. One of the CF₃ groups of the BArF₄⁻ counteranion was also refined over two positions (50:50). Other ADP had to be restrained likely due to the reduced quality of the crystal.

II. 3.2. Synthesis and characterization of rhodium compounds



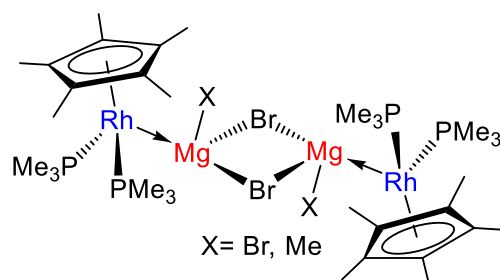
Compound 1a $[(\eta^5\text{-C}_5\text{Me}_5)\text{Rh}(\text{PMe}_3)_2]$. We used a slight modification of the procedure previously reported by Werner¹². A sodium amalgam was prepared by dissolving Na metal (172 mg, 7.5 mmol) onto mercury (4.5 mL) under argon atmosphere. Diethyl ether (20 mL), PMe_3 (6.8 mL, 6.66 mmol) and a toluene (5 mL) solution of $[(\eta^5\text{-C}_5\text{Me}_5)\text{RhCl}_2]_2$ (927 mg, 1.5 mmol) were subsequently added stepwise. The mixture was stirred for 8 hours after which it was filtrated and extracted with pentane (20 mL). The red solution was concentrated to *ca.* 5 mL and stored at $-78\text{ }^\circ\text{C}$. Rhombic brown crystals of **1a** were obtained after 5 days (750 mg, 60%).

^1H NMR (300 MHz, C_6D_6 , $25\text{ }^\circ\text{C}$) δ : 2.17 (s, 15 H, C_5Me_5), 1.3 (vt, 18 H, PMe_3). ^{31}P $\{^1\text{H}\}$ NMR (121 MHz, C_6D_6 , $25\text{ }^\circ\text{C}$) δ : -6.6 (d, $^1J_{\text{PRh}} = 216\text{ Hz}$). ^{103}Rh $\{^1\text{H}\}$ NMR (15.94 MHz, C_6D_6 , $25\text{ }^\circ\text{C}$) δ : -9165.



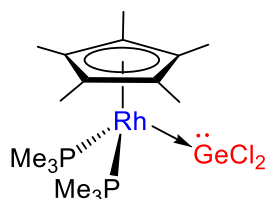
Compound 5a $[(\eta^5\text{-C}_5\text{Me}_5)\text{RhH}(\text{PMe}_3)_2]\text{PF}_6$. Compound **5a** was best prepared by adding NH_4PF_6 (50.0 mg, 0.12 mmol) over a THF (5 mL) solution of **1a** (20.9 mg, 0.12 mmol). The solution was stirred during 30 minutes, time after which addition of pentane (20 mL) caused precipitation of **5a**. The recorded spectroscopic data matched those previously reported by Werner¹².

^1H NMR (400 MHz, THF, 25 °C) δ : 1.99 (s, 15 H, C_5Me_5), 1.62 (br vt, 18 H, PMe_3 , $^2J_{\text{HP}} = 5.1\text{ Hz}$), -13.35 (td, RhH, $^2J_{\text{HP}} = 23.4\text{ Hz}$, $^1J_{\text{HRh}} = 34.9\text{ Hz}$). ^{13}C $\{^1\text{H}\}$ NMR (100 MHz, THF, 25 °C,) δ : 11.0 (C_5Me_5), 20.7 (vt, $^1J_{\text{CP}} = 16\text{ Hz}$, PMe_3), 103.0 (C_5Me_5). ^{31}P $\{^1\text{H}\}$ NMR (162 MHz, THF, 25 °C) δ : -1.4 (dd, $^1J_{\text{PRh}} = 137\text{ Hz}$, $^2J_{\text{PP}} = 14\text{ Hz}$).



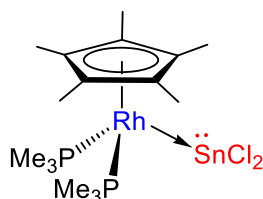
Compound 1a·MgMeBr. A toluene (4 mL) solution of **1a** (30 mg, 0.077 mmol) placed in a Schlenk flask was charged with a solution of the MeMgBr, 1M in Et₂O (77 μ L, 0.077 mmol) and stirred for one hour at 25 °C. Then pentane (10 mL) is added and the resulting solid is filtrated, dried under reduced pressure and washed with pentane to provide the resultant **1a·MgMeBr** as orange to brown solids in moderate to good yields (28 mg, 83%). Single crystal of compound **1a·MgMeBr** was grown from slow diffusion of pentane into their benzene solutions. The analogous procedures carried out in J. Young NMR tubes between **1a** (14 mg, 0.036 mmol) and equimolar amounts of the MeMgBr lead to formation of the reported **1a·MgMeBr** in quantitative spectroscopic yields. Anal. Calcd. for C_{16.25}H_{33.75}Br_{1.75}MgP₂Rh: C, 34.1; H, 5.9. Found: C, 34.4; H, 6.4.

¹H NMR (400 MHz, C₆D₆, 25 °C) δ : 1.87 (s, 15 H, C₅Me₅), 1.38 (vt, 18 H, ²J_{HP} = 6.4 Hz, PMe₃). Signal due to CH₃Mg could not be unambiguously identified. ¹³C {¹H} NMR (101 MHz, C₆D₆, 25 °C) δ : 99.3 (C₅Me₅), 21.9 (vt, ¹J_{CP} = 12 Hz, PMe₃), 11.3 (C₅Me₅), 3.1 (CH₃Mg). ³¹P {¹H} NMR (162 MHz, C₆D₆, 25 °C) δ : -10.2 (d, ¹J_{PRh} = 172 Hz). ¹⁰³Rh {¹H} NMR (15.9 MHz, C₆D₆, 25 °C) δ : -9404.



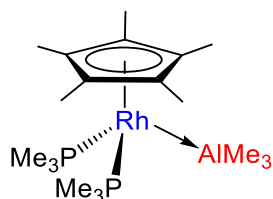
Compound $1a \cdot \text{GeCl}_2$. A solid mixture of **1a** (30 mg, 0.077 mmol) and $\text{GeCl}_2 \cdot \text{dioxane}$ (0.077 mmol, 36 mg) is placed in a Schlenk flask and dissolved in bromobenzene (4 mL) under argon atmosphere. The solution is stirred for one hour at 25 °C and pentane (10 mL) is subsequently added. The resulting solid is filtrated, dried under vacuum and washed with pentane to provide the resultant **$1a \cdot \text{GeCl}_2$** as orange to brown solids in moderate to good yields (31 mg, 76 %). Single crystal of compound **$1a \cdot \text{GeCl}_2$** was grown from slow diffusion of pentane into their bromobenzene solutions. The analogous procedures carried out in J. Young NMR tubes between **1a** (14 mg, 0.036 mmol) and equimolar amounts of $\text{GeCl}_2 \cdot \text{dioxane}$ lead to formation of the reported **$1a \cdot \text{GeCl}_2$** in quantitative spectroscopic yields. Anal. Calcd. for $\text{C}_{16}\text{H}_{33}\text{GeCl}_2\text{P}_2\text{Rh}$: C, 36.0; H, 6.2. Found: C, 36.3; H, 6.1.

^1H NMR (400 MHz, $\text{C}_6\text{D}_5\text{Br}$, 298 K): δ 1.67 (s, 15 H, C_5Me_5), 1.55 (t, $^2J_{\text{HP}} = 4.5$ Hz, 18 H, PMe_3). $^{13}\text{C}\{^1\text{H}\}$ NMR (101 MHz, $\text{C}_6\text{D}_5\text{Br}$, 298 K): δ 102.7 (s, C_5Me_5), 18.9 (t, $^1J_{\text{CP}} = 16$ Hz, PMe_3), 9.9 (s, C_5Me_5). $^{31}\text{P}\{^1\text{H}\}$ NMR (162 MHz, $\text{C}_6\text{D}_5\text{Br}$, 298 K): δ -7.0 (d, $^1J_{\text{PRh}} = 171$). $^{103}\text{Rh}\{^1\text{H}\}$ NMR (15.94 MHz, $\text{C}_6\text{D}_5\text{Br}$, 298 K): δ -8756.



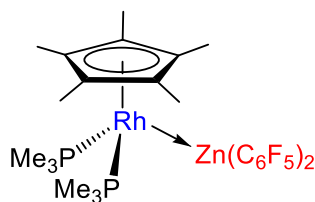
Compound 1a·SnCl₂. A solid mixture of **1a** (30 mg, 0.077 mmol) and SnCl₂ (0.077 mmol, 15 mg) is placed in a Schlenk flask and dissolved in bromobenzene (4 mL) under argon atmosphere. The solution is stirred for one hour at 25 °C and pentane (10 mL) is subsequently added. The resulting solid is filtrated, dried under vacuum and washed with pentane to provide the resultant **1a·SnCl₂** as orange to brown solids in moderate to good yields (29 mg, 69 %). Single crystal of compound **1a·SnCl₂** was grown from slow diffusion of pentane into their bromobenzene solutions. The analogous procedures carried out in J. Young NMR tubes between **1a** (14 mg, 0.036 mmol) and equimolar amounts of the SnCl₂ lead to formation of the reported **1a·SnCl₂** in quantitative spectroscopic yields. Anal. Calcd. for C₁₆H₃₃Cl₂P₂RhSn: C, 33.1; H, 5.7. Found: C, 33.4; H, 6.1.

¹H NMR (400 MHz, C₆D₅Br, 298 K): δ 1.67 (s, 15 H, C₅Me₅), 1.56 (t, ²J_{HP} = 4.1 Hz, 18 H, PMe₃). ¹³C{¹H} NMR (101 MHz, C₆D₅Br, 298 K): δ 101.7 (s, C₅Me₅), 19.5 (t, ¹J_{CP} = 16 Hz, PMe₃), 10.0 (s, C₅Me₅). ³¹P{¹H} NMR (162 MHz, C₆D₅Br, 298 K): δ -8.5 (d, ¹J_{PRh} = 169 Hz). ¹¹⁹Sn{¹H} NMR (149 MHz, C₆D₅Br, 298 K): δ 810.7 (br s). ¹⁰³Rh{¹H} NMR (15.94 MHz, C₆D₅Br, 298 K): δ -8836.



Compound 1a·AlMe₃. A toluene (4 mL) solution of **1a** (30 mg, 0.077 mmol) placed in a Schlenk flask was charged with a solution of the corresponding AlMe₃ 1M in toluene (77 μL, 0.077 mmol) and stirred for one hour at 25 °C. Then pentane (10 mL) is added and the resulting solid filtrated, dried under reduced pressure and washed with pentane to provide the resultant **1a·AlMe₃** as orange to brown solids in moderate to good yields (28 mg, 83 %). Single crystal of compound **1a·AlMe₃** was grown from slow diffusion of pentane into their bromobenzene solutions. The analogous procedures carried out in J. Young NMR tubes between **1a** (14 mg, 0.036 mmol) and equimolar amounts of AlMe₃ lead to formation of the reported **1a·AlMe₃** in quantitative spectroscopic yields. Anal. Calcd. for C₁₉H₄₂AlP₂Rh: C, 49.3; H, 9.2. Found: C, 49.4; H, 9.3.

¹H NMR (400 MHz, C₆D₆, 298 K): δ 1.67 (s, 15 H, CH₃), 1.10 (t, ²J_{HP} = 4.0 Hz, 18 H, PMe₃), -0.06 (s, 9 H, Al(CH₃)₃). ¹³C{¹H} NMR (101 MHz, C₆D₆, 298 K): δ 100.9 (s, C₅Me₅), 21.0 (t, ²J_{CP} = 15 Hz, PMe₃), 11.3 (s, C₅Me₅), 1.0 (s, Al(CH₃)₃). ³¹P{¹H} NMR (162 MHz, C₆D₆, 298 K): δ -6.9 (d, ¹J_{PRh} = 181 Hz). ¹⁰³Rh{¹H} NMR (15.94 MHz, C₆D₆, 298 K): δ -9272. Anal. Calcd. for C₁₉H₄₂AlP₂Rh: C, 49.3; H, 9.2. Found: C, 49.4; H, 9.3. Yield: 28 mg, 83 %.

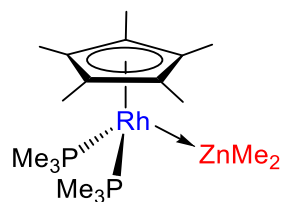


Compound 1a·Zn(C₆F₅)₂. A solid mixture of **1a** (30 mg, 0.077 mmol) and Zn(C₆F₅)₂ (0.077 mmol, 30 mg) is placed in a Schlenk flask and dissolved in toluene (4 mL) under argon atmosphere. The solution is stirred for one hour at 25 °C and pentane (10 mL) is subsequently added. The resulting solid is filtrated, dried under vacuum and washed with pentane to provide the resultant **1a·Zn(C₆F₅)₂** as orange to brown solids in moderate to good yields (28 mg, 83 %). Single crystal of compound **1a·Zn(C₆F₅)₂** was grown from slow diffusion of pentane into their benzene solutions. The analogous procedures carried out in J. Young NMR tubes between **1a** (14 mg, 0.036 mmol) and equimolar amounts of Zn(C₆F₅)₂ lead to formation of the reported **1a·Zn(C₆F₅)₂** in quantitative spectroscopic yields. Anal. Calcd. for C₂₈H₃₃F₁₀P₂Rh: C, 42.6; H, 4.2. Found: C, 42.2; H, 4.6. Yield: 28 mg, 83 %.

¹H NMR (400 MHz, C₆D₆, 25 °C) δ: 1.59 (s, 15 H, C₅Me₅), 1.06 (vt, 18 H, ²J_{HP} = 3.7 Hz, PMe₃). ¹³C {¹H} NMR (101 MHz, C₆D₆, 25 °C,) δ: 140-135 (br, C₆F₅), 98.8 (C₅Me₅), 20.6 (vt, ¹J_{CP} = 16 Hz, PMe₃), 10.2 (C₅Me₅). ¹³C {¹H} NMR (101 MHz, toluene-*d*₈, -10 °C) δ: 144.6 (dd, C₆F₅), 135.3 (br t, C₆F₅), 128.9 (t, C₆F₅), 97.0 (s, C₅Me₅), 91.5 (C_{ipso}(C₆F₅)), 18.3 (vt, ¹J_{CP} = 16 Hz, PMe₃), 8.2 (C₅Me₅). ¹³C signals due to C₆F₅ fragments partly resolved at -10C, but a fully unambiguous assignment could not be made; see spectra below. ¹⁹F {¹H} NMR (376 MHz, C₆D₆, 25 °C,) δ: -161.3 (t, ¹J_{CF} = 21 Hz, *m*-C₆F₅), -158.1 (t, ¹J_{CF} = 20 Hz, 2F, *p*-C₆F₅), -115.0 (d, ¹J_{CF} = 23 Hz, 4F, *o*-

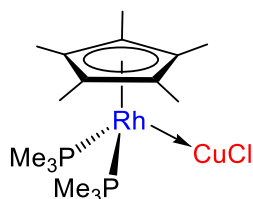
C_6F_5 . ^{31}P $\{^1\text{H}\}$ NMR (162 MHz, C_6D_6 , 25 °C) δ : -7.2 (d, $^1J_{\text{PRh}} = 167$ Hz).

^{103}Rh $\{^1\text{H}\}$ NMR (15.9 MHz, C_6D_6 , 25 °C) δ : -9355.



Compound 1a·ZnMe₂. A toluene (4 mL) solution of **1a** (30 mg, 0.077 mmol) placed in a Schlenk flask was charged with a solution of the ZnMe₂ 1M in toluene (77 μL, 0.077 mmol) and stirred for one hour at 25 °C. Then pentane (10 mL) is added and the resulting solid filtrated, dried by a flow of argon, since under reduced pressure ZnMe₂ is readily eliminated and washed with pentane to provide the resultant **1a·ZnMe₂** as orange to brown solids in moderate to good yields (20 mg, 53 %). Single crystal of compound **1a·ZnMe₂** was grown from slow diffusion of pentane into their benzene solutions. The analogous procedures carried out in J. Young NMR tubes between **1a** (14 mg, 0.036 mmol) and equimolar amounts of ZnMe₂ lead to formation of the reported **1a·ZnMe₂** in quantitative spectroscopic yields. Anal. Calcd. for C₁₈H₃₉P₂RhZn: C, 44.5; H, 8.1. Found: C, 45.0; H, 7.6.

¹H NMR (400 MHz, C₆D₆, 25 °C) δ: 1.76 (s, 15 H, C₅Me₅), 1.09 (br vt, 18 H, ²J_{HP} = 3.7 Hz, PMe₃), -0.41 (s, 6H, ZnMe₂). ¹³C {¹H} NMR (101 MHz, C₆D₆, 25 °C,) δ: 97.4 (s, C₅Me₅), 21.8 (vt, ¹J_{CP} = 14 Hz, PMe₃), 10.9 (s, C₅Me₅), -5.1 (ZnMe₂). ³¹P {¹H} NMR (162 MHz, C₆D₆, 25 °C) δ: -6.9 (d, ¹J_{PRh} = 192 Hz). ¹⁰³Rh {¹H} NMR (15.9 MHz, C₆D₆, 25 °C) δ: -9212.



Compound 1a·CuCl. A solid mixture of **1a** (30 mg, 0.077 mmol) and CuCl (0.077 mmol, 7.6 mg) is placed in a Schlenk flask and dissolved in bromobenzene (4 mL) under argon atmosphere. The solution is stirred for one hour at 25 °C and pentane (10 mL) is subsequently added. The resulting solid is filtrated, dried under vacuum and washed with pentane to provide the resultant **1a·CuCl** as orange to brown solids in moderate to good yields (23 mg, 66 %). The analogous procedures carried out in J. Young NMR tubes between **1a** (14 mg, 0.036 mmol) and equimolar amounts of CuCl lead to formation of the reported **1a·CuCl** in quantitative spectroscopic yields. Anal. Calcd. for C₁₆H₃₃CuClP₂Rh: C, 39.3; H, 6.8. Found: C, 39.5; H, 6.9.

¹H NMR (400 MHz, C₆D₅Br, 298 K): δ 1.66 (s, 15 H, C₅Me₅), 1.48 (br s, 18 H, PMe₃). ¹³C{¹H} NMR (101 MHz, C₆D₅Br, 298 K): δ 103.0 (s, C₅Me₅), 18.4 (t, ¹J_{CP} = 16 Hz, PMe₃), 10.3 (s, CH₃). ³¹P{¹H} NMR (162 MHz, C₆D₅Br, 298 K): δ -3.0 (d, ¹J_{PRh} = 144 Hz). ¹⁰³Rh{¹H} NMR (15.94 MHz, C₆D₅Br, 298 K): δ -8540.

II.4. References

1. a) B. Fuentes, M. García-Melchor, A. Lledós, F. Maseras, J. A. Casares, G. Ujaque, P. Espinet, *Chem. Eur. J.*, **2010**, *16*, 8596-8599.
b) M. García-Melchor, B. Fuentes, A. Lledós, J. A. Casares, G. Ujaque, P. Espinet, *J. Am. Chem. Soc.*, **2011**, *133*, 13519–13526.
c) J. del Pozo, G. Salas, R. Álvarez, J. A. Casares, P. Espinet, *Organometallics*, **2016**, *35*, 3604-3611; d) R. J. Oeschger, D. H. Ringger, P. Chen, *Organometallics*, **2015**, *34*, 3888-3892.
2. a) N. Hidalgo, C. Maya, J. Campos, *Chem. Commun.*, **2019**, *55*, 8812-8815.
b) S. Jamali, S. Abedanzadeh, N. K. Khaledi, H. Samouei, Z. Hendi, S. Zacchini, R. Kiaa, H. R. Shahsavari, *Dalton Trans.*, **2016**, *45*, 17644-17651.
c) M. K. Karunananda, N. P. Mankad NP *Organometallics*, **2017**, *36*, 220–227.
d) N. P. Mankad *Chem Comm.*, **2018**, *54*, 1291–1302.
e) Y. Zhang, M. K. Karunananda, H. –C. Yu, K. J. Clark, W. Williams, N. P. Mankad, D. H. Ess, D. H. *ACS Catal.*, **2019**, *9*, 2657-2663.
3. a) B. R. Barnett, C. E. Moore, P. Chandrasekaran, S. Sproules, A. L. Rheingold, S. DeBeerde, J. S. Figueroa, *Chem. Sci.*, **2015**, *6*, 7169-7178.
b) H. Yang, F. P. Gabbai, *J. Am. Chem. Soc.*, **2015**, *137*, 13425-13432.
c) S. Sen, I.-S. Ke, F. P. Gabbai, *Organometallics*, **2017**, *36*, 4224-4230.
4. T. A. Rokob, A. Hamza, A. Stirling, I. Pápai, *J. Am. Chem. Soc.*, **2009**, *131*, 2029-2036.
5. a) M. Devillard, R. Declercq, E. Nicolas, A. W. Ehlers, J. Backs, N. Saffon-Merceron, G. Bouhadir, J. C. Slootweg, W. Uhl, D. Bourissou, *J. Am. Chem. Soc.*, **2016**, *138*, 4917-4926.
b) J. Campos, *J. Am. Chem. Soc.*, **2017**, *139*, 2944-2947.

- c) N. Hidalgo, J. J. Moreno, M. Pérez-Jiménez, C. Maya, J. López-Serrano, J. Campos, *Chem. Eur. J.*, **2020**, *26*, 1-13.
6. M. J. Katz, K. Sakai, D. B. Leznoff, *Chem. Soc. Rev.*, **2008**, *37*, 1884-1895.
7. K. Omoto, S. Tashiro, M. Shionoya, *Z. Anorg. Allg. Chem.*, **2015**, *641*, 2056-2059.
8. For some recent examples see: a) H. Braunschweig, R. D. Dewhurst, F. Hupp, C. Schneider, *Chem. Commun.*, **2014**, *50*, 15685-15688.
- b) H. Braunschweig, R. D. Dewhurst, F. Hupp, J. Wolf, *Chem. Eur. J.*, **2015**, *21*, 1860-1862.
- c) B. R. Barnett, J. S. Figueroa, *Chem. Commun.*, **2016**, *52*, 13829-13839.
- d) U. Jayarathne, T. J. Mazzacano, S. Bagherzadeh, N. P. Mankad, *Organometallic*, **2013**, *32*, 3986-3992.
- e) S. Banerjee, M. K. Karunananda, S. Bagherzadeh, U. Jayarathne, S. R. Parmelee, G. W. Waldhart, N. P. Mankad, *Inorg. Chem.*, **2014**, *53*, 11307-11315.
- f) M. K. Karunananda, F. X. Vázquez, E. E. Alp, W. Bi, S. Chattopadhyay, T. Shibatade, N. P. Mankad, *Dalton Trans.*, **2014**, *43*, 13661-13671.
9. a) G. Aullón, S. Alvarez, *Inorg. Chem.*, **1996**, *35*, 3137-3144.
- b) M.-E. Moret in *Higher Oxidation State Organopalladium and Platinum Chemistry* (Ed.: A. J. Canty) *Topics in Organometallic Chemistry*, Springer: Berlin Heidelberg, **2011**, pp 157-184.
10. a) P. Pyykkö, J. Li, N. Runeberg, *Chem. Phys. Lett.*, **1994**, *218*, 133-138.
- b) P. Pyykkö, Y. Zhao, *Angew. Chem. Int. Ed. Engl.*, **1991**, *30*, 604-605.
11. a) R. J. Oeschger, P. Chen, *Organometallics*, **2017**, *36*, 1465-1468.
- b) Eno Paenurk, R. Gershoni-Poranne, P. Chen, *Organometallics*, **2017**, *36*, 4854-4863.

- c) G. Wang, T. T. Ponduru, Q. Wang, L. Zhao, G. Frenking, H. V. R. Dias, *Chem. Eur. J.*, **2017**, *23*, 17222 – 17226.
- d) M. Baya, U. Belío, D. Campillo, I. Fernández, S. Fuertes, A. Martín, *Chem. Eur. J.*, **2018**, *24*, 13879-13889.
12. B. Klingert, H. Werner, *Chem. Ber.*, **1983**, *116*, 1450-1462.
13. J. W. Kang, P. M. Maitlis, *J. Organomet. Chem.*, **1971**, *26*, 393-399.
14. A. K. Swarnakar, M. J. Ferguson, R. McDonald, E. Rivard, *Dalton Trans.*, **2016**, *45*, 6071-6078.
15. M. J. Butler, M. R. Crimmin, *Chem. Commun.*, **2017**, *53*, 1348-1365.
16. K. Jonas, C. Krüger, *Angew. Chem. Int. Ed. Engl.*, **1980**, *19*, 520-537.
17. B. Cordero, V. Gómez, A. E. Platero-Prats, M. Revés, J. Echeverría, E. Cremades, F. Barragán, S. Alvarez, *Dalton Trans.*, **2008**, 2832-2838.
18. R. M. Peltzer, O. Eisenstein, A. Nova, M. Cascella, *J. Phys. Chem. B.*, **2017**, *121*, 4226-4237.
19. L. Pauling, *J. Am. Chem. Soc.*, **1947**, *69*, 542-553.
20. O. Ekkert, A. J. P. White, H. Toms, M. R. Crimmin, *Chem. Sci.* **2015**, *6*, 5617-5622.
21. Previously reported magnesium MOLPs are based on cationic magnesium fragments. See for example:
- a) M. P. Blake, N. Kaltsoyannis, P. Mountford, *J. Am. Chem. Soc.*, **2015**, *137*, 12352-12368.
- b) J. Hicks, C. E. Hoyer, B. Moubaraki, G. L. Manni, E. Carter, D. M. Murphy, K. S. Murray, L. Gagliardi, C. Jones, *J. Am. Chem. Soc.*, **2014**, *136*, 5283-5286.
- c) M. P. Blake, N. Kaltsoyannis, P. Mountford, *Chem. Commun.*, **2013**, *49*, 3315-3317.
- d) J. T. Golden, T. H. Peterson, P. L. Holland, R. G. Bergman, R. A. Andersen, *J. Am. Chem. Soc.*, **1998**, *120*, 223-224.

- e) W. Kaschube, K.-R. Pörschke, K. Angermund, C. Krüger, G. Wilke, *Chem. Ber.*, **1988**, *121*, 1921-1929.
- f) M. Ohashi, K. Matsubara, T. Iizuka, H. Suzuki, *Angew. Chem., Int. Ed.*, **2003**, *42*, 937-940.
22. N. Sheng Loong Tan, G. L. Nealon, J. M. Lynam, A. N. Sobolev, M. R. Rowles, M. I. Ogden, M. Massi, A. B. Lowe, *Dalton Trans.*, **2019**, *48*, 16437-16447.
23. A. Hofmann, A. Lamprecht, J. O. C. Jiménez-Halla, T. Tröster, R. D. Dewhurst, C. Lenczyk, H. Braunschweig, *Chem. Eur. J.*, **2018**, *24*, 11795-11802.
24. a) A. V. Zabula, T. Pape, A. Hepp, F. E. Hahn, *Dalton Trans.*, **2008**, 5886-5890. b) D. Heitmann, T. Pape, A. Hepp, C. Muck-Lichtenfeld, S. Grimme, F. E. Hahn, *J. Am. Chem. Soc.*, **2011**, *133*, 11118-11120. c) H. Braunschweig, A. Damme, R. D. Dewhurst, F. Hupp, J. O. C. Jimenez-Halla, K. Radacki, *Chem. Commun.*, **2012**, *48*, 10410-10412. d) F. Hupp, M. Ma, F. Kroll, J. O. C. Jimenez-Halla, R. D. Dewhurst, K. Radacki, A. Stasch, C. Jones, H. Braunschweig *Chem. Eur. J.*, **2014**, *20*, 16888-16898.
25. H. Arp, J. Baumgartner, C. Marschner, P. Zark, T. Müller, *J. Am. Chem. Soc.*, **2012**, *134*, 10864-10875.
26. R. C. Haddon, *J. Phys. Chem. A.*, **2001**, *105*, 4164-4165.
27. a) L. Á. Ivarez-Rodríguez, J. A. Cabeza, J. M. Fernandez-Colinas, P. García-Álvarez, D. Polo, *Organometallics*, **2016**, *35*, 2516-2523. b) D. Matioszek, N. Saffon, J.-M. Sotiropoulos, K. Miqueu, A. Castel, J. Escudie, *Inorg. Chem.*, **2012**, *51*, 11716-11721. c) J.M. García, E. Ocando-Mavárez, T. Kato, D. Santiago-Coll, A. Briceno, N. Saffon-Merceron, A. Baceiredo, *Inorg. Chem.*, **2012**, *51*, 8187-8193. d) M. Veith, A. Müller, L. Stahl, M. Nötzel, M. Jarczyk, V. Huch, *Inorg. Chem.*, **1996**, *35*, 3848-3855. e) M. L. B. Ismail, F.-Q. Liu, W.-L. Yim, R. Ganguly, Y. Li, C.-W. So, *Inorg. Chem.*,

2017, 56, 5402-5410. f) M. Kilian, H. Wadepohl, L. H. Gad, *Eur. J. Inorg. Chem.*, **2008**, 1892-1900. g) J. Martincová, R. Dostálová, L. Dostál, A. Růžička, R. Jambo, *Organometallics*, **2009**, 28, 4823–4828.

28. a) J. Bauer, H. Braunschweig and K. Radacki, *Chem. Commun.*, **2012**, 48, 10407-10409. b) A related Rh/Al species was earlier disclosed, though the Rh—Al interaction may not be described as dative bond: J. M. Mayer and J. C. Calabrese, *Organometallics*, **1984**, 3, 1292-1298.

29. Previous examples contain AlMe₃ as a bridging motif or bound to *p*-block metals and metalloids: a) Z. Weng, S. Teo, L. L. Kohb, T. S. A. Hor, *Chem. Commun.*, **2006**, 1319-1321. b) M. Oishi, M. Oshima, H. Suzukib *Inorg. Chem.*, **2014**, 53, 6634-6654. c) S. Ogoshi, M. Ueta, T. Arai, H. Kurosawa, *J. Am. Chem. Soc.*, **2005**, 127, 12810-12811. d) S. Schulz, A. Kuczkowski, M. Nieger *J. Organomet. Chem.*, **2000**, 604, 202-207. e) K. Zeckert, *Dalton Trans.*, **2012**, 41, 14101-14106.

30. a) J. J. Gair, Y. Qiu, R. L. Khade, N. H. Chan, A. S. Filatov, Y. Zhang, J. C. Lewis, *Organometallics*, **2019**, 38, 1407-1412.

b) T. Cadenbach, T. Bollermann, C. Gemel, M. Tombul, I. Fernandez, M. V. Hopffgarten, G. Frenking, R. A. Fischer, *J. Am. Chem. Soc.*, **2009**, 131, 16063-16077.

c) M. Molon, T. Cadenbach, T. Bollermann, C. Gemel, R. A. Fischer, *Chem. Commun.*, **2010**, 46, 5677-5679.

d) O. Ekkert, A. J. P. White, M. R. Crimmin, *Angew. Chem.*, **2016**, 128, 16265-16268.

e) C. J. Pell, W.-C. Shih, S. Gatard, O. V. Ozerov, *Chem. Commun.*, **2017**, 53, 6456-6459.

f) M. D. Fryzuk, D. H. McConville, S. J. Rettig, *Organometallics*, **1990**, 9, 1359-1360.

31. a) H. Takahashi, S. Inagaki, N. Yoshii, F. Gao, Y. Nishihara, K. Takagi, *J. Org. Chem.*, **2009**, *74*, 2794-2797.
b) S. Ejiri, S. Odo, H. Takahashi, Y. Nishimura, K. Gotoh, Y. Nishihara, K. Takagi, *Org. Lett.*, **2010**, *12*, 1692-1695.
32. a) D. Schneider, H. Werne, *Organometallics*, **1993**, *12*, 4420-4430.
b) H. Werner, J. Wolf, G. Müller, C. Krüger, *J. Organomet. Chem*, **1988**, *342*, 381-398.
33. a) M. U. Pilotti, I. Topaloglu, F. G. A. Stone, *J. Chem. Soc. Dalton Trans.* **1991**, 1355-1360.
b) M. J. Fernandez, J. Modrego, L. A. Oro, M.-C. Apreda, F. H. Cano, C. Foces-Foce, *J. Chem. Soc. Dalton Trans.*, **1989**, 1249-1252.
c) C. G. Arena, F. Faraone, M. Lanfranchi, E. Rotondo, A. Tiripicchio. *Inorg. Chem.*, **1992**, *31*, 4797-4802.
34. G. Bruno, S. L. Schiavo, E. Rotondo, P. Piraino, F. Faraone, *Organometallics*, **1987**, *6*, 2502-2507.
35. R. F. W. Bader, *Atoms in Molecules: A Quantum Theory*, Oxford University Press, Oxford, **1995**.
36. a) J. P. Foster, F. Weinhold, *J. Am. Chem. Soc.*, **1980**, *102*, 7211-7218.
b) A. E. Reed, L. A. Curtiss, F. Weinhold, *Chem. Rev.*, **1988**, *88*, 899-926.
c) E. D. Glendening, C. R. Landis, F. Weinhold, *J. Comput. Chem.*, **2013**, *34*, 1429-1437.
d) E. D. Glendening, J. K. Badenhoop, A. E. Reed, J. E. Carpenter, J. A. Bohmann, C. M. Morales, C. R. Landis, F. Weinhold, NBO 6.0.; *Theoretical Chemistry Institute*, University of Wisconsin: Madison, **2013**. Available at: www.chem.wisc.edu
37. a) A. V. Marenich, C. J. Cramer, D. G. Truhlar, *J. Phys. Chem. B*, **2009**, *113*, 6378-6396.

- b) J.-D. Chai, M. Head-Gordon, *Phys. Chem. Chem. Phys.*, **2008**, *10*, 6615-6620.
- c) R. Ditchfield, W. J. Hehre, J. A. Pople, *J. Chem. Phys.*, **1971**, *54*, 724-728.
- d) J.-P. Blaudeau, M. P. McGrath, L. A. Curtiss, L. Radom, *J. Chem. Phys.*, **1997**, *107*, 5016-5021.
- e) M. M. Francl, W. J. Pietro, W. J. Hehre, J. S. Binkley, M. S. Gordon, D. J. DeFrees, J. A. Pople, *J. Chem. Phys.*, **1982**, *77*, 3654-3665.
- f) V. A. Rassolov, J. A. Pople, M. A. Ratner, T. L. Windus, *J. Chem. Phys.*, **1998**, *109*, 1223-1229.
38. Gaussian 09, Revisions B.01 and E.01, M. J. Frisch, G. W. Trucks, H. B. Schlegel, G. E. Scuseria, M. A. Robb, J. R. Cheeseman, G. Scalmani, V. Barone, G. A. Petersson, H. Nakatsuji, X. Li, M. Caricato, A. Marenich, J. Bloino, B. G. Janesko, R. Gomperts, B. Mennucci, H. P. Hratchian, J. V. Ortiz, A. F. Izmaylov, J. L. Sonnenberg, D. Williams-Young, F. Ding, F. Lipparini, F. Egidi, J. Goings, B. Peng, A. Petrone, T. Henderson, D. Ranasinghe, V. G. Zakrzewski, J. Gao, N. Rega, G. Zheng, W. Liang, M. Hada, M. Ehara, K. Toyota, R. Fukuda, J. Hasegawa, M. Ishida, T. Nakajima, Y. Honda, O. Kitao, H. Nakai, T. Vreven, K. Throssell, J. A. Montgomery, Jr., J. E. Peralta, F. Ogliaro, M. Bearpark, J. J. Heyd, E. Brothers, K. N. Kudin, V. N. Staroverov, T. Keith, R. Kobayashi, J. Normand, K. Raghavachari, A. Rendell, J. C. Burant, S. S. Iyengar, J. Tomasi, M. Cossi, J. M. Millam, M. Klene, C. Adamo, R. Cammi, J. W. Ochterski, R. L. Martin, K. Morokuma, O. Farkas, J. B. Foresman, and D. J. Fox, Gaussian, Inc., Wallingford CT, **2016**.
39. a) T. Lu, F. Chen, *J. Comput. Chem.*, **2012**, *33*, 580-592.
- b) Multiwfn, v. 6.0. <http://sobereva.com/multiwfn/>
40. a) A. D. McLean, G. S. Chandler, *J. Chem. Phys.*, **1980**, *72*, 5639-5648.

- b) R. Krishnan, J. S. Binkley, R. Seeger, J. A. Pople, *J. Chem. Phys.*, **1980**, 72, 650-654.
- c) B. P. Pritchard, D. Altarawy, B. Didier, T. D. Gibson, T. L. Windus, *J. Chem. Inf. Model.*, **2019**, 59, 4814-4820.
- d) T. Noro, M. Sekiya, T. Koga, *Theor. Chem. Acc.*, **2012**, 131, doi: 10.1007/s00214-012-1124-z
- e) Wavefunctions were exported from Gaussian09 as extended wavefunction .wfx files with an added electron density function (EDF) field to represent inner core electrons when using ECPs.
41. P. L. A. Popelier, *The QTAIM Perspective of Chemical Bonding. In The Chemical Bond* (Eds G. Frenking and S. Shaik). **2014** doi: <https://doi.org/10.1002/9783527664696.ch8>
42. Some figures have been rendered using the Cylview software. “CYLview, 1.0b; Legault, C. Y., Université de Sherbrooke, 2009 (<http://www.cylview.org>)”
43. R. K. Harris, E. D. Becker, S. M. Cabal de Menezes, P. Granger, R. E. Hoffman and K. W. Zilm, *Pure & Appl. Chem.*, **2008**, 80, 59-84.
44. G. M. Sheldrick, *Acta Cryst.*, **2008**, A64, 112–122.

CHAPTER III

III.1. Introductory comments

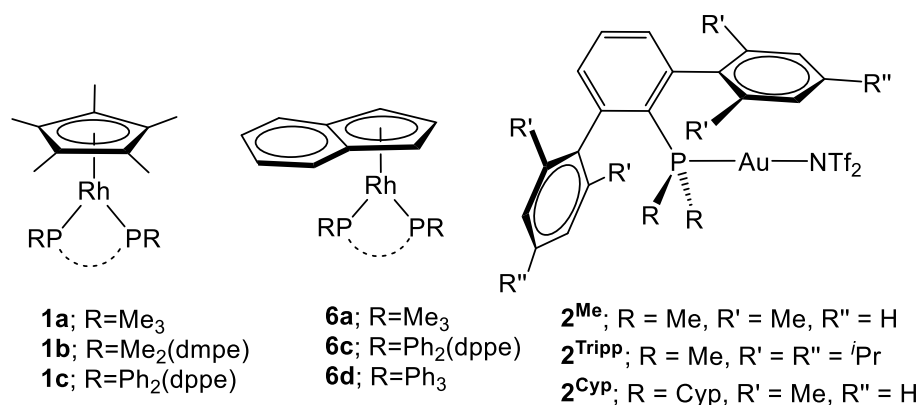
In the previous Chapter we demonstrated the Lewis basic behavior of compound $[(\eta^5\text{-C}_5\text{Me}_5)\text{Rh}(\text{PMe}_3)_2]$ (**1a**)¹ towards a series of electrophiles and its ability to form bimetallic structures containing a Rh→M dative bond. As described in the Introduction of this Thesis, there is increasing interest on the design of bimetallic frustrated Lewis pairs (FLPs), for which monometallic fragments under highly congested environments are necessary. The obvious target for us and the core of this Chapter is to increase the size of the Lewis acidic fragment to be combined with the Lewis basic Rh precursor **1a**. To do so, we have examined the combination of Rh(I) compound **1a** with the gold terphenyl phosphine complexes **2** represented in Scheme 1. These gold complexes were chosen because they have been developed by our group² and they have given very remarkable results in the chemistry of bimetallic FLPs thanks to their high electrophilicity and steric shielding.

In terms of intermolecular reactivity (small molecule activation), the Rh(I)/Au(I) pairs clearly render potential for bimetallic bond activation processes. Thus, as highly constrained metallic fragments of opposed electronics, they may behave as bimetallic frustrated Lewis pairs (FLPs). Beyond the Rh(I) precursor **1a**, we have carried out studies in which we have also modified the nature of this Lewis basic fragment. In particular, we have investigated the differences in reactivity between rhodium and gold complexes when the steric and electronic properties of their respective phosphine ligands are modified. Likewise, we have extended these studies

¹ B. Klingert, H. Werner, *Chem. Ber.*, **1983**, *116*, 1450-1462.

² J. Campos, M. F. Espada, J. López-Serrano, M. L. Poveda, E. Carmona, *Angew. Chemie, Int. Ed.* **2015**, *54*, 15379.

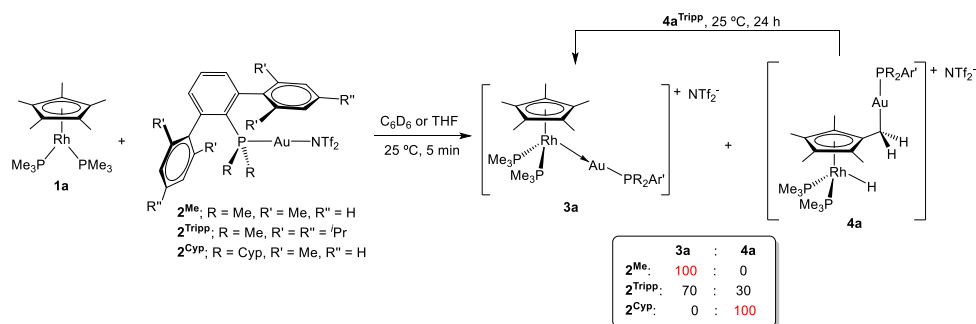
by investigating the bimetallic reactivity when the Cp* fragment of rhodium complexes is substituted by the also prevalent indenyl ($[\text{C}_9\text{H}_7]^-$) ligand.



Scheme 1. Rhodium and gold complexes studied in this chapter.

III.2. Reactions between rhodium complex $\text{Rh}(\text{C}_5\text{Me}_5)(\text{PMe}_3)_2$ (**1a**) and the gold complexes $(\text{PR}_2\text{Ar})\text{Au}(\text{NTf}_2)$ (**2**)

Reactions with the triflimide Au(I) complex $(\text{PR}_2\text{Ar})\text{Au}(\text{NTf}_2)$ (**2**) containing a bulky terphenyl phosphine have been examined. The selected phosphines, ordered by their steric profiles, are $\text{PMe}_2\text{Ar}^{\text{Xyl}2} < \text{PMe}_2\text{Ar}^{\text{Tripp}2} < \text{PCyp}_2\text{Ar}^{\text{Xyl}2}$ (Cyp = C₅H₁₀; see Scheme 2).



Scheme 2. Selectivity in the reaction between Rh(I) compound **1a** and electrophilic Au(I) species of type **2**.

Treatment of **1a** with $(\text{PMe}_2\text{Ar}^{\text{Xyl}2})\text{Au}(\text{NTf}_2)$ (**2^{Me}**) readily caused quantitative formation of the new metal-only Lewis pair (MOLP)³ **3a^{Me}** (Scheme 2). This was identified by a new AB₂ pattern in the ³¹P{¹H} NMR spectrum (Figure 1), where an apparent double triplet at 13.9 ppm (³J_{PP} = 12, ²J_{PRh} = 10 Hz) and a double doublet at -3.1 ppm (³J_{PP} = 12, ¹J_{PRh} = 155 Hz) due to $\text{PMe}_2\text{Ar}^{\text{Xyl}2}$ and the two PMe_3 ligands, respectively, are evidence for the formation of a bimetallic species.

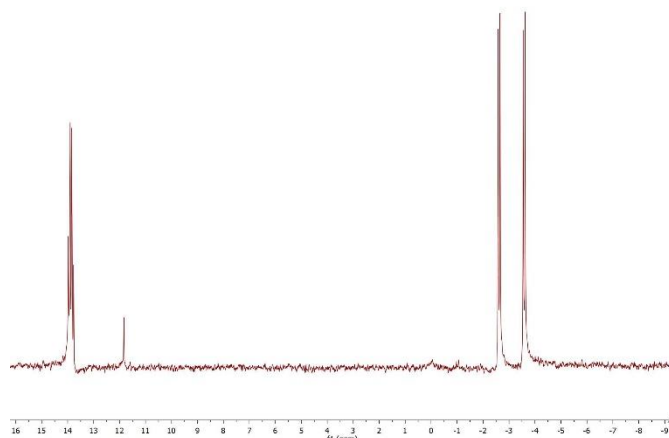


Figure 1. ³¹P{¹H} NMR of complex **3a^{Me}**.

In stark contrast, addition of $(\text{PCyp}_2\text{Ar}^{\text{Xyl}2})\text{Au}(\text{NTf}_2)$ (**2^{Cyp}**) to benzene or THF solutions of **1a** immediately led to compound **4a^{Cyp}**, which formed in quantitative spectroscopic yields (Scheme 2). ¹H NMR analysis (Figure 2) revealed the asymmetry of the cyclopentadienyl ring which, instead of the usual large singlet (observed in **3a^{Me}**), appeared as three

³ J. Bauer, H. Braunschweig, R. D. Dewhurst, *Chem. Rev.*, **2012**, *112*, 4329-4346.

resonances: two at 1.84 and 1.73 ppm for six protons each, and a doublet at 1.05 ppm ($^2J_{\text{HP}} = 9.6$ Hz) pertaining to the functionalized $\text{C}_5\text{Me}_4\text{—CH}_2\text{—Au}$ moiety. These were accompanied by a distinctive low-frequency signal at -13.34 ppm (dt, $^2J_{\text{HP}} = 35.8$, $^1J_{\text{HRh}} = 24.5$ Hz) due to a newly formed hydride ligand bound to the rhodium centre. As supported by isotopic labelling experiments (*vide infra*), this hydride originates from a methyl group of Cp^* , showing evidence that this type of hydrogen shuttle is viable in late transition metals.

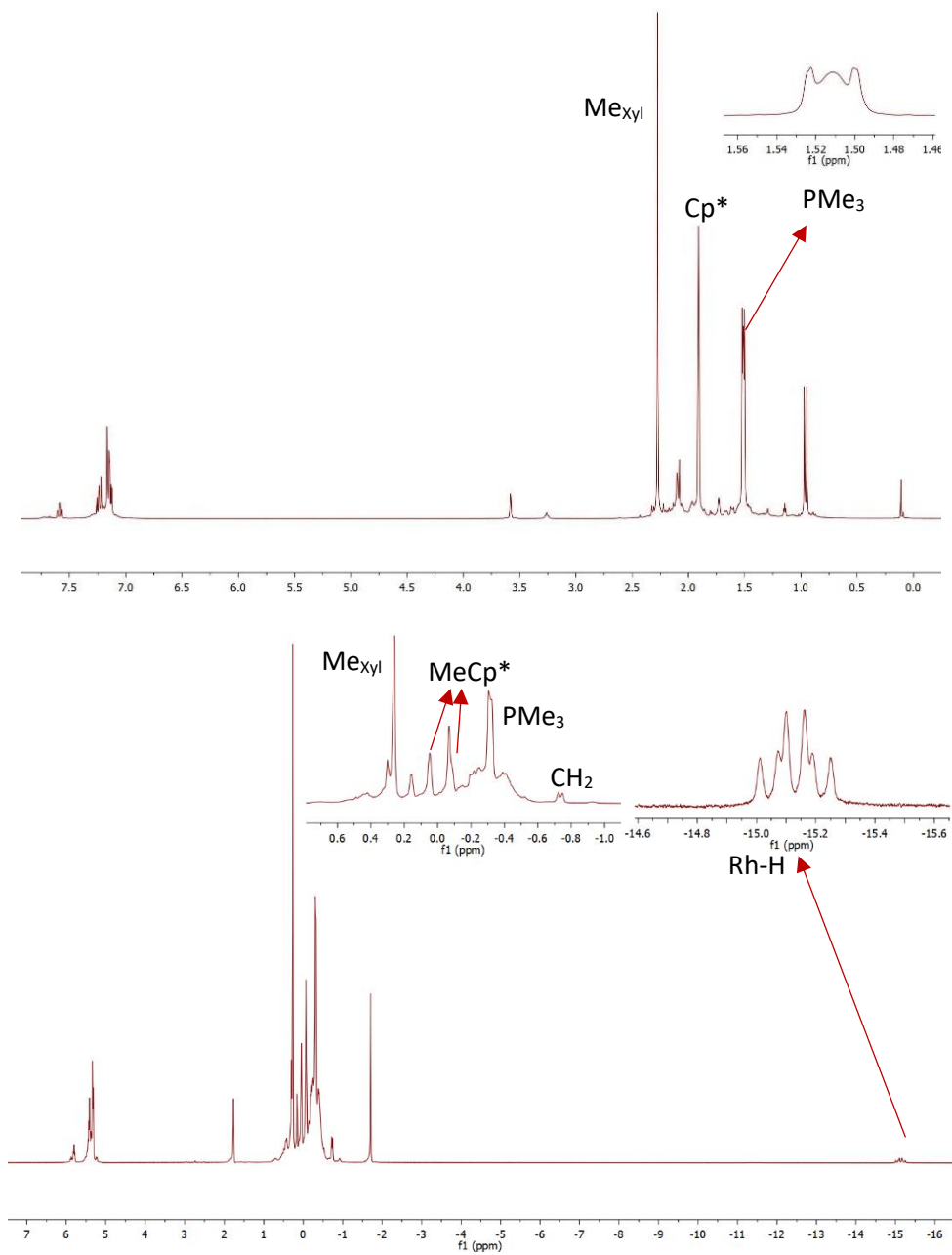


Figure 2. ^1H NMR of complexes 3a^{Me} (up) and 4a^{Cyp} (down).

The absence of ^{31}P - ^{103}Rh scalar coupling for the terphenyl phosphine, which resonates at 56.0 (t, $^5J_{\text{PP}} = 10$ Hz) is characteristic of compounds **4**, while PMe_3 ligands in **4a**^{Cyp} display a signal at -2.2 ppm (dd, $^5J_{\text{PP}} = 10$, $^1J_{\text{PRh}} = 140$ Hz) (Figure 3).

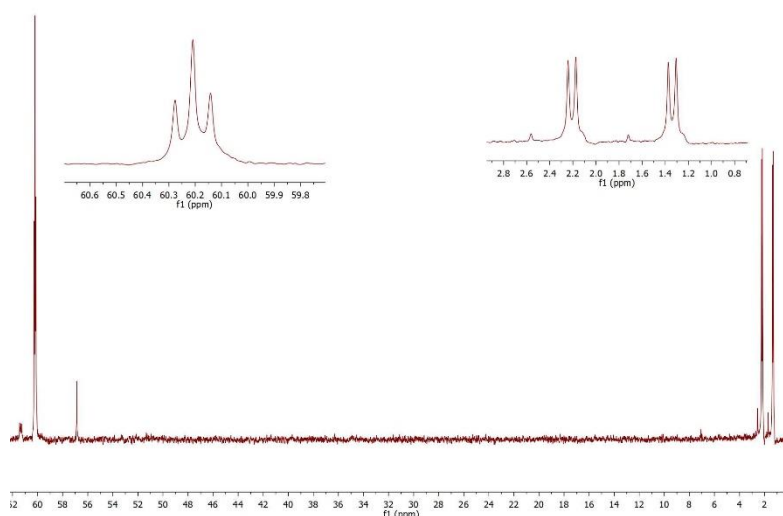


Figure 3. $^{31}\text{P}\{^1\text{H}\}$ NMR of complex **4a**^{Cyp}.

The molecular structure of **4a**^{Cyp} has been authenticated by X-ray diffraction studies (Figure 4), for which single crystals were grown by slow diffusion of pentane into their benzene solutions. This structure finds no previous precedent. In view of the isolobal analogy between H^+ and $[\text{LAu}]^+$ fragments, it could be described as the substitution of a methyl proton of the Cp^* ligand by the $[(\text{PCyp}_2\text{Ar}^{\text{Xyl}2})\text{Au}]^+$ unit, which is accommodated in an orthogonal fashion relative to the Cp^* plane (85.21°). The highly electrophilic character of gold(I) is likely responsible for shortening the C1—C6 distance to 1.483(10) Å (*c.f.* average 1.51 Å for $d_{(\text{Cp}^*)\text{C}-\text{CH}_3}$). It should be remarked that there is no previous demonstration for the migration

of a hydride from a methyl group of Cp* to a late transition metal, although the possibility has been invoked before⁴.

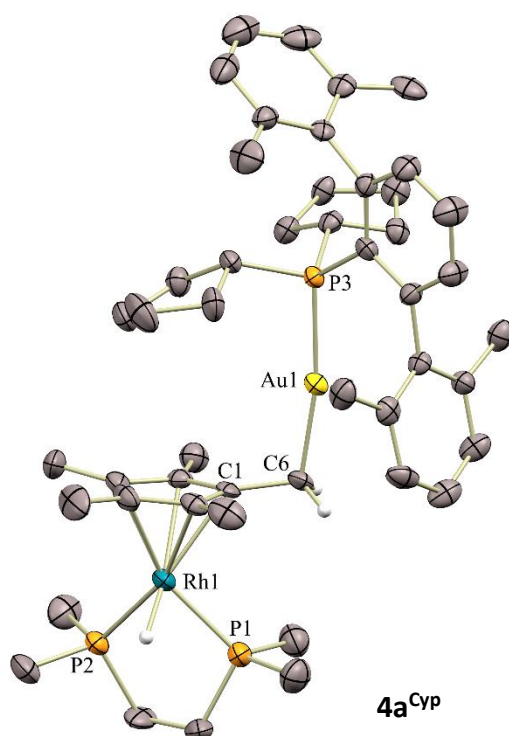


Figure 4. ORTEP diagram of compound **4a^{Cyp}**.

Interestingly, we noted an in-between scenario with the intermediate size phosphine ($\text{PMe}_2\text{Ar}^{\text{Tripp}2}$) of compound **2^{Tripp}**. Addition of

⁴ a) H.-J. Kraus, H. Werner, *Angew. Chem. Int. Ed. Engl.*, **1982**, *21*, 866-867.

b) H. Werner, G. T. Crisp, P. W. Jolly, H.-J. Kraus, C. Krüger, *Organometallics*, **1983**, *2*, 1369-1377.

c) A. Nutton, P. M. Maitlis, *Dalton Trans.*, **1981**, 2335-2338.

d) C. P. Lenges, P. S. White, M. Brookhart, *J. Am. Chem. Soc.*, **1999**, *121*, 4385-4396.

(PMe₂Ar^{Tripp2})Au(NTf₂) (**2**^{Tripp}) to solutions of **1a** results in the formation of both isomers, **3a**^{Tripp} and **4a**^{Tripp}, in a ca. 70:30 ratio, along with unidentified minor species. Compounds **3a**^{Tripp} and **4a**^{Tripp} have the same spectroscopic pattern as their PMe₂Ar^{Xyl2} and PCyp₂Ar^{Xyl2} analogues (Figure 5), which allowed us to easily assign their molecular formulation.

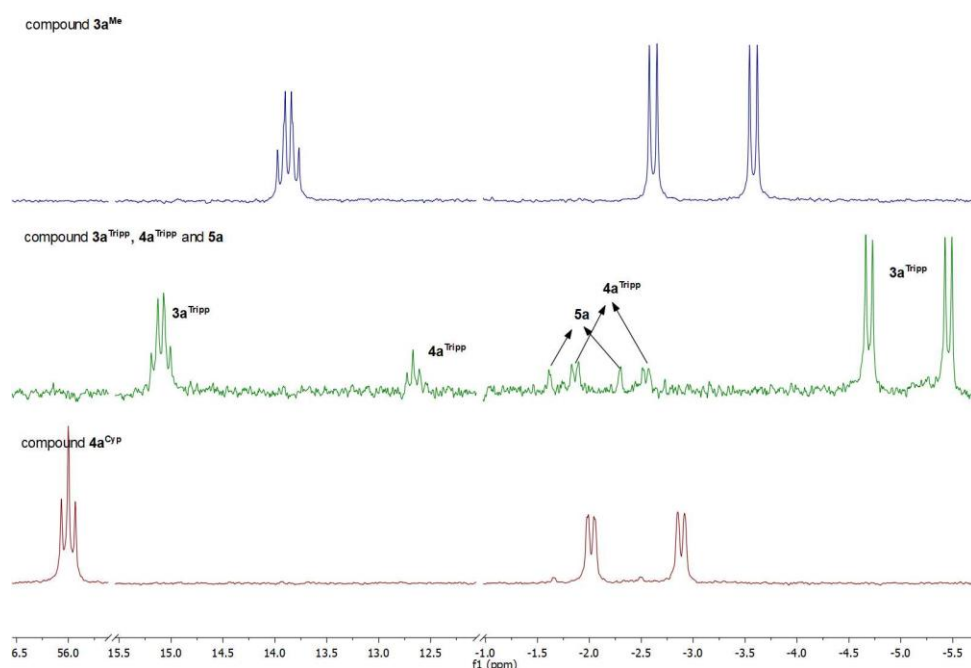


Figure 5. Superimposed representation of selected regions of ³¹P{¹H} NMR spectra of compounds **3a** and **4a** (Compound labelled as **5a** will be introduced in the next section).

That is, while the bimetallic adduct **3a**^{Tripp} exhibits ³¹P{¹H} resonances at 15.2 (dt, ³J_{PP} = 14, ²J_{PRh} = 12 Hz, PMe₂Ar^{Tripp2}) and -5.1 (dd, ³J_{PP} = 14, ¹J_{PRh} = 155 Hz, PMe₃) ppm, isomer **4a**^{Tripp} displays signals at 12.7 (t, ³J_{PP} = 12 Hz, PMe₂Ar^{Tripp2}) and -2.2 (dd, ³J_{PP} = 12 Hz, ¹J_{PRh} = 140 Hz, PMe₃), as well as a characteristic hydride peak at -13.48 (²J_{HP} = 35.8, ¹J_{HRh} = 24.1 Hz,) ppm. Low-temperature NMR monitoring of the reaction

revealed that isomer **3a**^{Tripp} forms as the exclusive product below $-40\text{ }^{\circ}\text{C}$, while the complex derived from C—H activation at the Cp* moiety requires higher temperatures to appear. Nevertheless, heating solutions of pure **3a**^{Tripp} did not cause the appearance of isomer **4a**^{Tripp}. We also observed that the stability of compounds **3a** and **4a** clearly differs. While the former remains intact for weeks in solution under a nitrogen atmosphere, the latter complexes slowly decompose under the same conditions. In the case of **4a**^{Tripp}, we were thrilled to note that at least part of this species evolves to its isomeric bimetallic adduct **3a**^{Tripp}, thus supporting the reversibility for the Cp* activation process.

X-ray crystallographic study of complex **3a**^{Tripp} was accomplished. Its solid-state molecular structure is presented in Figure 6 and exhibits a Rh—Au bond distance of $2.593(1)\text{ \AA}$, comparable to the only other example of a bimetallic Rh/Au unsupported MOLP of this kind⁵. This value is shortened by around 0.2 \AA with respect to the sum of their covalent radii (2.78 \AA)⁶, thus providing support for the existence of a dative Rh→Au bond. Similarly, the calculated formal shortness ratio (FSR)⁷, defined as the ratio between the M—M length and the sum of metallic radii, exactly accounts for 1.00.

⁵C. Bianchini, C. J. Elsevier, J. M. Ernsting, M. Peruzzini, F. Zanolini, *Inorg. Chem.*, **1995**, *34*, 84-92.

⁶B. Cordero, V. Gómez, A. E. Platero-Prats, M. Revés, J. Echeverría, E. Cremades, F. Barragán, S. Alvarez, *Dalton Trans.*, **2008**, 2832-2838.

⁷L. Pauling, *J. Am. Chem. Soc.*, **1947**, *69*, 542-553.

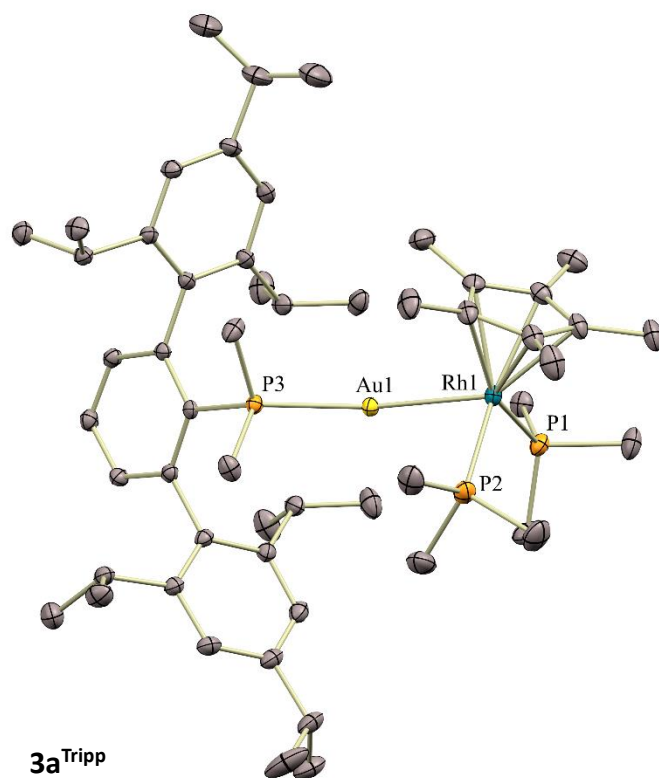


Figure 6. ORTEP diagram of compound **3a^{Tripp}**

III.3. DFT Mechanistic studies for the reaction between 1a and 2^{Tripp} towards the formation of 4^{Tripp}

In a joint work with Doctor Juan Jose Moreno Diaz, another member of our research group, we investigated the possible mechanism to account for the formation of complexes **3** and **4**. We focused on the complexes with Xyl and Tripp phosphines because they are simpler than the Cyp analogue to carry out computational investigations. We investigated different mechanisms for the highly unusual formation of compounds **4**. The first one

was the conceptually simplest mechanism for the formation of type **4** complexes, which would be the intramolecular conversion of **1a** into a hydride fulvene complex, which could then be trapped by the electrophilic species **2**. The concerted transition state for the direct transfer of the proton/hydride presented an exceedingly large barrier (TS1 in Figure 7, 59.7 kcal/mol) to yield the aforementioned fulvene hydride complex at 21.5 kcal/mol. Interestingly, Cp* slippage to form an agostic complex presented a much lower barrier (TS2, 31.0 kcal/mol), from which C–H bond breaking to form the hydride is much more facile (TS3, 25.4 kcal/mol). Subsequent partial restoration of the Cp* hapticity does not seem rate limiting either (TS4). These barriers are overly large to be consistent with experimental reaction conditions, which rules out an unassisted intramolecular equilibrium of **1a** to form a fulvene hydride complex.

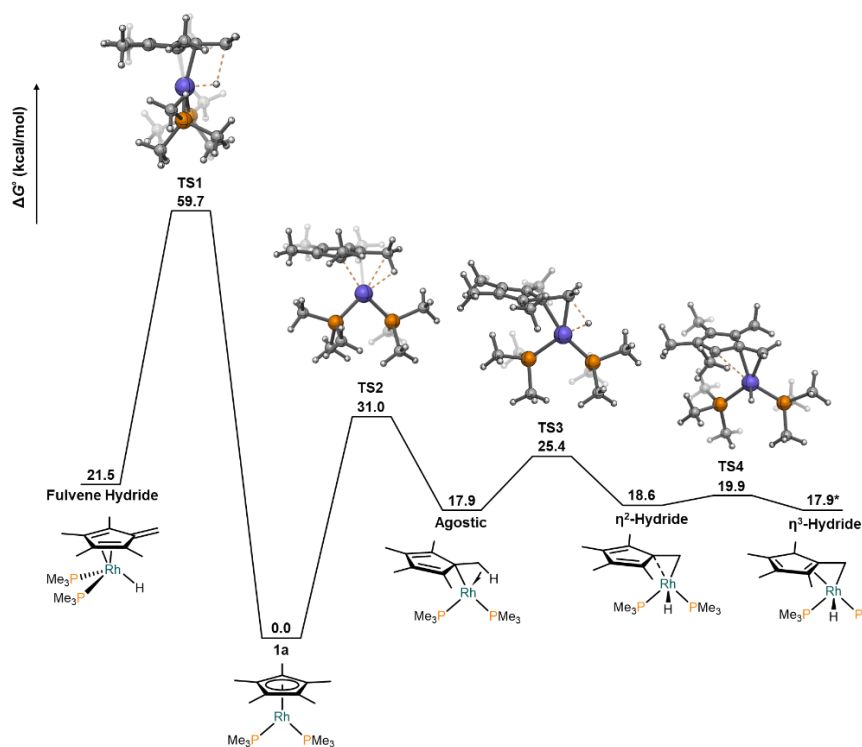


Figure 7. Free energy profile for the intramolecular conversion of **1a** into a fulvene hydride complex. * SCF energy relative to TS4.

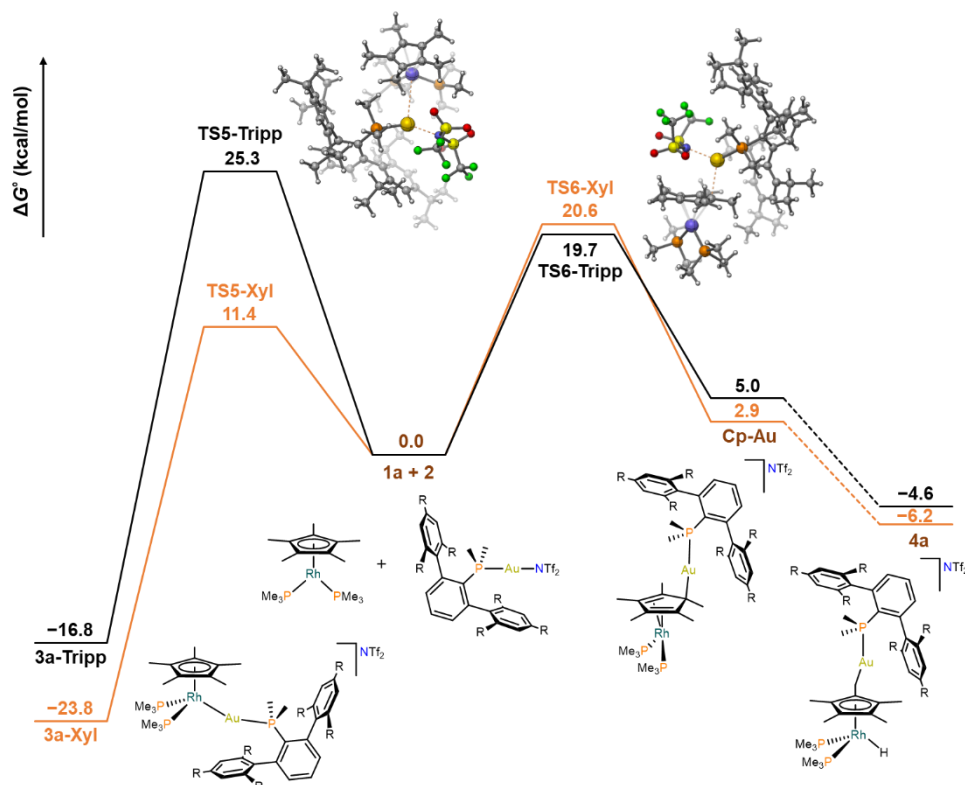


Figure 8. Free energy profile encompassing Lewis adduct formation, binding of Au(I) to the Cp* and thermodynamics of formation of **4a** species for Xyl (orange) and Tripp (black).

We then wondered whether type **2** complexes could facilitate any of these reaction pathways (figure 8). Both the Xyl and Tripp systems were computationally studied to gain insight into the role of steric hindrance in the reaction outcome (Figure 8). In agreement with experimental findings, the formation of species **4a**^{Tripp} is under kinetic control, as the thermodynamic product is the Lewis adduct. The Xyl system presents a low barrier (TS5-Xyl, 11.4 kcal/mol) for the formation of the Lewis adduct, as expected due to the lower steric demand of the phosphine. In turn, for the Tripp system the transition state lies at 25.3 kcal/mol, which we found to be

competitive (TS6-Tripp, 25.5 kcal/mol) with the binding of the gold center to a carbon atom of the anionic Cp* ring, forming a Rh-diene complex at 5.0 kcal/mol (**Cp-Au**). This species cannot be accessed by the Xyl system, as the barrier for the formation of **3a^{Xyl}** is much lower. We sought to investigate whether the binding of the electrophilic gold center to the Cp* was key to promote hydride transfer to the Rh center concomitant with the formation of the Au-CH₂ bond in order to form species **4a^{Tripp}**. Using **Cp-Au^{Xyl}** as a reference, it was clear that despite the pyramidalization that accompanies the formation of the Au-C bond pushing a methyl group towards rhodium, the concerted hydride transfer and gold migration to the nascent CH₂ moiety remains inaccessible (TS7 in Figure 9, 49.4 kcal/mol). In turn, the barrier to form an agostic complex via slippage drops to 22.5 kcal/mol (TS8-Xyl, *cf* TS2 at 31.0 kcal/mol), from which hydride formation (TS9-Xyl) lies at 25.0 kcal/mol, comparable to the unassisted pathway (TS3). We then moved to study the bulkier Tripp system, to ascertain whether these effects were not countered by increased steric demands (Figure 10).

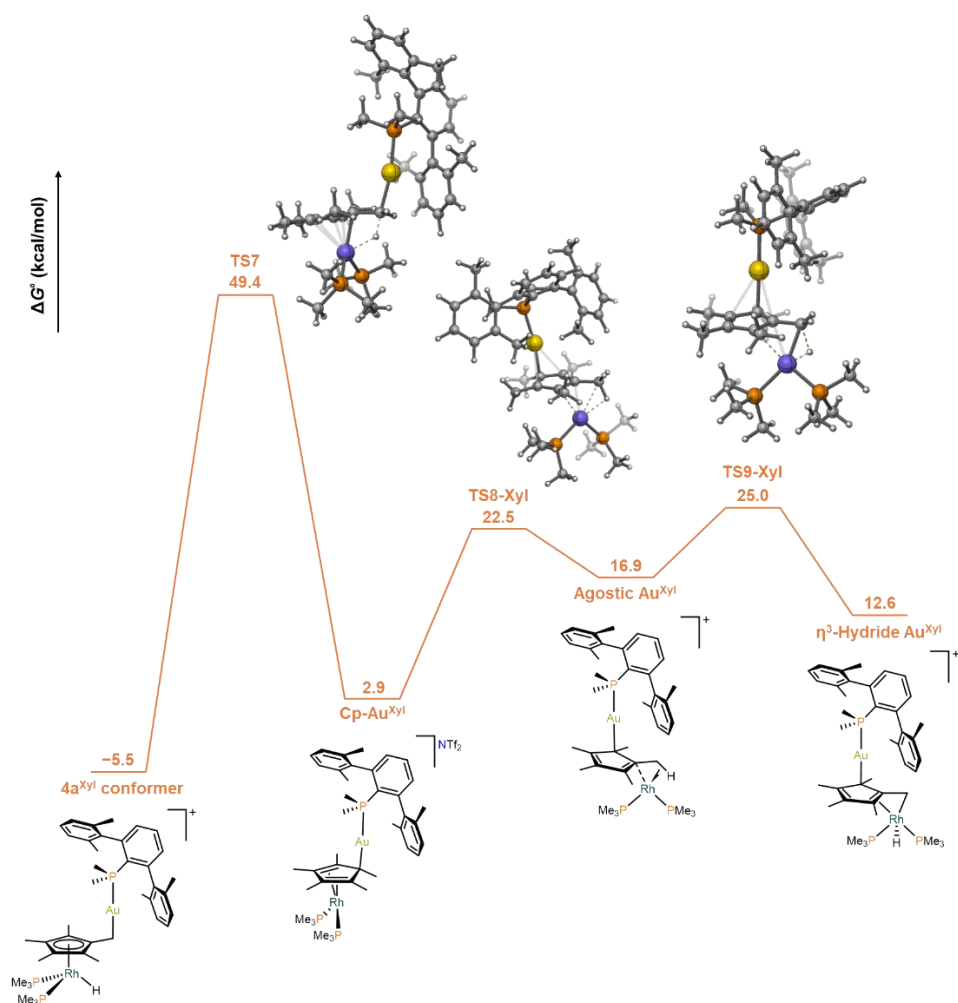


Figure 9. Free energy profile of the direct (left) and stepwise (right) transfer of a hydride from the Cp* to Rh for the Xyl system.

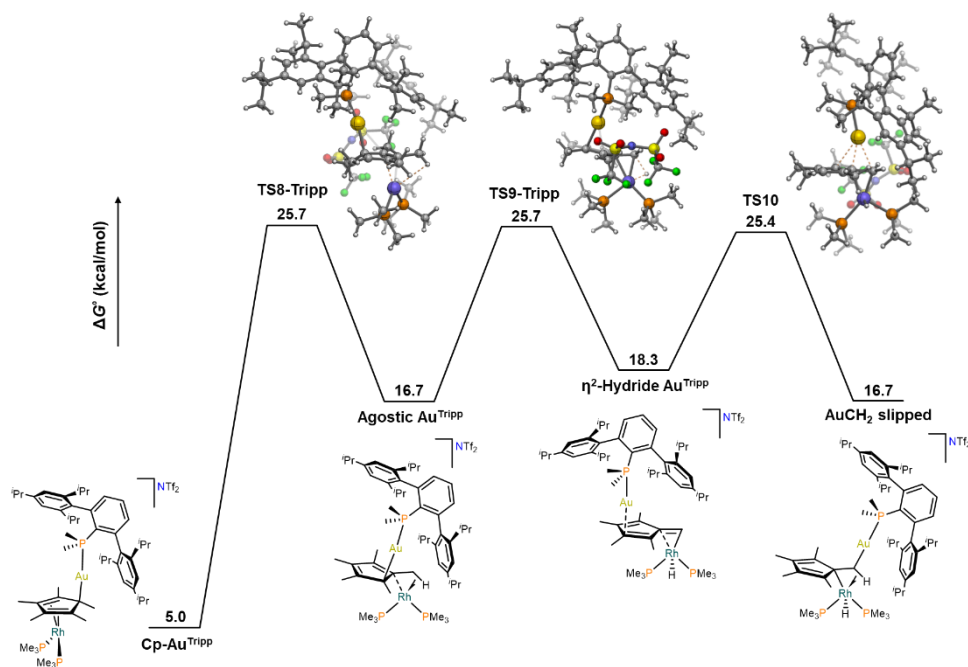


Figure 10. Free energy profile for the conversion of **Cp-Au^{Tripp}** into **4a^{Tripp}**.

The formation of the corresponding agostic complex for the Tripp system presents a barrier of 25.7 kcal/mol, competitive with that of the formation of the Lewis adduct (TS5-Tripp, 25.3 kcal/mol), consistent with the formation of a mixture of **3a^{Tripp}** and **4a^{Tripp}**. Subsequent barriers for the formation of the Rh hydride and for the migration of the gold center towards the CH₂ moiety present similar barriers of 25.7 and 25.4 kcal/mol, respectively (TS9-Tripp and TS10). Therefore, a plausible mechanism for this unusual transformation encompasses the binding of the Lewis acidic gold center to the Cp* inner ring. The bulkiness of the Lewis acid dictates selectivity, kinetically controlling Lewis adduct formation. Two alternative pathways, involving hydride abstraction by the Lewis acid and concerted Au–C bond formation concomitant with HNTf₂ release were found to be higher energy. Their key transition states are represented in Figures 11 and 12.

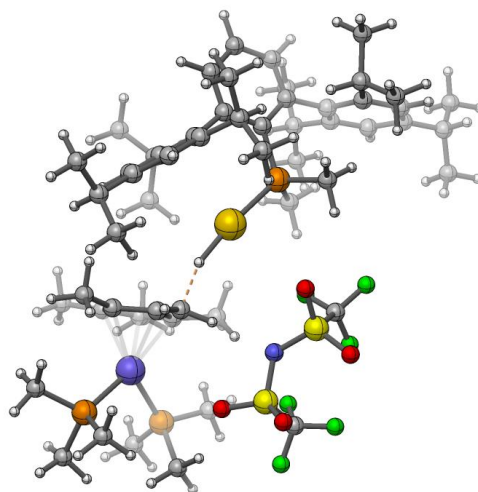


Figure 11. Transition state for the abstraction of a hydride from the Cp* by the gold center for the Tripp system (TS11, 28.1 kcal/mol).

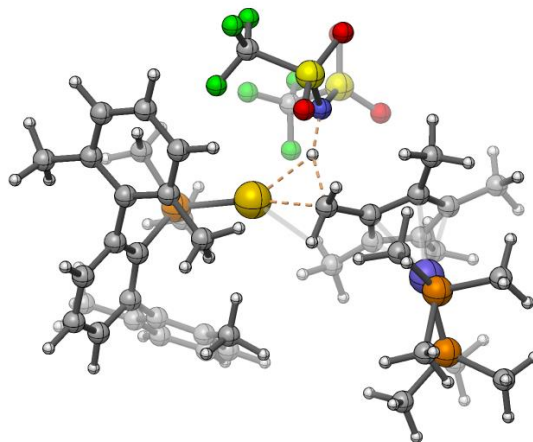
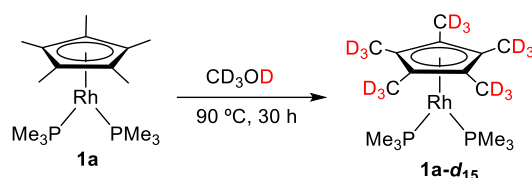


Figure 12. Transition state for the concerted formation of Au-C and N-H bonds for the Xyl system (TS12, 41.2 kcal/mol).

III.4. Isotopic labelling studies on the Rh/CH₃ hydride migration in complex **4a^{Cyp}**

In order to demonstrate the origin of the hydride ligand in compounds **4a** we aimed to access a perdeuterated isotopologue of **1a**. The

cyclopentadienyl ligand in **1a** was fully labelled by heating in CD₃OD solution at 90 °C for 30 hours without any apparent decomposition (Scheme 3, Figure 13). Full deuteration of Cp* is well documented; however, it usually requires either the addition of an external base to favour deprotonation/protonation routes or the presence of a basic ligand for the same purpose^{6a,8}.



Scheme 3. Isotopic labelling of **1a** in CD₃OD.

⁸ See for example: a) J.-R. Hamon, P. Hamon, S. Sinbandhit, P. Guenot, D. Astruc, *J. Org. Chem.*, **1991**, *413*, 243-255.

b) C. S. Wei, C. A. Jiménez-Hoyos, M. F. Videa, J. F. Hartwig, M. B. Hall, *J. Am. Chem. Soc.*, **2010**, *132*, 3078-3091.

c) G. Ciancaleoni, S. Bolaño, J. Bravo, M. Peruzzini, L. Gonsalvi, A. Macchioni, *Dalton Trans.*, **2010**, *39*, 3366-3368.

d) M. Carmona, J. Ferrer, R. Rodríguez, V. Passarelli, F. J. Lahoz, P. García-Orduña, L. Cañadillas-Delgado, D. Carmona, *Chem. Eur. J.*, **2019**, *25*, 13665-13670.

e) R. Poli, *Chem. Rev.*, **1991**, *91*, 509-551

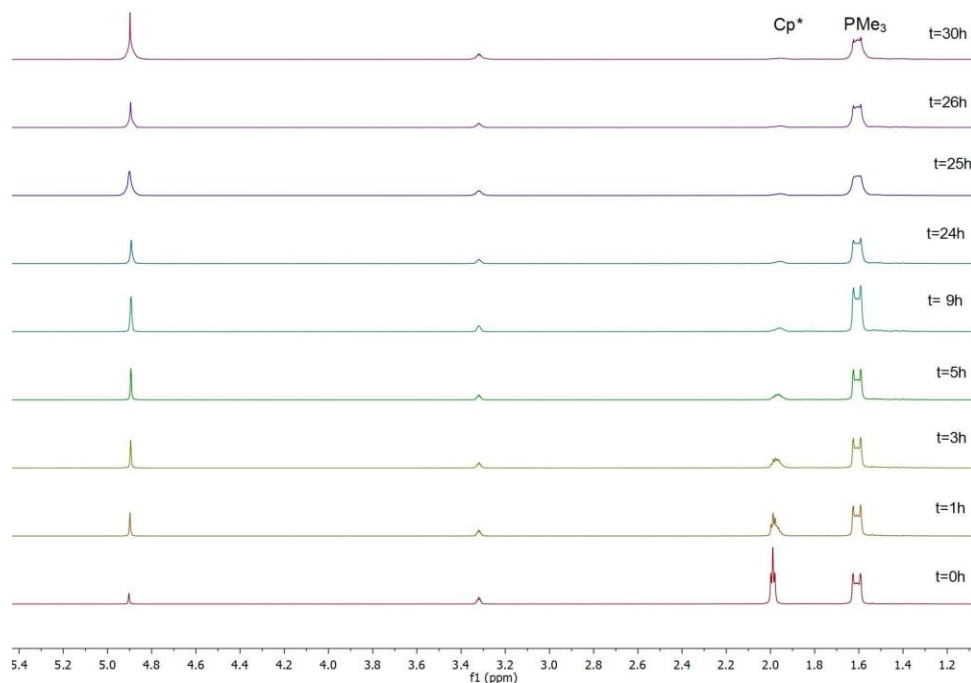


Figure 13. ^1H NMR monitoring of the deuteration the cyclopentadienyl ligand in compound **1a**.

The deuteration of **1a** in the absence of external additives speaks in favour of the basic role played by the rhodium centre. Brookhart has suggested that deuteration of related $[(\eta^5\text{-C}_5\text{Me}_5)\text{Rh}(\text{olefin})_2]$ compounds may proceed through a bimolecular route⁹, though it does not seem to apply in this case, where the disappearance of the ^1H NMR signal due to Cp* follows first-order kinetics ($k_1 = 6.66 \cdot 10^{-5} \text{ s}^{-1}$; Figure 14).

⁹ P. H. Budzelaar, J. J. Engelberts, J. H. van Lenthe, *Organometallics*, **2003**, 22, 1562–1576.

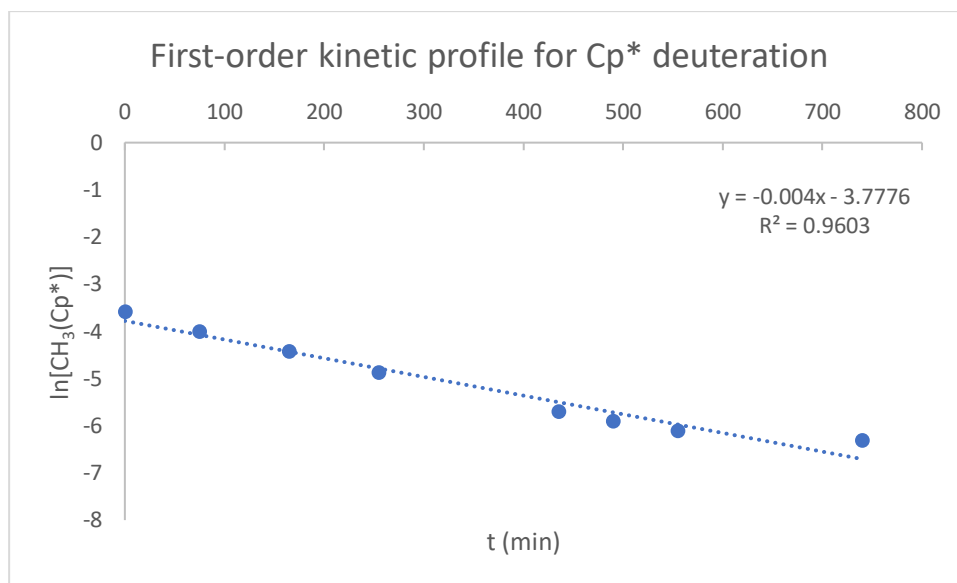
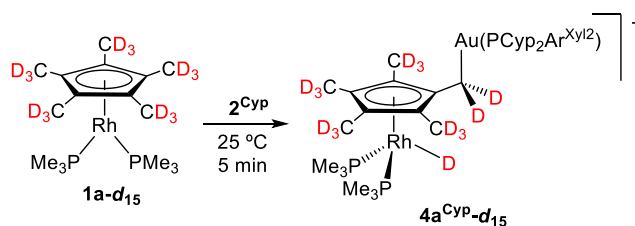


Figure 14. First-order kinetic representation for the deuteration of the cyclopentadienyl ligand in **1a**, accounting for a k_1 of $6.66 \cdot 10^{-5} \text{ s}^{-1}$.

As anticipated, treatment of isotopologue **1a-d₁₅** with [(PCyp₂Ar^{Xyl2})Au(NTf₂)] (**2^{Cyp}**) immediately yields the corresponding bimetallic product derived from Cp* activation, for which the absence of a low-frequency ¹H NMR signal illustrates the migration of the deuterium from a methyl group of the Cp* ring (Scheme 4).



Scheme 4. Synthesis of isotopologue **4a^{Cyp}-d₁₅** by reaction of **1a-d₁₅** and **2^{Cyp}**.

III.5. Reactivity of Rh/Au bimetallic compounds **3a** and **4a** towards polar E—H bonds (E = O, N)

We gained further evidence for the reversibility of the Rh/CH₃ hydride migration process by conducting reactivity studies and taking advantage of additional isotopic labelling experiments. We explored the reactivity of Rh/Au bimetallic compounds **3a** and **4a** towards polar E—H bonds, particularly those of NH₃, MeOH and H₂O. Their activation by transition metal complexes is often challenging, particularly for the case of the N—H bonds in ammonia¹⁰. This is due to the formation of Werner-type complexes that typically quench any further reactivity at the metal site. There are, however, examples that demonstrate the potential of bimetallic entities to tackle these difficulties¹¹. In the present case, we noticed that metal adducts **3a** exhibit no reactivity towards the explored E—H bonds, while compounds of type **4a** were active even under very mild conditions (Scheme 5), particularly for N—H activation.

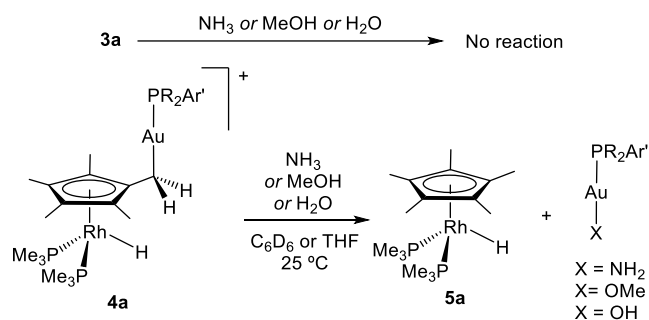
¹⁰ Selected examples of ammonia activation by transition metal complexes: a) J. Zhao, A. S. Goldman, J. F. Hartwig, *Science*, **2005**, *307*, 1080-1082.

b) C. M. Fafard, D. Adhikari, B. M. Foxman, D. J. Mindiola, O. V. Ozerov, *J. Am. Chem. Soc.*, **2007**, *129*, 10318-10319.

c) J. Abbenseth, M. Kinauer, F. W. Heinemann, C. Würtele, B. de Bruin, S. Schneider, M. G. Scheibel, *Inorg. Chem.*, **2015**, *54*, 9290-9302.

¹¹ a) S. Jamali, S. Abedanzadeh, N. K. Khaledi, H. Samouei, Z. Hendi, S. Zacchini, R. Kia, H. R. Shamsavari, *Dalton Trans.*, **2016**, *45*, 17644-17651.

b) N. Hidalgo, C. Maya, J. Campos, *Chem. Commun.*, **2019**, *55*, 8812-8815.



Scheme 5. Reactivity studies of bimetallic Rh/Au compounds towards E—H bonds of ammonia, methanol and water.

This behaviour was especially obvious for the mixture of $\mathbf{3a}^{\text{Tripp}}$ and $\mathbf{4a}^{\text{Tripp}}$, where only the Cp*-activated compound ($\mathbf{4a}^{\text{Tripp}}$) evolved and the bimetallic adduct ($\mathbf{3a}^{\text{Tripp}}$) remained unaltered (Figure 15).

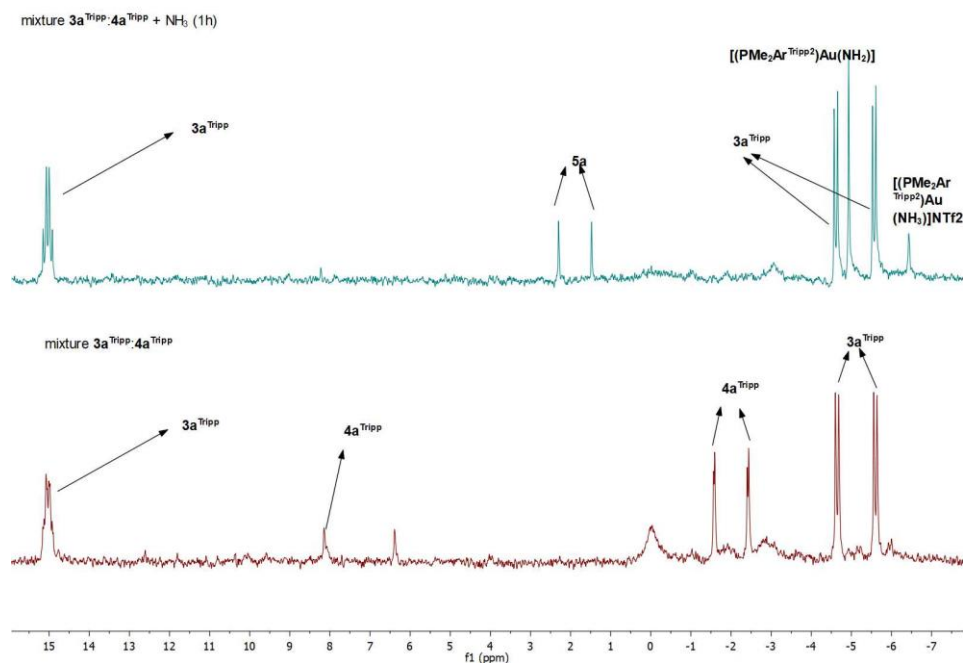
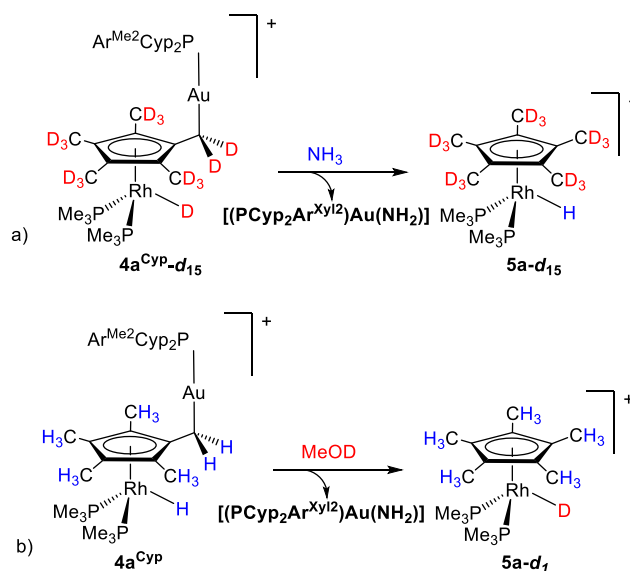


Figure 15. Superimposed representation of $^{31}\text{P}\{^1\text{H}\}$ NMR spectra of the isomeric mixture $\mathbf{3a}^{\text{Tripp}}$: $\mathbf{4a}^{\text{Tripp}}$ before and after exposure to NH_3 (0.5 bar).

For convenience, we focused on the reactivity of **4a^{Cyp}** to inspect these reactions in more detail. This compound evolved into equimolar mixtures of cation $[(\eta^5\text{-C}_5\text{Me}_5)\text{Rh}(\text{PMe}_3)_2\text{H}]^+$ (**5a**)¹ and the corresponding neutral gold complex $[(\text{PCyp}_2\text{Ar}^{\text{Xyl}2})\text{Au}(\text{X})]$ (where X stands for NH_2 (**2^{Cyp}·NH₂**), OMe (**2^{Cyp}·OMe**) or OH (**2^{Cyp}·OH**); Scheme 5).

Regarding the Rh/Au bimetallic reactivity, the rate of E—H bond activation varied markedly for the three substrates. While the N—H bond in ammonia was readily cleaved ($t_{1/2} \approx 30$ min), the activation of methanol and water was significantly slower (MeOH: $t_{1/2} \approx 48$ h; H₂O: $t_{1/2} \approx 5$ days). We hypothesized that the reduced activity of **4a^{Cyp}** towards methanol and water is likely derived from the low oxophilicity of gold¹², and in the latter case because of solubility issues. Importantly, when the reaction with ammonia was carried out using labelled **4a^{Cyp}-d₁₅**, a distinctive hydridic signal became discernible by ¹H NMR spectroscopy (Scheme 6).



¹² K. P. Keep, *Inorg. Chem.*, **2016**, 55, 9461-9470.

Scheme 6. Isotopic labelling experiments. (a) reaction between isotopically labelled **4c-d₁₅** and ammonia; reaction between **4c** and deuterated methanol.

Similarly, the reaction of non-deuterated **4a^{Cyp}** with CD₃OD yields $[(\eta^5\text{-C}_5\text{Me}_5)\text{Rh}(\text{PMe}_3)_2\text{D}]^+$ as the major Rh-containing species. These results provide further evidence for reversibility concerning hydride migration. As discussed in the previous section, one possibility that finds precedent in Cp* complexes of early transition metals involve hydride migration to the metal with the formation of a fulvene intermediate¹³. Such an intermediate could subsequently be trapped by electrophilic gold, as seen in a related system based on cobaltocene and an acidic iron species¹⁴. However, our already discussed computational studies have clearly ruled out that mechanism and instead favour the active participation of gold during hydride transfer.

The notion of reversibility is also in agreement with an FLP-type activation of E—H bonds in the more congested system based on PCyp₂Ar^{Xyl₂}, where small amounts of monometallic Lewis base (**1a**) and acid (**2^{Cyp}**) may form in solution, behaving as an unusual thermally induced bimetallic FLP¹⁵. In fact, treatment of independently prepared $[(\text{PCyp}_2\text{Ar}^{\text{Xyl}_2})\text{Au}(\text{NH}_3)](\text{NTf}_2)$ with **1a** provide the same reaction outcome,

¹³ a) J. E. Bercaw, *J. Am. Chem. Soc.*, **1974**, *96*, 5087-5094.

b) C. McDade, J.C. Green, J. E. Bercaw, *Organometallics*, **1982**, *1*, 1629-1634.

c) A. R. Bulls, W. P. Schaefer, M. Serfas, J. E. Bercaw, *Organometallics*, **1987**, *6*, 1219-1226.

d) F. G. N. Cloke, J. P. Day, J. C. Green, C. P. Morley, A.C. Swain, *J. Chem. Soc. Dalton Trans.*, **1991**, 789-796.

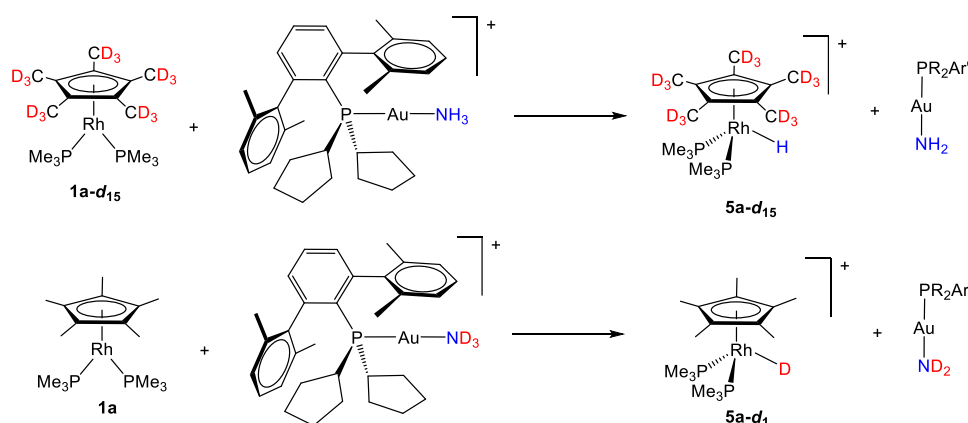
f) H. J. Kraus, H. Werner, *Angew. Chem. Int. Ed. Engl.*, **1982**, *21*, 866-867.

g) H. Werner, G. T. Crisp, P. W. Jolly, H.-J. Kraus, C. Krüger, *Organometallics*, **1983**, *2*, 1369-1377.

¹⁴ Y. Ohki, A. Murata, M. Imada, K. Tatsumi, *Inorg. Chem.*, **2009**, *48*, 4271-4273.

¹⁵ M. J Chalkley, T. J. Del Castillo, B. D. Matson, J. C. Peters, *J. Am. Chem. Soc.* **2018**, *140*, 6122-6129.

that is, quantitative formation of equimolar amounts of compounds **5a** and **2^{Cyp}·NH₂**. Accordingly, when isotopologue **1a-d₁₅** was used instead, compound **5a-d₁₅** was formed with no deuteration at the hydride position, whereas the reaction between **1a** and [(PCyp₂Ar^{Xyl2})Au(ND₃)](NTf₂) yielded the corresponding **5a-d₁** deuteride.



Scheme 7. Isotopic labelling experiments between Rh compound **1a** and [(PCyp₂Ar^{Xyl2})Au(NH₃)](NTf₂) and their isotopologues.

To gain deeper knowledge on the cooperative activation of E-H bonds, the mechanism of the reaction between complexes **1a** and **2^{Tripp}** with ammonia was been studied by Dr. Juan José Moreno Díaz. Although this theoretical work is totally independent of this Thesis, a summary of the results is given below. A detailed mechanism for this reaction is obtained from a computational study of stationary points along the potential energy surface of the path from **1a** + **2^{Tripp}** to an amido bridge complex with a [Au₂(μ-NH₂)] core (Figure 16).

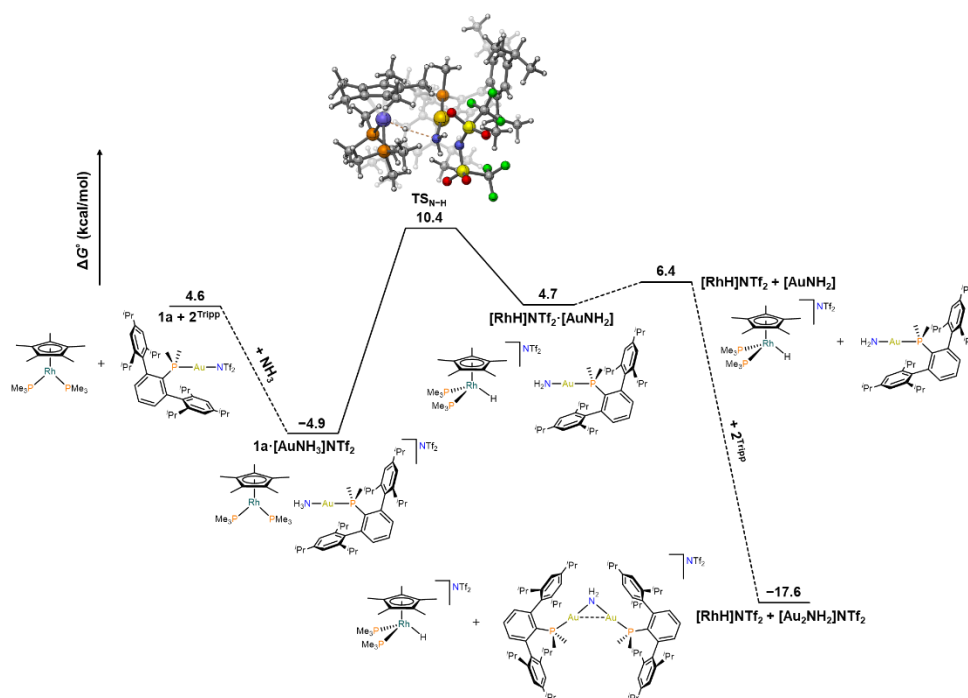


Figure 16. Free energy profile for the cooperative activation of NH_3 by combining **1a** and **2^{Tripp}**.

In solution, we have demonstrated that only compounds **4** are active towards E-H bond activation. Nonetheless, both metal centers in complex **4a^{Tripp}** are saturated, but the evolution of **4a^{Tripp}** towards the Lewis adduct **3a^{Tripp}** clearly indicates that the independent fragments are accessible in solution ($[\text{Rh}] + [\text{Au}]$ in Figure 8). DFT calculations locate the independent fragments solely 4.6 kcal/mol above **4a^{Tripp}**. Then, the weakly coordinating triflimide in **2^{Tripp}** is readily displaced by ammonia, a reaction that is largely exergonic (9.5 kcal/mol). Binding to the electrophilic gold(I) center lowers the barrier for deprotonation by the basic Rh center to 15.3 kcal/mol, in a way that is highly resembling of conventional FLPs. However, this reaction is thermoneutral relative to the fragments, but overall endergonic relative to **4a^{Tripp}**. We also computed these fragments independently to ensure translational entropy was not responsible for the endergonic. We therefore

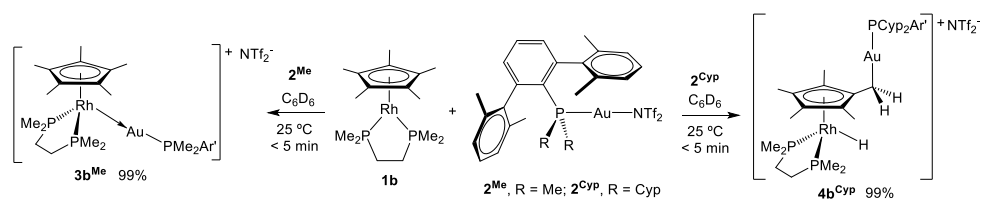
evaluated that, under the reaction conditions, the generated gold amido complex and unreacted **2^{Tripp}** could rapidly evolve to form a bridged amido, cationic digold complex featuring an aurophilic interaction, an event that is more than sufficiently exergonic to drive the reaction forward.

III.6. Modification of phosphine properties of Cp*Rh complexes **1**.

We first decided to examine the effects of modifying the simple trimethyl phosphine ligands in **1a**. To circumvent the possibility of ligand dissociation during Cp* and small molecule activation, we selected the chelating bisphosphines 1,2-bis(dimethylphosphino)ethane (dmpe) and 1,2-bis(diphenylphosphino)ethane (dppe), which led to compounds **1b** and **1c**, respectively. These compounds were prepared following the same procedure employed to access **1a**. In terms of the electrophilic gold fragment, we focus on compounds **2^{Me}** and **2^{Cyp}** which gave rise to only one product in their respective reactions with **1a**.

As anticipated, the combination of the rhodium precursor **1b** with gold compounds **2^{Me}** and **2^{Cyp}** led to analogous reactivity to that observed for the Rh(I) species **1a** (Scheme 8), owing to their similar stereoelectronic properties. Therefore, the smaller [(PMe₂Ar^{Xyl})Au]⁺ fragment leads to quantitative formation of the corresponding Rh(I)→Au(I) metal-only Lewis pair (MOLP)³ (**3b^{Me}**). In contrast, the more sterically congested [(PCyp₂Ar^{Xyl})Au]⁺ unit triggers the immediate migration of a hydride towards the rhodium centre with formation of a new Au-CH₂ bond in the Cp*-functionalized compound **4b^{Cyp}**, without any trace of bimetallic dative bonding. The formation of these bimetallic species is easily inferred from multinuclear NMR spectroscopy. A distinctive AB₂ pattern demonstrating the formation of a bimetallic species arises in the ³¹P{¹H} NMR spectrum

of **3b^{Me}**, with an apparent double triplet at 14.6 ppm ($^2J_{\text{PRh}} = 12$, $^3J_{\text{PP}} = 9$ Hz) and a double doublet at 45.5 ppm ($^1J_{\text{PRh}} = 154$, $^3J_{\text{PP}} = 9$ Hz), due to $\text{PMe}_2\text{Ar}^{\text{Xyl}2}$ and dmpe ligands, respectively. In turn, the ^1H NMR spectrum of **4b^{Cyp}** reveals the formation of a new hydride ligand resonating at -13.6 ppm (td, $^2J_{\text{HP}} = 34$, $^1J_{\text{HRh}} = 26$ Hz) and the distinctive asymmetry of the Cp* ligand, now transformed into the $\{\text{C}_5\text{Me}_4\text{CH}_2\text{AuP}\}$ moiety, leading to three resonances at 1.74, 1.69 and 1.21 ppm (d, $^2J_{\text{HP}} = 7.7$ Hz) in a 3:3:1 ratio. The molecular structure of **4b^{Cyp}** was authenticated by X-ray diffraction studies from single crystals grown by slow diffusion of pentane into a saturated benzene solution (Figure 17). The rhodium centre adopts a piano-stool conformation to accommodate the newly form hydride ligand, while the $[(\text{PCyp}_2\text{Ar}^{\text{Xyl}2})\text{Au}]^+$ unit displays an orthogonal arrangement relative to the Cp* plane (85.22°).



Scheme 8. Bimetallic reactivity between Lewis basic Rh(I) compound **1b** and Lewis acidic Au(I) compounds **2^{Me}** and **2^{Cyp}**.

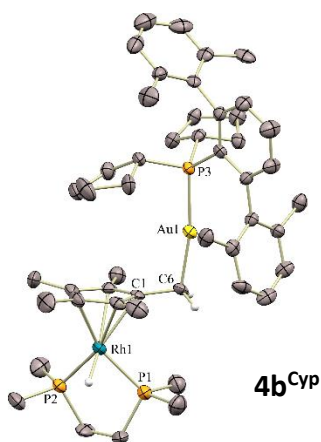
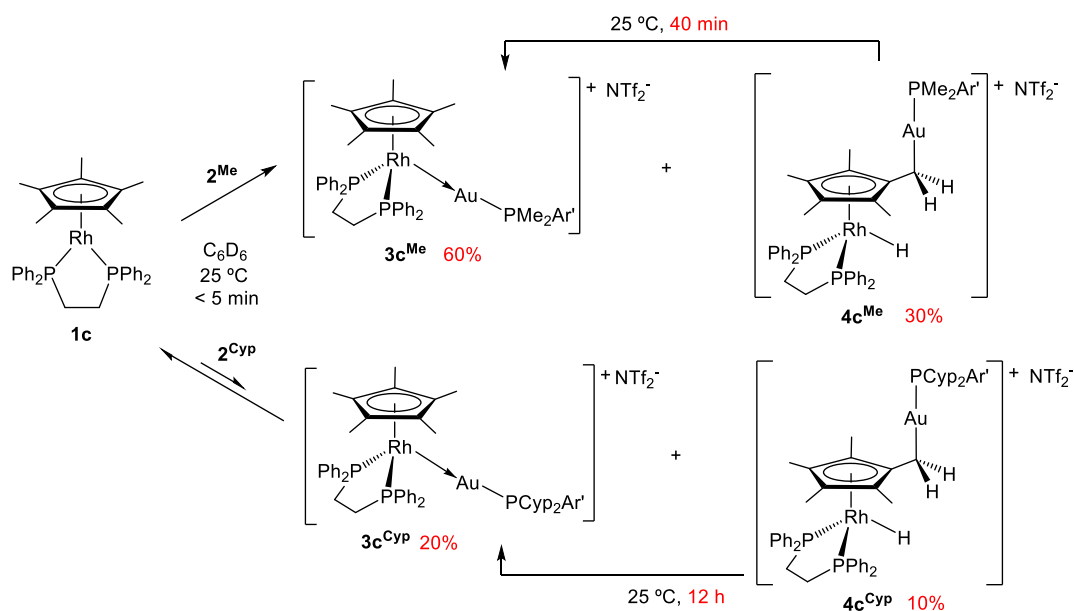


Figure 17. ORTEP diagram of compound **4b^{Cyp}**

We envisioned that the bulkier and less basic dppe ligand would induce differences in the bimetallic reactivity of precursor **1c** due to steric and electronic effects. In this case, reaction with the smaller $\text{PMe}_2\text{Ar}^{\text{Xyl}2}$ -based gold complex **2^{Me}** not only produced the predicted bimetallic Lewis adduct **3c^{Me}**, but also small amounts of the Cp*-functionalized product **4c^{Me}** in around 30% spectroscopic yield (Scheme 9). Nonetheless, the latter species rapidly evolve to the thermodynamic product **3c^{Me}**, though its formation suggest that the higher steric pressure exerted by dppe compared to dmpe partially hampers the approximation of the two metal sites and facilitates the detection of **4c^{Me}**, not discernible for neither **1a** or **1b** for the smaller $\text{PMe}_2\text{Ar}^{\text{Xyl}2}$ gold system. This finding also supports the reversibility of the proton migration from Cp* to rhodium. Although the isolation of the minor species **4c^{Me}** was not possible, its existence is corroborated by multinuclear NMR analysis. Thus, distinctive resonances in the ^1H NMR are found at -12.30 ppm for the hydride ligand and at 1.99, 1.91 and 0.37 (d, $^2J_{\text{HP}} = 9$ Hz) for the functionalized Cp* ring. $^{31}\text{P}\{^1\text{H}\}$ NMR signals recorded at 73.4 and 40.8 ppm due to dppe and $\text{PMe}_2\text{Ar}^{\text{Xyl}2}$ ligands, respectively, are also in agreement with the analogous signals associated to **4a^{Cyp}** and **4b^{Cyp}**.



Scheme 9. Bimetallic reactivity between Lewis basic Rh(I) compound **1c** and Lewis acidic Au(I) compounds **2^{Me}** and **2^{Cyp}**.

In stark contrast, when we carried out the same study with the bulkier gold complex **2^{Cyp}** a different scenario ensues: if the reaction is carried out at low temperature, the species in major proportion remain to be the two starting complexes **1c** and **2^{Cyp}**. At room temperature we observe the formation of both the Cp*-activated product **4c^{Cyp}** as minor species and the bimetallic Lewis adduct **3c^{Cyp}** while the monometallic precursors **1c** and **2^{Cyp}** remain as the major components (Scheme 9). It is important to remark that despite being the more congested Rh(I) compound, the formation of the bimetallic adduct **3c^{Cyp}** is viable, which differs from Rh(I) precursors **1a** and **1b**. We thus attribute this difference to the reduced donating capacity of dppe, leading to a less basic Rh(I) site and possibly to a less favoured metal protonation by migration from the Cp* ligand. In fact, the activation product **4c^{Cyp}** is initially formed but disappears after several hours in favour of a mixture of **1c**, **2^{Cyp}** and **3c^{Cyp}**, evincing the reversibility of the formation of

the Au–C bond and concomitant proton migration, as occurs for the $\text{PMe}_2\text{Ar}^{\text{Xyl}2}$ system. Furthermore, the latter three species are in dynamic equilibrium, which allowed us to spectroscopically investigate the thermodynamics of such a process. A solution of complexes **1c** and **2c**^{Cyp} in benzene-*d*₆ was monitored for 24 hours to ensure the complete absence of **4c**^{Cyp}, then a van't Hoff analysis (figure 18) over a 60 K range yielded thermal parameters for the equilibrium of $\Delta H = 0.34$ kcal/mol and $\Delta S = -2.52$ cal/K·mol, corresponding to $\Delta G_{298} = 1.09$ kcal/mol for the formation of the bimetallic adduct **3c**^{Cyp}. The very small and positive enthalpic value enables the persistence of the monometallic fragments in solution, a prerequisite for exhibiting bimetallic FLP reactivity. In turn, we attribute the mildly negative entropic parameter to the release of the triflimidate anion upon formation of the Rh→Au dative bond.

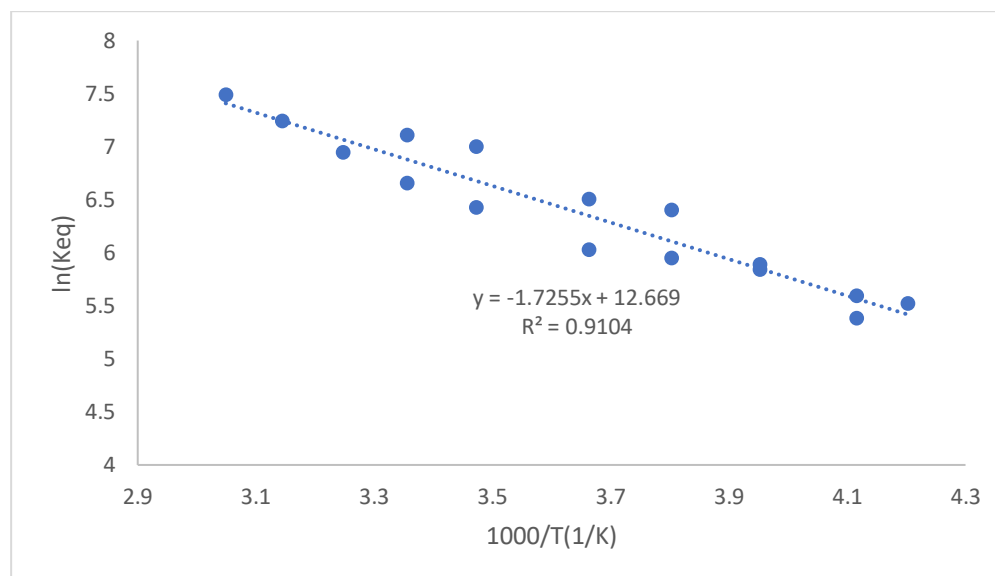


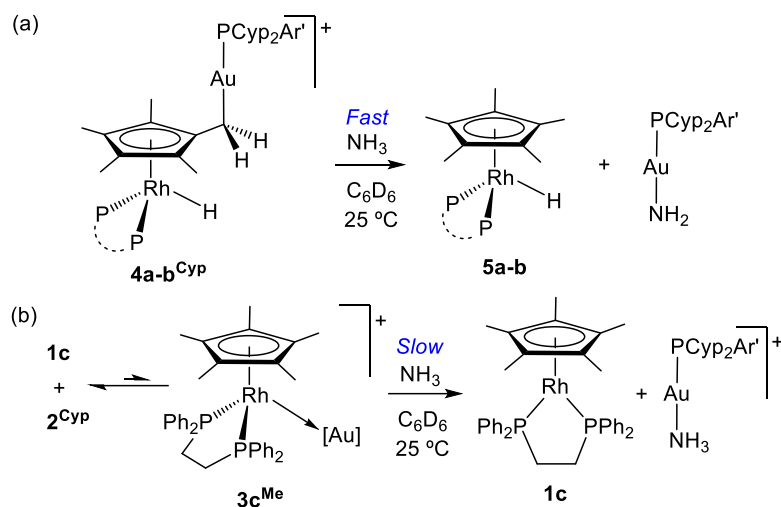
Figure 18. Van't Hoff plot derived from variable temperature ¹H NMR spectra of the equilibrium between **1c** and **2c**^{Cyp} with **3c**^{Cyp} from 298 K to 238 K.

Therefore, it seems that the higher steric profile of dppe compared to PMe_3 and dmpe partly impede the formation of an inactive bimetallic

adduct, while the reduced basicity of the resulting Rh(I) precursor **1c** limits its capacity to accommodate a hydride ligand from the Cp* moiety with the resulting oxidation to Rh(III). We tested whether this modulation in bimetallic reactivity has a direct effect on the activation of small molecules, for which we selected the activation of the N–H bond in ammonia that we already described for **4a**^{Cyp}. Compound **4b**^{Cyp} also mediates the heterolytic cleavage of ammonia under mild conditions (1 bar, 25 °C; Scheme 10) to yield mononuclear species $[(\eta^5\text{-C}_5\text{Me}_5)\text{Rh}(\text{L}_2)\text{H}]^+$ (**5b**, L₂ = dmpe) and **2**^{Cyp}·NH₂¹⁶.

Contrarily, the equilibrium mixture comprised of **1c**, **2**^{Cyp} and **3c**^{Cyp} fails to cleavage the N–H bond under similar conditions. Instead, only **2**^{Cyp} readily converts into the corresponding ammonia adduct $[(\text{PCyp}_2\text{Ar}^{\text{Xyl}_2})\text{Au}(\text{NH}_3)](\text{NTf}_2)$. Subsequently, the mixture slowly evolves to a solution containing the latter adduct and Rh(I) precursor **1c** in detriment of the bimetallic pair **3c**^{Cyp}. Therefore, the reduced basicity of dppe compared to dmpe or PMe₃ hampers the use of the corresponding Lewis basic Rh(I) precursor as a metallic FLP component under these conditions.

¹⁶ M. G. Alférez, J. J. Moreno, N. Hidalgo, J. Campos. *Angew. Chem. Int. Ed.*, **2020**, *59*, 20863-20867.



Scheme 10. (a) FLP-type N–H bond activation in ammonia by Rh(I)/Au(I) bimetallic pairs vs (b) no cooperative activation and ammonia adduct formation.

III.7. Substituting the Cp* ligand in compounds 1 by the Indenyl ligand in Rh complexes 6

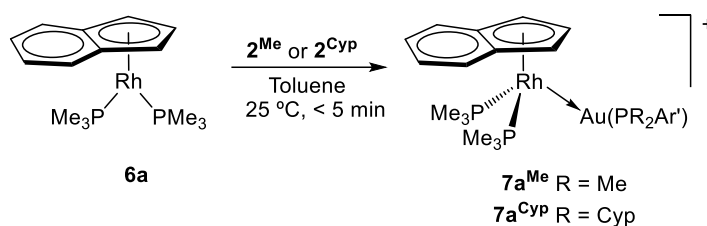
With the aim of circumventing the discussed non-innocence character of Cp* to access a broader family of Rh(I)/Au(I) bimetallic FLPs we decided to study analogous Rh(I) precursors based on the well-known indenyl ligand ($[C_9H_7]^-$)¹⁷. Besides, we postulated that the greater capacity of the latter ligand to navigate through variable hapticities (from η^1 to η^5) might offer a richer reactivity after FLP-type bimetallic bond activation. Initially, we prepared the previously reported compound $[(\eta^5-C_9H_7)Rh(PMe_3)_2]$ ¹⁸ (**6a**) as our benchmark indenyl-based species. To carry out comparative studies we synthesized analogous Rh(I) species bearing both dppe (**6c**) and the non-chelating and more sterically demanding PPh₃

¹⁷ V. B. Kharitonov, D. V. Muratov, D.A. Loginov, *Coordination chemistry reviews*, **2019**, 399, 213027.

¹⁸ T. B. Marder, J. C. Calabrese, D. C. Roe, T. H. Tulip, *Organometallics*, **1987**, 6(9), 2012-2014.

(**6d**), though we omitted a related dmpe version, anticipating identical behavior to **6a** in line to the previously discussed results.

Not surprisingly, the equimolar reaction of **6a** and the smaller gold precursor **2^{Me}** led to the corresponding bimetallic adduct **7a^{Me}** (Scheme 11).



Scheme 11. Bimetallic reactivity between Lewis basic indenyl-Rh(I) compound **6a** with Lewis acidic Au(I) compounds **2^{Me}** and **2^{Cyp}**.

In this case, the reaction with the bulkier **2^{Cyp}** similarly yielded the metal-metal bonded adduct **7a^{Cyp}**, which we attribute to the reduced steric pressure exerted by the indenyl ligand compared to Cp*. The two new adducts exhibit a similar pattern in their $^{31}\text{P}\{^1\text{H}\}$ NMR spectra, with two doublets due to PMe_3 (**7a^{Me}**, 3.9 ppm, $^1J_{\text{PRh}} = 158$ Hz; **7a^{Cyp}**, -6.2 ppm, $^1J_{\text{PRh}} = 159$ Hz) and the terphenyl phosphine (**7a^{Me}**, 4.6 ppm, $^2J_{\text{PRh}} = 18$ Hz; **7a^{Cyp}**, 43.4 ppm, $^2J_{\text{PRh}} = 19$ Hz). At variance with bimetallic adduct **3a^{Me}**, there is no observable scalar coupling between PMe_3 and PPh_3 phosphines, a feature attributable to the slightly different geometric environment around rhodium, as evidenced by X-ray diffraction studies (Figure 19). For instance, the Rh–Au–P angles in the indenyl systems are wider (**7a^{Me}**, 171.61(7); **7a^{Cyp}**, 168.21(10) $^\circ$) than in the Cp* complex **3a^{Tripp}** (157.90 $^\circ$), while the greater coordination flexibility of indenyl reflects into wider offset angles between the rhodium centre and the centroid of the η^5 -coordinated ring (**3a^{Tripp}**, 1.85 $^\circ$; **7a^{Me}**, 10.88 $^\circ$; **7a^{Cyp}**, 12.35 $^\circ$). Nonetheless, the three structures exhibit comparable Rh–Au bond distances of 2.593(1) (**3a^{Tripp}**), 2.5541(8) (**7a^{Me}**) and 2.5970(12) (**7a^{Cyp}**) Å, in all cases slightly lower than the sum of their

covalent radii (2.78 Å)⁸. Analogously, the calculated formal shortness ratio (FSR)¹⁹, namely the ratio between the M–M bond distance and the sum of their metallic radii, are almost identical and accounts for 1.00 (**3a**^{Tripp}), 0.99 (**7a**^{Me}) and 1.00 (**7a**^{Cyp}).

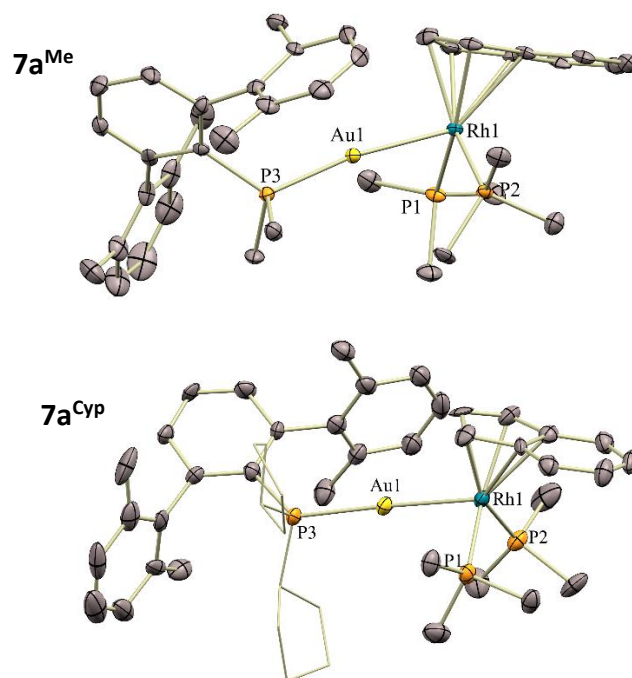
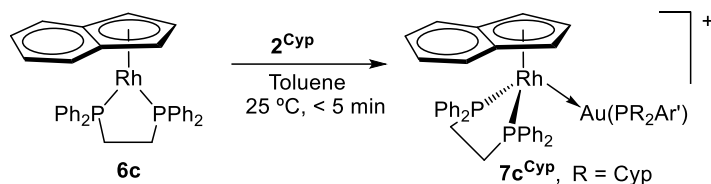


Figure 19. ORTEP diagrams of indenyl compounds **7a**^{Me} and **7a**^{Cyp}. Selected bond distances (Å) and angles(°): complex **7a**^{Me}: Rh1–P1, 2.2581(3); Rh1–P2, 2.248(2); Rh1–Au1, 2.5541(8); Au1–P3 2.250(3); P1–Rh1–P2, 98.16(9); P1–Rh1–Au1, 84.55(7); P2–Rh1–Au1, 83.95(7); P3–Au1–Rh1, 170.61(7). Complex **7a**^{Cyp}: Rh1–P1, 2.246(4); Rh1–P2, 2.262(4); Rh1–Au1, 2.597 (12); Au1–P3, 2.302(3); P1–Rh1–P2, 95.90(15); P1–Rh1–Au1, 89.02(10); P2–Rh1–Au1, 92.77(11); P3–Au1–Rh1, 168.21(10).

The combination of the more congested Rh(I) precursor **6c** with the bulkier Au(I) complex **2**^{Cyp} was then examined. Despite increasing the steric pressure, this mixture cleanly evolves to the corresponding metallic Lewis

¹⁹ L. Pauling, J. Am. Chem. Soc. 1947, 69, 542–553.

pair $7c^{Cyp}$ (Scheme 12), as inferred from two doublets in the $^{31}P\{^1H\}$ NMR spectrum at 74.7 and 47 ppm associated to dppe and $PCyp_2Ar^{Xyl_2}$, respectively.



Scheme 12. Bimetallic reactivity between Lewis basic indenyl-Rh(I) compound $6c$ with Lewis acidic Au(I) compounds 2^{Me} and 2^{Cyp} .

Crystals suitable for X-ray diffraction studies were grown by slow diffusion of pentane into a saturated benzene solution of $7c^{Cyp}$. Interestingly, its ORTEP diagram (Figure 20) reveals an elongated Rh–Au bond length of 2.6314(10) Å, though still within the sum of the corresponding covalent radii and with a FSR value of 1.02.

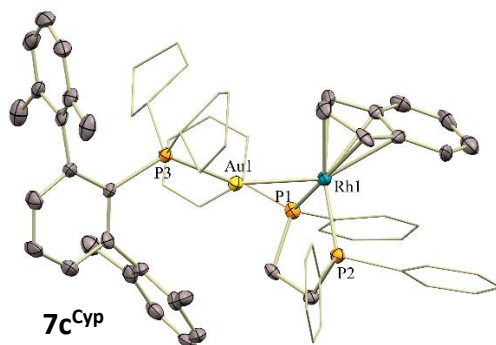
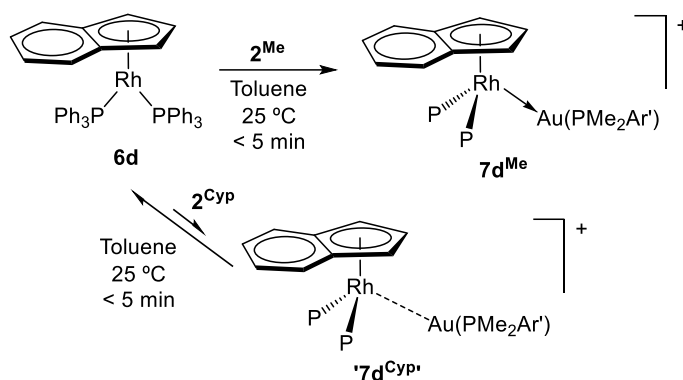


Figure 20. ORTEP diagram of indenyl compound $7c^{Cyp}$. Selected bond distances (Å) and angles (°): Rh1–P1, 2.232(3); Rh1–P, 2 2.243(3); Rh1–Au1, 2.6314(10); Au1–P3, 2.307(3); P1–Rh1–P2, 85.05(13); P1–Rh1–Au1 83.71(9); P2–Rh1–Au1, (90.77(9); P3–Au1–Rh1, 156.56(8).

Moving towards more congested systems, the analogous reaction with the PPh₃ containing rhodium complex **6d** was examined, in which case the formation of the bimetallic adduct does not take place (Scheme 13).



Scheme 13. Bimetallic reactivity between Lewis basic indenyl-Rh(I) compound **6d** with Lewis acidic Au(I) compounds **2^{Me}** and **2^{Cyp}**.

Instead, we observe broad ³¹P{¹H} NMR resonances associated to the corresponding monometallic precursors, indicating dynamic behaviour between these species and the bimetallic adduct that is not favoured in this case. When the reaction is monitored at -20 °C in the NMR probe the resonances narrow, as previously observed for other bimetallic FLPs investigated in our group²⁰. The reluctance to form a Rh→Au dative bond in this case is most likely due to steric reasons. In fact, treating compound **6d** with the smaller gold complex **2^{Me}** does yield the corresponding bimetallic pair **7d^{Me}**, which was fully characterized by spectroscopic means.

²⁰ a) J. Campos, *J. Am. Chem. Soc.*, **2017**, *139*, 2944-2947.

b) N. Hidalgo, J. J. Moreno, M. Pérez-Jiménez, C. Maya, J. López-Serrano, J. Campos, *Chem. Eur. J.*, **2020**, *26*, 5982-5993.

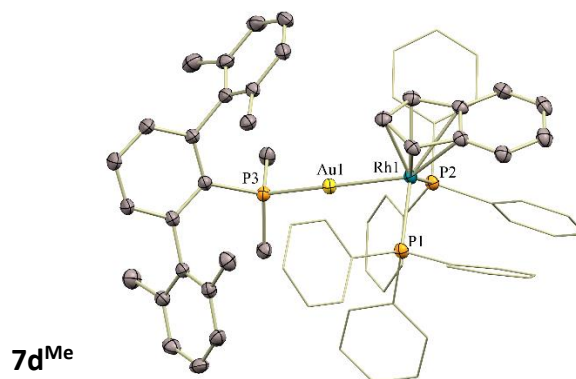


Figure 21. ORTEP diagram of indenyl compounds **7d^{Me}**. Selected bond distances (Å) and angles(°): Rh1–P1, 2.2876 (10); Rh1–P2, 2.3114(10); Rh1–Au1, 2.5828(3); Au1–P3, 2.2748(10); P1–Rh1–P2, 107.77(9); P1–Rh1–Au1, 87.49(3); P2–Rh1–Au1, 79.51(2); P3–Au1–Rh1, 171.83(3).

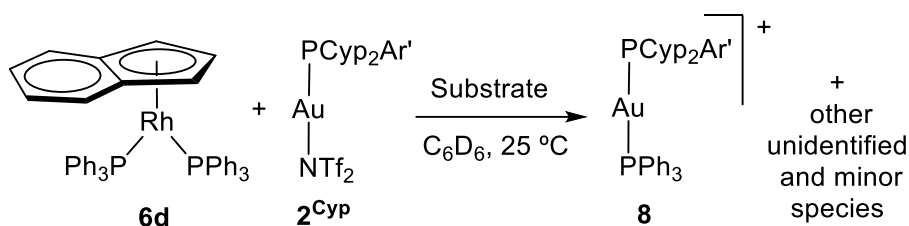
Besides, its molecular formulation was authenticated by X-ray diffraction studies (Figure 21), demonstrating the presence of a dative Rh→Au bond characterized by a length of 2.5828(3) Å.

We have previously demonstrated the importance of accessing monometallic fragments in highly polarized and unsupported bimetallic pairs to enhance their cooperative reactivity^{11b,21}. As such, we promptly explored the reactivity of the non-bonded pair **6d:2^{Cyp}** towards a variety of small molecules containing both non-polar or weakly polarized (H₂, C₂H₂, C₂H₄) and polar bonds (NH₃, H₂O, MeOH). However, instead of the foreseen FLP-type bond activation, we rapidly detected the formation of the heteroleptic gold compound [Au(PCyp₂Ar^{Xyl2})(PPh₃)] (**8**), defined by two distinctive doublets (²J_{PP} = 309 Hz) at 59.4 and 44.3 ppm by ³¹P{¹H} NMR spectroscopy.

²¹ a) N. Hidalgo, F. de la Cruz-Martínez, M. T. Martín, M. C. Nicasio, J. Campos, *Chem. Commun.*, **2022**, 58, 9144-9147.

b) N. Hidalgo, C. Romero-Pérez, C. Maya, I. Fernández, J. Campos, *Organometallics*, **2021**, 40, 1113-1119.

c) N. Hidalgo, C. Maya, J. Campos, *Chem. Commun.*, **2019**, 55, 8812-8815.



Scheme 13. Attempts to carry out bimetallic bond activation with a range of substrates (H_2 , C_2H_2 , C_2H_4 , NH_3 , H_2O , MeOH and 2,6-dimethylphenylisocyanide) leading to formation of $[\text{Au}(\text{PCyp}_2\text{Ar}^{\text{Xyl}2})(\text{PPh}_3)]^+$.

To assure its formulation this compound was independently prepared and fully characterized (see Experimental Section). Compound **8** is the major and, in some cases, the only discernible gold species obtained during our reactivity studies. Interestingly, the lability of PPh_3 is only evidenced upon addition of small molecules, but it also requires the presence of the gold precursor, since no phosphine dissociation was observed in the absence of $\mathbf{2^{Cyp}}$. Further evidence of phosphine lability was obtained after attempts to activate ethylene, which led among other species to the formation of $[(\eta^5\text{-C}_9\text{H}_7)(\text{PPh}_3)(\text{C}_2\text{H}_4)\text{Rh} \rightarrow \text{Au}(\text{PCyp}_2\text{Ar}^{\text{Xyl}2})](\text{NTf}_2)$, whose cationic part was detected by mass spectrometry analysis (MS (electrospray, m/z): calcd for $[\text{M}^+]$ 1179.39, found 1179.56; Figure 22)

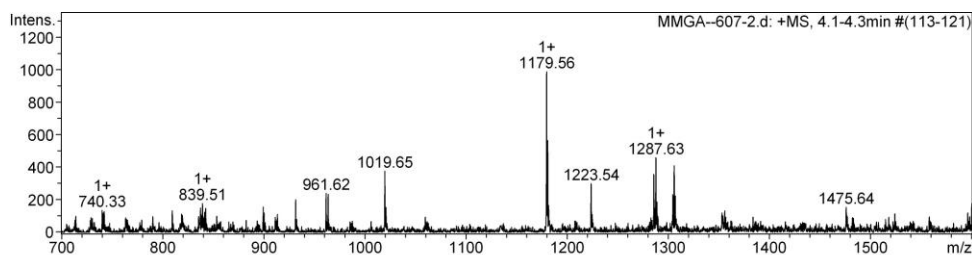


Figure 22. Mass spectrum of the reaction crude after exposing a solution of **6d** and $\mathbf{2^{Cyp}}$ to ethylene atmosphere (0.5 atm). MS (electrospray, m/z): calcd for $[\text{M}^+]$ 1179.39, found 1179.56.

Herein, we postulate that substitution of PPh₃ by the smaller ethylene ligand likely facilitates the formation of the dative Rh→Au bond. Likewise, initial efforts to activate isocyanides in an FLP-like manner (i.e. 1,1- or 1,2-addition)^{13,22} led to similar results. As an example, addition of 2,6-dimethylphenylisocyanide to a solution of **6d:2**^{Cyp} led to a complex mixture from which a small crop of crystals of [(η⁵-C₉H₇)(PPh₃)(XylNC)Rh→Au(PCyp₂Ar^{Xyl2})](NTf₂) could be grown and studied by X-ray diffraction (Figure 23), once more revealing the lability of PPh₃ from Rh(I) and thus speaking against its use as a metallic FLP component.

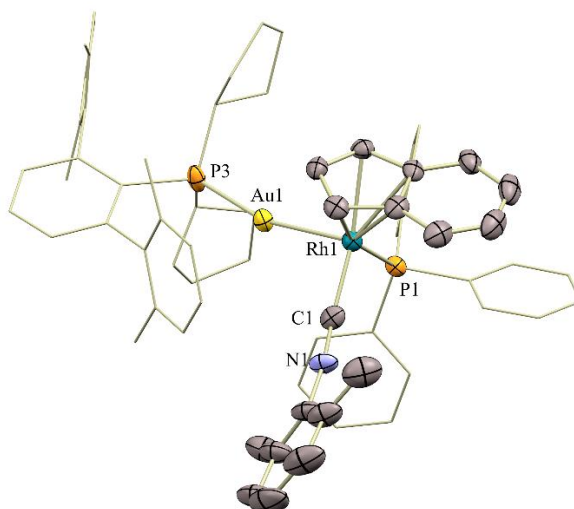


Figure 23. ORTEP diagram of indenyl compound [(η⁵-C₉H₇)(PPh₃)(XylNC)Rh→Au(PCyp₂Ar^{Xyl2})](NTf₂). Selected bond distances (Å) and angles(°): Rh1–P1, 2.2657(12); Rh1–C1, 1.919(6); N1–C1, 1.159(7); Rh1–Au1, 2.5978(4); Au1–P3, 2.2865(13); P1–Rh1–C1, 90.77(14); P1–Rh1–Au1, 87.75(3); C1–Rh1–Au1, 94.91(16); P3–Au1–Rh1, 164.36(4).

²² See for instance: a) R. Liedtke, F. Scheidt, J. Ren, B. Schirmer, A. J. P. Cardenas, C. G. Daniliuc, H. Eckert, T. H. Warren, S. Grimme, G. Kehrer, G. Erker, *J. Am. Chem. Soc.*, **2014**, *136*(25), 9014–9027.

b) O. Ekkert, G. G. Miera, T. Wiegand, H. Eckert, B. Schirmer, J. L. Petersen, C. G. Daniliuc, R. Fröhlich, S. Grimme, G. Kehra, G. Erker, *Chem. Sci.*, **2013**, *4*, 2657–2664.

c) A. C. McQuilken, Q. M. Dao, A. J. P. Cardenas, J. A. Bertke, S. Grimme, T. H. Warren, *Angew. Chem. Int. Ed.*, **2016**, *55*, 14335–14339.

We wondered whether the superior kinetic stability of the chelating dppe ligand would circumvent this drawback while still facilitating the prevalence of the monometallic fragments (bearing in mind the aforesaid elongated Rh→Au bond). However, similar studies based on precursor **6c** led to identical results, since the major gold-containing species in all our studies was digold compound $[(\text{PCyp}_2\text{Ar}^{\text{Xyl}2})\text{Au}]_2(\mu\text{-dppe})(\text{NTf}_2)_2$, characterized by $^{31}\text{P}\{^1\text{H}\}$ NMR resonances at 74.9 and 46.5 ppm ($^2J_{\text{PP}} = 164$ Hz) and X-ray diffraction (Figure 24). We attribute, at least in part, the unexpected facility by which phosphines dissociate in the presence of gold due to the weakening of the Rh–P bonds upon the approach of electrophiles. In the second chapter the strength of the dative bonding between the Rh centre in compound **1a** and a range of metallic electrophiles was computed concluding that this strength correlates with a greater contribution of $\sigma_{(\text{Rh-P})}$ orbital, thus weakening Rh–P bonds²³.

²³ S. Bajo, M. G. Alférez, M. M. Alcaide, J. López-Serrano, J. Campos, *Chem. Eur. J.*, **2020**,26,16833–16845.

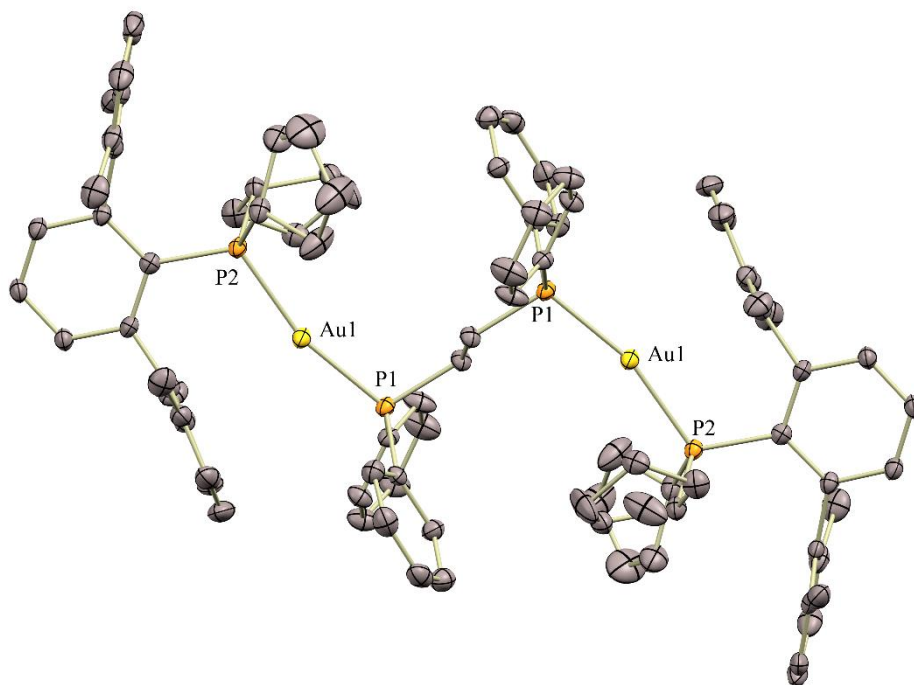


Figure 24. ORTEP diagram of indenyl compounds $[\{(PCyp_2Ar^{Xyl_2})Au\}_2(\mu\text{-dpppe})](NTf_2)_2$.

In summary, we provide a systematic study on a series of Rh(I)/Au(I) bimetallic pairs under sterically congested environments. This study evidences the potential for bimetallic cooperation and contrasting reactivity of two metals together compared to their individual mononuclear species. The nature of phosphine ligands bound to either Rh(I) or Au(I) precursors is crucial to control selectivity, which is dominated by kinetic effects. Thus, in the case of $[(\eta^5\text{-C}_5\text{Me}_5)\text{Rh}(\text{PR}_3)_2]$ compounds, a highly unusual Cp* non-innocence behavior has been described upon addition of the bulkier gold species $[(\text{PR}_2\text{Ar}^{\text{Cyp}})\text{Au}(\text{NTf}_2)]$, while the less congested $[(\text{PR}_2\text{Ar}^{\text{Xyl}})\text{Au}(\text{NTf}_2)]$ system leads to the formation of Rh→Au bimetallic adducts. The unusual activation of the Cp* ligand provides an opportunity to investigate late transition metal catalyzed transformations in which

methyl groups of the commonly-employed C_5Me_5 ligand act as proton shuttles.

The basicity of the phosphines bound to Rh also play an important role, since for the more congested but less basic dppe ligand, the Cp^* -activated complexes only appear as transient species. In addition, the stereoelectronic properties of the phosphines dictate the equilibrium between bimetallic adducts and individual monometallic compounds for the $[(\eta^5-C_9H_7)Rh(PR_3)_2]$ precursors. This equilibrium is directly associated to the ability of bimetallic pairs to exhibit frustrated Lewis pair (FLP) behavior, which was observed only for the more congested Cp^* -based Rh system. In contrast, the indenyl analogues were unable to mediate FLP-type bond activation due to the lability of the Rh–P bonds in the presence of gold.

Computational investigations rule out a mechanism defined by the intramolecular formation of a fulvene structure trapped by electrophilic gold, as invoked for mononuclear systems based on early transition metals. At variance, we postulate a genuine bimetallic pathway that involves the initial binding of gold to the inner Cp^* ring, which facilitates proton migration to the basic Rh site and exemplify the potential of bimetallic synergisms. Besides, our theoretical studies provide insights about the kinetic control that dominate the divergent bimetallic pathways described in this work and the cooperative N-H bond activation of ammonia.

III.8. Experimental procedures

III.8.1. General considerations

All preparations and manipulations were carried out using standard Schlenk and glove-box techniques, under argon or high-purity nitrogen atmosphere, respectively. All solvents were dried, stored over 4 Å molecular sieves, and degassed prior to use. Toluene (C₇H₈) and *n*-pentane (C₅H₁₂) were distilled under nitrogen over sodium. Benzene-*d*₆ and toluene-*d*₈ were dried over molecular sieves (4 Å). THF-*d*₈ was distilled under nitrogen over sodium/benzophenone. [Au(THT)Cl]²⁴, **1a**¹, **2**^{Me2}, **2**^{Cyp20b} and **5a**¹, **6a**¹⁸, **6d**²⁵ were prepared according to previously reported procedures. Other chemicals were commercially available and used as received. Solution NMR spectra were recorded on Bruker AMX-300, DRX-400 and DRX-500 spectrometers. Spectra were referenced to external SiMe₄ (δ: 0 ppm) using the residual proton solvent peaks as internal standards (¹H NMR experiments), or the characteristic resonances of the solvent nuclei (¹³C{¹H} NMR experiments), while ³¹P was referenced to H₃PO₄. Spectral assignments were made by routine one- and two-dimensional NMR experiments where appropriate. For elemental analyses a LECO TruSpec CHN elementary analyzer was utilized. Infrared spectra were recorded on a Bruker Vector 22 spectrometer in Nujol.

III.8.2. Crystallographic details

²⁴ A. Uson, M. Laguna, D. A. Briggs, H. H. Murray and J. P. Fackler, *Inorg. Synth.*, **1989**, 26, 85-91.

²⁵ C. N. Garon, D. I. McIsaac, C. M. Vogels, A. Decken, I. D. Williams, C. Kleeberg, T. B. Marder, S. A. Westcott, *Dalton Trans.*, **2009**, 1624–1631

Crystals of compounds were grown by slow diffusion of pentane into their benzene or THF solutions, respectively. Low-temperature diffraction data were collected on a Bruker APEX-II CCD diffractometer using monochromatic radiation $\lambda(\text{Mo K}\alpha_1) = 0.71073 \text{ \AA}$ (**3a**^{Tripp} and **4a**^{Cyp}) on a D8 Quest APEX-III single crystal diffractometer with a Photon III detector and a I μ S 3.0 microfocus X-ray source (**4b**^{Cyp}, **7a**^{Me}, **7a**^{Cyp}, **6d**, **7d**^{Me}, $[(\eta^5\text{-C}_9\text{H}_7)(\text{PPh}_3)(\text{XylNC})\text{Rh}\rightarrow\text{Au}(\text{PCyp}_2\text{Ar}^{\text{Xyl}_2})](\text{NTf}_2)$, **6c**, **7c**^{Cyp} and $[\{(\text{PCyp}_2\text{Ar}^{\text{Xyl}_2})\text{Au}\}_2(\mu\text{-dppe})](\text{NTf}_2)_2$) at the Instituto de Investigaciones Químicas de Sevilla.

For crystals of **3a**^{Tripp} and **4a**^{Cyp}: data collections were processed with APEX-W2D-NT (Bruker, 2004), cell refinement and data reduction with SAINT-Plus (Bruker, 2004)²⁶ and the absorption was corrected by multi-scan method applied by SADABS²⁷. The structures were solved with SHELXT and was refined against F^2 on all data by full-matrix least squares with SHELXL²⁸.

For crystals of **4b**^{Cyp}, **7a**^{Me}, **7a**^{Cyp}, **6d**, **7d**^{Me}, $[(\eta^5\text{-C}_9\text{H}_7)(\text{PPh}_3)(\text{XylNC})\text{Rh}\rightarrow\text{Au}(\text{PCyp}_2\text{Ar}^{\text{Xyl}_2})](\text{NTf}_2)$, **6c**, **7c**^{Cyp} and $[\{(\text{PCyp}_2\text{Ar}^{\text{Xyl}_2})\text{Au}\}_2(\mu\text{-dppe})](\text{NTf}_2)_2$: data were collected by means of ω and φ scans using monochromatic radiation $\lambda(\text{Mo K}\alpha_1) = 0.71073 \text{ \AA}$. The diffraction images collected were processed and scaled using APEX-III software. Using Olex2²⁹, the structures **7a**^{Me}, **6d** and **6c** were solved with SHELXS (direct methods) and the structures **4b**^{Cyp}, **7a**^{Cyp}, **7c**^{Cyp}, $[(\eta^5\text{-C}_9\text{H}_7)(\text{PPh}_3)(\text{XylNC})\text{Rh}\rightarrow\text{Au}(\text{PCyp}_2\text{Ar}^{\text{Xyl}_2})](\text{NTf}_2)$ and

²⁶ SAINT 6.02, BRUKER-AXS, Inc., Madison, WI 53711-5373 USA, 1997–1999.

²⁷ SADABS George Sheldrick, Bruker AXS, Inc., Madison, Wisconsin, USA, 1999.

²⁸ G. M. Sheldrick, *Acta Cryst.* **2008**, A64, 112-122.

²⁹ a) L. J. Bourhis, O. V. Dolomanov, R. J. Gildea, J. A. K. Howard, H. Puschmann, *Acta Cryst.*, 2015, A71, 59-75.

b) O. V. Dolomanov, L. J. Bourhis, R. J. Gildea, J. A. K. Howard, H. Puschmann, *J. Appl. Cryst.*, **2009**, 42, 339-341.

c) G. M. Sheldrick, *Acta Cryst.*, **2015**, C71, 3-8.

[{(PCyp₂Ar^{Xyl₂})Au}₂(μ-dppe)](NTf₂)₂ were solved with olex2.solve1.3 and all was refined against F² on all data by full-matrix least squares with SHELXL.

All non-hydrogen atoms were refined anisotropically. Hydrogen atoms were included in the model at geometrically calculated positions and refined using a riding model. The isotropic displacement parameters of all hydrogen atoms were fixed to 1.2 times the U value of the atoms to which they are linked (1.5 times for methyl groups). The hydride ligand directly bound to rhodium in structure **4a**^{Cyp} and **4b**^{Cyp} was located at the difference electron density map and its Rh—H bond distance restrained to typical values. Both structures contain solvent molecules in the unit cell (benzene and pentane in **3a**^{Me} and THF in **4a**^{Cyp}) with variable degrees of disorder to which several restraints were applied.

III. 8. 3. Computational details

Calculations were performed at the DFT level with the Gaussian 09 (Revision E.01) program³⁰. The hybrid functional PBE0³¹ was used throughout the computational study, and dispersion effects were accounted for by using Grimme's D3 parameter set with Becke–Johnson (BJ) damping³². Geometry optimizations were carried out without geometry constraints, using the 6-31G(d,p)³³ basis set to represent the C, H, P, O, S, F and N atoms and the Stuttgart/Dresden Effective Core Potential and its associated basis set (SDD)³⁴ to describe the Rh and Au atoms. Bulk solvent effects (dichloromethane) were included at the optimization stage with the SMD continuum model³⁵. The stationary points and their nature as minima or saddle points (TS) were characterized by vibrational analysis, which also produced zero-point (ZPE), enthalpy (H), entropy (S) and Gibbs energy (G)

³⁰ M. J. Frisch, G. W. Trucks, H. B. Schlegel, G. E. Scuseria, M. A. Robb, J. R. Cheeseman, G. Scalmani, V. Barone, B. Mennucci, G. A. Petersson, H. Nakatsuji, M. Caricato, X. Li, H. P. Hratchian, A. F. Izmaylov, J. Bloino, G. Zheng, J. L. Sonnenberg, M. Hada, M. Ehara, K. Toyota, R. Fukuda, J. Hasegawa, M. Ishida, T. Nakajima, Y. Honda, O. Kitao, H. Nakai, T. Vreven, J. A. J. Montgomery, J. E. Peralta, F. Ogliaro, M. Bearpark, J. J. Heyd, E. Brothers, K. N. Kudin, V. N. Staroverov, R. Kobayashi, J. Normand, K. Raghavachari, A. Rendell, J. C. Burant, S. S. Iyengar, J. Tomasi, M. Cossi, N. Rega, J. M. Millam, M. Klene, J. E. Knox, J. B. Cross, V. Bakken, C. Adamo, J. Jaramillo, R. Gomperts, R. E. Stratmann, O. Yazyev, A. J. Austin, R. Cammi, C. Pomelli, J. W. Ochterski, R. L. Martin, K. Morokuma, V. G. Zakrzewski, G. A. Voth, P. Salvador, J. J. Dannenberg, S. Dapprich, A. D. Daniels, O. Farkas, J. B. Foresman, J. V. Ortiz, J. Cioslowski, D. J. Fox. Gaussian 09, Revision E.01, Gaussian, Inc.: Wallingford CT, **2013**.

³¹ J. P. Perdew, K. Burke, M. Ernzerhof, *Phys. Rev. Lett.*, **1996**, *77*, 3865–3868.

³² S. Grimme, J. Antony, S. Ehrlich, H. Krieg, *J. Chem. Phys.*, **2010**, *132*, 154104.

³³ a) W. J. Hehre, R. Ditchfield, J. A. Pople, *J. Phys. Chem.*, **1972**, *56*, 2257–2261.

b) P. C. Hariharan, J. A. Pople, *Theor. Chim. Acta.*, **1973**, *28*, 213–222.

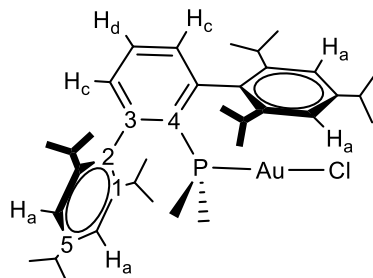
c) M. M. Francl, W. J. Pietro, W. J. Hehre, J. S. Binkley, M. S. Gordon, D. J. Defrees, J. A. Pople, *J. Chem. Phys.*, **1982**, *77*, 3654–3665.

³⁴ D. Andrae, U. Haeussermann, M. Dolg, H. Stoll, H. Preuss, *Theor. Chim. Acta*, **1990**, *77*, 123–141.

³⁵ A. V. Marenich, C. J. Cramer, D. G. Truhlar, *J. Phys. Chem. B*, **2009**, *113*, 6378–6396.

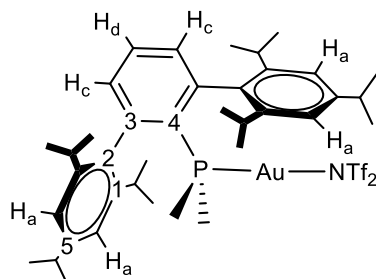
data at 298.15 K. The minima connected by a given transition state were determined by perturbing the transition states along the TS coordinate and optimizing to the nearest minimum.

III.8.4. Synthesis and characterization of new compounds



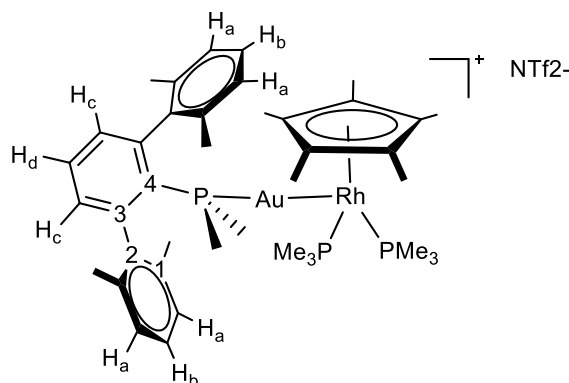
Compound [(PMe₂Ar^{Tripp2})AuCl]. A solution of terphenyl phosphine PMe₂Ar^{Tripp2} (510 mg, 0.940 mmol) in toluene (10 mL) was added under nitrogen over a suspension of [Au(THT)Cl] (THT = tetrahydrothiophene) (300 mg, 0.940 mmol) in toluene (5 mL). The initial white suspension was stirred for 8 hours, becoming a solution and then the solvent was removed under vacuum. The resulting white solid was washed with pentane and dried to yield [(PMe₂Ar^{Tripp2})AuCl] as a fine white powder (619 mg, 85%). Anal. Calcd. for C₃₈H₅₅AuClP: C, 58.87; H, 7.15. Found: C, 58.5; H, 7.2.

¹H NMR (400 MHz, CDCl₃, 25 °C) δ: 7.49 (td, 1 H, ³J_{HH} = 7.5 Hz, ⁵J_{HP} = 2.0, H_d), 7.25 (dd, 2 H, ²J_{HH} = 7.5 Hz, ⁴J_{HP} = 3.5, H_c), 7.12 (s, 4 H, H_a), 2.99 (hept, 2 H, ³J_{HH} = 6.9 Hz, *p*-(CH(CH₃)₂), 2.55 (hept, 4 H, ³J_{HH} = 6.8 Hz, *o*-(CH(CH₃)₂)), 1.35 (m, 24 H, *o*, *p*-(CH(CH₃)₂)), 1.26 (d, 6 H, ²J_{HP} = 10.3 Hz, PMe₂), 1.06 (d, 12 H, ³J_{HH} = 6.9 Hz, *o*-(CH(CH₃)₂)). ¹³C{¹H} NMR (125 MHz, CDCl₃, 25 °C) δ: 150.1 (C₅), 145.9 (C₁), 145.5 (d, ²J_{CP} = 11 Hz, C₃), 135.8 (d, ³J_{CP} = 5 Hz, C₂), 132.7 (d, ³J_{CP} = 8 Hz, CH_c), 129.4 (CH_d), 128.7 (C₄), 121.5 (CH_a), 34.3 (*p*-(CH(CH₃)₂), 31.3 (*o*-(CH(CH₃)₂), 25.7 (*o*-(CH(CH₃)₂), 24.3 (*o/p*-(CH(CH₃)₂)), 23.0 (*o/p*-(CH(CH₃)₂)), 17.7 (d, ¹J_{CP} = 39 Hz, PMe₂). ³¹P{¹H} NMR (202 MHz, CD₂Cl₂, 25 °C) δ: -5.8.



Compound 2^{Tripp}. A solution of [(PMe₂Ar^{Tripp2})AuCl] (333 mg, 0.430 mmol) in toluene (10 mL) was added over AgNTf₂ (167mg, 0.430 mmol) under inert atmosphere. The mixture was stirred at 0°C for one hour and subsequently filtrated, evaporated and washed with pentane. The residue was dried under vacuum to provide compound 2^{Tripp} as a temperature-sensitive white solid (145 mg, 40%).

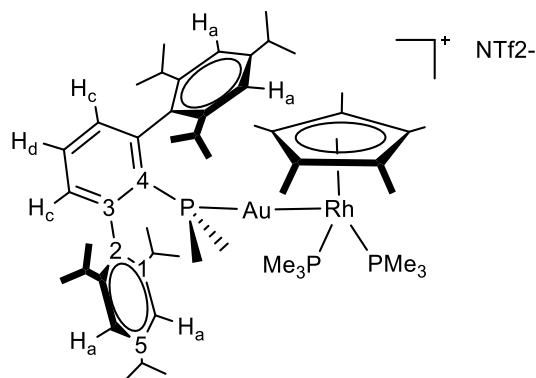
¹H NMR (300 MHz, C₆D₆, 25 °C) δ: 7.42 (m, 1 H, H_d), 7.21 (d, 2 H, ²J_{HH} = 7.5 Hz, H_c), 6.91 (m, 4 H, H_a), 2.95 (hept, 2 H, ³J_{HH} = 7.0 Hz, *p*-(CH(CH₃)₂)), 2.49 (hept, 4 H, ³J_{HH} = 6.6 Hz, *o*-(CH(CH₃)₂)), 1.35 (d, 12 H, ³J_{HH} = 7.1 Hz, *p*-(CH(CH₃)₂)), 1.32 (d, 12 H, ³J_{HH} = 6.6Hz, *o*-(CH(CH₃)₂)), 1.06 (d, 6 H, ²J_{HP} = 9.4 Hz, PMe₂), 0.95 (d, 12 H, ³J_{HH} = 6.8 Hz, *o*-(CH(CH₃)₂)). ¹³C{¹H} NMR (100 MHz, C₆D₆, 25 °C) δ: 150.5 (C₅), 146.3 (C₁), 146.1 (d, ²J_{CP} = 11 Hz, C₃), 135.7 (d, ³J_{CP} = 5 Hz, C₂), 133.1 (d, ³J_{CP} = 8 Hz, CH_c), 130.1 (CH_d), 128.8 (d, ¹J_{CP}= 76 Hz, C₄), 122.1 (CH_a), 120.0 (q, ¹J_{CF} = 320 Hz, CF₃), 34.6 (*p*-(CH(CH₃)₂)), 31.7 (*o*-(CH(CH₃)₂)), 25.7 (*o*-(CH(CH₃)₂)), 24.3 (*p*-(CH(CH₃)₂)), 22.8 (*o*-(CH(CH₃)₂)), 17.4 (d, ¹J_{CP} = 40 Hz, PMe₂). ³¹P {¹H} NMR (121 MHz, C₆D₆, 25 °C) δ: -24.6.



Compound 3a^{Me}. A solid mixture of compounds **1a** (24 mg, 0.061 mmol) and **2^{Me}** (50 mg, 0.061 mmol) was dissolved in toluene (5ml) and stirred at room temperature for 30 minutes. Reaction monitoring revealed that formation of **3a^{Me}** was immediate and proceeded quantitatively by NMR spectroscopy. The solution was concentrated to half of its volume and precipitated with pentane. The residue was then filtered and dried under vacuum (49 mg, 66 %). To increase purity, compound **3a^{Me}** was crystallized by slow diffusion of pentane over a toluene solution to provide a brownish crystalline material. Anal. Calcd. For C₄₂H₆₀AuF₆NO₄P₃RhS₂: C, 41.56; H, 4.98; N, 1.15; S, 5.28. Found: C, 42.04; H, 4.79; N, 1.18; S, 5.42.

¹H NMR (400 MHz, THF-*d*₈, 25 °C,) δ: 7.60 (td, 1 H, ³J_{HH} = 7.5 Hz, ³J_{HP} = 1.9 Hz, H_d), 7.24 (m, 2 H, H_b), 7.13 (m, 6 H, H_c and H_a), 2.27 (s, 12 H, Me_{Xyl}), 1.91 (s, 15 H, C₅Me₅), 1.50 (m, 18 H, PMe₃) 0.96 (d, 6 H, ³J_{HH} = 8.6 Hz, PMe₂). ¹³C{¹H} NMR (100 MHz, THF-*d*₈, 25 °C) δ: 146.1 (d, ²J_{CP} = 9 Hz, C₃), 142.4 (d, ³J_{CP} = 2 Hz, C₂), 137.2 (C₁), 132.2 (d, ⁴J_{CP} = 3 Hz, CH_d), 131.8 (d, ³J_{CP} = 8 Hz, CH_c), 129.7 (CH_b), 129.2 (d, ¹J_{CP} = 77 Hz, C₄), 128.7 (CH_a), 121.2 (q, ¹J_{CF} = 323 Hz, CF₃), 101.3 (C₅Me₅), 23.7 (vt, ¹J_{CP} = 17 Hz, PMe₃), 22.4 (Me_{Xyl}), 18.1 (d, ¹J_{PC} = 33 Hz, PMe₂),

11.8 (C_5Me_5). $^{31}P\{^1H\}$ NMR (162 MHz, THF- d_8 , 25 °C,) δ : 13.9 (td, $^3J_{PP} = 12$ Hz, $^2J_{PRh} = 10$ Hz PAu), -3.1 (dd, $^1J_{PRh} = 155$ Hz, $^3J_{PP} = 12$ Hz, PMe_3).



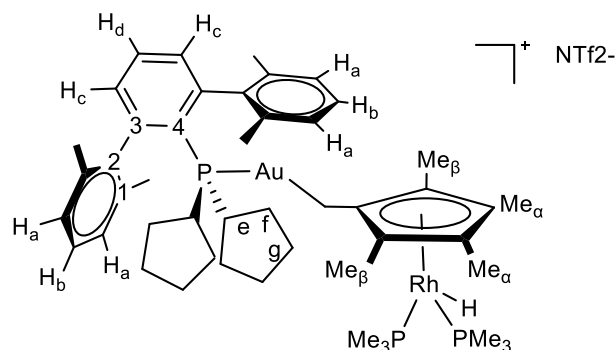
Compound 3a^{Tripp}. A solid mixture of compounds **1a** (19 mg, 0.049 mmol) and **2^{Tripp}** (50 mg, 0.049 mmol) was dissolved in toluene (5ml) at $-60\text{ }^{\circ}\text{C}$ and stirred for 30 minutes at that temperature. Reaction monitoring revealed that formation of **3a^{Tripp}** was immediate and proceeded almost quantitatively (*ca.* 90%) by NMR spectroscopy. The solution was gently warmed up to $25\text{ }^{\circ}\text{C}$, concentrated to half of its initial volume and then precipitated with pentane. The residue was then filtered and dried under vacuum (30 mg, 44 %). To increase purity, compound **3a^{Tripp}** was crystallized by slow diffusion of pentane over a toluene solution to provide a brownish crystalline material. Anal. Calcd. for $\text{C}_{56}\text{H}_{88}\text{AuF}_6\text{O}_5\text{P}_3\text{RhS}_2$: C, 47.70; H, 6.29; N, 0.99; S, 4.55. Found C, 47.71; H, 6.20; N, 1.31; S, 4.58.

^1H NMR (300 MHz, $\text{THF-}d_8$, $25\text{ }^{\circ}\text{C}$) δ : 7.28 (t, 1 H, $^3J_{\text{HH}} = 7.6\text{ Hz}$, H_d), 7.09 to 6.99 (m, 6 H, H_c and H_a), 3.03 (m, 2 H, $p\text{-}(\text{CH}(\text{CH}_3)_2)$), 2.85 (m, 4 H, $o\text{-}(\text{CH}(\text{CH}_3)_2)$), 1.63 (s, 15 H, C_5Me_5), 1.53 (d, 12 H, $^3J_{\text{HH}} = 7.5\text{ Hz}$, $p\text{-}(\text{CH}(\text{CH}_3)_2)$), 1.44 (d, 12 H, $^3J_{\text{HH}} = 7.1\text{ Hz}$, $o\text{-}(\text{CH}(\text{CH}_3)_2)$), 1.38 (t, 18 H, PMe_3), 1.30 (d, 6 H, $^3J_{\text{HH}} = 8.9\text{ Hz}$, PMe_2), 1.11 (d, 12 H, $^3J_{\text{HH}} = 7.2\text{ Hz}$, $o/p\text{-}(\text{CH}(\text{CH}_3)_2)$). $^{13}\text{C}\{^1\text{H}\}$ NMR (100 MHz, C_6D_6 , $25\text{ }^{\circ}\text{C}$) δ : 150.0 (C_5), 146.8 (C_1), 144.9 (d, $^2J_{\text{CP}} = 11\text{ Hz}$, C_3), 137.2 (d, $^3J_{\text{CP}} = 4\text{ Hz}$, C_2), 133.2 (d, $^3J_{\text{CP}} = 7\text{ Hz}$, CH_c), 131.5 (CH_d), 128.8 (d, $^1J_{\text{CP}} = 83\text{ Hz}$, C_4),

120.9 (CH_a), 120.7 (q, $^1J_{CF} = 327$ Hz, CF₃), 96.0 (C₅Me₅), 34.6 (*p*-(CH(CH₃)₂)), 31.7 (*o*-(CH(CH₃)₂)), 25.8 (*o*-(CH(CH₃)₂)), 24.1 (*p*-(CH(CH₃)₂)), 23.2 (vt, $^1J_{CP} = 17$ Hz, PMe₃), 22.7 (*o*-(CH(CH₃)₂)), 14.3 (d, $^1J_{CP} = 33$ Hz, PMe₂), 11.7 (C₅Me₅). $^{31}\text{P}\{^1\text{H}\}$ NMR (121 MHz, THF-*d*₈, 25 °C,) δ : 15.2 (dt, $^3J_{PP} = 14$ Hz, $^2J_{PRh} = 12$ Hz PMe₂), -5.1 (dd, $^1J_{PRh} = 155$ Hz, $^3J_{PP} = 14$ Hz, PMe₃).

Compound 4a^{Tripp}. Compound **4a^{Tripp}** cannot be isolated in pure form as it represents the minor isomer during the reaction of **1a** and **2^{Tripp}** (maximum conversion of around 30%, *c.f.* major isomer **3a^{Tripp}**: *ca.* 70%) and exhibits a pronounced reactivity and thermal instability. Nevertheless, multinuclear NMR analysis permitted identification of its ^1H and $^{31}\text{P}\{^1\text{H}\}$ NMR resonances in isomeric mixtures of **3a^{Tripp}**: **4a^{Tripp}**.

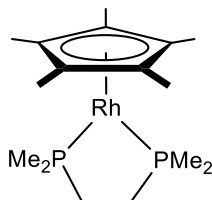
^1H NMR (400 MHz, THF-*d*₈, 25 °C,) δ : 7.26 to 6.90 (aromatic-CH), 2.73 (m, 2 H, *p*-(CH(CH₃)₂)), 2.55 (m, 4 H, *o*-(CH(CH₃)₂)), 1.60 (s, 12 H, C₅Me₅), 1.48 (d, 12 H, $^3J_{HH} = 7.5$ Hz, *p*-(CH(CH₃)₂)), 1.39 (d, 12 H, $^3J_{HH} = 7.1$ Hz, *o*-(CH(CH₃)₂)), (d, 6 H, $^3J_{HH} = 8.9$ Hz, PMe₂), 1.30 (t, 18 H, PMe₃), 1.07 (d, 12 H, $^3J_{HH} = 7.2$ Hz, *o*-(CH(CH₃)₂)), -13.5 (dt, 1 H, $^2J_{HP} = 35.8$ Hz, $^1J_{HRh} = 24.1$ Hz, RhH). $^{31}\text{P}\{^1\text{H}\}$ NMR (162 MHz, THF-*d*₈, 25 °C,) δ : 12.7 (dt, $^3J_{PP} = 12$ Hz, PMe₂), -2.2 (dd, $^1J_{PRh} = 140$ Hz, $^3J_{PP} = 12$ Hz, PMe₃).



Compound 4a^{Cyp}. A solid mixture of compounds **1a** (21 mg, 0.054 mmol) and **2^{Cyp}** (50 mg, 0.054 mmol) was dissolved in toluene (5ml) and stirred for 30 minutes under argon atmosphere at 25 °C. Reaction monitoring revealed that formation of **4a^{Cyp}** was immediate and proceeded almost quantitatively (*ca.* 95%) by NMR spectroscopy. The solution was concentrated to *ca.* half of its original volume and the bimetallic product was precipitated with pentane. The residue was filtered dried under vacuum (108 mg, 81 %). For better purity, compound **4a^{Cyp}** was crystallized by slow diffusion of pentane into a toluene solution to provide a brownish crystalline material. Anal. Calcd. For C₅₁H₇₆AuF₆NO₄P₃RhS₂: C, 45.78; H, 5.73; S, 4.79; N, 1.04. Found: C, 45.84; H, 5.22; S, 5.27; N, 1.15.

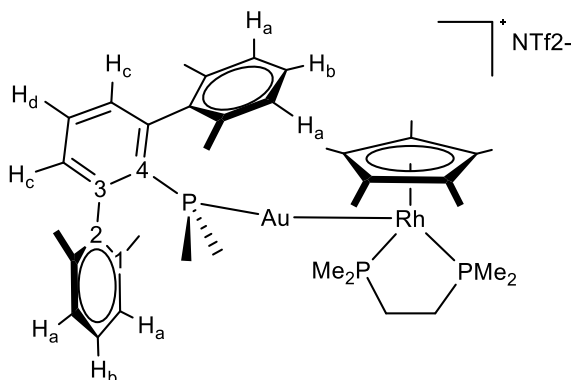
¹H NMR (400 MHz, THF-*d*₈, 25 °C) δ: 7.59 (t, 1 H, ³J_{HH} = 7.6 Hz, H_d), 7.21 (m, 2 H, H_b), 7.11 (m, 6 H, H_c and H_a), 2.24 (m, 2 H, Cyp(CH)), 2.06 (s, 12 H, Me_{Xyl}), 1.84 (s, 6 H, Me_α), 1.73 (s, 6 H, Me_β) 1.55 (m, 8 H, Cyp(CH₂)), 1.48 (m, 18 H, PMe₃), 1.39 (m, 8 H, Cyp(CH₂)), 1.05 (d, 2 H, ²J_{HP} = 9.6 Hz, CH₂-Au), -13.3 (dt, 1 H, ²J_{HP} = 35.8 Hz, ¹J_{HRh} = 24.5 Hz, RhH). ¹³C{¹H} NMR (100 MHz, THF-*d*₈, 25 °C) δ: 149.5 (d, ²J_{CP} = 10 Hz, C₃), 143.2 (d, ³J_{CP} = 5 Hz, C₂) 137.3 (C₁), 133.0 (d, ³J_{CP} = 6 Hz, CH_c), 132.1 (d, ⁴J_{CP} = 4 Hz, CH_d), 129.6 (d, ¹J_{CP} = 72 Hz, C₄), 128.6 (CH_a), 128.3 (CH_b), 121.2 (q, ¹J_{CF} = 322 Hz, CF₃), 102.7 (CCH₂), 100.7 (CMe_α),

91.6 (CMe β), 38.6 (d, $^1J_{CP} = 28$ Hz, Cyp(CH)), 35.3 (d, $^3J_{CP} = 9$ Hz, Cyp(CH $_2$)), 32.8 (d, $^3J_{CP} = 10$ Hz, Cyp(CH $_2$)), 26.4 (d, $^2J_{CP} = 10$ Hz, Cyp(CH $_2$)), 21.9 (Me $_{Xyl}$), 21.7 (d, $^2J_{CP} = 10$ Hz, Cyp(CH $_2$)), 20.3 (t, $^2J_{CP} = 17$ Hz, PMe $_3$), 11.5 and 11.3 (Me $_{\alpha}$ and Me $_{\beta}$), 1.3 (d, $^2J_{CP} = 3$ Hz, CCH $_2$). ^{31}P { ^1H } NMR (162 MHz, THF- d_8 , 25 °C) δ : 56.0 (t, $^5J_{PP} = 10$ Hz, PMe $_2$), -2.2 (dd, $^1J_{PRh} = 140$ Hz, $^5J_{PP} = 10$, PMe $_3$).



Compound 1b. Sodium amalgam was prepared by adding sodium (58 mg, 2.5 mmol) to mercury (1.5 mL, 102 mmol) under argon atmosphere. The mixture was suspended in diethyl ether (20 mL) to which a solution of dmpe (0.2 mL, 1.13 mmol) was added first and $[\text{C}_5\text{Me}_5\text{RhCl}_2]_2$ (309 mg, 0.5 mmol) in toluene (5 mL) second. The mixture was stirred for 8 hours, after which it was filtrated, the solvent evaporated under reduced pressure and the residue extracted with pentane (20 mL). The solution volume was reduced to 5 mL and stored at $-78\text{ }^\circ\text{C}$ to crystallize. Rhombic pink crystals were obtained after 5 days (750 mg, 60 %). Anal. Calcd. for $\text{C}_{16}\text{H}_{31}\text{P}_2\text{Rh}$: C, 49.5; H, 8.1. Found: C, 49.6; H, 8.0.

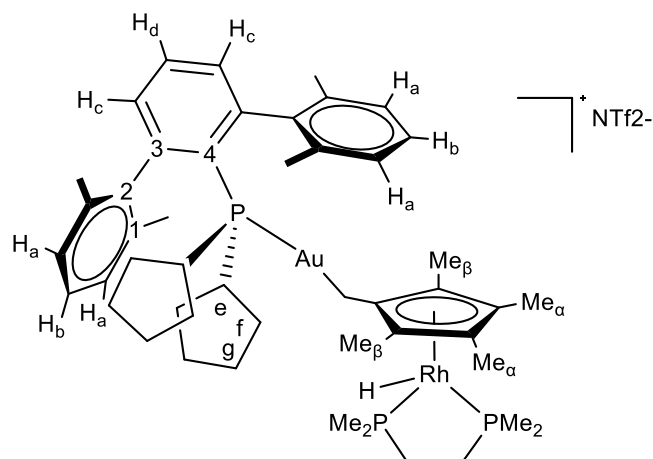
^1H NMR (400 MHz, C_6D_6 , $25\text{ }^\circ\text{C}$) δ : 2.17 (s, 15H, C_5Me_5), 1.19 (vt, 12H, $^2J_{\text{HP}} = 4\text{ Hz}$, PMe_2), 1.13 (d, 4H, $^2J_{\text{HP}} = 16\text{ Hz}$, CH_2). $^{13}\text{C}\{^1\text{H}\}$ NMR (100 MHz, C_6D_6 , $25\text{ }^\circ\text{C}$) δ : 94.9 (m, C_5Me_5), 31.8 (vtd, $^1J_{\text{CP}} = 27$, $^2J_{\text{CRh}} = 4\text{ Hz}$, CH_2), 20.4 (vt, $^1J_{\text{CP}} = 9\text{ Hz}$, PMe_2), 12.4 (C_5Me_5). $^{31}\text{P}\{^1\text{H}\}$ NMR (162 MHz, C_6D_6 , $25\text{ }^\circ\text{C}$) δ : 42.2 (d, $^1J_{\text{PRh}} = 220\text{ Hz}$).



Compound 3b^{Me}. A solid mixture of compounds **1b** (33 mg, 0.085 mmol) and **2^{Me}** (70 mg, 0.085 mmol) was dissolved in toluene (5 mL) and stirred at room temperature for 5 minutes. Reaction monitoring revealed that formation of **3b^{Me}** was immediate and proceeded quantitatively by NMR spectroscopy. The solution was concentrated to half and precipitated with pentane. The orange residue was then filtered and dried under vacuum (77 mg, 64%). Anal. Calcd. for C₄₄H₆₆AuF₆NO₄P₃RhS₂: C, 42.4; H, 5.4; N, 1.1; S, 5.2. Found: C, 41.9; H, 5.2; N, 1.3; S, 5.2.

¹H NMR (500 MHz, C₆D₆, 25 °C) δ: 7.20 (t, 2H, ³J_{HH} = 7.7 Hz, H_b), 7.02 (d, 4H, ³J_{HH} = 7.7 Hz, H_a), 6.98 (td, 1H, ³J_{HH} = 7.6, ⁵J_{HP} = 1.6 Hz, H_d), 6.63 (dd, 2H, ³J_{HH} = 7.6, ⁴J_{HP} = 3.0 Hz, H_c), 2.09 (s, 12H, Me_{Xyl}), 1.76 (d, 4H, ²J_{HP} = 12.4 Hz, CH₂), 1.64 (s, 15H, C₅Me₅), 1.25 (d, 6H, ²J_{HP} = 9.5 Hz, PMeMe (dmpe)), 1.13 (d, 6H, ²J_{HP} = 9.5 Hz, PMeMe(dmpe)), 0.77 (d, 6H, ²J_{HP} = 8.6 Hz, PMe₂Ar^{Xyl2}). ¹³C{¹H} NMR (125 MHz, C₆D₆, 25 °C) δ: 144.8 (d, ²J_{CP} = 9 Hz, C₃), 141.7 (d, ³J_{CP} = 3 Hz, C₂), 135.9 (C₁), 131.5 (d, ¹J_{CP} ≈ 40Hz, C₄), 130.5 (overlapped CH_c and CH_d), 128.5 (CH_a), 127.2 (CH_b), 121.3 (q, ¹J_{CF} = 324 Hz, CF₃), 98.7 (C₅Me₅), 34.1 (CH₂), 22.4 (PMeMe (dmpe)), 21.7 (Me_{Xyl}), 17.7-17.4 (overlapped PMe₂Ar^{Xyl2} and PMeMe (dmpe)), 11.2 (C₅Me₅). ¹⁹F{¹H} NMR (471 MHz, C₆D₆, 25 °C) δ: -78.3.

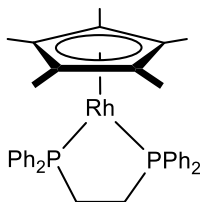
$^{31}\text{P}\{^1\text{H}\}$ NMR (202 MHz, C_6D_6 , 25 °C) δ : 45.5 (dd, $^1J_{\text{PRh}} = 154$, $^3J_{\text{PP}} = 9$ Hz, dmpe), 14.6 (dt, $^2J_{\text{PRh}} = 12$, $^3J_{\text{PP}} = 9$ Hz, $\text{PMe}_2\text{Ar}^{\text{Xyl}2}$).



Compound 4b^{Cyp}. A solid mixture of compounds **1b** (21 mg, 0.054 mmol) and **2^{Cyp}** (50 mg, 0.054 mmol) was dissolved in toluene (5 mL) and stirred at room temperature for 5 minutes. Reaction monitoring revealed that formation of **4b^{Cyp}** was immediate and proceeded quantitatively by NMR spectroscopy. The solution was concentrated to half volume and precipitated with pentane. The brown residue was then filtered and dried under vacuum (40 mg, 30%). To increase purity, compound **4b^{Cyp}** was crystallized by slow diffusion of pentane over a benzene solution to provide a yellow/brownish crystalline material. Anal. Calcd. for C₅₀H₇₅AuF₆NO₄P₃RhS₂: C, 45.3; H, 5.7; N, 1.1; S, 4.8. Found: C, 44.6; H, 5.7; N, 1.1; S, 4.9.

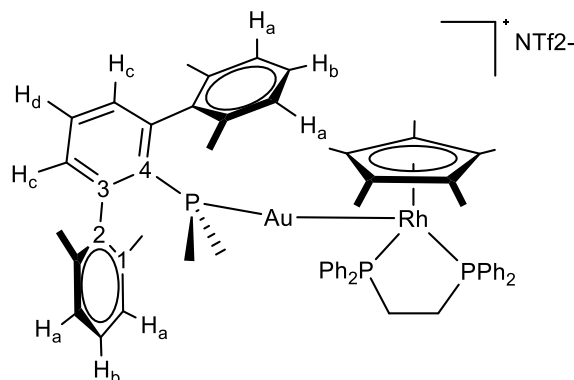
¹H NMR (400 MHz, C₆D₆, 25 °C) δ: 7.23 (t, 2H, ³J_{HH} = 7.4 Hz, H_b), 7.08 to 7.05 (m, 5H, H_a and H_d), 6.68 (brd, 2H, ³J_{HH} ≈ 7.4 Hz, H_c), 2.18 (m, 2H, H_e), 1.99 (s, 12H, Me_{Xyl}), 1.74 (s, 6H, Me_α), 1.69 (s, 6H, Me_β), 1.65 (m, 8H, H_g), 1.43 (d, 4H, ²J_{HP} = 9 Hz, CH₂dmpe), 1.35 (m, 8H, H_f), 1.28 (d, 6H, ²J_{HP} = 9.8 Hz, PMeMe), 1.21 (d, 2H, ²J_{HP} = 7.7 Hz, CH₂Au), 1.12 (d, 6H, ²J_{HP} = 9.8 Hz, PMeMe), -13.6 (td, 1H, ²J_{HP} = 34, ¹J_{HRh} = 26 Hz, RhH). ¹³C{¹H} NMR (100 MHz, C₆D₆, 25 °C) δ: 148.4.0 (d, ²J_{CP} = 8 Hz, C₃), 142.2 (C₂), 136.3 (br s, C₁), 131.7 (br, CH_c), 131.4 (d, ¹J_{CP} ≈ 30Hz, C₄) 130.8

(CH_d), 127.9 and 127.7 (CH_a and CH_b, overlapped with C₆D₆), 120.9 (q, $^1J_{CF}$ = 324 Hz, CF₃), 98.8 (CMe_β), 90.9 (CMe_α), 37.8 (d, $^1J_{CP}$ = 31 Hz, CH_e), 34.4 (CH_g), 31.9 (CH_f), 27.1 (d, $^2J_{CP}$ = 75 Hz, CH₂Au), 25.4 (vdd, $^2J_{CRh}$ = 28, $^1J_{CP}$ = 9 Hz, CH₂dmpe), 21.4 (Me_{xy1}), 18.9 (vt, $^1J_{CP}$ = 22 Hz, P*MeMe*), 13.4 (vt, $^1J_{CP}$ = 18 Hz, P*MeMe*), 10.6 and 10.5 (Me_α and Me_β). $^{19}\text{F}\{^1\text{H}\}$ NMR (376 MHz, C₆D₆, 25 °C) δ: -78.3. $^{31}\text{P}\{^1\text{H}\}$ NMR (162 MHz, C₆D₆, 25 °C) δ: 57.0 (t, $^3J_{PP}$ = 10 Hz), 42.9 (dd, $^1J_{PRh}$ = 137, $^3J_{PP}$ = 10 Hz).



Compound 1c. Sodium amalgam was prepared by adding sodium (173 mg, 7.5 mmol) to mercury (4.5 mL, 306 mmol) under argon atmosphere. The mixture was suspended in ether (20 mL), dppe (1343 mg, 2.25 mmol) was added first and $[\text{C}_5\text{Me}_5\text{RhCl}_2]_2$ (907 mg, 1.4 mmol) in toluene (5 mL) second. The mixture was stirred for 8 hours, after which time was filtrated, the solvent evaporated under reduced pressure and the residue extracted with pentane (20 mL). The solution volume was reduced to 5 mL and stored at $-78\text{ }^\circ\text{C}$ to crystallize. Rhombic pink crystals were obtained after 5 days (950 mg, 66 %). Anal. Calcd. for $\text{C}_{36}\text{H}_{39}\text{P}_2\text{Rh}$: C, 67.9; H, 6.2. Found: C, 67.9; H, 6.4.

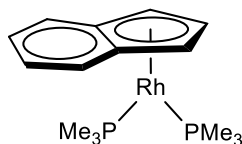
^1H NMR (400 MHz, C_6D_6 , $25\text{ }^\circ\text{C}$) δ : 7.68 (m, 8H, *o*-Ph₂), 7.17 (m, 8H, *m*-Ph₂), 7.09 (m, 4H, *p*-Ph₂), 1.85 (d, 4H, $^2J_{\text{HP}} = 19\text{ Hz}$, CH₂), 1.79 (s, 15H, C₅Me₅). $^{13}\text{C}\{^1\text{H}\}$ NMR (100 MHz, C_6D_6 , $25\text{ }^\circ\text{C}$) δ : 139.6 (vt, $^1J_{\text{CP}} = 16\text{ Hz}$, C_{*ipso*}Ph₂), 132.9 (vt, $^2J_{\text{CP}} = 6\text{ Hz}$, C_{*o*}Ph₂), 128.3 (overlapped, C_{*m*}Ph₂ and C_{*p*}Ph₂), 95.4 (m, C₅Me₅), 32.2 (vtd, $^1J_{\text{CP}} = 27$, $^2J_{\text{CRh}} = 2\text{ Hz}$, CH₂), 10.8 (C₅Me₅). $^{31}\text{P}\{^1\text{H}\}$ NMR (162 MHz, C_6D_6 , $25\text{ }^\circ\text{C}$) δ : 81.2 (d, $^1J_{\text{PRh}} = 219\text{ Hz}$).



Compound 3c^{Me}. A solid mixture of compounds **1c** (38.7 mg, 0.061 mmol) and **2^{Me}** (50 mg, 0.061 mmol) was dissolved in toluene (5 mL) and stirred at room temperature for 5 minutes. Reaction monitoring revealed that formation of **3c^{Me}** was immediate and proceeded quantitatively by NMR spectroscopy. The solution was concentrated to half and precipitated with pentane. The green residue was then filtered and dried under vacuum (40 mg, 45 %). Anal. Calcd. for C₆₂H₆₆AuF₆NO₄P₃RhS₂: C, 51.0; H, 4.6; N, 1.0; S, 4.4. Found: C, 50.6; H, 4.7; N, 1.2; S, 4.8.

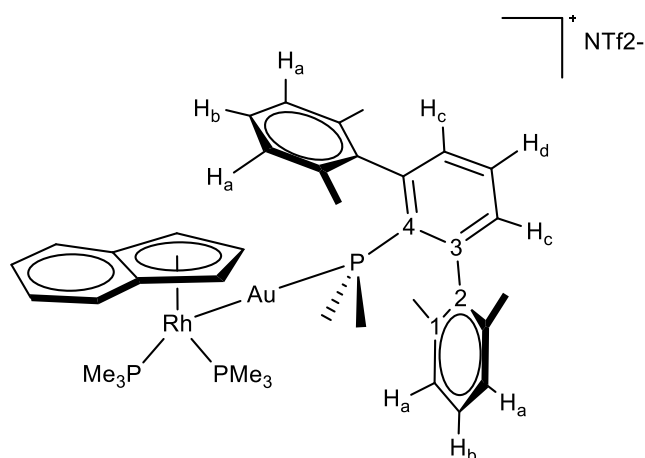
¹H NMR (500 MHz, C₆D₆, 25 °C) δ: 7.57 (m, 4H, *o*-Ph₂), 7.38 (m, 4H, *o*-Ph₂), 7.32 (m, 2H, H_b), 7.13 to 7.03 (m, 16H, overlapping *m*-Ph₂, *p*-Ph₂, H_a), 6.90 (m, 1H, H_d), 6.52 (dd, 2H, ³J_{HH} = 7.3, ⁴J_{HP} = 2.4 Hz, H_c), 2.62 (m, 4H, CH₂(dmpe)), 1.86 (s, 12H, Me_{Xyl}), 1.54 (s, 15H, C₅Me₅), 0.37 (d, 6H, ²J_{HP} = 8.8 Hz, PMe₂). ¹³C{¹H} NMR (125 MHz, C₆D₆, 25 °C) δ: 144.9 (d, ¹J_{CP} = 8 Hz, C₃), 141.2 (d, ¹J_{CP} = 2 Hz, C₂), 137.4 (m, C_{ipso}Ph₂), 136.1 (C₁), 132.5 (m, C_oPh₂), 131.5 (m, C_mPh₂), 130.5 (overlapped C₄ and CH_c), 130.4 (CH_d), 128.8 (m, C_pPh₂), 128.4 (CH_a), 127.2 (CH_b), 121.5 (q, ¹J_{CF} = 324 Hz, CF₃), 100.5 (C₅Me₅), 34.1 (CH₂), 21.4 (Me_{Xyl}), 17.5 (d, ¹J_{CP} = 32 Hz, PMe₂Ar^{Xyl2}), 10.9 (C₅Me₅). ¹⁹F{¹H} NMR (471 MHz, C₆D₆, 25 °C) δ:

-77.9. $^{31}\text{P}\{^1\text{H}\}$ NMR (202 MHz, C_6D_6 , 25 °C) δ : 74.1 (dd, $^1J_{\text{PRh}} = 164$, $^3J_{\text{PP}} = 6$ Hz), 12.1 (q, $^1J_{\text{PRh}} = ^3J_{\text{PP}} = 6$ Hz).



Compound 6a. Following a previously reported procedure,³⁶ (C₉H₇)Li (120 mg, 0.962 mmol) was added to a solution of [RhCl(COE)₂]₂ (332 mg, 0.461 mmol) in toluene (10 mL). The solution was stirred at room temperature overnight, filtered through celite and solvent was removed under vacuum. PMe₃ (1.25 mL, 1.23 mmol) was slowly added to a solution of the resulting product (268 mg, 0.616 mmol) in THF at -80 °C, stirring overnight. Solvent was removed under vacuum and the resulting green solid was coevaporated with pentane (329 mg, 72%).

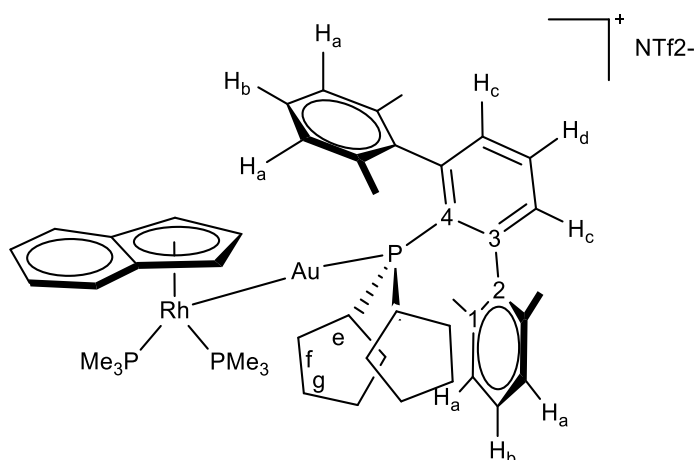
³⁶ H. Werner, R. Feser, *Z. Naturforsch.*, **1980**, 35 b, 689-693.



Compound 7a^{Me}. A solid mixture of compounds **6a** (32 mg, 0.085 mmol) and **2^{Me}** (70 mg, 0.085 mmol) was dissolved in toluene (5 mL) and stirred at room temperature for 5 minutes. Reaction monitoring revealed that formation of **7a^{Me}** was immediate and proceeded quantitatively by NMR spectroscopy. The solution was concentrated to half and precipitated with pentane. The brown residue was then filtered and dried under vacuum (58 mg, 57 %). Anal. Calcd. for C₄₁H₅₃AuF₆NO₄P₃RhS₂: C, 41.2; H, 4.5; N, 1.2; S, 5.4. Found: C, 41.0; H, 4.3; N, 1.2; S, 5.5.

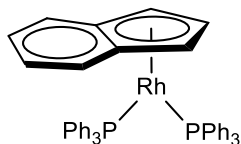
¹H NMR (500 MHz, C₆D₆, 25 °C) δ: 7.20 (m, 2H, H_b), 7.04 (m, 4H, H_a), 6.93-6.87 (m, 5H, overlapping Ind and H_d), 6.65 (dd, 2H, ³J_{HH} = 7.6, ⁴J_{HP} = 3.3 Hz, H_c), 5.79 (m, 1 H, Ind), 4.89 (m, 2H, Ind), 2.09 (s, 12H, Me_{Xyl}), 1.07 (vt, dar *J* del vt, 18H, PMe₃), 0.88 (d, 6H, ²J_{HP} = 9.6 Hz, PMe₂Ar^{Xyl2}). ¹³C{¹H} NMR (125 MHz, C₆D₆, 25 °C) δ: 145.9 (br, C₃), 140.5 (d ³J_{CP} = 9 Hz, C₂), 135.9 (C₁), 131.9 (CH_d), 130.8 (CH_c), 128.8 (d, ¹J_{CP} = 24 Hz, C₄), 127.9 and 127.8 (CH_a and CH_b, overlapped with C₆D₆), 124.9 (Ind), 119.6 (q, ¹J_{CF} = 326 Hz, CF₃), 115.8 (Ind), 94.6 (Ind), 82.8 (Ind), 74.0 (Ind), 22.5 (m, PMe₃), 21.3 (Me_{Xyl}), 16.3 (d, ¹J_{CP} = 16 Hz, PMe₂Ar^{Xyl2}). ¹⁹F{¹H} NMR (471 MHz, C₆D₆, 25 °C) δ: -78.4. ³¹P{¹H} NMR (162 MHz, C₆D₆, 25 °C) δ: 10.1, 10.1, 10.1.

NMR (202 MHz, C₆D₆, 25 °C) δ : 4.6 (d, $^2J_{\text{PRh}} = 18$ Hz), -3.9 (d, $^1J_{\text{PRh}} = 158$ Hz).



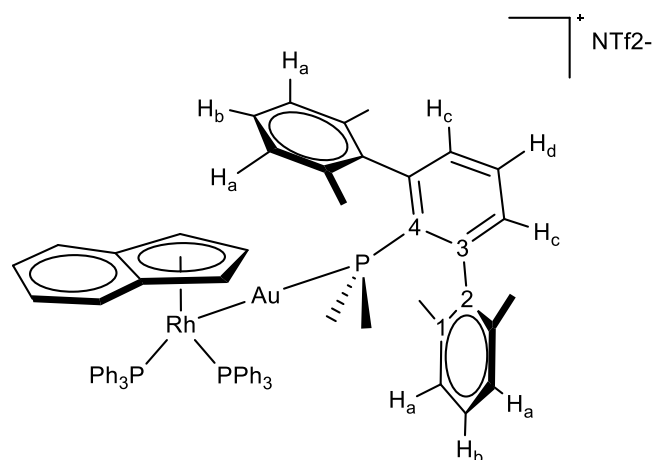
Compound 7a^{Cyp}. A solid mixture of compounds **6a** (40 mg, 0.107 mmol) and **2^{Cyp}** (100 mg, 0.107 mmol) was dissolved in toluene (5 mL) and stirred at room temperature for 5 minutes. Reaction monitoring revealed that formation of **7a^{Cyp}** was immediate and proceeded quantitatively by NMR spectroscopy. The solution was concentrated to half volume and precipitated with pentane. The green residue was then filtered and dried under vacuum (80 mg, 57 %). Anal. Calcd. for C₄₉H₆₇AuF₆NO₄P₃RhS₂: C, 45.1; H, 5.2; N, 1.1; S, 5.9. Found: C, 45.1; H, 5.0; N, 1.3; S, 5.8.

¹H NMR (500 MHz, C₆D₆, 25 °C) δ: 7.12 (m, 2H, H_b), 6.99 (m, 4H, H_a), 6.94 to 6.91 (m, 5H, H_d and Ind), 6.48 (dd, 2H, ³J_{HH} = 7.5, ⁴J_{HP} = 3.3 Hz, H_c), 5.75 (m, 1H, Ind), 4.86 (m, 2H, Ind), 2.30 (m, 2H, H_e), 1.99 (s, 12H, Me_{Xyl}), 1.65 to 1.57 (m, 8H, H_f), 1.42 (m, 8H, H_g), 1.13 (vt, 18H, PMe₃). ¹³C{¹H} NMR (125 MHz, C₆D₆, 25 °C) δ: 147.5 (d, ²J_{CP} = 9 Hz, C₃), 142.1 (d ³J_{CP} = 4 Hz, C₂), 137.5 (C₁), 132.7 (d, ¹J_{CP} = 30 Hz, C₄), 132.3 (CH_d), 131.9 (CH_c), 128.9 (CH_a), 128.1 (CH_b), 125.2 (Ind), 121.3 (q, ¹J_{CF} = 326 Hz, CF₃), 119.1 (Ind), 116.5 (Ind), 94.2 (Ind), 73.3 (Ind), 39.1 (d, ¹J_{CP} = 28 Hz, CH_e), 34.1 (CH_f), 31.9 (CH_g), 21.3 (Me_{Xyl}), 21.5 (m, PMe₃). ¹⁹F{¹H} NMR (471 MHz, C₆D₆, 25 °C) δ: -78.3. ³¹P{¹H} NMR (202 MHz, C₆D₆, 25 °C) δ: 43.3 (d, ²J_{PRh} = 19 Hz), -6.2 (d, ¹J_{PRh} = 159 Hz).



Compound 6d. $(C_9H_7)Li$ (360 mg, 2.8 mmol) is added to a solution of $[RhCl(COE)_2]_2$ (1 g, 1.4 mmol) in toluene (10 mL), stirred at room temperature overnight and filtered through celite. The solvent was removed under vacuum and PMe_3 (738 mg, 2.8 mmol) was slowly added to a solution of the resulting product (600 mg, 1.4 mmol) in THF at $-80\text{ }^\circ\text{C}$, stirring the solution upon warming to room temperature and heating at $60\text{ }^\circ\text{C}$ overnight. Solvent was removed under vacuum and the resulting red solid was coevaporated with pentane (840 mg, 84 %). The 1H NMR spectrum of the compound fits perfectly with prior literature precedent (REF). Besides, its still unreported $^{31}P\{^1H\}$ NMR data is given below.

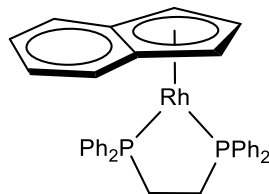
$^{31}P\{^1H\}$ NMR (162 MHz, C_6D_6 , $25\text{ }^\circ\text{C}$) δ : 50.9 (d, $^2J_{PRh} = 223\text{ Hz}$).



Compound 7d^{Me}. A solid mixture of compound **6d** (61 mg, 0.085 mmol) and **2^{Me}** (70 mg, 0.085 mmol) was dissolved in toluene (5 mL) and stirred at room temperature for 5 minutes. Reaction monitoring revealed that formation of **7d^{Me}** was immediate and proceeded quantitatively by NMR spectroscopy. The solution was concentrated to half volume and precipitated with pentane. The yellow residue was then filtered and dried under vacuum (40 mg, 31 %). Anal. Calcd. for C₇₁H₆₅AuF₆NO₄P₃RhS₂: C, 54.4; H, 4.2; N, 0.9; S, 4.1. Found: C, 54.4; H, 4.2; N, 1.0; S, 4.2.

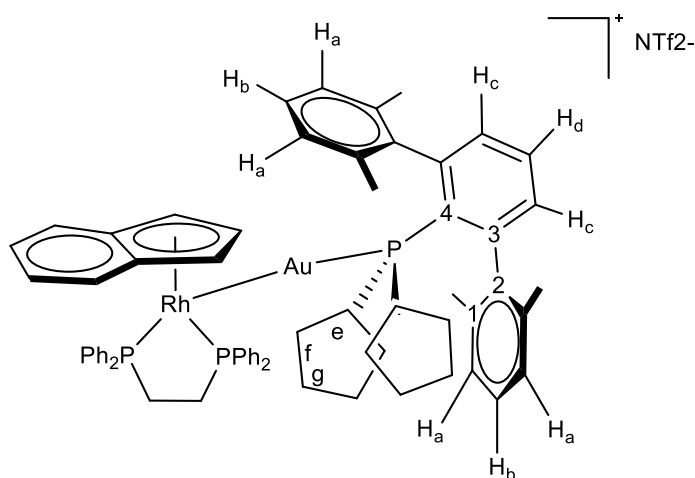
¹H NMR (500 MHz, THF-*d*₈, 25 °C) δ: 7.74 (m, 1H, H_a), 7.44 to 7.41 (m, 8H, overlapped *p*-Ph₃ and H_b), 7.23 to 7.20 (m, 18H, overlapped *m*-Ph₃, H_c and H_a), 7.06 to 7.01 (m, 3H, overlapping Ind), 6.90 (m, 12H, *o*-Ph₃), 5.83 (m, 2H, Ind), 5.00 (m, 2H, Ind), 2.22 (s, 12 H, Me_{Xyl}), 0.77 (d, 6H, ²J_{HP} = 10.0 Hz, PMe₂Ar^{Xyl2}). ¹³C{¹H} NMR (125 MHz, THF-*d*₈, 25 °C) δ: 145.3 (d, ²J_{CP} = 9 Hz, C₃), 141.3 (d, ³J_{CP} = 4 Hz, C₂), 136.4 (C₁), 135.8 (d, ¹J_{CP} = 47 Hz, C₄), 133.6 (t, ³J_{CP} = 5 Hz, C_oPh₃), 131.8 (CH_d), 131.3 (d, ³J_{CP} = 8 Hz, CH_c), 130.2 (C_pPh₃), 128.4 (CH_b), 128.1 (t, ³J_{CP} = 5 Hz, C_mPh₃ overlapped s, CH_a), 127.9 (Ind), 120.2 (Ind), 119.9 (q, ¹J_{CF} = 330 Hz, CF₃), 94.9 (br, Ind), 79.6 (br, Ind), 21.5 (Me_{Xyl}), 17.4 (d, ¹J_{CP} = 35 Hz, PMe₂Ar^{Xyl2}). ¹⁹F{¹H}

NMR (471 MHz, THF-*d*₈, 25 °C) δ : -78.3. ³¹P{¹H} NMR (202 MHz, THF-*d*₈, 25 °C) δ : 40.1 (d, ¹J_{PRh} = 168 Hz), 1.6 (d, ¹J_{PRh} = 15 Hz).



Compound 6c (C_9H_7)Li (360 mg, 2.8 mmol) is added to a solution of $[RhCl(COE)_2]_2$ (1 g, 1.4 mmol) in toluene (10 mL), stirred at room temperature overnight and filtered through celite. Solvent was removed under vacuum and dppe (273 mg, 0.69 mmol) was slowly added to a solution of the resulting product (300 mg, 0.69 mmol) in THF (5 mL) at $-80\text{ }^\circ\text{C}$, stirring the solution upon warming to room temperature and heating at $60\text{ }^\circ\text{C}$ overnight. Solvent was removed under vacuum yielding a yellow solid (320 mg, 77 %). Anal. Calcd. for $C_{35}H_{31}P_2Rh$: C, 68.2; H, 5.1. Found: C, 68.2; H, 5.4.

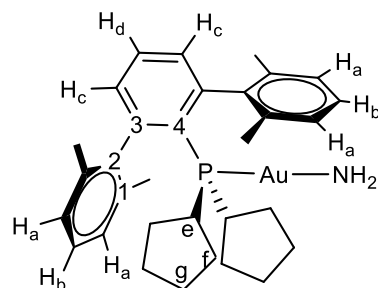
^1H NMR (500 MHz, C_6D_6 , $25\text{ }^\circ\text{C}$) δ : 7.45 (m, 8H, *o*-Ph₂), 7.11 (m, 8H, *m*-Ph₂), 7.07 (m, 4H, *p*-Ph₂), 7.05 to 6.92 (m, 4H, Ind), 6.14 (m, 1H, Ind), 5.52 (m, 2H, Ind), 1.63 (d, 4H, $^2J_{HP} = 18\text{ Hz}$, CH₂). $^{13}\text{C}\{^1\text{H}\}$ NMR (125 MHz, C_6D_6 , $25\text{ }^\circ\text{C}$) δ : 139.9 (m, $C_{ipso}\text{Ph}_2$), 132.6 (m, $C_o\text{Ph}_2$), 128.8 ($C_p\text{Ph}_2$), 127.7 (overlapped with C_6D_6 , $C_m\text{Ph}_2$) 120.5 (Ind), 117.2 (Ind), 116.5 (Ind), 95.1 (m, Ind), 73.1 (m, Ind), 28.9 (vt, $^1J_{CP} = 25\text{ Hz}$, CH₂). $^{31}\text{P}\{^1\text{H}\}$ NMR (202 MHz, C_6D_6 , $25\text{ }^\circ\text{C}$) δ : 75.9 (d, $^1J_{PRh} = 223\text{ Hz}$).



Compound 7c^{Cyp}. A solid mixture of compound **6c** (10 mg, 0.0816 mmol) and **2^{Cyp}** (8 mg, 0.0816 mmol) was dissolved in toluene (5 mL) and stirred at room temperature for 5 minutes. Reaction monitoring revealed that formation of **7c^{Cyp}** was immediate and proceeded quantitatively by NMR spectroscopy. The solution was concentrated to half volume and precipitated with pentane. The brown residue was then filtered and dried under vacuum (57.5 mg, 57 %). Anal. Calcd. for C₆₉H₇₀AuF₆NO₄P₃RhS₂: C, 53.6; H, 4.6; N, 0.9; S, 4.4. Found: C, 53.6; H, 4.3; N, 1.1; S, 4.5.

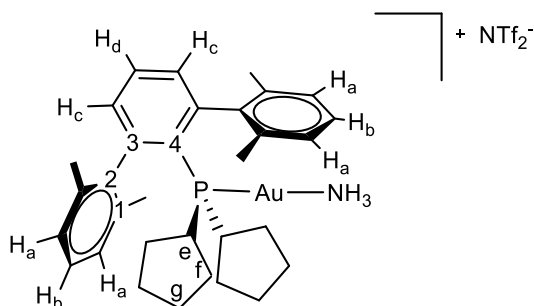
¹H NMR (400 MHz, THF-*d*₈, 25 °C) δ: 7.88 (br, 2H, H_b), 7.59 (br, 4H, H_a), 7.39 (m, 1H, H_d), 7.28 (m, 5H, overlapped *p*-PPh₃ and Ind), 7.24 (m, 6H, PPh₃), 7.15 (m, 10H, PPh₃), 7.07 (m, 1H, Ind), 6.92 (m, 2H, H_c), 6.83 (m, 1H, Ind), 6.64 (m, 2H, Ind), 6.24 (m, 2H, Ind), 5.92 (br, 2H, Ind), 2.34 (s, 12H, Me_{Xyl}), 2.23 (m, 2H, H_e), 2.12 (m, 4H, CH₂^{dpppe}), 1.54 (m, 8H, H_f), 1.39 (m, 8H, H_g). ¹³C{¹H} NMR (100 MHz, THF-*d*₈, 25 °C) δ: 147.1 (C₃), 142.4 (C^PPh₃), 137.4 (C₂), 128.7 (overlapped PPh₃, Ind, CH_b, CH_a), 127.9 (overlapped PPh₃, CH_c, CH_d), 125.1 (overlapped PPh₃, Ind), 118.9 (Ind), 117.4 (Ind), 39.4 (C_e), 33.7 (C_f), 26.3 (C_g), 20.5 (overlapped CH₂^{dpppe} and Me_{Xyl}). ³¹P{¹H} NMR (162 MHz, THF-*d*₈, 25 °C) δ: 74.7 (d, ¹J_{PRh} = 161 Hz), 47.0 (d, ³J_{PP} = 18 Hz).

III.8.5. X-H (X = H, C, O, N) bond activation studies using Rh and Au



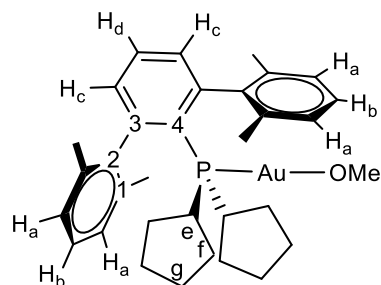
Compound $2^{\text{Cyp}}\cdot\text{NH}_2$. A solution of 2^{Cyp} (50 mg, 0.054 mmol) in toluene (5 ml) was treated with one equivalent of LiNH_2 (1.2 mg, 0.054 mmol) and the suspension stirred at 25 °C under argon for 24 hours. The resulting solution was evaporated and extracted with pentane (4 x 5 mL) to yield a mixture of two species in ca 3:1 ratio. While the major compound is attributed to $2^{\text{Cyp}}\cdot\text{NH}_2$ (whose spectroscopic resonances are reported and assigned below), the minor species is ascribed to cation $[(\text{PCyp}_2\text{Ar}^{\text{Xyl}2})\text{Au}(\text{NH}_3)]^+$ (also described below). Although we did not separate the two species, we estimate an overall yield for $2^{\text{Cyp}}\cdot\text{NH}_2$ of around 64 %.

^1H NMR (500 MHz, C_6D_6 , 25 °C) δ : 7.44 to 7.21 (m, 7 H, H_a , H_d , H_c), 6.85 (m, 2 H, H_b), 2.51 (s, 2 H, NH_2), 2.31 (s, 2 H, $\text{Cyp}(\text{CH})$), 2.15 (s, 12 H, Me_{Xyl}), 1.92 to 1.77 (m, 8 H, $\text{Cyp}(\text{CH}_2)$), 1.61 (s, 8 H, $\text{Cyp}(\text{CH}_2)$). $^{13}\text{C}\{^1\text{H}\}$ NMR (100 MHz, C_6D_6 , 25 °C) δ : 147.9 (br, C_3), 144.4 (br, C_2), 137.3 (C_1), 132.3 (d, $^3J_{\text{CP}} = 7$ Hz, CH_c), 132.1 (d, $^4J_{\text{CP}} = 4$ Hz, CH_d), 131.6 (CH_b), 129.3 (C_4), 125.7 (CH_a), 38.2 (d, $^1J_{\text{CP}} = 36$ Hz, $\text{Cyp}(\text{CH})$), 35.6 ($\text{Cyp}(\text{CH}_2)$), 32.8 ($\text{Cyp}(\text{CH}_2)$), 25.2 (d, $^2J_{\text{CP}} = 11$ Hz, $\text{Cyp}(\text{CH}_2)$), 21.5 (s, Me_{Xyl}). $^{31}\text{P}\{^1\text{H}\}$ NMR (202 MHz, C_6D_6 , 25 °C) δ : 49.8. IR (Nujol): $\nu_{\text{NH}} = 3257, 3311 \text{ cm}^{-1}$.



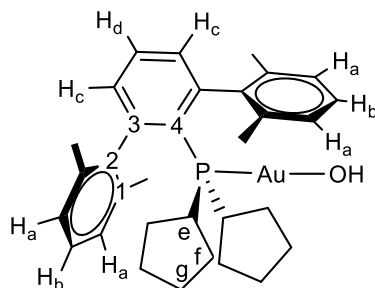
Compound [(PCyp₂Ar^{Xyl2})Au(NH₃)]NTf₂ A solution of **2**^{Cyp} (50 mg, 0.054 mmol) in toluene (5 ml) was placed under dry ammonia atmosphere (0.5 bar) in a pressure vessel and the solution stirred for 24 hours. Then it was evaporated and washed up with pentane (3 x 5 mL) to yield compound [(PCyp₂Ar^{Xyl2})Au(NH₃)]NTf₂ as a white powder (30 mg, 59 %).

¹H NMR (400 MHz, C₆D₆, 25 °C) δ: 7.26 to 7.03 (m, 7 H, H_a, H_d, H_c), 6.63 (m, 2 H, H_b), 2.55 (s, 3 H, NH₃), 2.04 (s, 2 H, Cyp(CH)), 1.96 (s, 12 H, Me_{Xyl}), 1.83 (s, 4 H, Cyp(CH₂)), 1.70 (s, 2 H, Cyp(CH₂)), 1.59 (s, 2 H, Cyp(CH₂)), 1.40 (s, 8 H, Cyp(CH₂)). ¹³C{¹H} NMR (100 MHz, C₆D₆, 25 °C,) δ: 148.1 (br, C₃), 144.5 (br, C₂), 137.3 (C₁), 132.2 (d, ³J_{CP} = 7 Hz, CH_c), 131.6 (CH_d), 128.6 (CH_b), 120.9 (q, ¹J_{CF} = 320 Hz, CF₃), 38.1 (d, ²J_{CP} = 36 Hz, Cyp(CH)), 35.6 (d, ³J_{CP} = 6 Hz, Cyp(CH₂)), 32.8 (d, ³J_{CP} = 6 Hz, Cyp(CH₂)), 25.2 (d, ²J_{CP} = 116 Hz, Cyp(CH₂)) 25.1 (d, ²J_{CP} = 13 Hz, Cyp(CH₂)), 21.3 (s, Me_{Xyl}). Signals due to C₄ and CH_a could not be precisely assigned. ³¹P{¹H} NMR (162 MHz, C₆D₆, 25 °C) δ: 50.2. IR (Nujol): ν_{NH} = 3186, 3271, 3378 cm⁻¹.



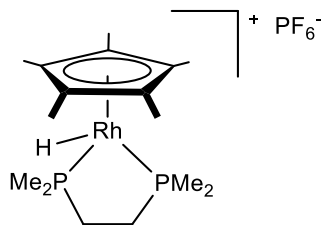
Compound 2^{Cyp}·OMe. A solution of 2^{Cyp} (50 mg, 0.054 mmol) in toluene (5 ml) was treated with one equivalent of CH₃ONa (2.9 mg, 0.054 mmol) and the solution stirred for 24 hours. Then it was evaporated and extracted with toluene (4 x 5 mL). The filtrate was dried under vacuum and the residue washed with pentane to yield compound 2^{Cyp}·OMe as a white powder (20 mg, 56 %).

¹H NMR (400 MHz, C₆D₆, 25 °C) δ: 7.32 (s, 2 H, H_c), 7.16 to 6.96 (m, 5 H, H_a, H_d), 6.62 (s, 2 H, H_b), 2.11 (s, 2 H, Cyp(CH)), 1.95 (s, 12 H, Me_{Xyl}), 1.70 to 1.14 (m, 16 H, Cyp(CH₂)). ¹³C{¹H} NMR (100 MHz, C₆D₆, 25 °C) δ: 148.1 (br, C₃), 142.3 (br, C₂), 137.3 (C₁), 132.3 (d, ²J_{CP} = 7 Hz, C_c), 131.2 (CH_d), 128.9 (d, ¹J_{CP} ≈ 72 Hz, C₄), 127.4 (CH_a), 125.7 (CH_b), 38.3 (d, ¹J_{CP} = 37 Hz, Cyp(CH)), 35.7 (d, ²J_{CP} = 6 Hz, Cyp(CH₂)), 33.0 ((OMe)), 25.1 (d, ³J_{CP} = 12 Hz, Cyp(CH₂)), 21.5 (Me_{Xyl}). ³¹P{¹H} NMR (162 MHz, C₆D₆, 25 °C) δ: 47.7.



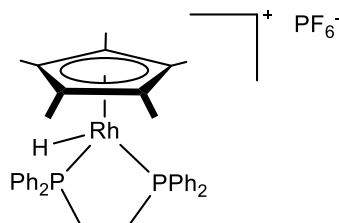
Compound 2^{Cyp}·OH. A solution of compound [(PCyp₂Ar^{Xyl2})AuCl] (50 mg, 0.072mmol) in benzene (5 ml) was treated with one equivalent of KOH (4.0 mg, 0.072 mmol) and the suspension stirred at room temperature for 24 hours. The resulting solution was then evaporated and extracted with pentane (4 x 5 mL). The filtrate was dried under reduced pressure to provide compound 2^{Cyp}·OH as a white powder (28 mg, 57 %).

¹H NMR (400 MHz, C₆D₆, 25 °C) δ: 7.20 (q, 2 H, ³J_{HH} = 7.1 Hz, H_b), 7.07 (d, 4 H, ²J_{HH} = 7.5 Hz, H_a), 6.92 (td, 1 H, ³J_{HH} = 7.4 Hz, ⁵J_{HP} = 1.6 Hz, H_d), 6.55 (dd, 2 H, ²J_{HH} = 7.6 Hz, ²J_{HP} = 3.2 Hz, H_c), 2.02 to 1.85 (m, 2 H, Cyp(CH)), 1.90 (s, 12 H, Me_{Xyl}), 1.65 to 1.15 (m, 16 H, Cyp(CH₂)). ¹³C{¹H} NMR (100 MHz, C₆D₆, 25 °C,) δ: 148.1 (br, C₃), 142.3 (br, C₂), 136.4 (C₁), 131.7 (d, ³J_{CP} = 7 Hz, CH_c), 130.4 (CH_d), 128.4 (CH_b), 127.5 (CH_a), 38.1 (d, ²J_{CP} = 36 Hz, Cyp(CH)), 34.8 (d, ³J_{CP} = 6 Hz, Cyp(CH₂)), 32.2 (d, ³J_{CP} = 6 Hz, Cyp(CH₂)), 24.9 (d, ²J_{CP} = 16 Hz, Cyp(CH₂)) 24.8 (d, ²J_{CP} = 13 Hz, Cyp(CH₂)), 21.3 (s, Me_{Xyl}). Signals due to C₄ could not be precisely assigned. ³¹P{¹H} NMR (162 MHz, C₆D₆, 25 °C) δ: 47.7. IR (Nujol): ν_{OH} = 3503 cm⁻¹.



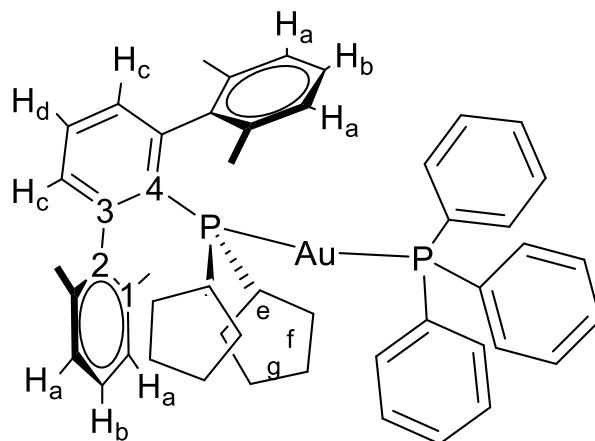
Compound 5b. NH_4PF_6 (42 mg, 0.258 mmol) was added to a solution of **1b** (100 mg, 0.258 mmol) in THF (10 mL) and stirred for 1 hour. Concentration to half volume and precipitation with pentane (20 mL) yielded a solid brown residue (77 mg, 77%). Anal. Calcd. for $\text{C}_{16}\text{H}_{32}\text{P}_2\text{Rh}$: C, 49.4; H, 8.3. Found: C, 49.6; H, 8.4.

^1H NMR (400 MHz, $\text{THF-}d_8$, 25 °C) δ : 2.02 (s, 15H, C_5Me_5), 1.92 to 1.75 (br m, 4H, CH_2), 1.62 (dd, 12H, $^3J_{\text{HRh}} = 15.0$, $^2J_{\text{HP}} = 11.5$ Hz, PMe_2), -13.60 (dt, 1H, $^2J_{\text{HP}} = 31.9$, $^1J_{\text{HRh}} = 27.8$ Hz, RhH). $^{13}\text{C}\{^1\text{H}\}$ NMR (100 MHz, $\text{THF-}d_8$, 25 °C) δ : 94.9 (C_5Me_5), 28.8 (m, CH_2), 18.8 and 13.6 (m, PMe_2), 9.72 (C_5Me_5). $^{31}\text{P}\{^1\text{H}\}$ NMR (162 MHz, $\text{THF-}d_8$, 25 °C) δ : 45.9 (d, $^1J_{\text{PRh}} = 134$ Hz, PMe_2), -144.2 (q, $^1J_{\text{PF}} = 710$ Hz PF_6)



Compound 5c. NH_4PF_6 (26 mg, 0.157 mmol) was added to a solution of **1c** (100 mg, 0.157 mmol) in THF (10 mL) and stirred for 1 hour. Concentration to half volume and precipitation with pentane (20 mL) yielded a solid brown residue (73 mg, 73%). Anal. Calcd. for $\text{C}_{36}\text{H}_{40}\text{P}_2\text{Rh}$: C, 67.8; H, 6.3. Found: C, 67.5; H, 6.7.

^1H NMR (400 MHz, THF- d_8 , 25 °C) δ : 7.74, 7.65, 7.61, 7.45 (m, 20H, overlapped *m*-Ph₂, *o*-Ph₂, *p*-Ph₂), 2.56 (d, 4H, $^2J_{\text{HP}} = 18.3$ Hz, CH₂), 1.60 (s, 15H, C₅Me₅), -12.26 (m, RhH). $^{13}\text{C}\{^1\text{H}\}$ NMR (100 MHz, THF- d_8 , 25 °C) δ : 132.9, 131.4 and 128.9 (C_oPh₂, C_mPh₂, C_pPh₂), 130.0 (d, $^1J_{\text{CP}} = 43$ Hz, C_{ipso}Ph₂), 132.9 (vt, $^3J_{\text{CP}} = 6$ Hz, C_oPh₂), 128.3 (C_pPh₂), 95.0 (C₅Me₅), 31.9 (vtd, $^1J_{\text{CP}} = 27$, $^2J_{\text{CRh}} = 2$ Hz, CH₂), 10.7 (C₅Me₅). $^{31}\text{P}\{^1\text{H}\}$ NMR (162 MHz, THF- d_8 , 25 °C) δ : 73.5 (d, $^1J_{\text{PRh}} = 139$ Hz, PPh₂), -144.2 (q, $^1J_{\text{PF}} = 690$ Hz PF₆)



Compound 8. PPh₃ (5.62 mg, 0.021 mmol) was added to a solution of gold complex **2^{Cyp}** (20 mg, 0.021 mmol) in benzene, and stirred for 5 minutes. Solvent was removed under vacuum to yield the desired product (10 mg, 40%).

¹H NMR (400 MHz, THF-*d*₈, 25 °C) δ: 7.41 to 7.33 (br t, PPh₃), 7.27 to 7.16 (m, PPh₃), 7.06 to 6.9 (m, PPh₃), 6.83 (d, 4H, ³J_{HH} = 7.6 Hz, H_a), 6.61 (br, 1H, H_d) 6.54 (br d, 2H, ³J_{HH} = 7.6 Hz, H_c), 2.44 to 2.31 (m, 2H, PCH), 1.98 (s, 12H, Me_{Xyl}), 1.89 to 1.52 (m, 16H, CH₂). ¹³C{¹H} NMR (100 MHz, THF-*d*₈, 25 °C) δ: 134.1 (PPh₃), 132.3 (PPh₃), 131.9 (CH_c), 128.3 (CH_a), 37.9 (d, ¹J_{CP} = 29 Hz, PCH), 25.7 (d, ²J_{CP} = 10 Hz, CH₂), 25.6 (d, ³J_{CP} = 11 Hz, CH₂), 21.6 (Me_{Xyl}). ³¹P{¹H} NMR (162 MHz, THF-*d*₈, 25 °C) δ: 59.4 (d, ¹J_{PP} = 309 Hz), 44.3 (d, ¹J_{PP} = 309 Hz).

III.8.6. Variable temperature van't Hoff study of the equilibrium of **1c** and **2^{Cyp}** with **3c^{Cyp}**

Complexes **1c** and **2^{Cyp}** were dissolved in benzene-*d*₆ in a young NMR tube. The reaction was monitored for 24 hours. For complex **4c^{Cyp}**, the C–H activation product disappears, rendering a mixture comprising complexes **1c**, **2^{Cyp}** and **3c^{Cyp}**. To study the equilibrium between the precursors and the adduct, the tube was inserted into a temperature-controlled NMR probe and ¹H NMR spectra were collected at 5 K intervals from 298 K to 238 K and back to 298 K, allowing 5 minutes for equilibration at each temperature. Concentrations were determined by NMR. The equilibrium constant of the reaction was calculated according to the expression:

$$K_{obs} = \frac{[10c]}{[9][2c]}$$

The plot of ln(*K*_{obs}) as a function of T⁻¹ was fit by a line according to the expression:

$$\ln(K_{obs}) = \frac{-\Delta H}{RT} + \frac{\Delta S}{R}$$

The enthalpy and entropy of the reaction were extracted from the slope and intercept, respectively.

III.9. References

1. B. Klingert, H. Werner, *Chem. Ber.*, **1983**, *116*, 1450-1462.
2. J. Campos, M. F. Espada, J. López-Serrano, M. L. Poveda, E. Carmona, *Angew. Chemie, Int. Ed.* **2015**, *54*, 15379-15384.
3. J. Bauer, H. Braunschweig, R. D. Dewhurst, *Chem. Rev.*, **2012**, *112*, 4329-4346.
4. a) H.-J. Kraus, H. Werner, *Angew. Chem. Int. Ed. Engl.*, **1982**, *21*, 866-867.
b) H. Werner, G. T. Crisp, P. W. Jolly, H.-J. Kraus, C. Krüger, *Organometallics*, **1983**, *2*, 1369-1377.
c) A. Nutton, P. M. Maitlis, *Dalton Trans.*, **1981**, 2335-2338.
d) C. P. Lenges, P. S. White, M. Brookhart, *J. Am. Chem. Soc.*, **1999**, *121*, 4385-4396.
5. C. Bianchini, C. J. Elsevier, J. M. Ernsting, M. Peruzzini, F. Zanobini, *Inorg. Chem.*, **1995**, *34*, 84-92.
6. B. Cordero, V. Gómez, A. E. Platero-Prats, M. Revés, J. Echeverría, E. Cremades, F. Barragán, S. Alvarez, *Dalton Trans.*, **2008**, 2832-2838.
7. L. Pauling, *J. Am. Chem. Soc.*, **1947**, *69*, 542-553.
8. See for example: a) J.-R. Hamon, P. Hamon, S. Sinbandhit, P. Guenot, D. Astruc, *J. Org. Chem.*, **1991**, *413*, 243-255.
b) C. S. Wei, C. A. Jiménez-Hoyos, M. F. Videa, J. F. Hartwig, M. B. Hall, *J. Am. Chem. Soc.*, **2010**, *132*, 3078-3091.
c) G. Ciancaleoni, S. Bolaño, J. Bravo, M. Peruzzini, L. Gonsalvi, A. Macchioni, *Dalton Trans.*, **2010**, *39*, 3366-3368.
d) M. Carmona, J. Ferrer, R. Rodríguez, V. Passarelli, F. J. Lahoz, P. García-Orduña, L. Cañadillas-Delgado, D. Carmona, *Chem. Eur. J.*, **2019**, *25*, 13665-13670.
e) R. Poli, *Chem. Rev.*, **1991**, *91*, 509-551

9. P. H. Budzelaar, J. J. Engelberts, J. H. van Lenthe, *Organometallics*, **2003**, *22*, 1562–1576.
10. Selected examples of ammonia activation by transition metal complexes:
- a) J. Zhao, A. S. Goldman, J. F. Hartwig, *Science*, **2005**, *307*, 1080-1082.
- b) C. M. Fafard, D. Adhikari, B. M. Foxman, D. J. Mindiola, O. V. Ozerov, *J. Am. Chem. Soc.*, **2007**, *129*, 10318-10319.
- c) J. Abbeneth, M. Kinauer, F. W. Heinemann, C. Würtele, B. de Bruin, S. Schneider, M. G. Scheibel, *Inorg. Chem.*, **2015**, *54*, 9290-9302.
11. a) S. Jamali, S. Abedanzadeh, N. K. Khaledi, H. Samouei, Z. Hendi, S. Zacchini, R. Kia, H. R. Shahsavari, *Dalton Trans.*, **2016**, *45*, 17644-17651.
- b) N. Hidalgo, C. Maya, J. Campos, *Chem. Commun.*, **2019**, *55*, 8812-8815.
12. K. P. Keep, *Inorg. Chem.*, **2016**, *55*, 9461-9470.
13. a) J. E. Bercaw, *J. Am. Chem. Soc.*, **1974**, *96*, 5087-5094.
- b) C. McDade, J.C. Green, J. E. Bercaw, *Organometallics*, **1982**, *1*, 1629-1634.
- c) A. R. Bulls, W. P. Schaefer, M. Serfas, J. E. Bercaw, *Organometallics*, **1987**, *6*, 1219-1226.
- d) F. G. N. Cloke, J. P. Day, J. C. Green, C. P. Morley, A.C. Swain, *J. Chem. Soc. Dalton Trans.*, **1991**, 789-796.
- f) H. J. Kraus, H. Werner, *Angew. Chem. Int. Ed. Engl.*, **1982**, *21*, 866-867.
- g) H. Werner, G. T. Crisp, P. W. Jolly, H.-J. Kraus, C. Krüger, *Organometallics*, **1983**, *2*, 1369-1377.
14. Y. Ohki, A. Murata, M. Imada, K. Tatsumi, *Inorg. Chem.*, **2009**, *48*, 4271-4273.
15. M. J Chalkley, T. J. Del Castillo, B. D. Matson, J. C. Peters, *J. Am. Chem. Soc.* **2018**, *140*, 6122-6129.
16. M. G. Alférez, J. J. Moreno, N. Hidalgo, J. Campos. *Angew. Chem. Int. Ed.*, **2020**, *59*, 20863-20867.

17. V. B. Kharitonov, D. V. Muratov, D.A. Loginov, *Coordination chemistry reviews*, **2019**, 399, 213027.
18. T. B. Marder, J. C. Calabrese, D. C. Roe, T. H. Tulip, *Organometallics*, **1987**, 6(9), 2012-2014.
19. L. Pauling, *J. Am. Chem. Soc.* 1947, 69, 542–553.
20. a) J. Campos, *J. Am. Chem. Soc.*, **2017**, 139, 2944-2947.
b) N. Hidalgo, J. J. Moreno, M. Pérez-Jiménez, C. Maya, J. López-Serrano, J. Campos, *Chem. Eur. J.*, **2020**, 26, 5982-5993.
21. a) N. Hidalgo, F. de la Cruz-Martínez, M. T. Martín, M. C. Nicasio, J. Campos, *Chem. Commun.*, **2022**, 58, 9144-9147.
b) N. Hidalgo, C. Romero-Pérez, C. Maya, I. Fernández, J. Campos, *Organometallics*, **2021**, 40, 1113-1119.
c) N. Hidalgo, C. Maya, J. Campos, *Chem. Commun.*, **2019**, 55, 8812-8815.
22. See for instance: a) R. Liedtke, F. Scheidt, J. Ren, B. Schirmer, A. J. P. Cardenas, C. G. Daniliuc, H. Eckert, T. H. Warren, S. Grimme, G. Kehr, G. Erker, *J. Am. Chem. Soc.*, **2014**, 136(25), 9014–9027.
b) O. Ekkert, G. G. Miera, T. Wiegand, H. Eckert, B. Schirmer, J. L. Petersen, C. G. Daniliuc, R. Fröhlich, S. Grimme, G. Kehra, G. Erker, *Chem. Sci.*, **2013**, 4, 2657-2664.
c) A. C. McQuilken, Q. M. Dao, A. J. P. Cardenas, J. A. Bertke, S. Grimme, T. H. Warren, *Angew. Chem. Int. Ed.*, **2016**, 55, 14335–14339.
23. S. Bajo, M. G. Alférez, M. M. Alcaide, J. López-Serrano, J. Campos, *Chem. Eur. J.*, **2020**, 26, 16833–16845.
24. A. Uson, M. Laguna, D. A. Briggs, H. H. Murray and J. P. Fackler, *Inorg. Synth.*, **1989**, 26, 85-91.
25. C. N. Garon, D. I. McIsaac, C. M. Vogels, A. Decken, I. D. Williams, C. Kleeberg, T. B. Marder, S. A. Westcott, *Dalton Trans.*, **2009**, 1624–1631

26. SAINT 6.02, *BRUKER-AXS*, Inc., Madison, WI 53711-5373 USA, **1997–1999**.
27. SADABS George Sheldrick, *Bruker AXS, Inc.*, Madison, Wisconsin, USA, **1999**.
28. G. M. Sheldrick, *Acta Cryst.* **2008**, *A64*, 112-122.
29. a) L. J. Bourhis, O. V. Dolomanov, R. J. Gildea, J. A. K. Howard, H. Puschmann, *Acta Cryst.*, 2015, *A71*, 59-75.
- b) O. V. Dolomanov, L. J. Bourhis, R. J. Gildea, J. A. K. Howard, H. Puschmann, *J. Appl. Cryst.*, **2009**, *42*, 339-341.
- c) G. M. Sheldrick, *Acta Cryst.*, **2015**, *C71*, 3-8.
30. M. J. Frisch, G. W. Trucks, H. B. Schlegel, G. E. Scuseria, M. A. Robb, J. R. Cheeseman, G. Scalmani, V. Barone, B. Mennucci, G. A. Petersson, H. Nakatsuji, M. Caricato, X. Li, H. P. Hratchian, A. F. Izmaylov, J. Bloino, G. Zheng, J. L. Sonnenberg, M. Hada, M. Ehara, K. Toyota, R. Fukuda, J. Hasegawa, M. Ishida, T. Nakajima, Y. Honda, O. Kitao, H. Nakai, T. Vreven, J. A. J. Montgomery, J. E. Peralta, F. Ogliaro, M. Bearpark, J. J. Heyd, E. Brothers, K. N. Kudin, V. N. Staroverov, R. Kobayashi, J. Normand, K. Raghavachari, A. Rendell, J. C. Burant, S. S. Iyengar, J. Tomasi, M. Cossi, N. Rega, J. M. Millam, M. Klene, J. E. Knox, J. B. Cross, V. Bakken, C. Adamo, J. Jaramillo, R. Gomperts, R. E. Stratmann, O. Yazyev, A. J. Austin, R. Cammi, C. Pomelli, J. W. Ochterski, R. L. Martin, K. Morokuma, V. G. Zakrzewski, G. A. Voth, P. Salvador, J. J. Dannenberg, S. Dapprich, A. D. Daniels, O. Farkas, J. B. Foresman, J. V. Ortiz, J. Cioslowski, D. J. Fox. Gaussian 09, Revision E.01, Gaussian, Inc.: Wallingford CT, **2013**.
31. J. P. Perdew, K. Burke, M. Ernzerhof, *Phys. Rev. Lett.*, **1996**, *77*, 3865–3868.

32. S. Grimme, J. Antony, S. Ehrlich, H. Krieg, *J. Chem. Phys.*, **2010**, *132*, 154104.
33. a) W. J. Hehre, R. Ditchfield, J. A. Pople, *J. Phys. Chem.*, **1972**, *56*, 2257–2261.
- b) P. C. Hariharan, J. A. Pople, *Theor. Chim. Acta.*, **1973**, *28*, 213–222.
- c) M. M. Francl, W. J. Pietro, W. J. Hehre, J. S. Binkley, M. S. Gordon, D. J. Defrees, J. A. Pople, *J. Chem. Phys.*, **1982**, *77*, 3654–3665.
34. D. Andrae, U. Haeussermann, M. Dolg, H. Stoll, H. Preuss, *Theor. Chim. Acta*, **1990**, *77*, 123–141.
35. A. V. Marenich, C. J. Cramer, D. G. Truhlar, *J. Phys. Chem. B*, **2009**, *113*, 6378–6396.
36. H. Werner, R. Feser, *Z. Naturforsch.*, **1980**, *35 b*, 689-693.

CHAPTER IV

IV.1. Introductory comments

The broad concept of metal-ligand cooperation, already discussed in some detail in Chapter 1, has enriched the traditional notion of an active metal site surrounded by spectator ligands¹. Among the wide variety of ligands that directly cooperate with transition metals, those bearing a Lewis acidic site enjoy increasing popularity². Not surprisingly, ligands containing group 13 elements are the preferred choice, with boron as the more prevalent³. As discussed in the introduction chapter, catalytic applications that rely on the cooperative action of a transition metal and a borane are rapidly increasing.

Borane containing ligands are usually tethered to the metal by two or more supporting groups to provide stability³. While phosphine and nitrogen-based donors have been amply used, the functionalization of widespread cyclopentadienyl (Cp) and indenyl (Ind) ligands with boron fragments remain little explored⁴. More precisely, they have only been

¹ a) C. Gunanathan, D. Milstein, *Acc. Chem. Res.*, **2011**, *44*, 588-602.

b) J. R. Khusnutdinova, D. Milstein, *Angew. Chem. Int. Ed.*, **2015**, *54*(42), 12236-12273.

c) M. R. Elsbey, R. T. Baker, *Chem. Soc. Rev.*, **2020**, *49*, 8933-8987.

² a) I. Kuzu, I. Krummenacher, J. Meyer, F. Armbruster, F. Breher, *Dalton Trans.*, **2008**, 5836-5865.

b) A. Amgoune, D. Bourissou, *Chem. Commun.*, **2011**, *47*, 859-871.

c) M. Devillard, G. Bouhadir, D. Bourissou, *Angew. Chem. Int. Ed.*, **2015**, *54*, 730-732.

d) J. S. Jones, F. P. Gabbai, *Acc. Chem. Res.*, **2016**, *49*, 857-867.

e) W. Guan, G. Zeng, H. Kameo, Y. Nakao, S. Sakaki, *Chem. Rec.*, **2016**, *16*, 2405-2425.

f) D. You, F. P. Gabbai, *Trends Chem.*, **2019**, *1*, 485-496.

³ a) H. Braunschweig, R. D. Dewhurst, A. Schneider, *Chem. Rev.*, **2010**, *110*, 3924-3957.

b) D. R. Owen, *Chem. Soc. Rev.*, **2012**, *41*, 3535-3546.

c) H. Kameo, H. Nakazawa, *Chem. Asian J.*, **2013**, *8*, 1720-1734.

d) D. R. Owen, *Chem. Commun.*, **2016**, *52*, 10712-10726

To see some relevant examples: e) A. J. M. Miller, J. A. Labinger, J. E. Bercaw, *J. Am. Chem. Soc.*, **2008**, *130*(36), 11874-11875.

f) J. J. Kiernicki, M. Zeller, N. K. Szymczak, *J. Am. Chem. Soc.*, **2017**, *139*, 18194-18197.

g) A. Iannetelli, G. Tizzard, S. J. Coles, G. R. Owen, *Inorg. Chem.*, **2018**, *57*, 446-456.

h) A. Iannetelli, R. C. Da Costa, A. J. Guwy, G. J. Tizzard, S. J. Coles, G. R. Owen, *Organometallics*, **2020**, *39*, 1976-1988.

⁴ a) Z. G. Lewis, A. J. Welch, *J. Organomet. Chem.*, **1992**, *438*, 353-369.

investigated in the narrow context of olefin polymerization with early transition metals (i.e. Zr, Ti, Hf)⁵. Therein, they have served as self-activating catalysts⁶ and to develop a new class of highly tunable donor/acceptor metallocenes⁷. However, it seems surprising that further applications have not yet emerged given the paramount position occupied by cyclopentadienyl and indenyl ligands in organometallic chemistry and homogeneous catalysis.

Besides, in terms of synthetic approaches, prior examples are mainly restricted to the simplest C₅H₅ moiety⁸, which places the borane functionality further from the metal center and thus reduces its potential for cooperation. At variance, the functionalization of its prominent permethylated version (Cp*) positions the boron atom in a more convenient location for partnering with the metal. This has been unexpectedly observed for cobaltocene, where borylation yields zwitterionic species alike [(η^5 -C₅Me₅)Co(η^5 -C₅Me₄CH₂BR₃)]⁹. In most cases, this likely proceeds through

b) E. Bardaya, B. Frangea, B. Hanqueta, G. E. Herberich, *J. Organomet. Chem.*, **1999**, 572, 225–232.

⁵ a) H. Braunschweig, R. Dörfler, M. Friedrich, M. Kraft, A. Oechsner, *Z. Anorg. Allg. Chem.*, **2011**, 2125–2128.

b) K. Rufanov, E. Avtomonov, N. Kazennova, V. Kotov, A. Khvorost, D. Lemenovskii, J. Lorberth, *J. Organomet. Chem.*, **1997**, 536-537, 361-373.

c) Y. Sun, W. E. Piers, G. P. A. Yap, *Organometallics*, **1997**, 16, 2509-2513.

⁶ a) Y. Sun, R. E. v. H. Spence, W. E. Piers, M. Parvez, G. P. A. Yap, *J. Am. Chem. Soc.*, **1997**, 119, 5132-5143.

b) R. Duchateau, S. J. Lancaster, M. Thornton-Pett, M. Bochmann, *Organometallics*, **1997**, 16, 4995-5005.

c) X. Song, M. Bochmann, *J. Organomet. Chem.*, **1997**, 545-546, 597-600.

d) S. Kohrt, G. Kehr, C. G. Daniliuc, R. S. Rojas, B. Rieger, C. Troll, G. Erker, *Organometallics*, **2016**, 35, 2689–2693.

⁷ K. A. O. Starzewski, W. M. Kelly, A. Stumpf, D. Freitag, *Angew. Chem. Int. Ed.*, **1999**, 38, 2439-2443.

⁸ a) J. C. Kotz, E. W. Post, *J. Am. Chem. Soc.*, **1968**, 90(16), 4503-4504.

b) J. C. Kotz, E. W. Post, *Inorg. Chem.*, **1970**, 9, 1661-1669.

⁹ a) J. Bauer, H. Braunschweig, C. Hörl, K. Radacki, J. Wahler, *Chem. Eur. J.*, **2013**, 19, 13396-13401.

b) V. Hosseininasab, I. M. DiMucci, P. Ghosh, J. A. Bertke, S. Chandrasekharan, C. J. Titus, D. Nordlund, J. H. Freed, K. M. Lancaster, T. H. Warren, *Nat. Chem.*, **2022**, 14, 1265-1269.

initial deprotonation of a methyl group from the Cp* moiety and subsequent trapping of the electrophilic borane in solution by fulvene or tuck-in type structures, as suggested for related systems^{5,10}. Radical mechanisms and direct electrophilic substitution with liberation of dihydrogen has also been proposed as an alternative pathway¹¹.

Nonetheless, these fortuitous examples do not offer a systematic approach to access this type of potentially cooperative structures. In this chapter, an in-depth study is carried out on a variety of rhodium/boron systems starting from the same rhodium complexes (**1** and **6**) investigated in the previous chapter. Their reactivity against pentafluorophenylborane (B(C₆F₅)₃) and the Pier's Borane (HB(C₆F₅)₂) has been investigated and will be the crux of the present chapter. In particular, we have focused on compounds **1a** and **6d** as representative Rh(I) precursors based on Cp* and indenyl ligands, respectively.

IV.2. Reaction of complex **1a** with B(C₆F₅)₃ and HB(C₆F₅)₂

We first treated a benzene solution of compound **1a** with the highly electrophilic B(C₆F₅)₃ borane. A rapid inspection of the resulting ¹H NMR spectrum points out to the analogous unusual activation of the Cp* ligand that we described in our prior chapter with Rh(I)/Au(I) pairs. Thus, the appearance of a low-frequency multiplet at -13.65 ppm aligns with the formation of a new Rh-H bond in compound **9^B** (Scheme 1), while the

¹⁰ a) H. J. Liu, M. S. Ziegler, T. D. Tilley, *Polyhedron*, **2014**, *84*, 203-208.

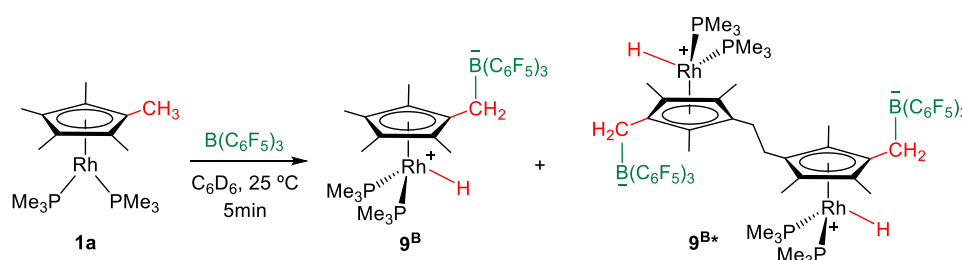
b) V. Varga, P. Šindelář, I. Čisářová, M. Horáček, J. Kubišta, K. Mach, *Inorg. Chem. Commun.*, **2005**, *8*, 222-226.

¹¹ a) A. Wong, J. Chu, G. Wu, J. Telsler, R. Dobrovetsky, G. Menard, *Inorg. Chem.*, **2020**, *59*, 10343-10352.

b) L. L. Cao, J. Zhou, Z. W. Qu, D. W. Stephan, *Angew. Chem. Int. Ed.*, **2019**, *58*, 18487-18491.

c) V. V. Burlakov, P. M. Pellny, P. Arndt, W. Baumann, A. Spannenberg, V. B. Shur, U. Rosenthal, *Chem. Commun.*, **2000**, 241-242.

characteristic intense signal of the Cp* ligand has disappeared due to its asymmetry after being functionalized at one of the methyl groups. To facilitate the reading, we have decided to label compounds derived from $B(C_6F_5)_3$ or $HB(C_6F_5)_2$ with 'B' or 'HB' as superindexes, respectively.



Scheme 1. Activation of the Cp* ligand in compound **1a** through proton migration upon addition of perfluorinated borane $B(C_6F_5)_3$.

Further careful NMR analysis reveals a more complicated situation than initially assumed. In the hydridic region of the 1H NMR spectrum, there are additional resonances. One of them ($\delta -13.26$, $^2J_{HP} = 36.1$, $^1J_{HRh} = 20.5$ Hz, RhH) is attributed to the known cationic $[(\eta^5-C_5Me_5)Rh(PMe_3)_2H]^+$ **5a** complex, which appears along with anion $[(HO)B(C_6F_5)_3]^-$ ($^{11}B\{^1H\} -12.7$ ppm; Figure 1) due to cooperative activation of an O–H bond of adventitious water. More importantly, the hydridic resonance of **9B** is not well-defined and its minute examination suggests that it pertains to several hydrides of independent but highly similar species (Figure 1).

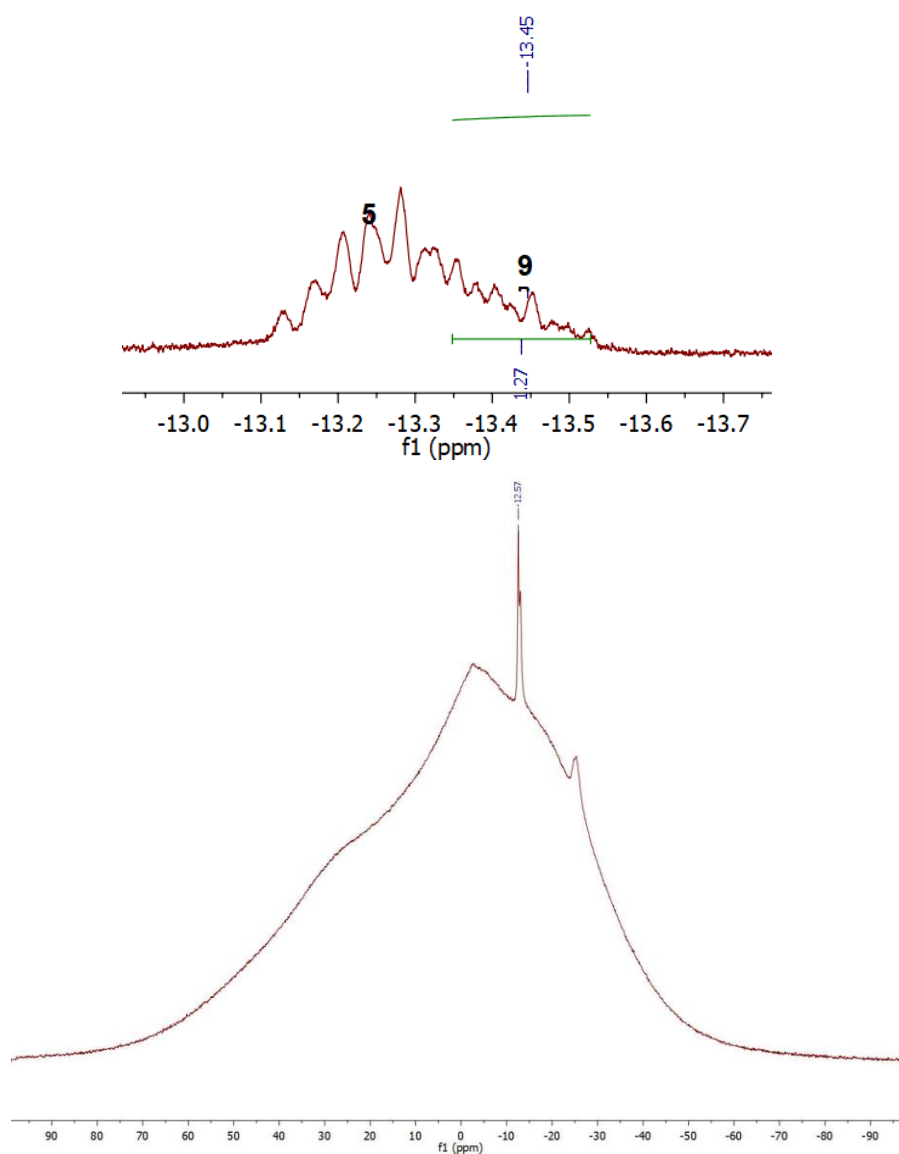
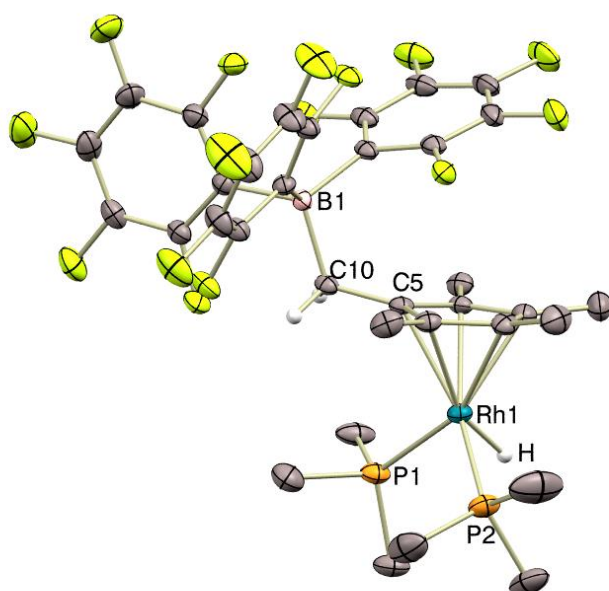


Figure 1. Zoom of the ^1H NMR spectrum of $\mathbf{9}^{\text{B}}$ at the low frequency where the mixture between the several hydrides is observed (top). $^{11}\text{B}\{^1\text{H}\}$ NMR spectrum of complex $\mathbf{9}^{\text{B}}$ containing also anion $[(\text{HO})\text{B}(\text{C}_6\text{F}_5)_3]^-$ (bottom).

The same may be inferred after examining the corresponding $^{31}\text{P}\{^1\text{H}\}$ NMR spectrum, where a complex set of overlapped resonances appear at -2 ppm. All attempts to isolate any of those species found no

success due to high instability and virtually identical solubilities. However, our suspicions were confirmed by X-ray diffraction studies. Crystals of compound **9^B** were grown by slow diffusion of pentane into its benzene solution at 5 °C. Surprisingly, apart from **9^B** the unit cell contains a second molecule of a binuclear species (**9^{B*}**) consisting of a dehydrogenative dimerization of the former by coupling two Cp*-methyl groups from adjacent molecules (Figure 2), with a C–C bond distance of the bridging unit of 1.555(8) Å.



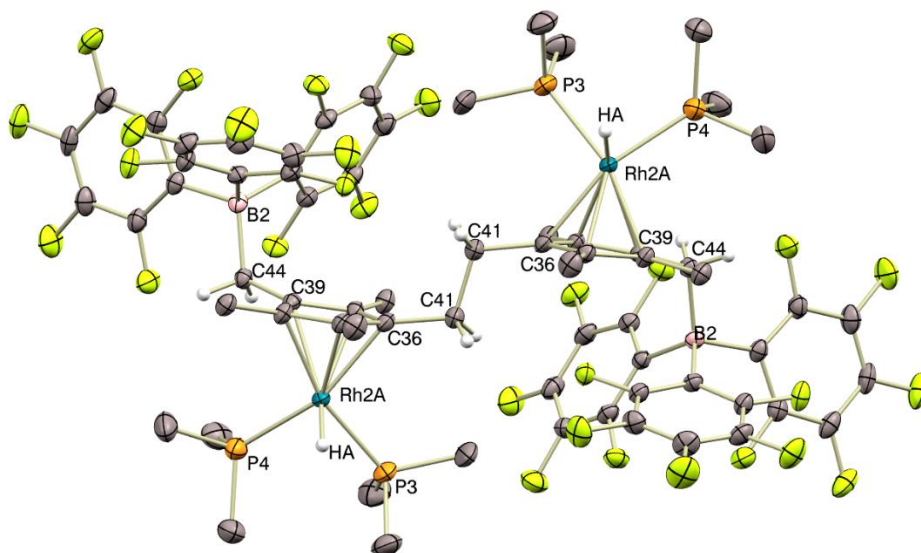


Figure 2. ORTEP diagrams of compounds **9^B** and **9^{B*}** as co-crystals that are present in the same unit cell. Selected bond distances (Å) and angles(°): Rh1–P1, 2.2651(12); Rh1–P2, 2.2761(12); Rh1–C5, 2.307(4); Rh1–H, 1.46(5); C5–C10, 1.489(6); C10–B1, 1.680(6); P1–Rh1–P2, 94.47(5); P1–Rh1–C5, 96.46(10); P1–Rh1–H, 79.5(18); P2–Rh1–C5, 139.27(11); P2–Rh1–H, 81.9(7); C5–Rh1–H, 138.7(17); C10–C5–Rh1, 131.9(3); C5–C10–B1, 117.7(3); Rh2A–P3, 2.2788(16); Rh2A–P4, 2.287(3); Rh2A–C36, 2.225(5); Rh2A–C39, 2.290(4); Rh2A–HA, 1.51(6); C36–C41, 1.518(6); C39–C44, 1.504(6); C44–B2, 1.673(6); P3–Rh2A–P4, 92.72(9); P3–Rh2A–HA, 77(2); P4–Rh2A–C39, 97.26(11); P4–Rh2A–HA, 87(2); C36–Rh2A–P3, 101.34(13); C36–Rh2A–P4, 158.73(13); C36–Rh2A–C39, 61.61(16); C36–Rh2A–HA, 112(2); C39–Rh2A–C39, 145(2); C41–C36–Rh2A, 134.7(3); C44–C39–Rh2A, 132.3(3); C39–C44–B2, 117.0(3).

Further confirmation for this rare reactivity emerges from electrospray ionization mass spectrometry (ESI-MS) analysis of the crude reaction mixture, where we detected a peak at m/z 1291.26 corresponding to the organic ionic fragment $[(C_6F_5)_3BCH_2C_5Me_3(\mu-CH_2)]_2$ (calcd m/z = 1292.19; Figure 3). This formal homocoupling suggests that a radical pathway may be operating to account for the activation of the Cp* ligand,

an avenue that finds precedent in the nascent area of frustrated radical pairs using perfluorinated boranes¹².

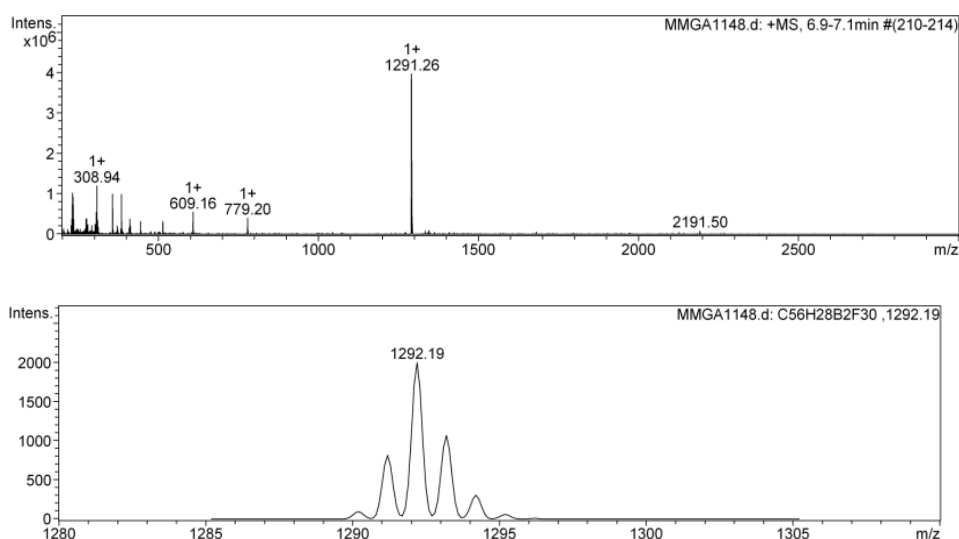


Figure 3. Mass spectrum of the reaction mixture depicted in Scheme 1 without additional purification (top: experimental; bottom: calculated). MS (electrospray, m/z): calcd for $C_{56}H_{28}B_2F_{30}$: $[M^+]$ 1292.19, found 1292.26

Aside from trisubstituted $B(C_6F_5)_3$, the Piers' borane $HB(C_6F_5)_2$ ¹³ seems more suitable to access an active pendant borane functionality, since the resulting borate moiety would contain a B–H bond susceptible of participating in chemical transformations.^{3c,d,6a} Despite its reduced electrophilicity, this borane similarly reacts with compound **1a** to yield the corresponding Cp* activated product **9^{HB}** (Scheme 2). The previously discussed homocoupling to yield dirhodium structures was not observed in

¹² a) L. Liu, L. L. Cao, Y. Shao, G. Ménard, D. W. Stephan, *Chem*, **2017**, *3*, 259–267.

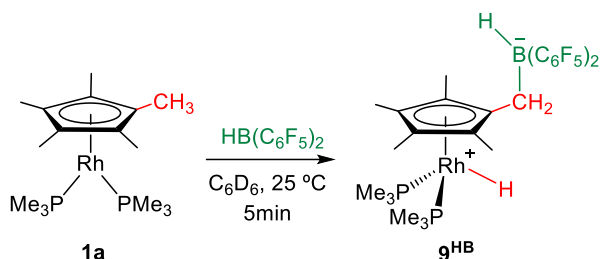
b) A. Dasgupta, E. Richards, R. L. Melen, *Angew. Chem. Int. Ed.*, **2021**, *60*, 53–65.

c) F. Holtrop, A. R. Jupp, B. J. Kooij, N. P. van Leest, B. de Bruin, J. C. Slootweg, *Angew. Chem., Int. Ed.*, **2020**, *59*, 22210–22216.

d) A. R. Jupp, *Dalton Trans.*, **2022**, *51*, 10681–10689.

¹³ D. J. Parks, W. E. Piers, G. P. A. Yap, *Organometallics*, **1998**, *17*, 5492–5503.

this case. The newly formed hydridic ligand likewise resonates at -13.51 ppm as a triple doublet ($^2J_{HP} = 39$, $^1J_{HRh} = 23$ Hz), and the loss of symmetry in the Cp* is reflected by resonances at 1.55, 1.42 and 0.47 ppm in a 2:2:1 ratio. In turn, a new signal appears in the $^{11}\text{B}\{^1\text{H}\}$ NMR spectrum at -21.2 ppm, which agrees with its tetracoordinated environment. The piano-stool conformation of the Rh site is accompanied by a decreased in the $^1J_{PRh}$ scalar-coupling observed by $^{31}\text{P}\{^1\text{H}\}$ NMR, shifting from 216 in precursor **1a** to 138 Hz in **9^{HB}**.



Scheme 2. Activation of the Cp* ligand in compound **1a** through proton migration upon addition of $\text{HB}(\text{C}_6\text{F}_5)_2$.

Single crystals of **9^{HB}** suitable for X-ray diffraction analysis were grown by diffusion of pentane into its benzene solution, which allowed us to authenticate the proposed molecular formulation (Figure 4).

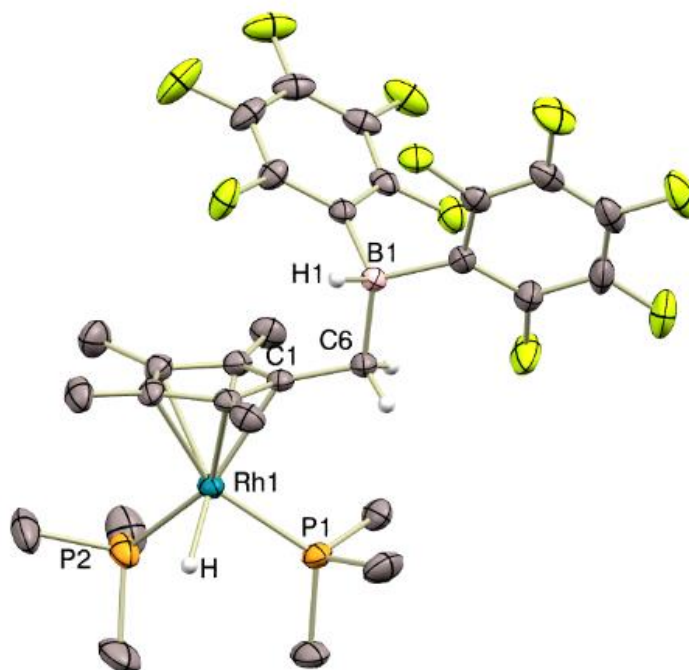
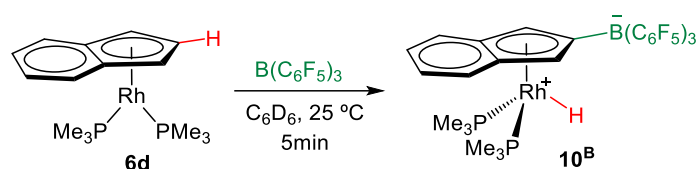


Figure 4. ORTEP diagram of compound **9^{HB}**. Selected bond distances (Å) and angles(°): Rh1–P1, 2.2787(10); Rh1–P2, 2.2643(11); Rh1–C1, 2.290(3); Rh1–H, 1.75(6); C1–C6, 1.490(5); C6–B1, 1.656(5); P1–Rh1–P2, 98.27(4); P1–Rh1–C1, 93.50(9); P1–Rh1–H, 83.2(18); P2–Rh1–C1, 154.50(10); P2–Rh1–H, 76.8(19); C1–Rh1–H, 127.3(19); C6–C1–Rh1, 134.5(2); C1–C6–B1, 109.0(3).

IV.3. Reaction of complex **6d** with $B(C_6F_5)_3$ and $HB(C_6F_5)_2$

We next moved forward towards the indenyl rhodium precursor **6d**. In the previous chapter, we have described that combining **6d** with several electrophilic Au(I) fragments of type $[(PR_2Ar)Au]^+$ led to either formation of unreactive bimetallic species defined by a dative $Rh \rightarrow Au$ bond or to the abstraction of a phosphine from rhodium to yield heteroleptic gold bisphosphine species. In stark contrast, addition of either $B(C_6F_5)_3$ or

HB(C₆F₅)₂ to solutions of **6d** leads to C–H bond activation of the indenyl fragment at the C2 position. Thus, the equimolar reaction with B(C₆F₅)₃ proceeds readily towards compound **10^B** (Scheme 3), where the new C–B bond results in a down-shifted ¹¹B{¹H} NMR resonance at -14.5 ppm (*cf* 60 ppm B(C₆F₅)₃). The migration of a hydride from the C2 position of the indenyl moiety generates a Rh–H bond that resonates at -13.08 ppm in the ¹H NMR spectrum. This complex remains stable in solution for prolonged periods of time under inert atmosphere.



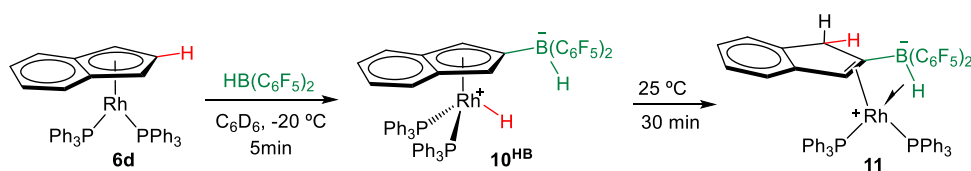
Scheme 3. Activation of the indenyl ligand in compound **6d** upon addition of perfluorinated borane B(C₆F₅)₃.

The spontaneous formation of **10^B** represents a rare case of electrophilic substitution of the coordinated indenyl fragment and a very convenient route to access bifunctional ligands of this kind. In fact, all prior examples that install highly acidic BR₂ functions at indenyl ligands requires the independent synthesis of the borylated indene precursor and usually the use of hard to handle haloboranes^{9a,10b,11b,12,14}. Moreover, all prior examples result in the borylation of indenyl at the C1 position, while placing the borane at the C2 site has remained elusive and only accessed in very low-yielding synthesis^{10b}.

¹⁴ a) M. T. Reetz, R. Brümmer, M. Kessler, J. Kuhnigk, *Chimia*, **1995**, *49*, 501–503.

b) E. Barday B. Frange B. Hanquet G. E. Herberich, *J. Organomet. Chem.*, **1999**, *572*, 225–232.

We next moved to the reaction with Piers' borane. Similarly, the activation of the indenyl ligand proceeds immediately to yield compound **10^{HB}** (Scheme 4), whose spectroscopic multinuclear NMR signature is analogous to that of **10^B** except for a new resonance in the ¹H NMR spectrum at 4.70 ppm attributable to the B–H terminus and that sharpens upon decoupling from ¹¹B. Remarkably, this compound readily evolves at room temperature in solution (*t*_{1/2} ≈ 10 min) to form the new species **11** (Scheme 4) that clearly differs from compounds **10** by NMR spectroscopy.



Scheme 4. Activation of the indenyl ligand in compound **6d** upon addition of HB(C₆F₅)₂.

The asymmetry of **11** is exemplified by two resonances in its ³¹P{¹H} NMR spectrum at 42.2 (dd, ³J_{PP} = 42, ¹J_{PRh} = 179 Hz) and 38.1 (dd, ³J_{PP} = 42, ¹J_{PRh} = 183 Hz), contrasting with single peaks in case of compounds **10** (37.8, **10^B**; 41.2 ppm, **10^{HB}**) (Figure 5). ¹⁹F{¹H} NMR reveals the presence of two different fluorinated arenes that do not interconvert in the NMR time-scale, a feature that is exclusive of this system among all complexes reported in this chapter. Thus, two clearly separated signals due to the *ortho*-fluorine atoms of the fluorinated rings are recorded by ¹⁹F{¹H} NMR at -129.8 and 128.1 ppm, which speaks in favor of a rigid structure in which the borane strongly interacts with the metal. Besides, the preceding symmetry of the indenyl ligand is also broken, and a new distinctive resonance due to two protons emerges at 3.78 ppm in the ¹H NMR spectrum that suggests loss of aromaticity. Finally, the hydridic signal in the ¹H NMR spectrum exhibits a

notable shift to higher frequencies from -13.72 ppm in **10^{HB}** to -7.21 ppm in **11**.

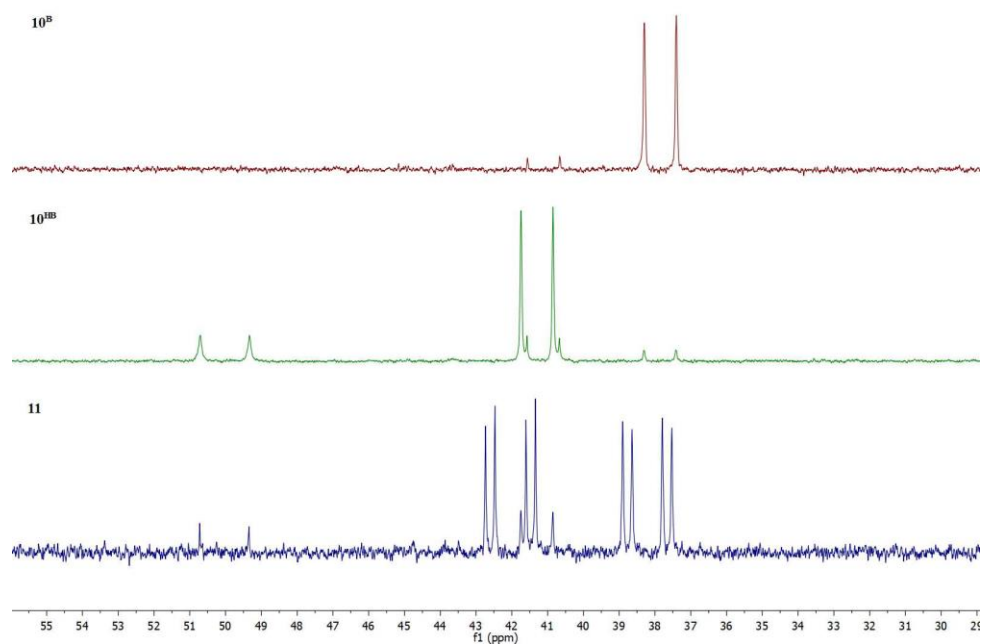
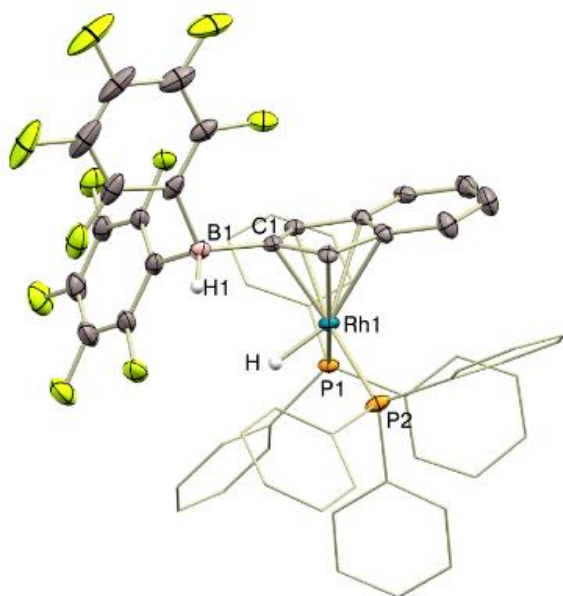
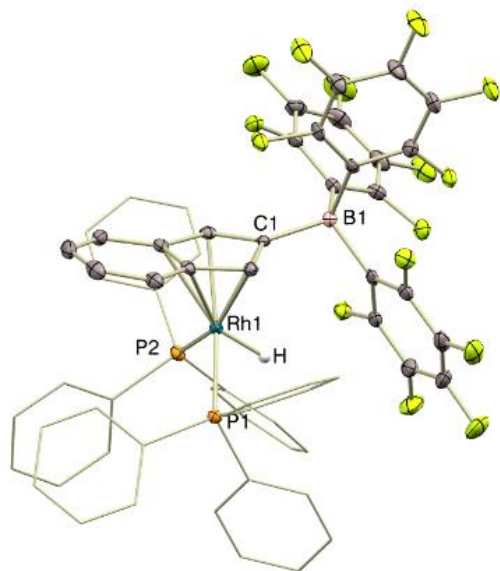


Figure 5. Comparison between ³¹P{¹H} NMR spectra of **10^B**, **10^{HB}** and **11**.

The structures of compounds **10^B**, **10^{HB}** and **11** was authenticated by X-ray diffraction studies (Figure 6). Compounds **10^B** and **10^{HB}** exhibit the expected structure anticipated by spectroscopic analysis, with C–B bond distances (1.650(5), **10^B**; 1.616(6) Å, **10^{HB}**) comparable to prior examples and other geometric parameters ranging normal values.



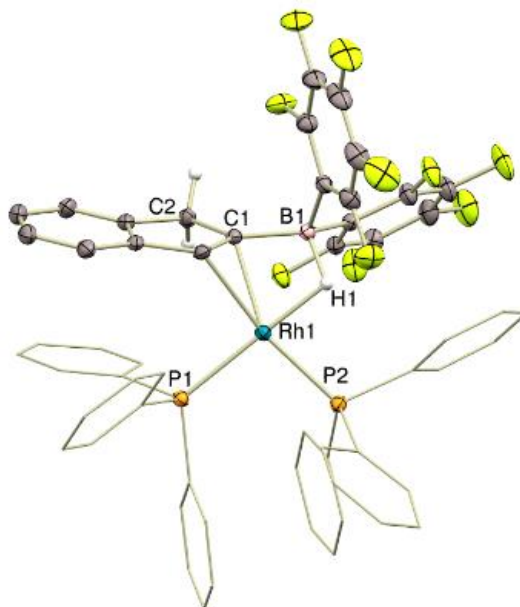


Figure 6. ORTEP diagrams for compounds **10^B**, **10^{HB}** and **11**. Selected bond distances (Å) and angles(°): Compound **10^B** Rh1–P1, 2.3105(9); Rh1–P2, 2.3234(9); Rh1–C1, 2.286(3); Rh1–H, 1.39(4); C1–B1, 1.650(5); P1–Rh1–P2, 101.68(3); P1–Rh1–C1, 134.21(9); P1–Rh1–H, 77.8(15); P2–Rh1–C1, 157.01(9); P2–Rh1–H, 80.8(14); C1–Rh1–H, 94.9(14); B1–C1–Rh1, 130.9(2). Compound **10^{HB}** Rh1–P1, 2.3005(6); Rh1–P2, 2.2991(7); Rh1–C1, 2.246(2); Rh1–H, 1.42(4); C1–B1, 1.620(4); P1–Rh1–P2, 100.61(2); P1–Rh1–C1, 130.05(6); P1–Rh1–H, 81.1(15); P2–Rh1–C1, 126.90(6); P2–Rh1–H, 83.5(15); C1–Rh1–H, 89.21(15); B1–C1–Rh1, 124.03(16); C1–B1–H1, 108.5(15). Compound **11**: Rh1–P1, 2.2804(6); Rh1–P2, 2.2701(6); Rh1–C1, 2.208(2); Rh1–H1, 1.74(3); Rh1–B1, 2.412 (3); C1–B1, 1.595(3); P1–Rh1–P2, 97.86(2); P1–Rh1–C1, 111.71(6); P1–Rh1–H1, 176.3(9); P1–Rh1–B1, 151.61(6); P2–Rh1–C1, 144.12(6); P2–Rh1–H1, 81.7(9); P2–Rh1–B1, 107.57(6); C1–Rh1–H1, 70.0(9); C1–Rh1–B1, 40.09(8); B1–Rh1–H1, 30.5(9).

The structure of **11** is more intriguing and can be described as a distorted square-planar Rh(I) species with two phosphine ligands, an η^2 -indene fragment coordinated as an olefin that chelates the metal through an additional interaction with a BH fragment. The latter interaction could in principle be described either as a 3-center-2-electron σ -borane complex (**I**) or as a bridging hydride between Rh and B. In turn, this bridging hydride

may be formally rationalized as a boron-hydride stabilized by an electrophilic Rh site (**II**, Rh \cdots H–B)¹⁵ or as a Lewis basic rhodium hydride that interacts with the pendant borane function (**III**, Rh–H \cdots B)¹⁶ (Figure 7).

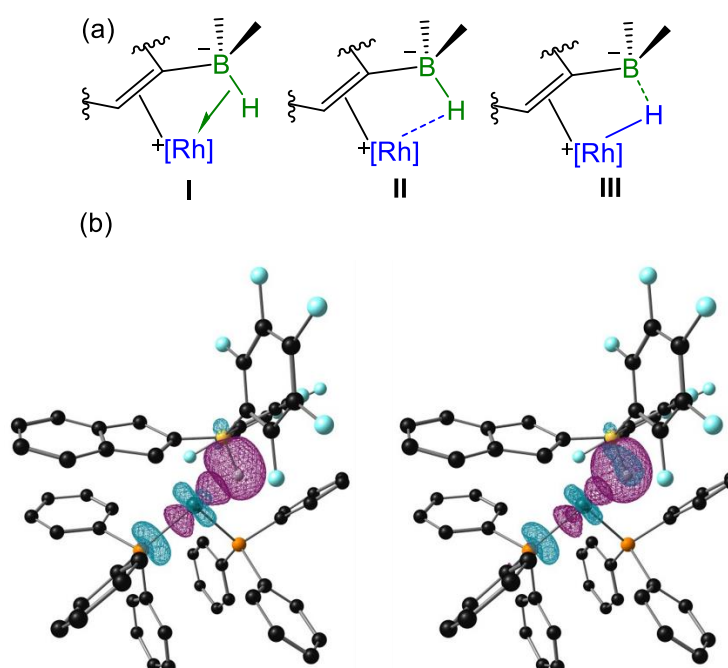


Figure 7. (a) Alternative possible representations of the interaction involving boron, hydride and rhodium; (b) NBOs (left) and NLMOs (right) 261 (donor, BD B–H) and 262 (acceptor, BD* Rh–P).

Bearing in mind the intrinsic uncertainty of locating hydrogen atoms by X-ray diffraction techniques, the structure is defined by Rh–B and Rh–H bond distances of 2.412(2) and 1.80(3), respectively, and an acute B–H–Rh

¹⁵ a) M. W. Drover, E. G. Bowes, J. A. Love, L. L. Schafer, *Organometallics*, **2017**, *36*, 331–341.

b) M. W. Drover, H. C. Johnson, L. L. Schafer, J. A. Love, A. S. Weller, *Organometallics*, **2015**, *34*, 3849–3856.

c) M. W. Drover, L. L. Schafer, J. A. Love, *Angew. Chem. Int. Ed.*, **2016**, *55*, 3181–3186.

¹⁶ B. E. Cowie, D. J. H. Emslie, *Can. J. Chem.*, **2018**, *96*(5), 484–491.

angle of 103.55(10)°, likely imposed by its intramolecular nature in a four-membered ring heterocycle. Among the structures depicted in Figure 6, the bridging hydride (**II** or **III**) fits better with the low-frequency signal recorded by ¹H NMR (δ -7.21)¹⁷. However, the relatively short Rh–B distance of 2.41, only moderately above the sum of their covalent radii (2.26Å),¹⁸ does not rule out the direct participation of the three elements in a σ -type complex.

The QTAIM analysis of complex **11** (Figure 8) shows bond critical points and paths between H and both Rh and B, but not between Rh and B. The Lewis-type NBO analysis describes the B–H–Rh interaction as a B–H bond delocalizing into a σ^* Rh–P orbital. This does not agree with the bonding scenario represented by a Lewis-basic Rh hydride (**II**), but fits well a borohydride σ complex (**I**). However, the electrostatic contributions to this bond, which would dominate scenario **III**, cannot be overlooked.

It is worth noting that the formation of **11** implies the migration of a hydride from the rhodium atom to the C1 position of the indenyl ligand, which loses its C₅-aromaticity. Moreover, that precise hydride ligand originates from a prior migration from the C2 position of the indenyl moiety upon addition of Piers' borane. Therefore, we disclose here a rare non-innocent behavior of the indenyl ligand that consists of an overall sequential two-step 1,2-H migration promoted by an electrophile, a unique process that to the best of our knowledge has remained undisclosed and that adds to the already rich chemistry of indenyl ligands. We naturally questioned ourselves about the precise mechanism to account for this process, which we investigated by computational means (Figure 8). The electrophilic attack of the borane to the indenyl presents a very low barrier (TS1) to give a square

¹⁷ T. M. Douglas, A. B. Chaplin, A. S. Weller, X. Yang, M. B. Hall, *J. Am. Chem. Soc.*, **2009**, *131*(42), 15440–15456.

¹⁸ B. Cordero, V. Gómez, A. E. Platero-Prats, M. Revés, J. Echeverría, E. Cremades, F. Barragán, S. Alvarez, *Dalton Trans.*, **2008**, 2832-2838.

planar, Rh(I) diene complex (B–C), from which hydride transfer to Rh, concomitant with the restoration of aromaticity, is both facile (TS2) and largely exergonic. The most challenging steps are the formation of an agostic B–H complex via TS3, which precedes the transfer of the metal hydride to the indenyl (TS4). Once the CH₂ moiety has been formed, the straightforward coordination of the olefin to Rh gives complex **11**. The direct hydride transfer to the indenyl from Rh–H at –22.4 kcal/mol was found to be only slightly higher energy (TS6 at 3.3 kcal/mol) and cannot therefore be ruled out. For both scenarios, the electrophilic attack of the borane to the indenyl ligand is key.

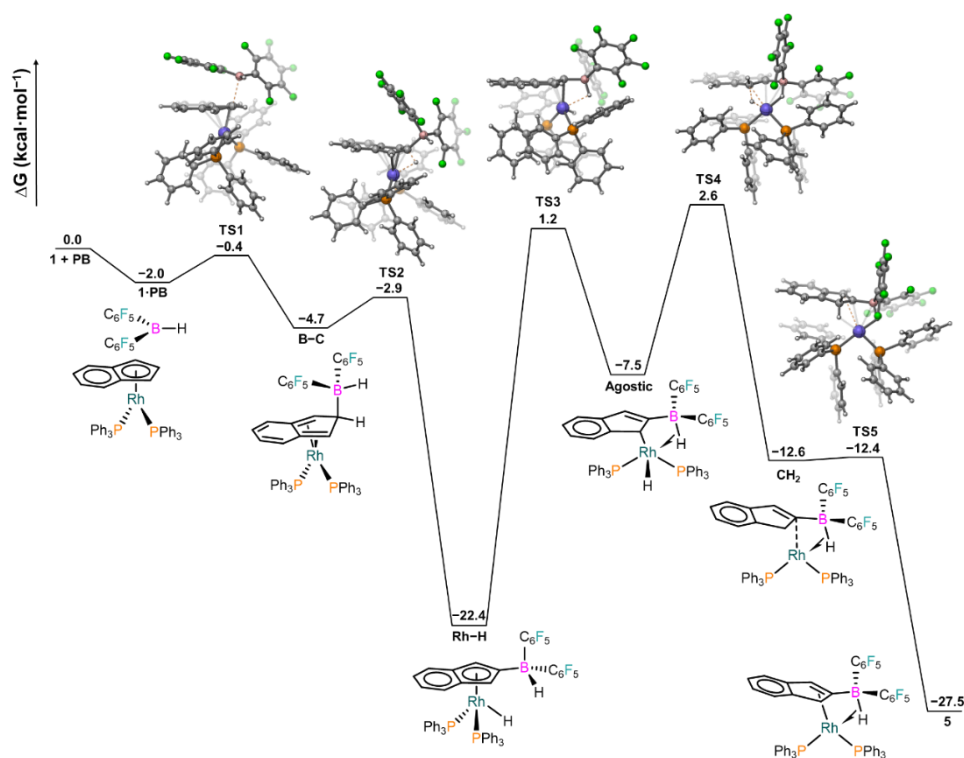


Figure 8. Free energy profile for the conversion of **6d** and Piers' borane into **11**.

IV.4. Catalytic studies

The non-innocent behavior of the indenyl ligand upon reaction with Piers' borane suggests that a catalytic cycle involving metal-ligand cooperation through sequential hydride migrations can be developed. To explore this possibility, we have carried out preliminary investigations on the catalytic hydrogenation of olefins using the rhodium complexes developed in this study. For convenience, we have selected the hydrogenation of styrene as a benchmark reaction to gauge the effect of the pendant borates in compounds **9**, **10** and **11** compared to precursors **1a** and **6d**. Hydrogenation of styrene towards ethylbenzene under mild conditions (25 °C, 0.5 atm, 0.5 mol% [Rh]) proceeds in low to good yields after one hour of reaction (Table 1) and, more importantly, provides a first hint on the effect of incorporating boron functionalities into the Cp* and Ind ligands.

Table 1. Catalyst screening for the hydrogenation of styrene^a

Entry	Cat	Yield (%)	TOF (h ⁻¹)
1	1^a	36	72
3	9^B	5	10
4	9^{HB}	10	20
2	6d	50	100
5	10^B	63	126
6	11	81	162

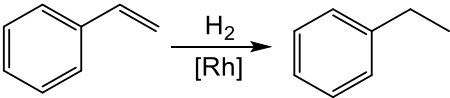
^aConditions: [Rh] 0.5 mol%, H₂ (0.5 atm), 25 °C, 1 h, C₆D₆ (0.6 mL).

From the results depicted in Table 1 it is evidenced that the instalment of a pendant borate at the Cp* ligand has a detrimental effect on

catalysis, with yields dropping from 36% for precursor **1a** (entry 1) to 5 and 10% using **9^B** and **9^{HB}**, respectively (entries 2 and 3). The opposite scenario arises with the Ind-system, where enhanced catalysis is observed in the presence of the borate site, from 50% yield of ethylbenzene formation for Rh(I) precursor **6d** (entry 4) up to 63 and 81% for the bifunctional systems **10^B** and **11**, respectively (entries 5 and 6). As foreseen, the best catalytic performance is achieved with compound **11**, where the cooperation between the metal and the boron function was already demonstrated in our described stoichiometric studies. In the same vein, the X-ray diffraction structures depicted in Figures 1, 2 and 6 already revealed a considerably longer Rh···B distance for the structures based on Cp* (4.978(6) Å, **9^B**; 4.834(5) Å, **9^{HB}**) compared to the short distance found in compounds **10^B** (3.580(5) Å) and especially **11** (2.412(2) Å), which makes the latter more suitable for chemical cooperation.

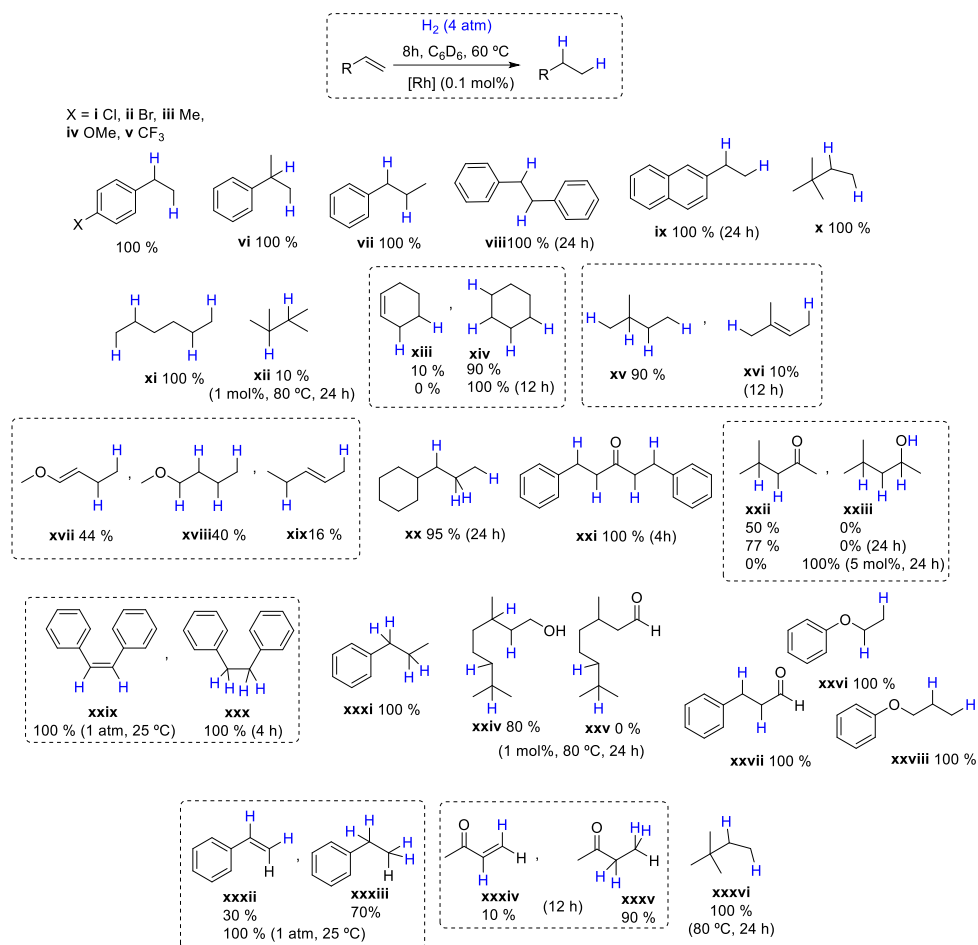
Further screening of catalytic conditions using compound **11** allowed us to reach turnover numbers (TON) of up to $2.5 \cdot 10^6$, associated to turnover frequencies (TOF) of around $1.25 \cdot 10^5 \text{ h}^{-1}$, when performing the catalysis in the absence of solvent (Table 2). Besides, poisoning experiments with mercury and carbon disulfide pointed out to the homogeneous nature of the active species.

Table 2. Results of catalytic conditions optimization for styrene hydrogenation with complex **11**.

									
Entry	Rh (mol%)	H ₂ (atm)	T (°C)	t (h)	Solvent	Additive	Yield (%)	TON	TOF (h ⁻¹)
1	1	0.5	25	3	Benzene	-	100	100	33
2	0.1	1	25	41	Benzene	-	100	1,000	24

3	0.1	1	25	16	Benzene	-	40	400	25
4	0.1	4	25	3	Benzene	-	100	1,000	333
5	0.01	1	25	70	Benzene	-	70	7,000	100
6	0.01	4	40	8	-	-	100	10,000	1,250
7	0.01	4	40	8	-	Hg	100	10,000	1,250
8	0.01	4	40	8	-	CS ₂	0	0	0
9	0.01	4	40	8	-	CS ₂ (10 %)	90	9,000	1,125
10	0.001	4	60	12	-	-	100	100,000	8,333
11	1 ppm	4	60	17	-	-	100	1,000,000	58,823
12	0.1 ppm	4	60	20	-	-	25	2,500,000	125,000

We also performed some preliminary investigations on substrate scope demonstrating that compound **11** is active for the hydrogenation of a variety of unsaturated species (Scheme 5). Styrene derivatives with electron donating and electron withdrawing groups were successfully hydrogenated. Internal olefins could be hydrogenated as well, though longer reaction times were required in some cases. The more hindered tetra-substituted 2,3-dimethylbutene olefin was only hydrogenated in 10 mol% yield even under slightly more forcing conditions (1 mol% **11**, 80 °C, 24 h). Several selected dienes, allenes and vinyl ethers were partially or totally hydrogenated, with specific selectivity in terms of overreduction being controlled by tuning experimental conditions. The regioselectivity was also analyzed for α,β -unsaturated compounds, which were primarily hydrogenated at the C=C position, though more forcing conditions allowed to reduce the carbonylic function as well. Once more, the addition of one or two molecules of dihydrogen in terminal and internal alkynes could be controlled by tuning the experimental conditions.



Scheme 5. Scope of hydrogenation reactions catalyzed by complex **11**.

Experimentally, the hydrogenation reactions described in Scheme 5 were carried out, depending on the H₂ pressure, in an ampoule (1 atm) or in a high-pressure vessel (4 atm). When the amount of catalyst is suitable to be weighed complex **1a** and **HB(C₆F₅)₂** were placed in the corresponding set-up, dissolved in benzene to form complex **11** and the olefin added. In cases where the amount of catalyst precursors is too small a stock solution in benzene is previously prepared and used for several catalytic runs. In all cases, the reaction solution was freeze-pumped to remove the nitrogen gas, filled with the corresponding H₂ pressure and heated if necessary. After the reaction was completed, the conversion was checked by ¹H NMR analysis. All hydrogenated compounds were identified through ¹H

NMR spectroscopy and by comparison with pure samples of those species obtained from commercial sources, except for compound **v**, whose spectroscopic data were compared to prior literature¹⁹.

IV.5. Mechanistic investigations

Aside from its direct use in catalysis, we decided to rather focus on shedding some light into the mechanism by which compound **11** hydrogenates unsaturated molecules in order to devise future and more challenging applications. To investigate the mechanism of the hydrogenation reaction, we initially carried out some kinetic studies. We first performed several exploratory experiments on our model hydrogenation of styrene under pseudo-first order conditions to measure the orders on catalyst, hydrogen and styrene. The initial exploration consisted in dissolving complex **11** (0.0002 mmol) and styrene (0.004 mmol) in C₆D₆ (0.2 mL) in a high-pressure NMR tube. The tube was freeze-pumped to remove the nitrogen gas and then filled with 6 bar of H₂ pressure. The reaction was monitored by ¹H NMR spectroscopy at different times. Figure 9 shows all the proton NMR spectra collected in which the regions that have been integrated and compared are indicated. Notice the appearance and the disappearance of a set of resonances, corresponding to styrene and the corresponding ethylbenzene.

¹⁹a) CSID:4482215, <http://www.chemspider.com/ChemicalStructure.4482215.html>.
b) <https://spectrabase.com/compound/KKKkq1TeEDX>.

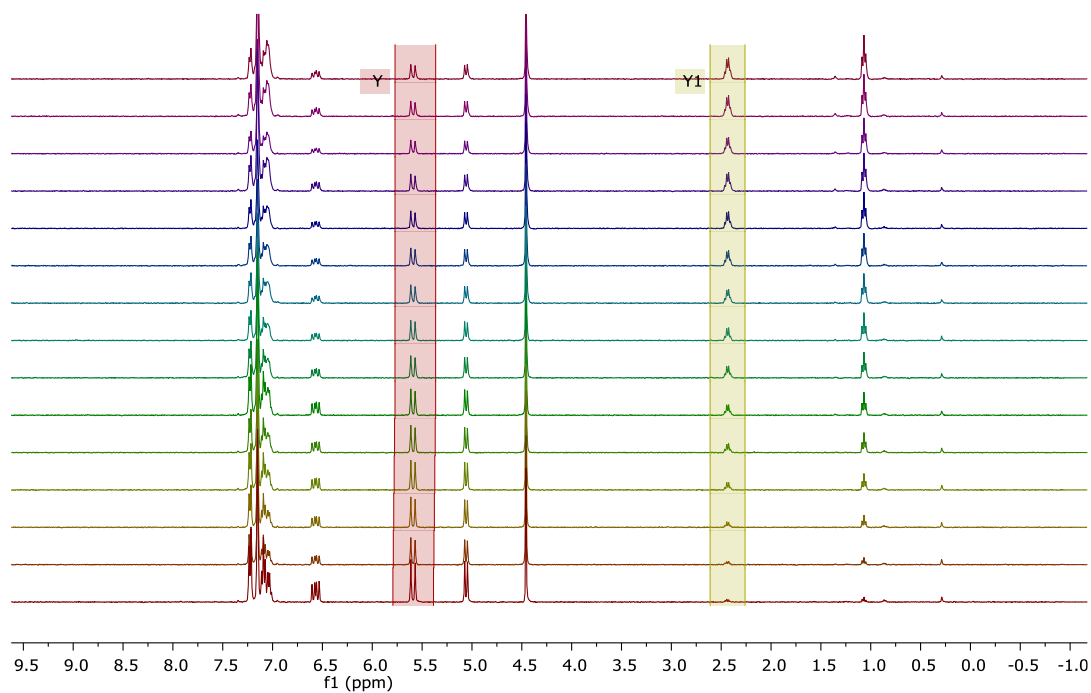


Figure 9. ^1H NMR monitoring of the catalytic hydrogenation of styrene by complex **11** (the proton signals of styrene are marked in red and the proton signals of the hydrogenated product are marked in yellow). Each spectrum is obtained with 4 min delay during 1 hour, the first spectrum being already delayed by 4 min.

A graphical representation of the variation of the styrene concentration with time (Figure 10) clearly indicates a zero-order dependence on the concentration of styrene, while pseudo-first order dependences were measured for catalyst and dihydrogen (Figures 11 and 12) after carrying out the same experiments at different H_2 pressures and catalyst loadings.

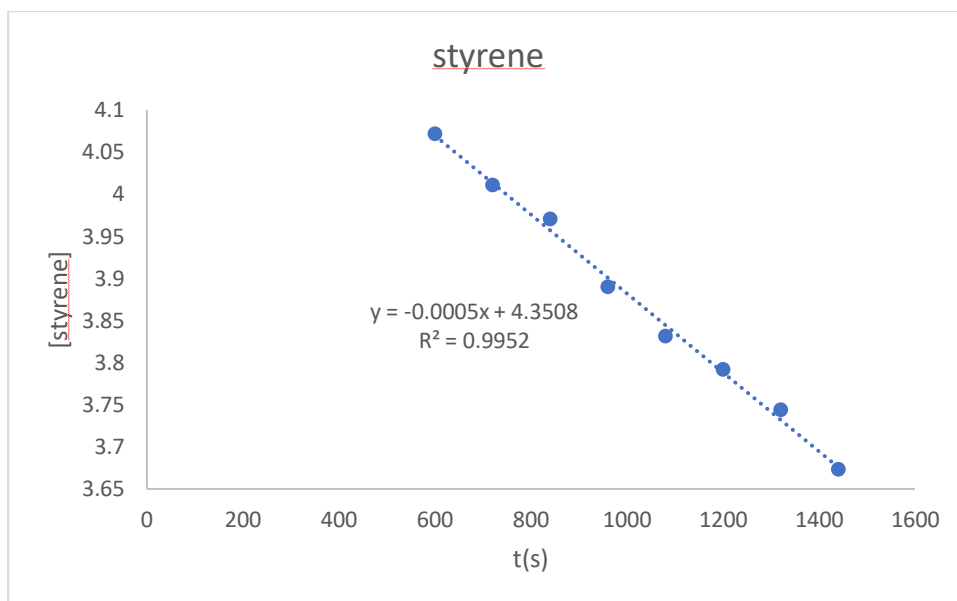


Figure 10. Plot of styrene concentration vs. time.

Conditions: 0.0087 mg of **11**, 6 bar H₂, 25°C, 0.2 mL C₆D₆.

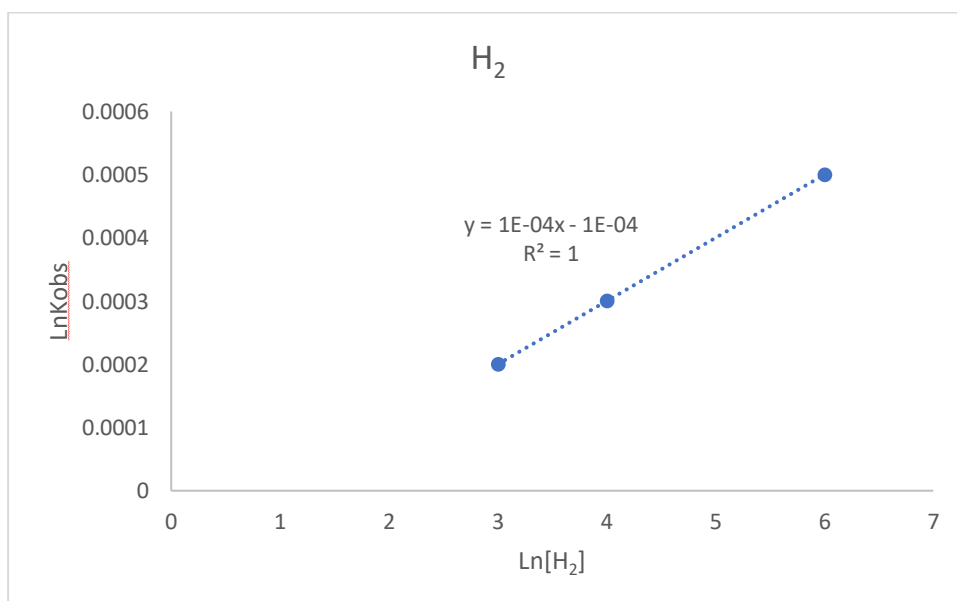


Figure 11. Plot of ln K_{obs} vs. ln[H₂] revealing pseudo first-order on H₂.

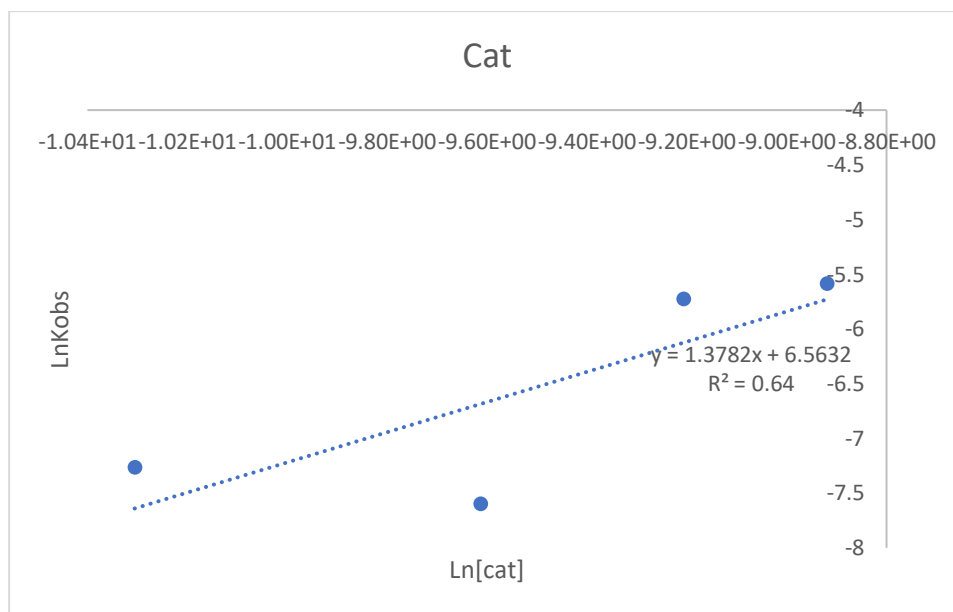
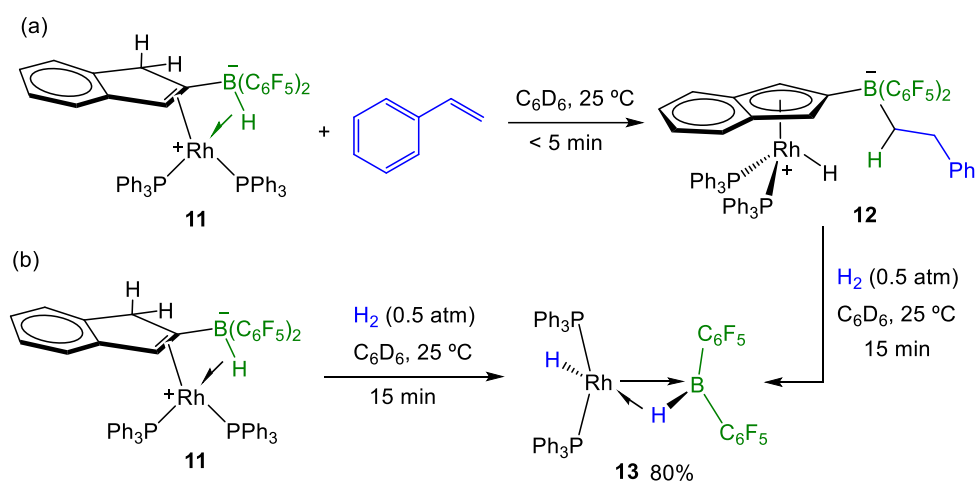


Figure 12. Plot of $\ln K_{obs}$ vs. $\ln[\text{cat}]$ revealing pseudo first-order on catalyst.

With the aim to look deeper into the mechanism, stoichiometric reactions were also performed. Thus, the addition of one equivalent of styrene to a freshly prepared C_6D_6 solution of **11** resulted in the immediate full conversion into a new species **12** (Scheme 6). Its formation is accompanied by a simplification of the corresponding $^{31}\text{P}\{^1\text{H}\}$ NMR spectrum from two resonances at 42.2 (dd, $^3J_{\text{PP}} = 42$, $^1J_{\text{PRh}} = 179$ Hz) and 38.1 (dd, $^3J_{\text{PP}} = 42$, $^1J_{\text{PRh}} = 183$ Hz) due to **11** to a single signal at 36.5 (d, $^1J_{\text{PRh}} = 145$ Hz) ppm in **12**.



Scheme 6. Stoichiometric reactivity of compound **11** towards styrene (a) and dihydrogen (b).

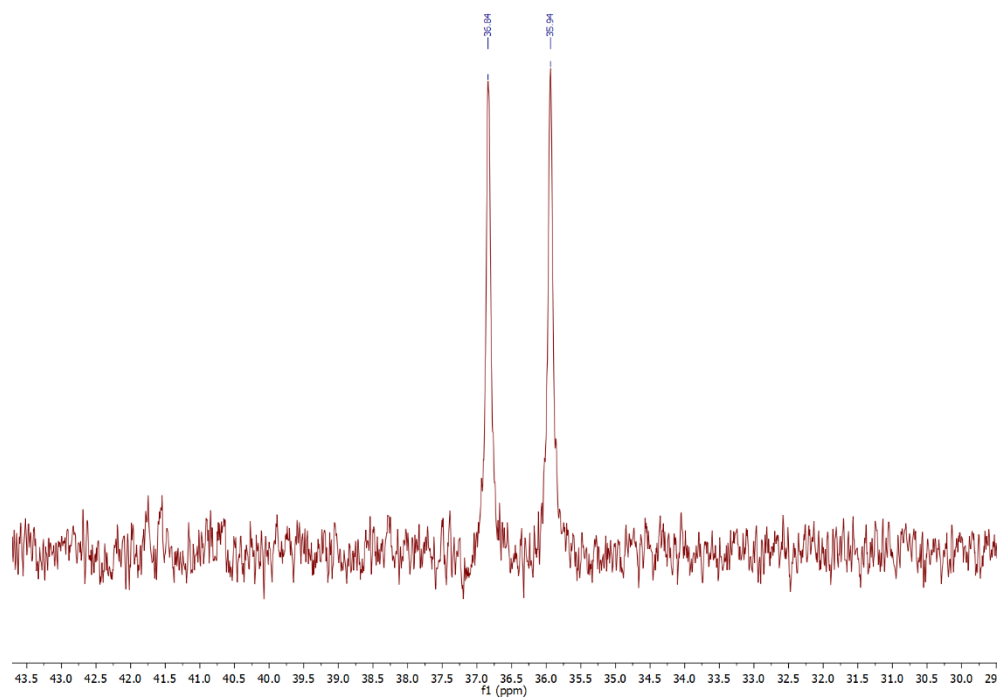


Figure 13. $^{31}\text{P}\{^1\text{H}\}$ NMR of complex **12** (C_6D_6 , 25 °C).

The higher symmetry of the latter species is further certified by the simpler ^1H NMR pattern exhibited by the indenyl ligand (δ 6.96, 6.37 and

5.21 due to two protons each), which has recovered its aromaticity and η^5 -coordination. In accordance, a low-frequency signal is now apparent at -13.70 ppm due to a Rh–H ligand, which along with the absence of additional signals due to B–H units, suggests the olefin to be inserted into the B–H bond. This occurs with concomitant return of a proton from the C1 position of the indenyl moiety to rhodium, demonstrating the reversible nature of the proton migrations between the metal, the indenyl ring and the borane function. Figure 14 depicts the X-ray diffraction structure of **12**, which corroborates our NMR-based formulation. The structure is analogous to that of **9^{HB}** according to all geometric parameters, though in this case the absence of a stabilizing B–H unit seems to prevent the migration of the rhodium hydride towards the indenyl ring which would otherwise result in a highly unsaturated metal site.

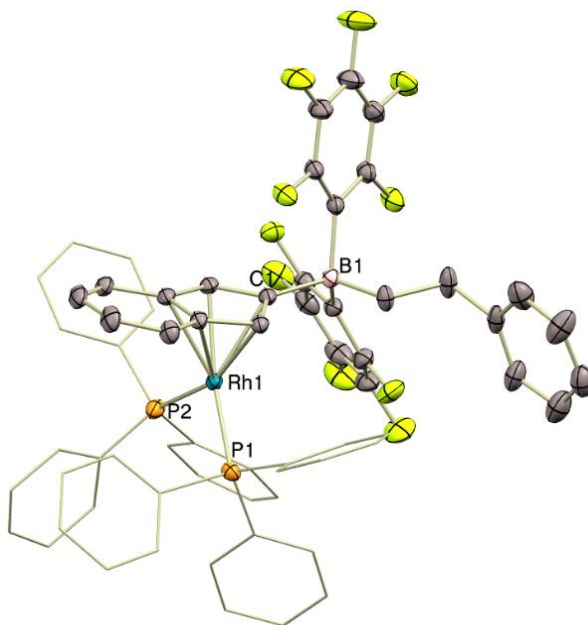


Figure 14. ORTEP diagram of compound **12**. The rhodium-hydride ligand has not been located in the Fourier electron density map and is not represented. Selected bond distances (Å) and angles(°): Compound **12** Rh1–P1, 2.3318 (5);

Rh1–P2, 2.3337(5); Rh1–C1, 2.2720(19); C1–B1, 1.639(3); C58–B1, 1.635(3); P1–Rh1–P2, 102.31(2); P1–Rh1–C1, 128.14(5); P2–Rh1–C1, 126.07(5); B1–C1–Rh1, 130.01(12); C58–B1–C1, 169.86(16).

In agreement with a first-order dependence on the concentration of dihydrogen, exposure of C₆D₆ solutions of **11** to H₂ atmosphere under catalytically relevant conditions did not provoke the immediate disappearance of the complex as occurred after styrene addition. In this case, working under moderately higher pressure (H₂ 6 bar, 25 °C) requires longer times (*ca.* 15 min) to produce a new species **13** in around 80% spectroscopic yield (Scheme 6), reaching complete conversion after several hours. The most distinctive feature of this compound is the presence of two low-frequency signals in the ¹H NMR spectrum at -1.23 and -16.33 ppm due to one proton each. Decoupling from either ¹¹B or ³¹P causes the respective aforesaid resonances to clearly sharpen (Figure 15), suggesting that the lower-field resonance is directly coupled to the boron centre as a B–H unit, while the higher-field signal is more influenced by the phosphine ligands.

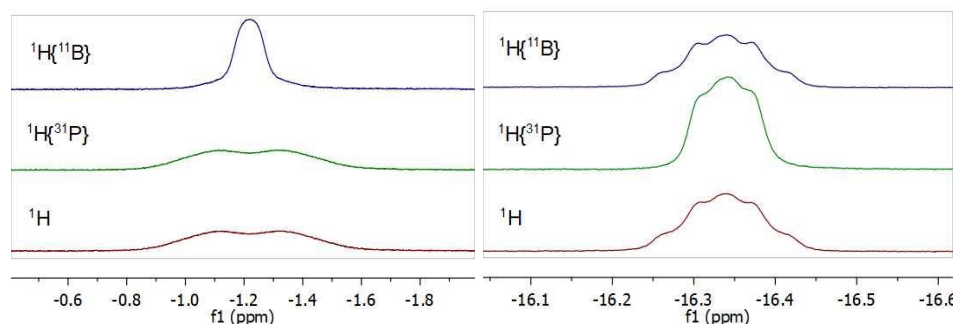


Figure 15. Superimposed zoom of the low-frequency ¹H NMR region of normal spectrum vs its decoupled ¹H{¹¹B} and ¹H{³¹P} NMR spectra of complex **13**.

The chemical shift of the BH unit along with the geometrical parameters commented below are indicative of a σ -borane complex, as later

discussed in the context of computational studies. Besides, it has been recognized that the separation between *meta* and *para* fluorine atoms ($\Delta_{m,p}$) of perfluorinated boranes is indicative of the coordination mode of the borane²⁰. For compound **13**, $\Delta_{m,p}$ equals 3.3 (δ_F -164.1 (F_m), -160,8 (F_p)), a slightly higher value than in compounds **10^{HB}** ($\Delta_{m,p} = 2.5$) and **12** ($\Delta_{m,p} = 2.8$), in agreement with a less anionic character of the boron atom. However, this value is mildly lower than for **11** ($\Delta_{m,p} = 4.6$), as expected for a stronger coordination of the boron centre to the metal in complex **13**. In solution, compound **13** exhibits dynamic behavior that accounts for the exchange of the B–H hydride with free dihydrogen and, at a lower rate, the intramolecular exchange between the two hydrides. Both processes were investigated by 2D-EXSY experiments and the details are discussed in the next section.

The molecular structure of **13** was also corroborated by X-ray diffraction studies (Figure 16), revealing the absence of the indenyl ligand, as deduced from NMR analysis, and the formation of a highly unsaturated σ -borane complex of rhodium. The departure of the indenyl ligand has facilitated the rearrangement of the phosphines ligands, which are now located in a *trans* disposition defined by a P–Rh–P angle of 156.58(5)°. The two hydride ligands could not be located in the Fourier electron density map, but the lowest-energy configuration found by DFT, which matches well the experimental geometry, suggests that they are also located *trans* to each other (Figure 17).

²⁰ T. Beringhelli, D. Donghi, D. Maggioni, G. D'Alfonso, *Coord. Chem. Rev.*, **2008**, 252, 2292-2313.

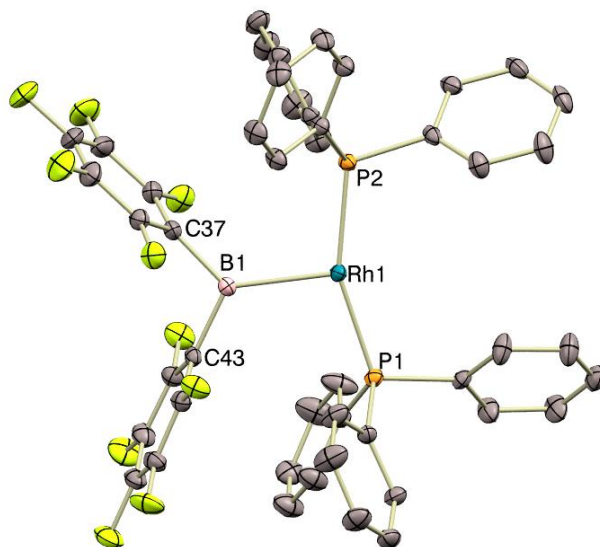


Figure 16. ORTEP diagram of compound **13**. The boron and rhodium-hydride ligand has not been located in the Fourier electron density map and is not represented. Selected bond distances (Å) and angles(°): Compound **13** Rh1–P1, 2.3069(11); Rh1–P2, 2.3049(11); Rh1–B1, 2.315(5); C37–B1, 1.622(6); C43–B1, 1.623(6); P1–Rh1–P2, 156.59(4); P1–Rh1–B1, 101.06(12); P2–Rh1–B1, 102.08(12); C37–B1–Rh1, 126.4(3); C43–B1–Rh1, 123.1(3); C37–B1–C43, 110.6(3).

The B–Rh distance is considerably shorter than in **11**, with a value of 2.316(5) Å. The geometry around the boron center (not accounting its hydride) is perfectly planar, as evinced by the sum of its three angles with Rh, C37 and C43 that accounts for an ideal 360.01°.

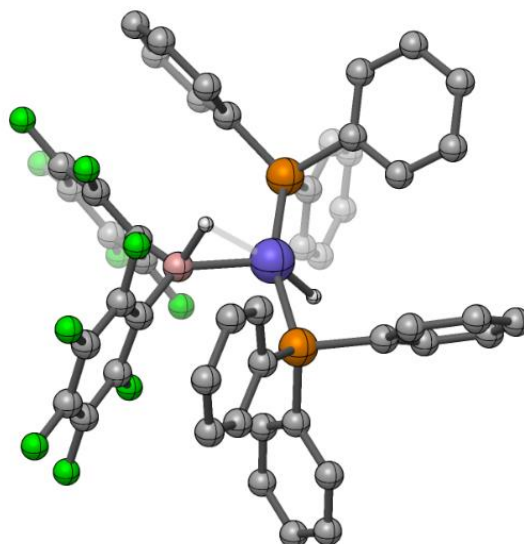


Figure 17. DFT-optimized structure of complex **13**.

We tested the catalytic competence of compounds **12** and **13** compared to precursor **11**, though the high instability of these species precluded a fully precise evaluation. In fact, while compound **12** could be isolated in acceptable purity and tested as a catalyst, the isolation of **13** in pure form escaped from our efforts. As such, we generated compound **13** *in situ* under hydrogen atmosphere and then added to the resulting solution styrene and fresh H₂ gas to monitor the catalytic reduction of the olefin by ¹H NMR. The resulting kinetic profile for the three catalysts was comparatively similar, however, while compounds **11** and **12** exhibited an apparent induction period of several minutes, that lapse was absent for the freshly prepared solution of **13**. Besides, hydrogenation of compound **12** leads to the formation of **13** as the major species. Altogether, these findings indicate that compound **13** might be the active species, while **12** would constitute an intermediate during catalyst activation. In any case, it is rather

clear that catalyst **11** containing the borane functionality, in whatever final form, is remarkably more efficient than its borane-free precursor **6d**. Thus, while **11** reduces styrene with full conversion even at catalyst loadings as low as 1ppm, the parent complex **6d** only produces around 4% of ethylbenzene under otherwise identical conditions, demonstrating the positive role of introducing the borane function.

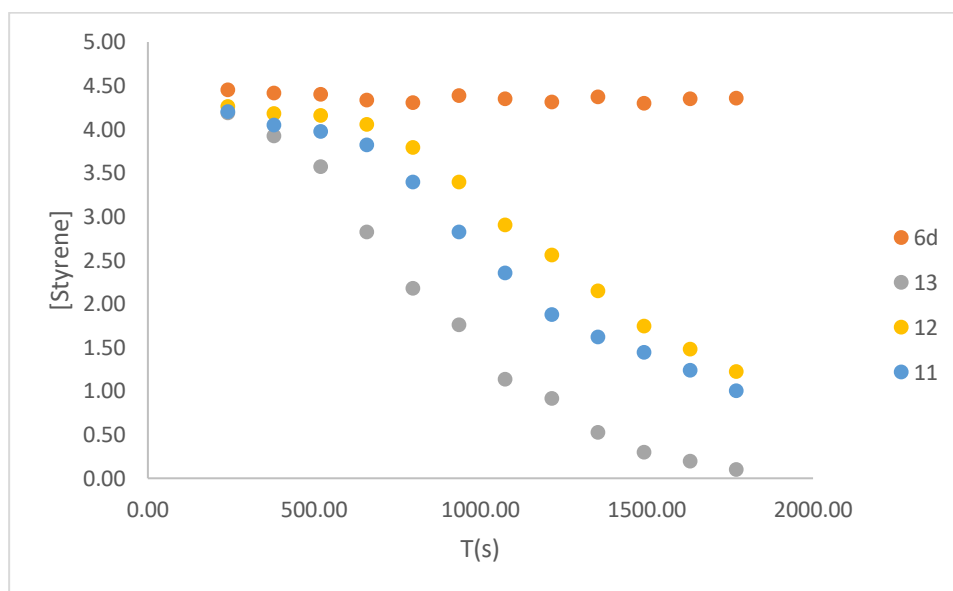


Figure 18. Comparison kinetic profile between complexes **6d**, **11**, **12** and **13**.

IV.7. Exchange Spectroscopy (EXSY) experiments for complex 13.

As aforesaid, our two-dimensional NMR studies carried out for the characterization of **13** reveal the presence of two chemical exchange processes taking place in solution, more precisely the intramolecular exchange between the two hydrides and the intermolecular exchange between the Rh–H unit and free H₂ in solution. To investigate further these processes, we carried out 2D-exchange spectroscopy (EXSY) studies.

Experimentally, complex **11** (0.138 mmol) was dissolved in C₆D₆ (0.2 mL) in a high-pressure NMR tube. The tube was freeze-pumped to remove the nitrogen gas, then filled with 6 bar of H₂ pressure. The tube was left to stand for 12 hours to secure full disappearance of complex **13**, then monitored by NOESY (or EXSY) spectroscopy at different temperatures. The intramolecular exchange between hydrides was observed only at higher temperatures, while the exchange of the rhodium hydride with free H₂ was more facile. Figures 18 and 19 contain representative examples of 2D-EXSY experiments at a mixing time where there is exchange (0.3 s) and when there is no exchange (0.005 s) for the intramolecular process. Similarly, Figures 21 and 22 are representative examples of similar experiments associated to the intermolecular exchange with H₂.

These studies were done in the temperature interval between 50 and 65 ° for the intramolecular exchange and from 0 to 25 °C for the exchange with H₂. The visible higher facility of the later exchange is in agreement with our Eyring analyses, which rendered values of $\Delta S = 2.03 \pm 0.11$ cal/Kmol and $\Delta H = 18.83 \pm 0.79$ Kcal/mol, corresponding to ΔG_{298} of 18.23 ± 2.73 Kcal/mol. The intramolecular exchange is characterized by a higher ΔG_{298} of 28.24 ± 0.49 Kcal/mol, and associated ΔS and ΔH values of 3.04 ± 0.1 cal/Kmol and 29.12 ± 0.68 Kcal/mol, respectively.

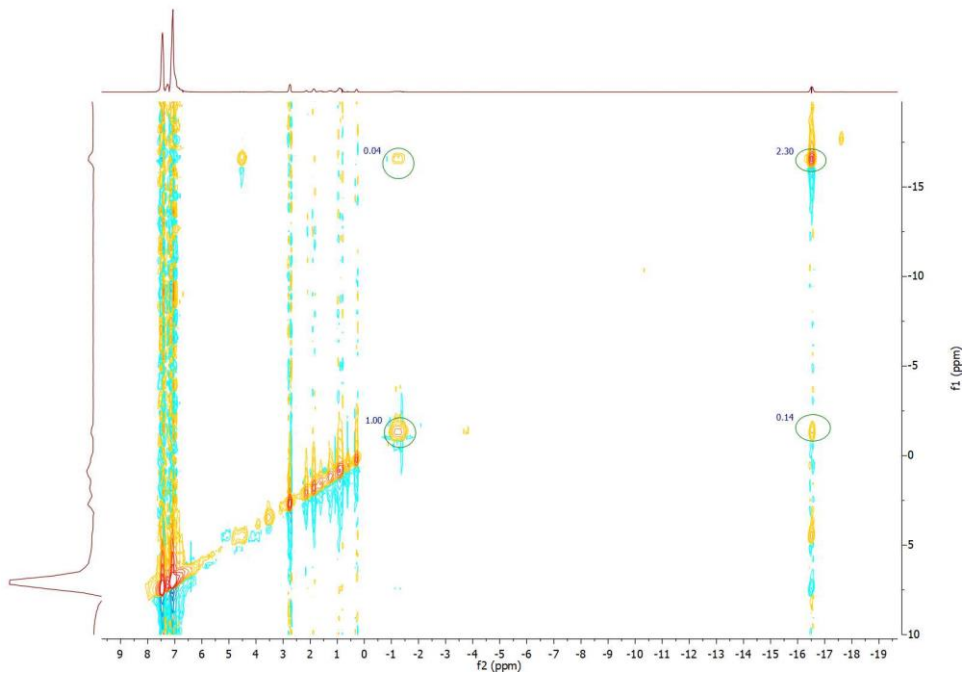


Figure 18. Example of NOESY experiment with mixing time of 0.3

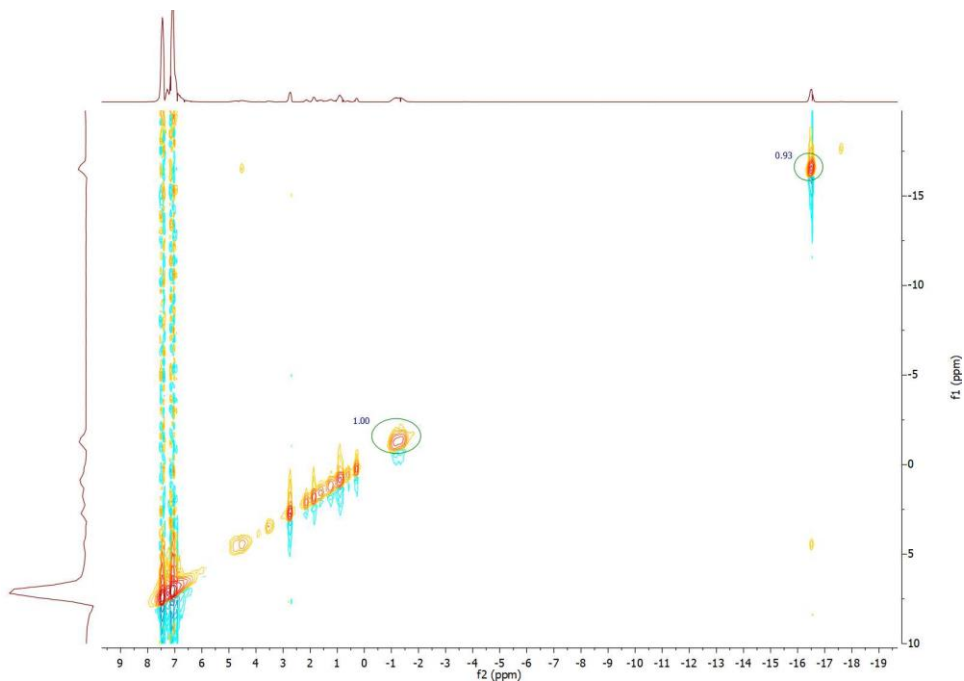


Figure 19. Example of NOESY experiment with mixing time of 0.005.

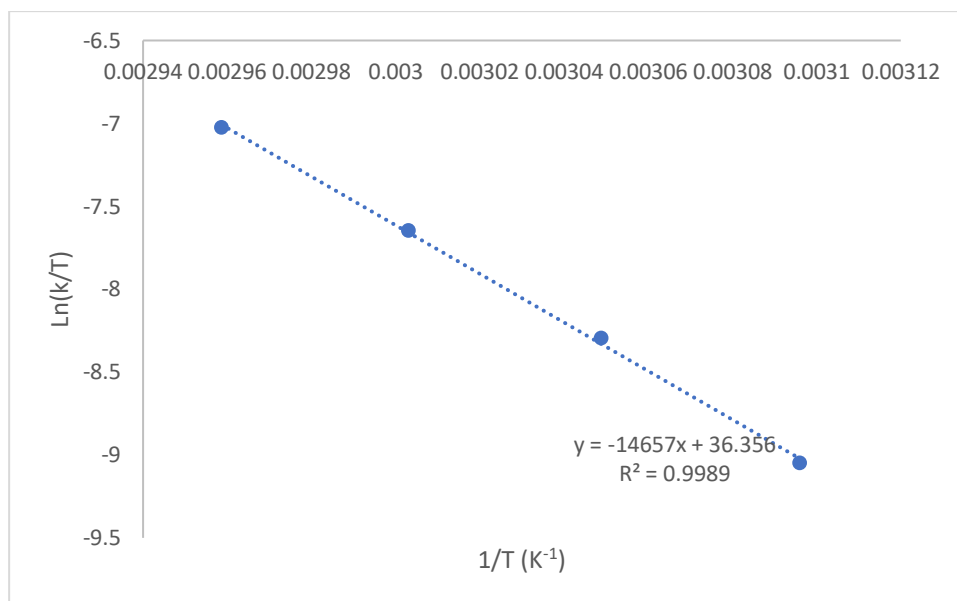


Figure 20. Eyring plot for the exchange of both hydride ligands in complex **11** from 65 to 50 °C.

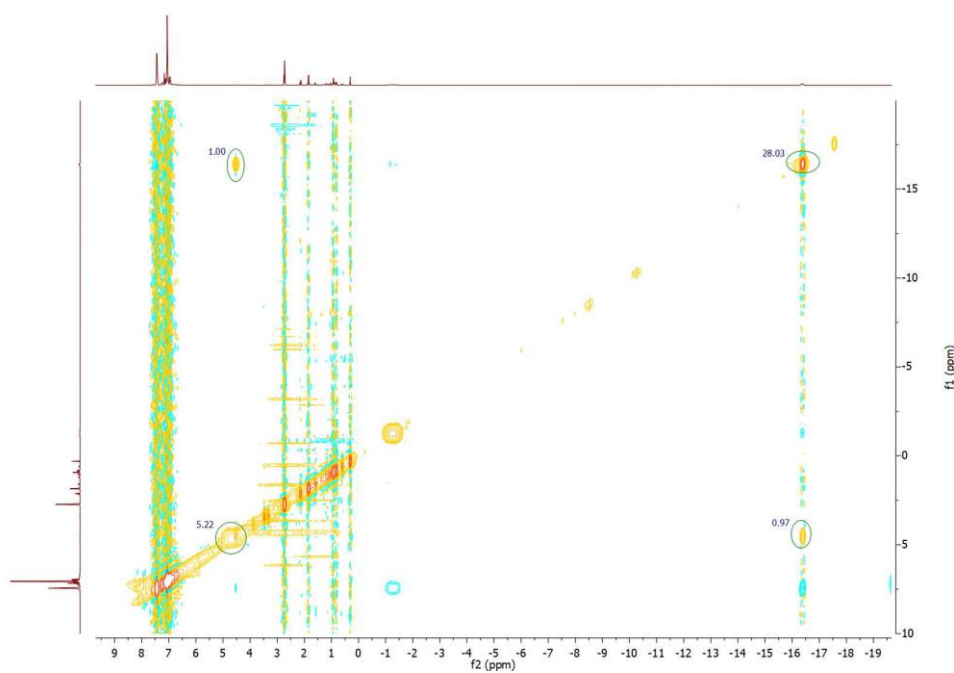


Figure 21. Example of NOESY experiment with mixing time of 0.3.

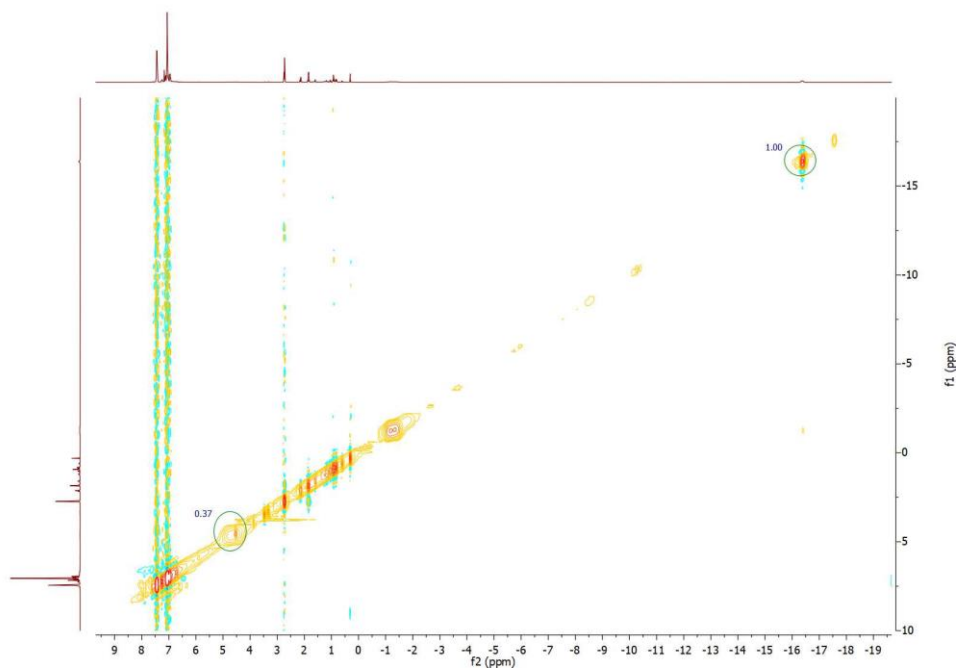


Figure 22. Example of NOESY experiment with mixing time of 0.005.

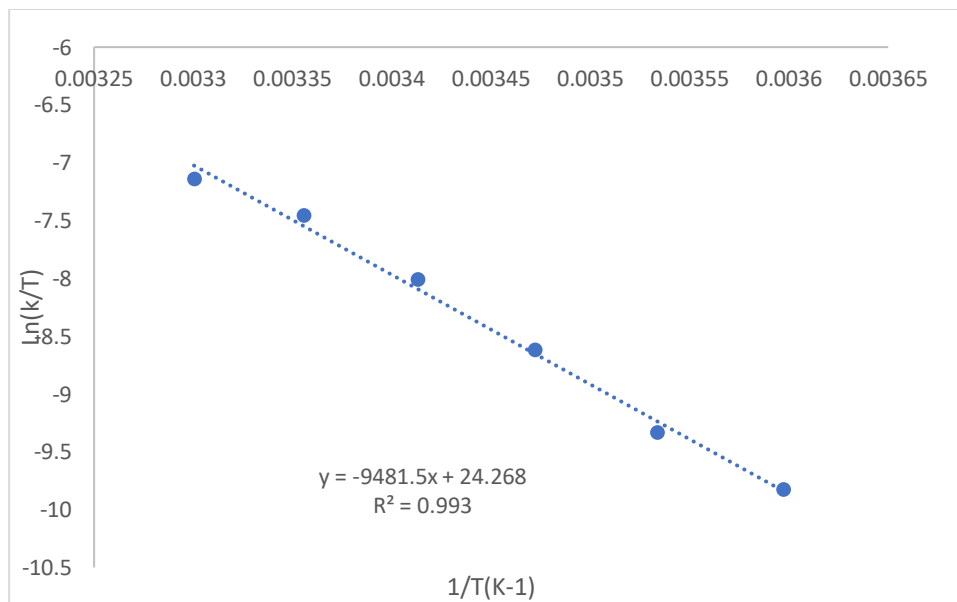


Figure 23. Eyring plot for the exchange of the terminal rhodium hydride in complex **11** and H₂ from 25 to 0 °C.

In summary, in this chapter we describe reactivity studies between compounds **1a** and **6d** with perfluorinated boranes $B(C_6F_5)_3$ and $HB(C_6F_5)_2$, demonstrating that the boron functionality readily incorporates into the aromatic ligand. The resulting complexes complement previous related systems, which are mostly based on highly acidic early transition metals. Moreover, they are genuine motifs to investigate metallic FLP-type cooperativity²¹ because of the contrasting Lewis basic and acidic nature of the Rh(I) and borane fragments, respectively. In this vein, we provide preliminary studies that evidence the potential of the boron functionality anchor to the indenyl system to enhance catalysis at the metal by using the hydrogenation of olefins as a model reaction. In particular, we have demonstrated that the catalytic system is effective for the hydrogenation of a broad variety of carbon-based unsaturated species with selectivity being controlled by tuning experimental conditions. Besides, we provide relevant mechanistic information from kinetic studies and stoichiometric experiments, revealing the direct participation of the indenyl ligand in a pre-activation step.

²¹ a) M. G. Alférez, N. Hidalgo, J. Campos, **2020**. Editors C. Sloatweg and A. Jupp. Springer.
b) M. Navarro, J. Campos, **2021**, *Chapter Three - Bimetallic frustrated Lewis pairs*, Editor(s): P. J. Pérez, *Advances in Organometallic Chemistry*, Academic Press, 75, 95-148.
c) M. Navarro, J. J. Moreno, M. Pérez-Jiménez, J. Campos, *Chem. Commun.*, **2022**, 58, 11220-11235.

IV.9. Experimental procedures

IV.9.1. General considerations

General considerations

All preparations and manipulations were carried out using standard Schlenk and glove-box techniques, under argon or high-purity nitrogen atmosphere, respectively. All solvents were dried, stored over 4 Å molecular sieves, and degassed prior to use. Toluene (C₇H₈) and *n*-pentane (C₅H₁₂) were distilled under nitrogen over sodium. Benzene-*d*₆ and toluene-*d*₈ were dried over molecular sieves (4 Å). THF-*d*₈ was distilled under nitrogen over sodium/benzophenone. Rhodium complex **1** and **2** were prepared according to previously reported procedures. B(C₆F₅)₃ was sublimated and Pier's Borane (HB(C₆F₅)₂) was synthesized by modification of the synthetic procedure for previously reported. Other chemicals were commercially available and used as received. Solution NMR spectra were recorded on Bruker AMX-300, DRX-400 and DRX-500 spectrometers. Spectra were referenced to external SiMe₄ (δ: 0 ppm) using the residual proton solvent peaks as internal standards (¹H NMR experiments), or the characteristic resonances of the solvent nuclei (¹³C{¹H} NMR experiments), while ³¹P was referenced to H₃PO₄. ¹⁹F is referenced to fluorotrichloromethane, and ¹¹B is referenced to BF₃·OEt₂. Spectral assignments were made by routine one- and two-dimensional NMR experiments where appropriate. For elemental analyses a LECO TruSpec CHN elementary analyzer was utilized.

IV.9.2. Crystallographic details.

Crystals of compounds were grown by slow diffusion of pentane into their benzene or toluene solutions, respectively. Low-temperature diffraction data were collected on a D8 Quest APEX-III single crystal diffractometer with a Photon III detector and a IμS 3.0 microfocus X-ray source (**9^B**, **9^{HB}**, **10^B**, **10^{HB}**, **11**, **12** and **13**) at the Instituto de Investigaciones

Químicas, Sevilla. Data were collected by means of ω and φ scans using monochromatic radiation $\lambda(\text{Mo K}\alpha 1) = 0.71073 \text{ \AA}$. The diffraction images collected were processed and scaled using APEX-III software. Using Olex2²², the structures **9^B** was solved with SHELXS (direct methods) and the structure **9^{HB}**, **10^B**, **10^{HB}**, **11**, **12** and **13** were solved with olex2.solve1.3 and all was refined against F^2 on all data by full-matrix least squares with SHELXL²³. All non-hydrogen atoms were refined anisotropically. Hydrogen atoms were included in the model at geometrically calculated positions and refined using a riding model, except the hydrides bonded to metal centres which have been identified on the Fourier map. The isotropic displacement parameters of all hydrogen atoms were fixed to 1.2 times the U value of the atoms to which they are linked (1.5 times for methyl groups).

In two (**12** and **13**) of these reported structures we used the program SQUEEZE to compensate for the contribution of disordered solvents.

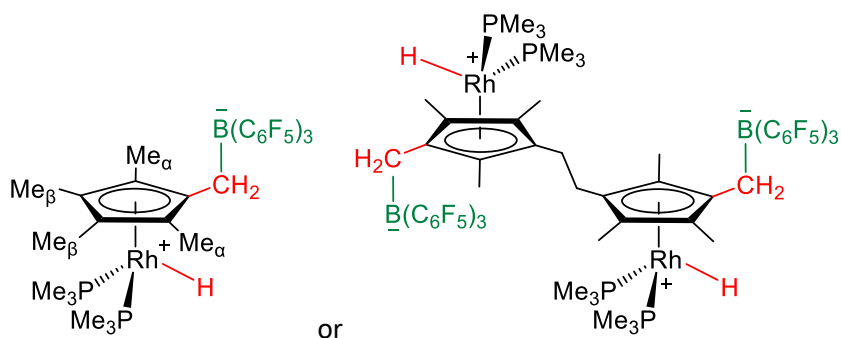
²² a) L. J. Bourhis, O. V. Dolomanov, R. J. Gildea, J. A. K. Howard, H. Puschmann, *Acta Cryst.*, **2015**, *A71*, 59-75.

b) O. V. Dolomanov, L. J. Bourhis, R. J. Gildea, J. A. K. Howard, H. Puschmann, *J. Appl. Cryst.*, **2009**, *42*, 339-341.

c) G. M. Sheldrick, *Acta Cryst.*, **2015**, *C71*, 3-8.

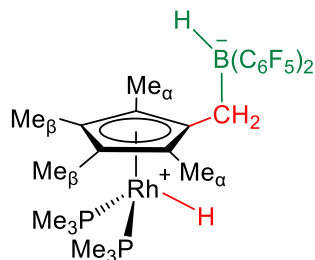
²³ G. M. Sheldrick, *Acta Cryst.* **2008**, *A64*, 112.

IV.9.3. Synthesis and characterization of new compounds



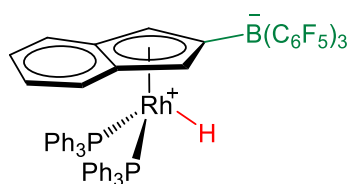
Compound 9^B and 9^{B*}. In a J. Young NMR tube a solid mixture of compound **1a** (30 mg, 0.077 mmol) and B(C₆F₅)₃ (40 mg, 0.079 mmol) was dissolved in toluene or benzene or THF (0.5 mL) at room temperature. Reaction monitoring revealed the formation of **9^B** and **9^{B*}** was immediate and proceeded quantitatively by NMR spectroscopy. Brown crystals were grown by slow diffusion of pentane into a benzene solution within the glove box. Anal. Calcd. for C₃₄H₃₃BF₁₅P₂Rh: C, 45.2; H, 3.7. Found: C, 45.1; H, 4.0.

¹H NMR (500 MHz, THF-*d*₈, 25 °C) δ: 1.91 (s, 6H, Me_α), 1.87 (s, 6H, Me_β), 1.33 (br, 6H, PMe₃), 1.17 (d, 2H, ²J_{HH} = 20.5 Hz, CH₂B), -13.65 (m, 1H, RhH). ¹¹B{¹H} NMR (128 MHz, C₆D₆, 25 °C) δ: -24.9 (brs). ¹³C{¹H} NMR (125 MHz, THF-*d*₈, 25 °C) δ: 25.44 (C₅Me₅), 15.5 (CH₂), 10.2 - 9.6 (m, overlapping PMe₃ C₅Me₅). ¹⁹F{¹H} NMR (471MHz, C₆D₆, 25 °C) δ: -167.0 (m, *m*-C₆F₅), -164.0 (m, *p*-C₆F₅), -132.3 (m, *o*-C₆F₅). ³¹P{¹H} NMR (162 MHz, THF-*d*₈, 25 °C) δ: -2.7 (dd, ¹J_{PRh} = 139, ³J_{PP} = 9 Hz).



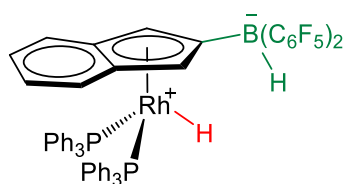
Compound 9^{HB}. In a J. Young NMR tube a solid mixture of compound **1a** (30 mg, 0.077 mmol) and HB(C₆F₅)₂ (30 mg, 0.086 mmol) was dissolved in toluene, benzene or THF (0.5 mL) at room temperature. Reaction monitoring revealed the formation of **9^{HB}** was immediate and proceeded quantitatively by NMR spectroscopy. Brown crystals were grown by slow diffusion of pentane into a benzene solution of **9^{HB}** in the freeze to the glove box. Anal. Calcd. for C₂₈H₃₄BF₁₀P₂Rh: C, 45.7; H, 4.7. Found: C, 45.5; H, 4.6.

¹H NMR (500 MHz, C₆D₆, 25 °C) δ: 1.55 (s, 6H, Me_α), 1.42 (s, 6H, Me_β), 0.72 (vt, 18H, PMe₃), 0.47 (d, 2H, ²J_{HH} = 12.9 Hz, CH₂B), -13.51 (td, 1H, ²J_{HP} = 39, ¹J_{HRh} = 23 Hz, RhH). ¹¹B{¹H} NMR (128 MHz, C₆D₆, 25 °C) δ: -21.2 (br). ¹³C{¹H} NMR (125 MHz, THF-*d*₈, 25 °C) δ: 95.4 (C₅Me₅), 18.7 (PMe₃), 10.5 (C₅Me₅). ¹⁹F{¹H} NMR (471MHz, C₆D₆, 25 °C) δ: -168.2 (m, *p*-C₆F₅), -166.2 (m, *p*-C₆F₅), -133.2 (m, *o*-C₆F₅) ppm. ³¹P{¹H} NMR (162 MHz, C₆D₆, 25 °C) δ: -2.66 (d, ¹J_{PRh} = 138 Hz).



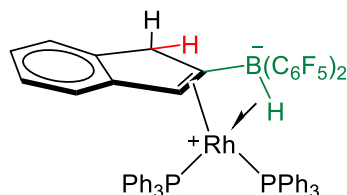
Compound 10^B. In a J. Young NMR tube a solid mixture of compound **6d** (42 mg, 0.059 mmol) and B(C₆F₅)₃ (30 mg, 0.059 mmol) was dissolved in toluene or benzene (0.5 mL) at room temperature. Reaction monitoring revealed the formation of **10^B** was immediate and proceeded quantitatively by NMR spectroscopy. Red crystals were grown by slow diffusion of pentane into a benzene solution of **10^B** in the glove box. Anal. Calcd. for C₆₃H₃₇BF₁₅P₂Rh: C, 60.3; H, 3.0. Found: C, 60.5; H, 3.1.

¹H NMR (400 MHz, toluene-*d*₈, -10 °C) δ: 6.98 (m, 4H, *o*-Ph₃), 6.82 (m, 8H, *o*-Ph₃), 6.75 (m, 20H, overlapping *p*-Ph₃, *m*-Ph₃, Ind), 6.05 (m, 2H, Ind), 5.35 (m, 2H, Ind), -13.08 (q, 1H, ²J_{HP} = 20.9 Hz, ¹J_{HRh} = 22.9 Hz, RhH). ¹¹B{¹H} NMR (128 MHz, toluene-*d*₈, -10 °C) δ: -14.5. ¹³C{¹H} NMR (125 MHz, toluene-*d*₈, -10 °C) δ: 133.3 (*m*-Ph₃), 132.80 (*p*-Ph₃), 130.1 (*o*-Ph₃), 127.7 (overlapping toluene signal, Ind), 122.0 (Ind), 117.5 (Ind), 88.7 (Ind). ¹⁹F{¹H} NMR (471MHz, toluene-*d*₈, -10 °C) δ: -164.1 (brt, *m*-C₆F₅), -160.7 (t, ³J_{FF}=21Hz, *p*- C₆F₅), -126.3 (brs, *o*- C₆F₅). ³¹P{¹H} NMR (162 MHz, toluene-*d*₈, -10 °C) δ: 37.8 (d, ¹J_{PRh} = 144 Hz).



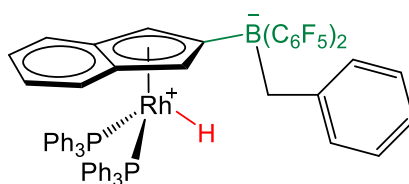
Compound 10^{HB}. In a J. Young NMR tube a solid mixture of compound **6d** (30 mg, 0.042 mmol) and HB(C₆F₅)₂ (20 mg, 0.057 mmol) was dissolved in toluene (0.5 mL) at -20 °C. Reaction monitoring at low temperature (-20 °C) revealed the formation of **10^{HB}** was immediate and proceeded quantitatively by NMR spectroscopy. Yellow crystals were grown by diffusion of pentane into a toluene solution in the glovebox freezer without allowing the reaction mixture to surpass the temperature of -10 °C during all reaction handling.

¹H NMR (400 MHz, toluene-*d*₈, -10 °C) δ: 6.90 (m, 30H, overlapping Ph₃), 6.81 (m, 2H, Ind), 5.73 (m, 2H, Ind), 5.27 (m, 2H, Ind), 4.70 (m, 1H, BH), -13.72 (q, 1H, ²J_{HP} = 23.9, ¹J_{HRh} = 23.9 Hz, RhH). ¹¹B{¹H} NMR (128 MHz, toluene-*d*₈, -10 °C) δ: -22.1 (brs). ¹³C{¹H} NMR (125 MHz, toluene-*d*₈, -10 °C) δ: 134.0 (PPh₃), 133.3 (PPh₃), 129.9 (PPh₃), 127.1 (Ind), 121.5 (Ind), 119.1 (Ind) 87.5(Ind). ¹⁹F{¹H} NMR (471MHz, toluene-*d*₈, -10 °C) δ: -165.1 (m, *m*-C₆F₅), -162.6 (t, ³J_{FF}=21Hz, *p*-C₆F₅), -130.5 (m, *o*-C₆F₅). ³¹P{¹H} NMR (162 MHz, toluene-*d*₈, -10 °C) δ: 41.2 (d, ¹J_{PRh} = 145 Hz).



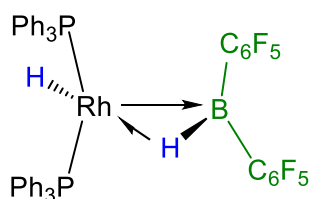
Compound 11. In a J. Young NMR tube a solid mixture of compound **6d** (30 mg, 0.042 mmol) and $\text{HB}(\text{C}_6\text{F}_5)_2$ (20 mg, 0.057 mmol) was dissolved in toluene or benzene (0.5 mL) at room temperature. Reaction monitoring revealed the formation of **11** was completed evolved in 5 minute and proceeded quantitatively by NMR spectroscopy. Orange crystals were grown by slow diffusion of pentane into a toluene solution of **11** in the glovebox freezer. Anal. Calcd. for $\text{C}_{57}\text{H}_{37}\text{BF}_{10}\text{P}_2\text{Rh}$: C, 63.0; H, 3.4. Found: C, 63.0; H, 3.2.

^1H NMR (500 MHz, toluene- d_8 , $-10\text{ }^\circ\text{C}$) δ : 7.63 (m, 6H, *o*-Ph₃), 7.13 (m, 6H, *o*-Ph₃), 6.82 (m, 12H, *m*-Ph₃), 6.70 (m, 7H, overlapping *p*-Ph₃, Ind), 6.54 (m, 1H, Ind), 6.03 (m, 1H, Ind), 5.73 (m, 1H, Ind), 3.78 (m, 2H, Ind), -7.21 (m, 1H, HB). $^{11}\text{B}\{^1\text{H}\}$ NMR (128 MHz, toluene- d_8 , $-10\text{ }^\circ\text{C}$) δ : -17.7 - -22.0 (brs). $^{13}\text{C}\{^1\text{H}\}$ NMR (125 MHz, toluene- d_8 , $-10\text{ }^\circ\text{C}$) δ : 133.8 (m, *m*-Ph₃), 127.1 (overlapping toluene *m*-Ph₃, *o*-Ph₃, *p*-Ph₃ and Ind), 124.3 (Ind), 122.7 (Ind) 106.7 (Ind), 44.2 (Ind). $^{19}\text{F}\{^1\text{H}\}$ NMR (471MHz, toluene- d_8 , $-10\text{ }^\circ\text{C}$) δ : -164.2 (m, *m*-C₆F₅), -159.6 (m, *p*-C₆F₅), -129.8 (m, *o*-C₆F₅), -128.1 (d, $^3J_{\text{FF}} = 22$ Hz, *o*-C₆F₅). $^{31}\text{P}\{^1\text{H}\}$ NMR (162 MHz, toluene- d_8 , $-10\text{ }^\circ\text{C}$) δ : 42.2 (dd, $^3J_{\text{PP}} = 42$, $^1J_{\text{PRh}} = 179$ Hz), 38.1 (dd, $^3J_{\text{PP}} = 42$, $^1J_{\text{PRh}} = 183$ Hz).



Compound 12. A solid mixture of compound **6d** (30 mg, 0.042 mmol) and $\text{HB}(\text{C}_6\text{F}_5)_2$ (20 mg, 0.057 mmol) was dissolved in toluene (2 mL), after which styrene was added (2 μL , 0.042 mmol) and the solution stirred at room temperature for 15 minutes. Reaction monitoring revealed the quantitative formation of **12** by NMR spectroscopy. Orange crystals were grown by diffusion of pentane into a toluene solution in the glovebox freezer. Anal. Calcd. for $\text{C}_{64}\text{H}_{44}\text{BF}_{10}\text{P}_2\text{Rh}$: C, 65.2; H, 3.8. Found: C, 65.3; H, 3.9.

^1H NMR (500 MHz, toluene- d_8 , -10°C) δ : 7.50 (m, 2H, *m*-styrene), 7.30 (m, 2H, *o*-styrene), 7.21 (m, 1H, *p*-styrene), 6.96 (m, 8H, Ind, Ph_3), 6.82 (m, Ph_3), 6.37 (m, 2H, Ind), 5.21 (m, 2H, Ind), 3.03 (m, 2H, CH_2 styrene), 2.01 (m, 2H, CH_2 styrene), -13.70 (q, 1H, $^2J_{\text{HP}} = 23.2$, $^1J_{\text{HRh}} = 22.8$ Hz, RhH). $^{11}\text{B}\{^1\text{H}\}$ NMR (128 MHz, toluene- d_8 , -10°C) δ : -15.2 - -12.1 (brs). $^{13}\text{C}\{^1\text{H}\}$ NMR (125 MHz, toluene- d_8 , -10°C) δ : 133.3 (PPh_3), 130.4 (PPh_3), overlapping toluene (Ind, *p,o*-styrene, PPh_3), 125.0 (*m*-styrene), 122.3 (Ind), 118.8 (Ind), 87.7 (Ind), . $^{19}\text{F}\{^1\text{H}\}$ NMR (471MHz, toluene- d_8 , -10°C) δ : -164.6 (m, *m*- C_6F_5), -161.8 (t, $^3J_{\text{FF}} = 20$ Hz, *p*- C_6F_5), -129.0 (brs, *o*- C_6F_5). $^{31}\text{P}\{^1\text{H}\}$ NMR (162 MHz, toluene- d_8 , -10°C) δ : 36.5 (d, $^1J_{\text{PRh}} = 145$ Hz).



Compound 13. In a NMR pressure tube or high-pressure reaction vessel a solid mixture of compound **6d** (30 mg, 0.042 mmol) and $\text{HB}(\text{C}_6\text{F}_5)_2$ (20 mg, 0.057 mmol) was dissolved in toluene or benzene (0.5-2 mL) at room temperature and stirred 18 hours under H_2 atmosphere (6 atm). Reaction monitoring revealed the formation of **13** was completed and proceeded quantitatively by NMR spectroscopy. Brown crystals were grown by slow diffusion of pentane into a toluene solution in the glovebox freezer. Anal. Calcd. for $\text{C}_{48}\text{H}_{32}\text{BF}_{10}\text{P}_2\text{Rh}$: C, 59.2; H, 3.3. Found: C, 59.1; H, 3.5.

^1H NMR (500 MHz, C_6D_6 , 25 °C) δ : 7.42 (m, 8H, o-Ph₃), 7.27 to 7.16 (m, 4H, o-Ph₃), 7.00 (m, 12H, m-Ph₃, p-Ph₃), 6.90 to 6.82 (m, 6H, m-Ph₃), -1.23 (m, 1H, BH), -16.33 (m, 1H, RhH). $^{11}\text{B}\{^1\text{H}\}$ NMR (128 MHz, C_6D_6 , 25 °C) δ : -1.2 (brs). $^{13}\text{C}\{^1\text{H}\}$ NMR (125 MHz, C_6D_6 , 25 °C) δ : 134.0 (Ph₃), 133.7 (o-Ph₃), 130.2 (p-Ph₃), 128.4 (o-Ph₃). $^{19}\text{F}\{^1\text{H}\}$ NMR (471 MHz, C_6D_6 , 25 °C) δ : -164.1 (m, p-C₆F₅), -160.8 (m, m-C₆F₅), -129.3 (br, o-C₆F₅). $^{31}\text{P}\{^1\text{H}\}$ NMR (162 MHz, C_6D_6 , 25 °C) δ : 38.2 (d, $^1J_{\text{PRh}} = 115$ Hz).

IV.9. Reference

1. a) C. Gunanathan, D. Milstein, *Acc. Chem. Res.*, **2011**, *44*, 588-602.
 - b) J. R. Khusnutdinova, D. Milstein, *Angew. Chem. Int. Ed.*, **2015**, *54*(42), 12236-12273.
 - c) M. R. Elsby, R. T. Baker, *Chem. Soc. Rev.*, **2020**, *49*, 8933-8987.
 2. a) I. Kuzu, I. Krummenacher, J. Meyer, F. Armbruster, F. Breher, *Dalton Trans.*, **2008**, 5836-5865.
 - b) A. Amgoune, D. Bourissou, *Chem. Commun.*, **2011**, *47*, 859-871.
 - c) M. Devillard, G. Bouhadir, D. Bourissou, *Angew. Chem. Int. Ed.*, **2015**, *54*, 730-732.
 - d) J. S. Jones, F. P. Gabbai, *Acc. Chem. Res.*, **2016**, *49*, 857-867.
 - e) W. Guan, G. Zeng, H. Kameo, Y. Nakao, S. Sakaki, *Chem. Rec.*, **2016**, *16*, 2405-2425.
 - f) D. You, F. P. Gabbai, *Trends Chem.*, **2019**, *1*, 485-496.
 3. a) H. Braunschweig, R. D. Dewhurst, A. Schneider, *Chem. Rev.*, **2010**, *110*, 3924-3957.
 - b) D. R. Owen, *Chem. Soc. Rev.*, **2012**, *41*, 3535-3546.
 - c) H. Kameo, H. Nakazawa, *Chem. Asian J.*, **2013**, *8*, 1720-1734.
 - d) D. R. Owen, *Chem. Commun.*, **2016**, *52*, 10712-10726
- To see some relevant examples: e) A. J. M. Miller, J. A. Labinger, J. E. Bercaw, *J. Am. Chem. Soc.*, **2008**, *130*(36), 11874-11875.
- f) J. J. Kiernicki, M. Zeller, N. K. Szymczak, *J. Am. Chem. Soc.*, **2017**, *139*, 18194-18197.
 - g) A. Iannetelli, G. Tizzard, S. J. Coles, G. R. Owen, *Inorg. Chem.*, **2018**, *57*, 446-456.
 - h) A. Iannetelli, R. C. Da Costa, A. J. Guwy, G. J. Tizzard, S. J. Coles, G. R. Owen, *Organometallics*, **2020**, *39*, 1976-1988.
4. a) Z. G. Lewis, A. J. Welch, *J. Organomet. Chem.*, **1992**, *438*, 353-369.

- b) E. Bardaya, B. Frangea, B. Hanqueta, G. E. Herberich, *J. Organomet. Chem.*, **1999**, 572, 225–232.
5. a) H. Braunschweig, R. Dörfler, M. Friedrich, M. Kraft, A. Oechsner, *Z. Anorg. Allg. Chem.*, **2011**, 2125–2128.
- b) K. Rufanov, E. Avtomonov, N. Kazennova, V. Kotov, A. Khvorost, D. Lemenovskii, J. Lorberth, *J. Organomet. Chem.*, **1997**, 536-537, 361-373.
- c) Y. Sun, W. E. Piers, G. P. A. Yap, *Organometallics*, **1997**, 16, 2509-2513.
6. a) Y. Sun, R. E. v. H. Spence, W. E. Piers, M. Parvez, G. P. A. Yap, *J. Am. Chem. Soc.*, **1997**, 119, 5132-5143.
- b) R. Duchateau, S. J. Lancaster, M. Thornton-Pett, M. Bochmann, *Organometallics*, **1997**, 16, 4995-5005.
- c) X. Song, M. Bochmann, *J. Organomet. Chem.*, **1997**, 545-546, 597-600.
- d) S. Kohrt, G. Kehr, C. G. Daniliuc, R. S. Rojas, B. Rieger, C. Troll, G. Erker, *Organometallics*, **2016**, 35, 2689–2693.
7. K. A. O. Starzewski, W. M. Kelly, A. Stumpf, D. Freitag, *Angew. Chem. Int. Ed.*, **1999**, 38, 2439-2443.
8. a) J. C. Kotz, E. W. Post, *J. Am. Chem. Soc.*, **1968**, 90(16), 4503-4504.
- b) J. C. Kotz, E. W. Post, *Inorg. Chem.*, **1970**, 9, 1661-1669.
9. a) J. Bauer, H. Braunschweig, C. Hörl, K. Radacki, J. Wahler, *Chem. Eur. J.*, **2013**, 19, 13396-13401.
- b) V. Hosseininasab, I. M. DiMucci, P. Ghosh, J. A. Bertke, S. Chandrasekharan, C. J. Titus, D. Nordlund, J. H. Freed, K. M. Lancaster, T. H. Warren, *Nat. Chem.*, **2022**, 14, 1265-1269.
10. a) H. J. Liu, M. S. Ziegler, T. D. Tilley, *Polyhedron*, **2014**, 84, 203-208.
- b) V. Varga, P. Šindelář, I. Císařová, M. Horáček, J. Kubišta, K. Mach, *Inorg. Chem. Commun.*, **2005**, 8, 222-226.
11. a) A. Wong, J. Chu, G. Wu, J. Telsler, R. Dobrovetsky, G. Menard, *Inorg. Chem.*, **2020**, 59, 10343-10352.

- b) L. L. Cao, J. Zhou, Z. W. Qu, D. W. Stephan, *Angew. Chem. Int. Ed.*, **2019**, *58*, 18487-18491.
- c) V. V. Burlakov, P. M. Pellny, P. Arndt, W. Baumann, A. Spannenberg, V. B. Shur, U. Rosenthal, *Chem. Commun.*, **2000**, 241-242.
12. a) L. Liu, L. L. Cao, Y. Shao, G. Ménard, D. W. Stephan, *Chem*, **2017**, *3*, 259-267.
- b) A. Dasgupta, E. Richards, R. L. Melen, *Angew. Chem. Int. Ed.*, **2021**, *60*, 53–65.
- c) F. Holtrop, A. R. Jupp, B. J. Kooij, N. P. van Leest, B. de Bruin, J. C. Slootweg, *Angew. Chem., Int. Ed.*, **2020**, *59*, 22210-22216.
- d) A. R. Jupp, *Dalton Trans.*, **2022**, *51*, 10681-10689.
13. D. J. Parks, W. E. Piers, G. P. A. Yap, *Organometallics*, **1998**, *17*, 5492–5503.
14. a) M. T. Reetz, R. Brümmer, M. Kessler, J. Kuhnigk, *Chimia*, **1995**, *49*, 501–503.
- b) E. Barday, B. Frange, B. Hanquet, G. E. Herberich, *J. Organomet. Chem.*, **1999**, *572*, 225–232.
15. a) M. W. Drover, E. G. Bowes, J. A. Love, L. L. Schafer, *Organometallics*, **2017**, *36*, 331–341.
- b) M. W. Drover, H. C. Johnson, L. L. Schafer, J. A. Love, A. S. Weller, *Organometallics*, **2015**, *34*, 3849–3856.
- c) M. W. Drover, L. L. Schafer, J. A. Love, *Angew. Chem. Int. Ed.*, **2016**, *55*, 3181–3186.
16. B. E. Cowie, D. J. H. Emslie, *Can. J. Chem.*, **2018**, *96*(5), 484-491.
17. T. M. Douglas, A. B. Chaplin, A. S. Weller, X. Yang, M. B. Hall, *J. Am. Chem. Soc.*, **2009**, *131*(42), 15440–15456.
18. B. Cordero, V. Gómez, A. E. Platero-Prats, M. Revés, J. Echeverría, E. Cremades, F. Barragán, S. Alvarez, *Dalton Trans.*, **2008**, 2832-2838.

19. a) CSID:4482215,
<http://www.chemspider.com/ChemicalStructure.4482215.html>.
b) <https://spectrabase.com/compound/KKKkq1TeEDX>
20. T. Beringhelli, D. Donghi, D. Maggioni, G. D'Alfonso, *Coord. Chem. Rev.*, 2008, 252, 2292-2313.
21. a) M. G. Alférez, N. Hidalgo, J. Campos, **2020**. Editors C. Sloatweg and A. Jupp. Springer.
b) M. Navarro, J. Campos, **2021**, *Chapter Three - Bimetallic frustrated Lewis pairs*, Editor(s): P. J. Pérez, *Advances in Organometallic Chemistry*, Academic Press, 75, 95-148.
c) M. Navarro, J. J. Moreno, M. Pérez-Jiménez, J. Campos, *Chem. Commun.*, **2022**, 58, 11220-11235.
22. a) L. J. Bourhis, O. V. Dolomanov, R. J. Gildea, J. A. K. Howard, H. Puschmann, *Acta Cryst.*, **2015**, A71, 59-75.
b) O. V. Dolomanov, L. J. Bourhis, R. J. Gildea, J. A. K. Howard, H. Puschmann, *J. Appl. Cryst.*, **2009**, 42, 339-341.
c) G. M. Sheldrick, *Acta Cryst.*, **2015**, C71, 3-8.
23. G. M. Sheldrick, *Acta Cryst.* **2008**, A64, 112.

Generals Conclusions

1. We present nine Rh-based metal-only Lewis pairs (MOLPs) using $[(\eta^5\text{-C}_5\text{Me}_5)\text{Rh}(\text{PMe}_3)]$ as a Lewis base. We provide X-ray diffraction structures for bimetallic compounds containing MgMeBr , AlMe_3 , GeCl_2 , SnCl_2 , $\text{Zn}(\text{C}_6\text{F}_5)_2$, and ZnMe_2 . It is surprising that despite the wide use of some of these Lewis acidic fragments, their corresponding MOLPs represent highly unusual examples of unsupported $\text{M}\rightarrow\text{M}$ bonding, particularly in cases like those with a $\text{Rh}\rightarrow\text{Mg}$ (**1a**·**MgMeBr**) or a $\text{Rh}\rightarrow\text{Al}$ (**1a**·**AlMe₃**) dative bond. The nature of the bimetallic dative bond has been investigated, revealing some interesting aspects, such as the fact that the bond covalency increases with the electronegativity of the electrophile, or the existence of an important contribution of the $\sigma(\text{Rh-P})$ orbitals within the $\text{Rh}\rightarrow\text{M}$ bonds.
2. We study the cooperative reactivity of $\text{Rh}(\text{I})/\text{Au}(\text{I})$ bimetallic pairs under sterically congested environments. The nature of phosphine ligands bound to either $\text{Rh}(\text{I})$ or $\text{Au}(\text{I})$ precursors is crucial to control selectivity. Thus, the less congested $[(\text{PR}_2\text{Ar}^{\text{Xyl}})\text{Au}(\text{NTf}_2)]$ system leads to the formation of $\text{Rh}\rightarrow\text{Au}$ bimetallic adducts, whereas the bulkier $[(\text{PR}_2\text{Ar}^{\text{Cyp}})\text{Au}(\text{NTf}_2)]$ leads to an unusual activation of the Cp^* ligand in compounds of type $[(\eta^5\text{-C}_5\text{Me}_5)\text{Rh}(\text{PR}_3)_2]$ defined by the concomitant migration of a proton to the Rh site and the formation of a new $\text{Au}\text{—C}$ bond.
3. The unusual activation of the Cp^* ligand provides an opportunity to investigate late transition metal catalyzed transformations in which methyl groups of the commonly-employed C_5Me_5 ligand

could act as proton shuttles. The reversible migration of the proton to the rhodium site has been demonstrated by isotopic labelling experiments. The overall mechanism has been assessed by computational means, suggesting the required direct participation of gold.

4. The Cp* activated species is active in small molecule activation, as demonstrated for the activation of N—H and O—H bonds in ammonia, water and methanol. We provide a computational investigation to elucidate the mechanism by which ammonia is activated in the presence of the two metals, which seems to occur by a stepwise route with initial coordination of ammonia to gold followed by deprotonation by the rhodium fragment.
5. We investigate the effects of changing the nature and basicity of the phosphines bound to Rh, which also play an important role. For instance, in the case of the more congested but less basic dppe ligand, the Cp*-activated complexes only appear as transient species. Changing the Cp* ligand by an indenyl fragment leads to the formation of Rh→Aubimetallic adducts in all cases, except for the combination of $[(\eta^5\text{-C}_9\text{H}_7)\text{Rh}(\text{PPh}_3)_2]$ with $[(\text{PCyp}_2\text{Ar}^{\text{Xyl}_2})\text{Au}(\text{NTf}_2)]$, that results in the independent monometallic compounds. Those are in equilibrium, an important aspect for their ability to exhibit frustrated Lewis pair (FLP) behavior. However, the lability of the Rh—P bonds in this system has precluded accessing an efficient bimetallic FLP.
6. We describe reactivity studies between compounds $[(\eta^5\text{-C}_5\text{Me}_5)\text{Rh}(\text{PMe}_3)]$ and $[(\eta^5\text{-C}_9\text{H}_7)\text{Rh}(\text{PPh}_3)_2]$ with perfluorinated boranes $\text{B}(\text{C}_6\text{F}_5)_3$ and $\text{HB}(\text{C}_6\text{F}_5)_2$. We observe in all the cases the non-innocent behavior of the aromatics rings of Cp* and indenyl

fragments, forming in both cases new carbon-boron bonds. The resulting bifunctional ligands are genuine motifs to investigate metallic FLP-type cooperativity because of the contrasting Lewis basic and acidic nature of the Rh(I) and borane fragments, respectively. In this vein, we provide preliminary studies that evidence the potential of the boron functionality to enhance catalysis at the metal by using the hydrogenation of olefins as a model reaction.

Conclusiones generales

1. Presentamos nueve pares de Lewis metálicos basados en Rh (MOLP) usando $[(\eta^5\text{-C}_5\text{Me}_5)\text{Rh}(\text{PMe}_3)]$ como base de Lewis. Proporcionamos estructuras de difracción de rayos X para estos compuestos bimetalicos que contienen MgMeBr , AlMe_3 , GeCl_2 , SnCl_2 , $\text{Zn}(\text{C}_6\text{F}_5)_2$ y ZnMe_2 . Es sorprendente que, a pesar del amplio uso de algunos de estos fragmentos ácidos de Lewis, sus MOLP correspondientes representan ejemplos muy inusuales de enlaces $\text{M}\rightarrow\text{M}$ sin soporte, particularmente en casos como aquellos con $\text{Rh}\rightarrow\text{Mg}$ (**1a**·**MgMeBr**) o $\text{Rh}\rightarrow\text{Al}$ (**1a**·**AlMe3**) enlace dativo. Se ha investigado la naturaleza del enlace dativo bimetalico, revelando algunos aspectos interesantes, como el hecho de que la covalencia del enlace aumenta con la electronegatividad del electrófilo, o la existencia de una importante contribución de los orbitales $\sigma(\text{Rh-P})$ dentro del Enlaces $\text{Rh}\rightarrow\text{M}$.
2. Estudiamos la reactividad cooperativa de pares bimetalicos $\text{Rh(I)}/\text{Au(I)}$ en ambientes estéricamente congestionados. La naturaleza de los ligandos de fosfina unidos a los precursores Rh(I) o Au(I) es crucial para controlar la selectividad. Por lo tanto, el sistema menos congestionado $[(\text{PR}_2\text{Ar}^{\text{Xyl}})\text{Au}(\text{NTf}_2)]$ conduce a la formación de aductos bimetalicos $\text{Rh}\rightarrow\text{Au}$, mientras que el más voluminoso $[(\text{PR}_2\text{Ar}^{\text{Cyp}})\text{Au}(\text{NTf}_2)]$ conduce a una activación inusual del ligando Cp^* en compuestos de tipo $[(\eta^5\text{-C}_5\text{Me}_5)\text{Rh}(\text{PR}_3)_2]$ definido por la migración concomitante de un protón al sitio Rh y la formación de un nuevo enlace $\text{Au}-\text{C}$.
3. La activación inusual del ligando Cp^* brinda la oportunidad de investigar las transformaciones catalizadas por metales de transición tardías en las que los grupos metilo del ligando C_5Me_5 comúnmente

empleado podrían actuar como lanzaderas de protones. La migración reversible del protón al sitio de rodio se ha demostrado mediante experimentos de marcaje isotópico. El mecanismo general ha sido evaluado por medios computacionales, lo que sugiere la participación directa requerida de oro.

4. La especie con el Cp* activado es activa en la activación de moléculas pequeñas, como se demostró para la activación de enlaces N—H y O—H en amoníaco, agua y metanol. Brindamos una investigación computacional para dilucidar el mecanismo por el cual se activa el amoníaco en presencia de los dos metales, lo que parece ocurrir por una ruta gradual con coordinación inicial de amoníaco a oro seguida de desprotonación por el fragmento de rodio.
5. Investigamos los efectos de cambiar la naturaleza y la basicidad de las fosfinas unidas a Rh, que también juegan un papel importante. Por ejemplo, en el caso del ligando dppe más congestionado, pero menos básico, los complejos activados por Cp* solo aparecen como especies transitorias. El cambio del ligando Cp* por un fragmento de indenilo conduce a la formación de aductos Rh→Au bimetálicos en todos los casos, excepto en la combinación de $[(\eta^5\text{-C}_9\text{H}_7)\text{Rh}(\text{PPh}_3)_2]$ con $[(\text{PCyp}_2\text{Ar}^{\text{Xyl}_2})\text{Au}(\text{NTf}_2)]$, que da como resultado los compuestos monometálicos independientes. Esos están en equilibrio, un aspecto importante para su capacidad de exhibir un comportamiento de par de Lewis frustrado (FLP). Sin embargo, la labilidad de los enlaces Rh-P en este sistema ha impedido acceder a un FLP bimetálico eficiente.
6. Describimos estudios de reactividad entre compuestos $[(\eta^5\text{-C}_5\text{Me}_5)\text{Rh}(\text{PMe}_3)]$ y $[(\eta^5\text{-C}_9\text{H}_7)\text{Rh}(\text{PPh}_3)_2]$ con boranos perfluorados $\text{B}(\text{C}_6\text{F}_5)_3$ y $\text{HB}(\text{C}_6\text{F}_5)_2$. Observamos en todos los casos el

comportamiento no inocente de los anillos aromáticos de Cp* y fragmentos de indenilo, formando en ambos casos nuevos enlaces carbono-boro. Los ligandos bifuncionales resultantes son motivos genuinos para investigar la cooperatividad de tipo FLP metálico debido a la naturaleza ácida y básica de Lewis contrastante de los fragmentos Rh (I) y borano, respectivamente. En este sentido, proporcionamos estudios preliminares que evidencian el potencial de la funcionalidad del boro para mejorar la catálisis en el metal mediante el uso de la hidrogenación de olefinas como reacción modelo.